



Impact of Moisture Variation on Strength and Deformation of Clays



Research Report 0-5430-1

TXDOT Project Number 0-5430

**Performed in cooperation with the
Texas Department of Transportation &
Federal Highway Administration**

October 2008

**Center for Transportation Infrastructure Systems
The University of Texas at El Paso
El Paso, TX 79968
(915) 747-6925
<http://ctis.utep.edu>**

This page replaces an intentionally blank page in the original.

-- CTR Library Digitization Team

TECHNICAL REPORT STANDARD TITLE PAGE

1. Report No. FHWA/TX-08/0-5430-1		2. Government Accession No.		3. Recipient's Catalog No.	
4. Title and Subtitle Impact of Moisture Variation on Strength and Deformation of Clays				5. Report Date October 2008	
				6. Performing Organization Code	
7. Authors A. Sabnis, T. Manosuthkij, I. Abdallah, S. Nazarian, A. J. Puppala				8. Performing Organization Report No. 0-5430-1	
9. Performing Organization Name and Address Center for Transportation Infrastructure Systems The University of Texas at El Paso, El Paso, Texas 79968-0516				10. Work Unit No.	
				11. Contract or Grant No. Project No. 0-5430	
12. Sponsoring Agency Name and Address Texas Department of Transportation Research and Technology Implementation Office P.O. Box 5080, Austin, Texas 78763-5080				13. Type of Report and Period Covered Technical Report 1/06 – 8/08	
				14. Sponsoring Agency Code	
15. Supplementary Notes Research Performed in cooperation with TxDOT and the Federal Highway Administration Research Study Title: Realistic Design Guidelines for Low Classification Roads in High PI Clays					
16. Abstract This research project was focused on low-volume roads over expansive clayey soils in Texas. In spite of the over conservative pavement designs recommended and widely used in Texas for roads in high PI clay areas, these pavements often fail prematurely. It is imperative to improve the design and laboratory procedures to address expansive subsoil conditions and then design pavements accordingly to extend the life expectancy of these roads. The intent of this research project was to cultivate the vital features of strategies for improving low-volume flexible pavement design and thus improving the overall low-volume road performance. These include: 1) Identify the most significant soil parameters directly related to the performance of these types of roads; 2) Propose practical laboratory test methods and analyzing models to address the problem of premature failure of low-volume roads on high PI expansive subgrade; 3) Qualify and quantify current remediation procedures, climatic effects and road condition assessment (both successful and unsuccessful) used to mitigate the shrink-swell problems; and 4) Develop a user-friendly expert system design tool to guide the designers through the process for more realistic designs and rehabilitations. This document provides information about the first two items. Static compaction in one lift was found to be the most practical procedure. The variations in modulus and shrinkage/expansion strains with moisture under a number of different moisture conditioning procedures were evaluated. For each moisture conditioning process, models were developed to estimate the variations in the modulus and shrinkage/expansion strains with moisture. Finally the fit parameters of those models were correlated to the index properties of the clays so that they can be readily used in practice. The developed models in this research project were implemented in the assessment of the pavement performance in Research Report 5430-2.					
17. Key Words High PI clay, Shrinkage strain, Expansion strain, Moisture content, Longitudinal Cracking, Moisture Variation, Swelling			18. Distribution Statement No restrictions. This document is available to the public through the National Technical Information Service, 5285 Port Royal Road, Springfield, Virginia 22161, www.ntis.gov		
19. Security Classified (of this report) Unclassified		20. Security Classified (of this page) Unclassified		21. No. of Pages 204	22. Price

DISCLAIMERS

The contents of this report reflect the view of the authors who are responsible for the facts and the accuracy of the data presented herein. The contents do not necessarily reflect the official views or policies of the Texas Department of Transportation or the Federal Highway Administration. This report does not constitute a standard, a specification or a regulation.

The material contained in this report is experimental in nature and is published for informational purposes only. Any discrepancies with official views or policies of the Texas Department of Transportation or the Federal Highway Administration should be discussed with the appropriate Austin Division prior to implementation of the procedures or results.

NOT INTENDED FOR CONSTRUCTION, BIDDING, OR PERMIT PURPOSES

Anup Sabnis, MSCE, EIT
Thammanoon Manosuthkij, PhD, EIT
Imad Abdallah, MSCE, EIT
Soheil Nazarian, Ph.D., P.E. (66495)
Anand J. Puppala, PhD, P.E. (Louisiana)

Impact of Moisture Variation on Strength and Deformation of Clays

by

**Anup Sabnis, MSCE, EIT
Thammanoon Manosuthkij, MSCE, EIT
Imad Abdallah, MSCE, EIT,
Soheil Nazarian, Ph.D., P.E.
and
Anand J. Puppala, PhD, PE**

Performed in cooperation with

**The Texas Department of Transportation and
The Federal Highway Administration**

Report Project 0-5430

Realistic Design Guidelines for Low Classification Roads in High PI Clays

Research Report 0-5430-1

October 2008

**The Center for Transportation Infrastructure Systems
The University of Texas at El Paso
El Paso, TX 79968-0516**

This page replaces an intentionally blank page in the original.

-- CTR Library Digitization Team

ACKNOWLEDGEMENTS

The successful progress of this project could not have happened without the help and input of many personnel of TxDOT. The authors acknowledge Mr. Patrick Downey, P.E., the project PD and Mr. Miles Garrison, P.E., the project PC for facilitating the collaboration with TxDOT Districts. They have also provided valuable guidance and input.

Special thanks are extended to the PAs, Mr. McDaniel, P.E., Mr. Mike Arellano, P.E., and Dr. German Claros, P.E. whom have been very supportive on this project and were helpful in finalizing this report.

ABSTRACT

This research project was focused on low-volume roads over expansive clayey soils in Texas. In spite of the over conservative pavement designs recommended and widely used in Texas for roads in high PI clay areas, these pavements often fail prematurely. This failure occurs primarily because of the highly variable properties of the clay throughout the year due to moisture fluctuations. The expansive nature of high PI clays, despite the fact that they are considered in the design, is also of concern since they contribute to the roughness of the road, and as such the loss of the functional serviceability of the roads. Therefore, it is imperative to improve the design and laboratory procedures to address expansive subsoil conditions and then design pavements accordingly to extend the life expectancy of these roads. The intent of this research project was to cultivate the vital features of strategies for improving low-volume flexible pavement design and thus improving the overall low-volume road performance. These include:

- 1). Identify the shortcomings of current design and construction practices associated with the less than desirable performance of pavements in low-volume roads constructed on high PI clays;
- 2). Identify the most significant soil parameters directly related to the performance of these types of roads;
- 3). Propose practical laboratory test methods and analyzing models to address the problem of premature failure of low-volume roads on high PI expansive subgrade;
- 4). Qualify and quantify current remediation procedures, climatic effects and road condition assessment (both successful and unsuccessful) used to mitigate the shrink-swell problems;
- 5). Develop a user-friendly expert system design tool to guide the designers through the process for more realistic designs and rehabilitations.

This document provides information about the second and third items above. Several different laboratory techniques to compact clay specimens were evaluated. Static compaction in one lift was found to be the most practical procedure.

The variations in modulus and shrinkage/expansion strains with moisture under a number of different moisture conditioning procedures were evaluated. The moisture conditioning procedures used were a) drying the specimens from the optimum moisture content, b) saturating the specimens from the optimum moisture content and c) drying after saturating the specimen prepared at the optimum moisture content (DFS). For each moisture conditioning process,

models were developed to estimate the variations in the modulus and shrinkage/expansion strains with moisture. Finally the fit parameters of those models were correlated to the index properties of the clays so that they can be readily used in practice.

The developed models in this research project were implemented in the assessment of the pavement performance in Research Report 5430-2. That report contains information about Items 1, 4 and 5 above.

IMPLEMENTATION STATEMENT

This report is one of two reports that documents the research and results of this project. One of the major products from this project was a program called ExSPRS (Expert System for Pavement Remediation Strategies) that can be used as a design guideline for low classification roads over high PI clays. The results and findings from this report were implemented in ExSPRS.

Some of the test methods described here can be implemented by TxDOT. Also, the expert system should be used for a pilot implementation on a number of projects to determine its applicability as a design check for roads with high PI clays.

TABLE OF CONTENTS

LIST OF FIGURES	xiii
LIST OF TABLES	xvii
CHAPTER 1 - INTRODUCTION.....	1
INTRODUCTION.....	1
ORGANIZATION OF REPORT	1
CHAPTER 2 - LITERATURE REVIEW.....	3
2.1 INTRODUCTION.....	3
2.2 HIGH-PI SOILS AND PAVEMENT DISTRESS	3
2.3 PREDICTION OF SWELLING OF EXPANSIVE CLAYS	5
2.4 STRENGTH AND STIFFNESS PROPERTIES OF SOILS	6
2.5 IMPACT OF SEASONAL CHANGES ON SOIL PROPERTIES.....	6
2.5.1 Strength Properties	7
2.5.2 Stiffness Properties	9
2.6 EFFECT OF MOISTURE VARIATION ON STIFFNESS PROPERTIES OF CLAYS	14
2.7 CRACKING OF PAVEMENT STRUCTURE.....	22
CHAPTER 3 - PREPARATION AND CONDITIONING OF SPECIMENS.....	27
3.1 INTRODUCTION.....	27
3.2 TxDOT COMPACTION TECHNIQUE.....	27
3.3 DIFFERENT COMPACTION AND CONDITIONING TECHNIQUES.....	27
3.4 STATIC COMPACTION FOR CYLINDRICAL SPECIMEN.....	33
3.5 PREPARATION OF RECTANGULAR SPECIMEN.....	35
3.6 DENSITY VARIATION ALONG THE LENGTH OF SPECIMENS.....	36
3.7 CONDITIONING	37
3.7.1 Drying Phase	37
3.7.2 Wetting Phase.....	38
CHAPTER 4 - TESTING METHODOLOGY.....	41
4.1 INTRODUCTION.....	41
4.2 TEST PROGRAM	41

4.3 CHEMICAL AND MINERALOGICAL TESTS	42
4.3.1 Determination of Soluble Sulfates Contents	42
4.3.2 Cation Exchange Capacity (CEC)	42
4.3.3 Determination of Clay Mineralogy	43
4.4 STRENGTH and STIFFNESS TESTS	43
4.4.1 Unconfined Compressive Strength (UCS) Test.....	43
4.4.2 Indirect Tensile Strength (IDT) Test.....	43
4.4.3 Flexural Test.....	43
4.4.4 Free-Free Resonant Column Test.....	46
4.4.5 Resilient Modulus Test.....	46
4.4.6 Permanent Deformation Test.....	48
4.5 VOLUMETRIC TESTS.....	49
4.5.1 Volumetric Shrinkage Test.....	50
4.5.2 Three-Dimensional Free Swell Testing.....	51
4.5.3 Swell Pressure Test.....	51
4.6 SUCTION TESTS.....	53
4.6.1 Pressure Plate Method.....	53
4.6.2 Filter Paper Method.....	54
CHAPTER 5 - PRESENTATION OF RESULTS	55
5.1 INTRODUCTION.....	55
5.2 INDEX PROPERTIES.....	55
5.3 MINERALOGICAL PROPERTIES.....	56
5.4 STRENGTH TESTS.....	57
5.5 STIFFNESS TESTS.....	57
5.6 VOLUMETRIC TESTS.....	62
CHAPTER 6 – DEVELOPMENT OF RELATIONSHIPS	69
6.1 INTRODUCTION.....	69
6.2 DRY FROM OPTIMUM PROCESS (DFO)	70
6.3 SATURATED FROM OPTIMUM PROCESS (SFO)	73
6.4 DRY FROM SATURATION PROCESS (DFS)	78
6.5 DEVELOPMENT OF RELATIONSHIP WITH INDEX PARAMETERS	87
6.6 APPLICATION OF MODELS	94
CHAPTER 7 - SUMMARY CONCLUSIONS.....	97
REFERENCES.....	99
APPENDIX A – PROTOCOLS.....	103
APPENDIX B – STATIC COMPACTOR APPARATUS DESIGN	115
APPENDIX C – NORMALIZED MODULUS VS NORMALIZED MOISTURE CONTENT – DFO RESULTS.....	119

APPENDIX D – NORMALIZED MODULUS VS SHRINKAGE STRAIN – DFO RESULTS.....	123
APPENDIX E – EXPANSION STRAIN VS NORMALIZED MOISTURE CONTENT – SFO RESULTS	131
APPENDIX F – NORMALIZED MODULUS VS NORMALIZED MOISTURE CONTENT – SFO RESULTS	139
APPENDIX G – NORMALIZED MODULUS VS EXPANSION STRAIN – SFO RESULTS	143
APPENDIX H – SHRINKAGE STRAIN VS NORMALIZED MOISTURE CONTENT – DFS RESULTS.....	151
APPENDIX I – NORMALIZED MODULUS VS NORMALIZED MOISTURE CONTENT – DFS RESULTS	159
APPENDIX J – NORMALIZED MODULUS VS SHRINKAGE STRAIN – DFS RESULTS.....	163
APPENDIX K – EXPANSION STRAIN VS TIME – SFO RESULTS	171

LIST OF FIGURES

Figure 2.1 – Map of the U.S. Showing Swell Potential of Expansive Soils.....	4
Figure 2.2 – Distortion and Cracking of Pavements.....	5
Figure 2.3 – Triaxial Test.....	8
Figure 2.4 – Typical Triaxial Test Results.....	8
Figure 2.5 – Indirect Tensile Strength Setup	9
Figure 2.6 – Cyclic Triaxial Test Apparatus.....	10
Figure 2.7 – Resilient Modulus Test.....	11
Figure 2.8 – Typical Resilient Modulus Test Results.....	11
Figure 2.9 – Typical Deformation Response in Permanent Deformation Test.....	12
Figure 2.10 – Typical Variation in Permanent Strain with Cycles	13
Figure 2.11 – Free-Free Resonant Column System	13
Figure 2.12 – Fixed-Free Resonant Column System	14
Figure 2.13 – Variation in Seismic Modulus with Moisture Content under Constant Compactive Effort for a Fine-Grained Material (Yuan and Nazarian, 2003).....	15
Figure 2.14 – Typical Variations of Modulus and Moisture Content with Time	16
Figure 2.15 – Typical Effect of Post-compaction Saturation on Resilient Responses (Drumm et al, 1997).....	17
Figure 2.16 – Typical Effect of Post-compaction Moisture Increase on Resilient Modulus (Drumm et al, 1997)	17
Figure 2.17 – Variation of Actual MR with Predicted MR Values	20
Figure 2.18 – Variation of Resilient Modulus with Moisture Content	21
Figure 2.19 – Three Point Bend Test.....	24
Figure 2.20 – Four Point Bend Test.....	25
Figure 2.21 – Different Stages of Cracking Mechanism	25
Figure 3.1 – Clay Specimen Subjected To Wetting by <i>Method 1</i>	28
Figure 3.2 – Clay Specimen Subjected To Wetting by <i>Method 2</i>	29
Figure 3.3 – Clay Specimen Subjected To Wetting by <i>Method 3</i>	29
Figure 3.4 – Change in Seismic Modulus and Moisture Content vs. Time	30
Figure 3.5 – Change in Dimension and Volume vs. Time.....	30
Figure 3.6 – Cracking of the Specimen Compacted by Method – 4 and Subjected to Drying.....	31
Figure 3.7 – Set-up for Wetting for Specimen Compacted by <i>Method 5</i>	31
Figure 3.8 – Change in Seismic Modulus and Moisture Content vs. Time during Wetting.....	32
Figure 3.9 – Completely Dry Specimen Compacted by <i>Method 5</i>	32

Figure 3.10 – Change in Seismic Modulus and Moisture Content vs. Time during Drying	33
Figure 3.11 – Change in Dimension and Volume vs. Time.....	33
Figure 3.12 – Preparation of Specimen.....	34
Figure 3.13 – Rectangular Specimen Preparation Using Static Compactor	35
Figure 3.14 –Variation in Density Using Different Compaction Techniques	36
Figure 3.15 – Drying Method for Clay Specimens.....	37
Figure 3.16 – Change in Dimensions and Volume vs Time.....	38
Figure 3.17 – Change in Seismic Modulus and Moisture Content vs Time.....	38
Figure 3.18 – Wetting Method for Clay Specimens	39
Figure 3.19 – Change in Dimensions and Volume vs. Time.....	40
Figure 3.20 – Change in Seismic Modulus and Moisture Content vs Time.....	40
Figure 4.1 – Steps in Flexural Test.....	44
Figure 4.2 – Flexural Test Set-up	45
Figure 4.3 – Typical Flexural Test Result	45
Figure 4.4 – Typical Free-Free Resonant Column Test Results.....	46
Figure 4.5 – Free-Free Resonant Column Test.....	47
Figure 4.6 – Typical Resilient Modulus Test Results.....	47
Figure 4.7 – Steps for Resilient Modulus Test	48
Figure 4.8 – Typical Permanent Deformation Test Result	49
Figure 4.9 – Typical Specimens.....	50
Figure 4.10 – Typical Photograph and Digital Image of a Specimen.....	51
Figure 4.11 – Three-Dimensional Free Swell Test Setup.....	52
Figure 4.12 – Modified Consolidation Test Setup for Swell Pressure Test.....	52
Figure 4.13 – Schematic Of Pressure Plate Apparatus (Soil-Moisture Equipment Corp., 2003).	53
Figure 4.14 – Pressure Plate Testing.....	54
Figure 4.15 – Calibration curves (Bulut, Lytton and Wray, 2001).....	54
Figure 5.1 – Typical Swell Strains from 3-D Swell Tests for Different Moisture Contents	65
Figure 5.2 – Soil Water Characteristic Curves of Soils.....	67
Figure 6.1 – Three Conditioning Processes	70
Figure 6.2 – Typical Variations in Moisture Content and Modulus with Time	71
Figure 6.3 – Typical Variations in Shrinkage Strains with Time	71
Figure 6.4 – Typical Variations in Shrinkage Strains with Normalized Moisture Content.....	71
Figure 6.5 – Typical Variation in Modulus with Moisture Content (DFO Process)	72
Figure 6.6 – Typical Variations in Modulus with Shrinkage Strains	74
Figure 6.7 – Typical Variations in Moisture Content and Modulus with Time (Wetting Process)	75
Figure 6.8 – Typical Variations in Expansion Strains with Time.....	75
Figure 6.9 – Typical Variations in Expansion Strains with Normalized Moisture Content (NMC _{SFO}).....	75
Figure 6.10 – Typical Variation in Seismic Modulus with Normalized Moisture Content (NMC _{SFO}).....	76
Figure 6.11 – Typical Variations in Modulus with Expansion Strains.....	77
Figure 6.12 – Typical Variations in Moisture Content and Modulus with Time	79

Figure 6.13 – Typical Variations in Expansion Strains with Time.....	79
Figure 6.14 – Typical Variations in Shrinkage Strains with Normalized Moisture Content (NMC _{DFS}).....	79
Figure 6.15 – Typical Variation in Normalized Modulus with Normalized Moisture Content (NMCDFS).....	80
Figure 6.16 – Typical Variations in Modulus with Expansion Strains.....	81
Figure 6.17 – Process in Predicting Shrinkage Strain.....	89
Figure 6.18 – Typical Trend Line for Parameter A with Plasticity Index	89
Figure 6.19 – Results of Sensitivity Study on the Shrinkage Models	92
Figure 6.20 – Comparison of Measured and Predicted Shrinkage Strain Data and Moisture Content for Three Specimen of the Houston Clay Material	93
Figure 6.21 – Histograms of Differences between Measured and Estimated Strains.....	94
Figure 6.22 – Application of Model	95

LIST OF TABLES

Table 2.1 – Resilient Modulus Results for Compacted Clay Specimens Tested without Further Conditioning.....	19
Table 2.2 – Resilient Modulus Results for Compacted Clay Specimens Tested after Moisture Conditioning.....	19
Table 2.3 – Resilient Modulus Results for Compacted Clay Specimens Tested after Drying.....	20
Table 4.1 – Test Matrix Carried Out in This Study	42
Table 4.2 – Typical Values for Three Basic Clay Minerals (Mitchell, 1976).	43
Table 4.3 – Loading Sequence for Resilient Modulus Test.....	49
Table 5.1 – Index Properties	55
Table 5.2 – Moisture Density Test Results.....	56
Table 5.3 – Chemical Parameters of Soils	56
Table 5.4 – Mineralogy Characteristics of Soils.....	57
Table 5.5 – UCS Test Results at Different Moisture Conditions	58
Table 5.6 – Indirect Tensile Strength Test Results at Different Moisture Conditions	58
Table 5.7 – Flexural Test Results at Different Moisture Conditions.....	59
Table 5.8 – Summary of Test Results during Drying Process.....	60
Table 5.9 – Summary of Test Results during Wetting Process	60
Table 5.10 – Resilient Modulus Test Results at Different Moisture Conditions.....	61
Table 5.11 – Permanent Deformation Test Results at Different Moisture Conditions.....	63
Table 5.12 – Volumetric Shrinkage Strain Results.....	64
Table 5.13 – Volumetric Swell Strain Tests Results	64
Table 5.14 – Swell Pressure Test Results	66
Table 6.1 – Typical Best Fit Parameters for Shrinkage Strain vs Normalized Moisture Content, NMC_{DFO}	72
Table 6.2 – Typical Best Fit Parameters between Normalized Modulus and Normalized Moisture Content (DFO).....	73
Table 6.3 – Typical Best Fit parameters between Normalized Modulus and Shrinkage Strains	74
Table 6.4 – Typical Best Fit Parameters (Expansion Strain vs Normalized Moisture Content, NMC_{SFO}).....	76

Table 6.5 – Typical Best Fit Parameters between Normalized Modulus and Normalized Moisture Content (NMC_{SFO})	76
Table 6.6 – Typical Best Fit parameters between Normalized Modulus and Expansion Strains.	78
Table 6.7 – Typical Best Fit Parameters between Shrinkage Strain and Normalized Moisture Content (DFS)	80
Table 6.8 – Typical Best Fit Parameters between Normalized Modulus and Normalized Moisture Content.....	80
Table 6.9 – Typical Best Fit parameters between Normalized Modulus and Expansion Strains.....	81
Table 6.10 – Summary of Equations Used to Establish Relationships.....	82
Table 6.11 – Best Fit Parameters (Shrinkage Strains vs. NMC_{DFO})	83
Table 6.12 – Best Fit Parameters (Normalized Modulus and NMC_{DFO})	83
Table 6.13 – Best Fit Parameters (Normalized Modulus vs. Shrinkage Strains after DFO Process)	84
Table 6.14 – Best Fit Parameters (Expansion Strain and NMC_{SFO})	84
Table 6.15 – Best Fit Parameters (Normalized Modulus and NMC_{SFO}).....	85
Table 6.16 – Best Fit Parameters (Normalized Modulus and Expansion Strain after SFO Process).....	85
Table 6.17 – Best Fit Parameters (Shrinkage Strain and NMC_{DFS}).....	86
Table 6.18 – Best Fit Parameters (Normalized Modulus and NMC_{DFS}).....	86
Table 6.19 – Best Fit Parameters (Normalized Modulus and Shrinkage Strain after DFS Process)	87
Table 6.20 – Correlation Analysis between Parameter A from Equation 6.4 and Index Properties of Clays.....	88
Table 6.21 – Relationships between Parameter and Index Properties of Soils.....	90
Table 6.22 – Weighting Functions for Each Index Parameter of San Antonio Clay	91
Table 6.23 – Estimated A* Parameter for Different Shrinkage Types Using all five Index Parameters for San Antonio Clay.....	91
Table 6.24 – Shrinkage Strains at 14% Moisture Content for San Antonio Clay	91

CHAPTER 1 - INTRODUCTION

INTRODUCTION

The Texas low-volume flexible pavement roadway system on high plasticity index (high PI) clay foundations often fail prematurely. A large number of these roads do not last as long as they are designed for. One reason is that the design procedures currently used does not account for the high-PI clay subgrades. It is therefore, important to improve the design and laboratory procedures to evaluate subsoil conditions and then design pavements accordingly to extend the life expectancy of these roads.

The main focus of this report is laboratory tests to evaluate strength and stiffness properties of high PI clays. Six different clay materials, consisting of on low PI clay and five high PI clays, were tested as part of a testing matrix to cover Texas conditions. Part of the data generated in this study was then used to carry out statistical analysis and to develop models predicting strains (shrinkage and expansion) and modulus of clays with change in moisture content.

ORGANIZATION OF REPORT

This documentation of work carried out for this study starts with a literature review (Chapter Two), in which the behaviors of high PI clays are critically analyzed with respect to change in moisture content. That chapter also covers pavement distresses due to the special properties (strength and stiffness) associated with these expansive soils. The impact of seasonal variation on strength and stiffness properties of clays is illustrated based on field and laboratory tests.

In Chapter Three, the laboratory tests for preparation of specimens are described. The current TxDOT compaction method and its drawbacks as related to clay materials are pointed out first. Alternative compaction methods were evaluated and compared with the current methods. Additionally, the drying and wetting processes of the specimen prepared at the optimum moisture content and tested at dry, optimum and saturated conditions are presented.

Chapter Four discusses the testing program in detail by explaining all strength and stiffness and shrink-swell tests which were performed in this study.

The results from all tests are presented in Chapter Five, while trends and observations between different parameters measured after dry and wet conditioning are documented in Chapter Six. Some of the data were used to develop mathematical models between index properties of clays and their modulus and shrinkage properties. These models are also described in Chapter Six.

CHAPTER 2 - LITERATURE REVIEW

2.1 INTRODUCTION

Many pavements fail prematurely due to moisture changes that affect the engineering and physical properties of the subgrade soils. Aubeny and Lytton (2002) investigated the modes of distress in pavements constructed on high-PI clays. The sources of distress involve the formation of surface cracks, moisture infiltration through the cracks, and therefore, a reduction in the strength of the soil. When these high-PI clays are subjected to drying in hot summer months, they tend to shrink significantly, causing distress, normally in the form of longitudinal cracking. This chapter provides a brief description of high-PI clays as problematic soils, pavement distresses as a result of expansive soils, and a literature review on evaluation of strength and stiffness properties of high-PI subgrades with changing moisture content.

2.2 HIGH-PI SOILS AND PAVEMENT DISTRESS

Soils that exhibit significant volume change from soil moisture fluctuations are known as expansive clay soils. Expansive clays contain highly active minerals that expand or shrink as moisture is added or removed. Soft clays usually have higher moisture contents and more voids than stiffer clays. If enough moisture fills the voids and the soil becomes saturated, the clay can lose nearly all of its strength and stiffness. Excessive moisture can cause costly construction problems.

Since clays have severe shrink and swell susceptibility, damage to roads, slabs, and foundations that are constructed on or near clays can occur. Approximately one-half of the land in the United States contains expansive soils (see Figure 2.1) causing billions of dollars in damage each year to roads, homes, pipelines and other structures (Krohn and Slosson, 1980).

Soil movements in highway environment caused by swell or shrinkage strains of expansive soils are attributed to subgrade moisture variation. The water content in the clay can change during or after construction of a structure in a number of ways. Rain, snowmelt, and poor drainage under roads can increase the moisture and trap it in the soil. Trees planted near pavement structures can reduce the water content in soils as the roots collect water during growth thus resulting in shrinkage problems in soils. Irrigation in the vicinity of the pavement structures can add

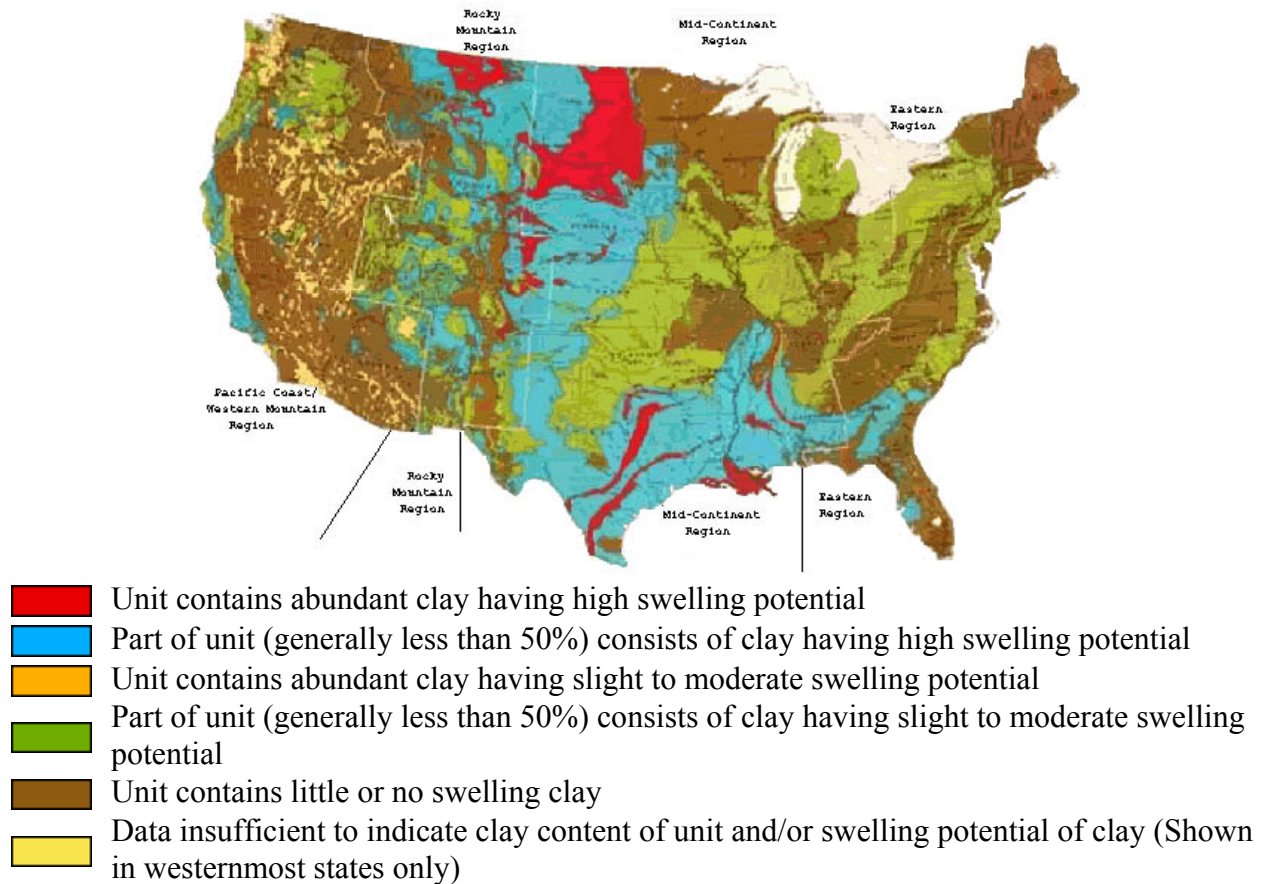


Figure 2.1 – Map of the U.S. Showing Swell Potential of Expansive Soils

moisture to the soil. Damages sustained by the pavements include distortion and cracking (see Figure 2.2) of pavements in all directions, as well as heave related bumps which may cause ride discomfort. Distortion may be caused by swelling of expansive subgrade soils, which sometimes lead to cracking. Longitudinal cracking is mainly attributed to shrinkage of underlying layers which may also be accelerated by repeated traffic loads (Engineering Manual 1110, 3-138, US Army Corps of Engineers, 1984). The cracks developed in pavements will further allow moisture infiltration to subgrade, which results in the weakening and loss of foundation support to pavements. In general, the magnitude and extent of damages to pavement structures can be extensive.

If the conditions are properly evaluated, the effect of shrink/swell susceptible clay soils on low traffic roads can be controlled. However, maintenance and repairs requirements can be extensive, often exceeding the capital costs.



Figure 2.2 – Distortion and Cracking of Pavements

2.3 PREDICTION OF SWELLING OF EXPANSIVE CLAYS

Changes in water content can greatly affect the engineering and physical properties of expansive soils, resulting in problems during and after construction. Also the volume changes resulting from shrinkage and swelling of fine-grained soil are large enough to seriously damage small buildings and highway pavements (Holtz and Kovacs, 1981). The swelling characteristics of the expansive clay soils should be predicted to make rational design of foundation of facilities to be constructed. The swelling could be inter-particle or intra-crystalline, which is based on the type of mineral present in the clay (Nwaiwu and Nuhu, 2006).

Factors influencing swelling potential and swelling pressure include: type and amount of clay, initial placement condition, stress history, nature of pore fluid, temperature, volume change permitted during swelling, shape size and thickness of sample as well as time (Nayak and Christensen, 1971). According to Holtz and Kovacs (1981), swelling depends on the clay minerals present in the soil, the soil structure and fabric and several physicochemical aspects of the soil such as cation valance, salt concentration, cementation and presence of organic matter.

Many investigators have conducted swelling pressure and/or swelling potential tests on expansive soils. Unfortunately, in most cases either the testing conditions differ from the ones adopted in investigation (Ladd, 1960) or the obtained data from testing is not sufficient enough to apply for the proposed equations to their soils (Seed et al. 1962).

The relationships among the index properties and physical state of expansive clay soils to their swelling characteristics have been the topic of extensive research. Komornik and David (1969) developed an equation in which the logarithm of swelling pressure was related to both the liquid limit and dry unit weight. El-Sohby and Mazen (1987) concluded that these two parameters are very significant in the determination of swelling pressure. Several regression equations were developed by Hossain et al. (1997) relating swelling to initial dry unit weight, initial water content, liquidity index, liquid limit or plasticity index. But none of the above equations incorporated the effects of physico-chemical factors on swelling properties of soils.

Nwaiwu and Nuhu (2006) carried out laboratory tests to evaluate the pH, electrical conductivity, loss on ignition of the soils, grain size distribution (Hydrometer test) and percentage free swell of expansive clay materials. They concluded that the swelling behavior can be predicted from a combination of physico-chemical/physico-mechanical and index properties of clays. According to Nwaiwu and Nuhu (2006), the specific gravity and electrical conductivity can be used to predict the swell potential, while the same factors along with clay content and plasticity index can be used to predict the free swell, swelling strain and swelling pressure of the clay from:

$$FS = -1263.41 - 14.43 \times Ec + 435.47 \times Gs + 4.88 \times C - 2.04 \times PI + \varepsilon \quad (2.1)$$

$$Sf = 11.17 + 0.16 \times Ec - 3.96 \times Gs + \varepsilon \quad (2.2)$$

$$Ps = 13720.02 + 149.24 \times Ec - 4940.1 \times Gs - 25.65 \times C + 20.33 \times PI + \varepsilon \quad (2.3)$$

where FS = free swell, Sf = swell strain, Ps = Swelling pressure, Ec = electrical conductivity, Gs = specific gravity, C = clay content in percent, PI = plasticity index, and ε = random error term.

2.4 STRENGTH AND STIFFNESS PROPERTIES OF SOILS

One of the major input parameters in many pavement design procedures for most subgrade materials is the seasonal variation in modulus with exposure to moisture. This issue should be addressed since expansive clays exhibit volume changes in accordance with seasonal fluctuations and because the rate at which moisture infiltrates into the soil is a key factor in assessing the magnitude to which strength degradation due to seasonal fluctuations in moisture is likely to occur (Aubeny and Lytton, 2002). In terms of performance, the water retention potentials of clay used as a subgrade have shown to have detrimental impact on the strength and stiffness parameters and, as such, their performance (Saarnketo and Scullion, 1997).

2.5 IMPACT OF SEASONAL CHANGES ON SOIL PROPERTIES

The variation in modulus with moisture in realistic pavement design is so important that significant research programs, such as the Federal Highway Administration (FHWA) and the long-term pavement performance (LTPP) monitoring program, have seriously focused on these issues for some time (Nazarian and Yuan, 2003). Aubeny and Lytton (2002) addressed two issues regarding the problem of strength degradation: (1) the degree of strength loss occurring in the soil and (2) the depth to which this strength degradation occurs.

In the summer months, the soil dries out with time. Such loss of moisture results in significant increase in the strength and stiffness (modulus) of the clay, which has a positive impact on the life of the pavement (Drumm et. al., 1995). However, the increase in stiffness results in the increase in the brittleness of the clay. The loss of moisture also contributes to the shrinkage of the clay. This tendency to shrink, along with the increase in the brittleness, causes cracks that will propagate to the surface of the road. These cracks, sometimes an inch or more wide, act as conduit for water to penetrate more rapidly in the subgrade, causing a vicious circle of

continuous damage to pavement. The depth and spacing of cracks will depend on the intensity and duration of the dry period as well as the type of vegetation in the vicinity.

In the rainy seasons, moisture penetrates into cracks and diffuses into the soil mass, and thus, clay exhibits exceptionally low strength and tends to expand. The low strength of the subgrade thus contributes to the structural damage of the road (Thompson and Elliot, 1985). In the saturated stage, the subgrade is so weak that the pavement would fail under much smaller loads than when the same subgrade is at its optimum state. This behavior of the subgrade is so predominant that the quality of the base layer on the structural performance of the pavement may become negligible.

The vulnerability of the clay subgrade to such seasonal and water content conditions has focused attention on the need to maintain more adequately the moisture content of the clay as constant as possible. Equilibrium moisture beneath highway pavements is critical to pavement design and construction because moisture directly affects the strength and stiffness of pavement systems. Therefore, a number of practical steps during the construction and rehabilitation should be considered to address the issue of maintaining constant moisture levels in the subgrade, including parameters such as widening the right of way, controlling the types and locations of trees and vegetations, and providing the appropriate drainage design (Pengelly and Addison, 2001).

2.5.1 STRENGTH PROPERTIES

Saturated clays are generally weak and thus are often a cause of premature distress of roads. For this reason, clays require a more careful analysis when dealing with their strength properties. Strength can be measured using both in the laboratory and in-situ methods.

Most laboratory strength measurements in Texas consist of the Texas Triaxial Test (Tex-117-E) and Standard Triaxial Test (Tex-143-E). The triaxial compression tests (see Figure 2.3) are used to measure the shear strength of a soil under controlled drainage conditions. In the conventional triaxial test, or Test Method Tex-143-E, a cylindrical specimen of soil encased in a rubber membrane is placed in a triaxial compression chamber, subjected to a confining pressure, and then loaded axially to failure.

For the standard triaxial tests (Tex-143-E), a minimum of three specimens are molded at the optimum moisture and maximum dry density for base and subgrade materials. A rubber membrane is placed over the sample, along with two o-rings, to prevent any water to infiltrate the specimen or any moisture to escape it. The specimens are then set aside for about 24 hrs. Each specimen is then tested in compression while being subjected to its assigned confining pressure (e.g. 3, 7, and 10 psi).

The same procedure is followed for the Texas Triaxial Test, or Test Method Tex-117-E, with the only difference being that immediately after extruding the specimens from the mold they are set aside for 24 hrs and then placed inside Texas triaxial cells. Following the drying process, the specimens are subjected to capillary wetting. The specimens are maintained under capillary wetting for a total of 24 hours. Each specimen is then subjected to its assigned confining pressure (e.g. 0, 5, 10, and 15 psi), and tested in compression.

Figure 2.4 shows typical triaxial test results (Mohr circles). The strength parameters obtained with these tests are the cohesion, angle of internal friction, and the Texas Triaxial classification of the materials. The Texas Triaxial design method is used to determine the required pavement thickness to ensure against subgrade shear failure due to heavy wheel loads. The thickness design can be performed based on the Texas Triaxial classification, the current and projected traffic, and a design wheel load.

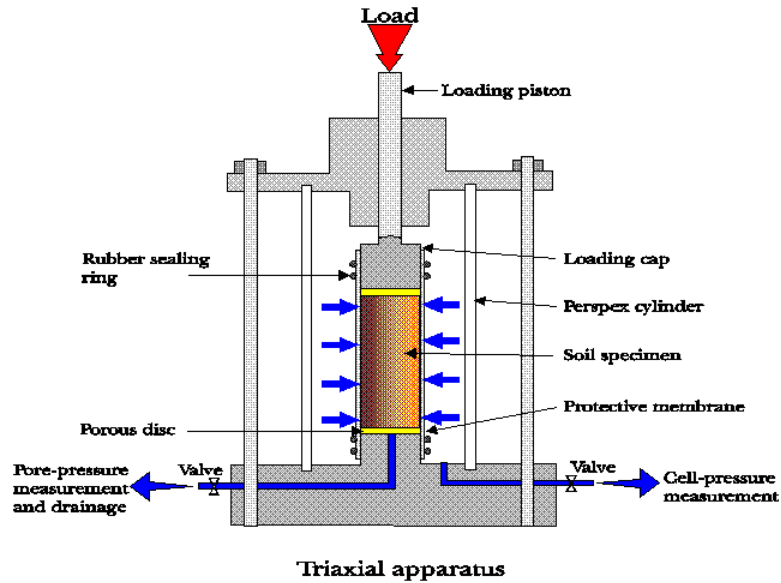


Figure 2.3 – Triaxial Test

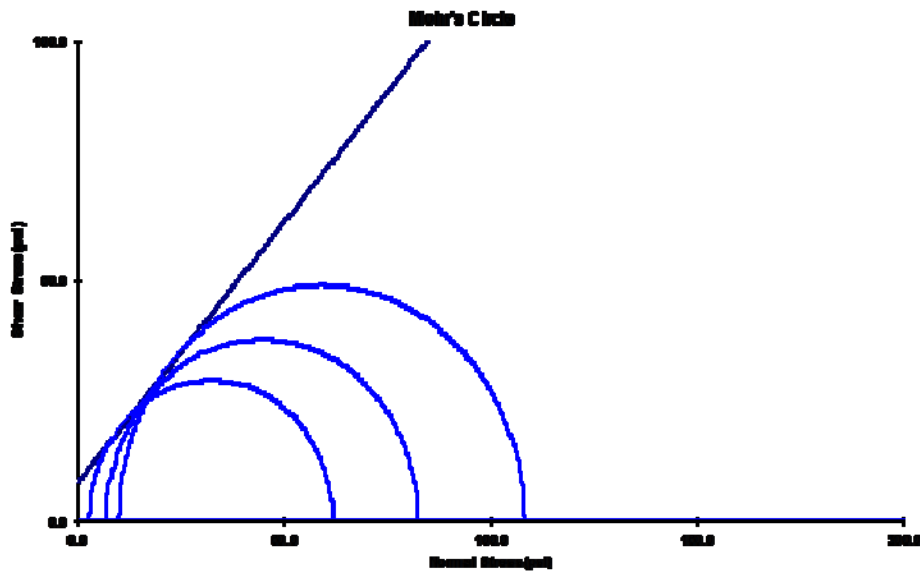


Figure 2.4 – Typical Triaxial Test Results

In the indirect tensile strength test (Tex-226-F, see Figure 2.5a) a cylindrical specimen is loaded diametrically across the circular cross section. Figure 2.5b shows the specimen set up for indirect tensile strength testing. The loading causes a tensile deformation perpendicular to the plane of loading ultimately resulting into a tensile failure. By knowing the load at failure and the dimensions of the test specimen, the indirect tensile strength can be calculated using:

$$IDT = \frac{2 \times P}{\pi \times D \times L} \quad (2.4)$$

where IDT = indirect tensile strength, P = load at failure, D = diameter of the specimen, and L = length of the specimen.

a) Indirect Tensile Strength Test



b) Specimen Setup for IDT



Figure 2.5 – Indirect Tensile Strength Setup

2.5.2 Stiffness Properties

The stiffness of subgrade soils is an important indicator of soil performance and a required input for a pavement design. Stiffness properties of subgrade soils are often determined and measured by conducting appropriate tests at compacted moisture levels. Stiffness tests can be carried out in the laboratory as well as in the field.

Laboratory stiffness measurement methods include the cyclic triaxial test, resilient modulus test, permanent deformation test, Free-free resonant column test, and fixed-free resonant column test.

Cyclic triaxial tests are carried out on samples prepared at optimum moisture content or at saturated condition to evaluate the behavior of soils. The test system is often a closed loop system, which controls the axial stress and confining pressure. An actuator applies the axial load. This cyclic load can be controlled according to the applied load or displacement or strain. The test method covers the determination of modulus and damping properties of soils in either undisturbed or reconstituted states by controlled cyclic triaxial techniques. The cyclic triaxial properties of the soil are then evaluated relative to a number of factors including the strain level, density, number of cycles, material type, saturation and effective stress (Matthew et. al., 2004).



Figure 2.6 – Cyclic Triaxial Test Apparatus

Figure 2.6 shows the cyclic triaxial test apparatus. A cylindrical specimen is prepared similar to the one prepared for the triaxial test. The specimen is subjected to cyclic deviator stress to study deformation response.

The resilient modulus (MR) is typically determined in the laboratory in accordance with the AASHTO T307 under conditions of maximum dry density and optimum moisture content. The resilient modulus is a measurement of the soil response when subjected to repeated loading. Resilient modulus tests are the primary means of determining the variation in modulus of base and subgrade materials with moisture. Most modern pavement design methods are based on the resilient modulus of the supporting subgrade soils.

The resilient modulus test provides a basic relationship between the applied stress and the resulting deformation of pavement materials (Matthew et al., 2004). This relationship can be used in the structural analysis of layered pavement systems. The resilient modulus test also provides a means of characterizing pavement construction materials when tested over a range of variable conditions, such as moisture, density, and stress conditions in a pavement subjected to moving wheel loads.

The resilient modulus system (Figure 2.7) applies cyclic loading to the soil specimen. The loading simulates conditions produced by traffic. The loading wave shape is typically a haversine. A double acting actuator applies axial load. The results of the resilient modulus test provide a relationship between stiffness and the state of stress of the material being tested. The typical test results are shown in Figure 2.8.

Majority of rutting or the vertical permanent deformation of the pavement structure is assumed to be contributed by the pavement layers such as base, sub-base and subgrade. In subsoils, 'subgrade' being the weakest, contributes maximum (approximately 40%) of the total permanent deformation. Hence it is very important to consider the permanent deformation aspects of the subgrade while estimating the total rutting magnitudes in a pavement section (Puppala et al., 1999).



Figure 2.7 – Resilient Modulus Test

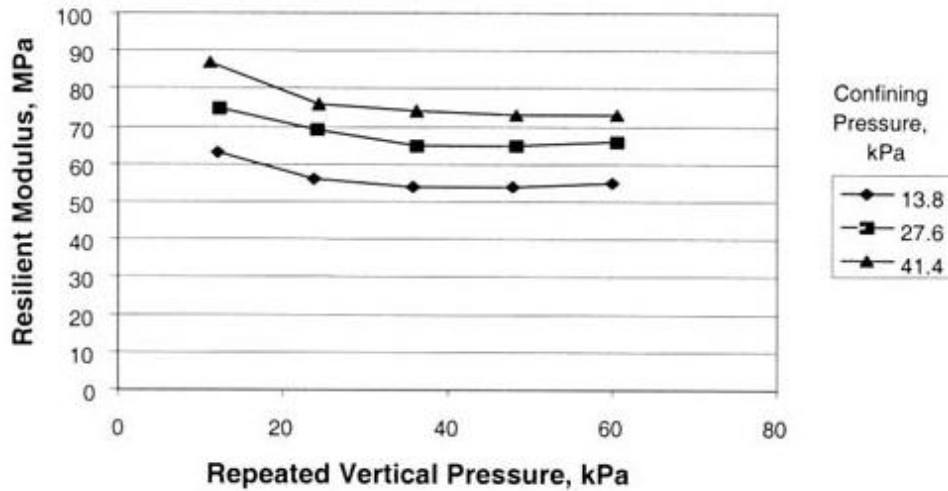


Figure 2.8 – Typical Resilient Modulus Test Results

Earlier studies regarding rut depth determination considered only top few layers such as asphalt base and subbase for analysis but later it was recognized the need to include permanent deformation caused by subgrade to calculate total rut depth. Thompson and Smith (1990) concluded that shear strength properties provide a better characterization of permanent deformation aspects of soils than the stiffness related properties. To characterize any subsoil, it is important to understand the soil's plastic strain response along with the resilient response. Repeated load triaxial test is used to calculate permanent deformation of subgrade specimens.

To minimize the imperfect contacts between the end platens and specimen, testing is started with the conditioning at prescribed confining and deviatoric stress level for 1,000 cycles. Actual testing is then followed by subjecting the sample at a particular combination of confining and deviatoric stress levels.

The vertical deformation from LVDTs were monitored and recorded continuously during testing. Figure 2.9 shows the typical deformation response monitored during testing. The elastic deformation recorded is used to determine the resilient modulus values while as plastic deformation is used to determine the permanent deformation values. A typical variation in permanent deformation with the number of cycles is shown in Figure 2.10. Initially, as the number of cycles increases, the permanent deformation accumulates rapidly. At higher cycles, the permanent deformation accumulates much slower.

The free-free resonant column (FFRC) device is a reasonably low cost device for measuring the modulus of pavement materials. Due to the nondestructive nature of this test, one specimen can be tested repeatedly to obtain the variation in modulus with moisture (Nazarian et al, 2002). Also, the same specimen can be used to measure the change in length and diameter of the specimen during to saturation and drying. Test results have shown that the modulus from the FFRC device is reasonably well-correlated to the modulus from the resilient modulus tests and the angle of internal friction from the triaxial tests (Nazarian, 2003).

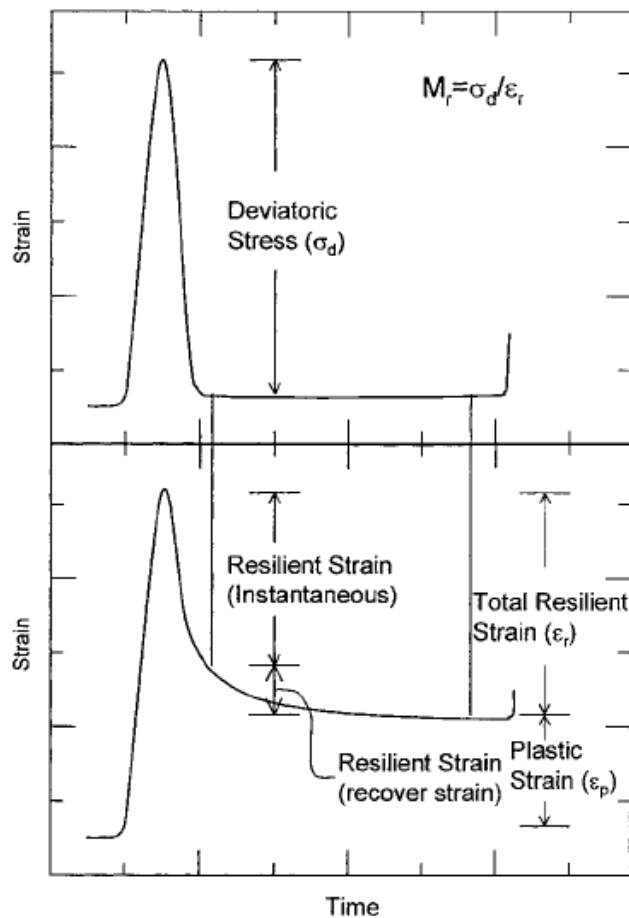


Figure 2.9 – Typical Deformation Response in Permanent Deformation Test

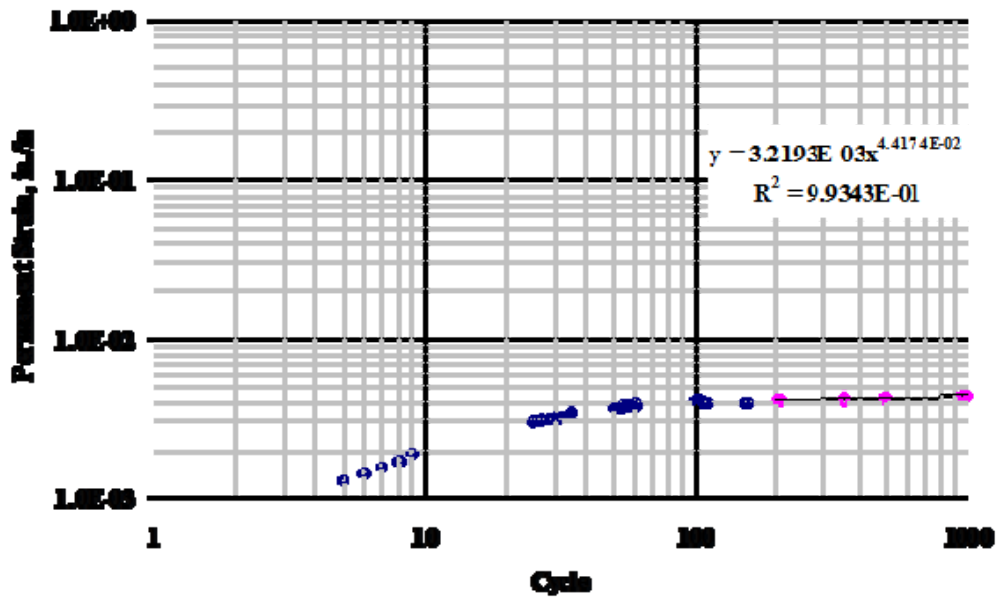


Figure 2.10 – Typical Variation in Permanent Strain with Cycles

To conduct the test, a specimen is prepared similar to the one prepared for the resilient modulus or triaxial tests. Since the test is nondestructive, the specimen can be tested after FFRC tests for strength (static triaxial tests) or stiffness (resilient modulus or cyclic triaxial test).

Figure 2.11 shows this procedure. An accelerometer is securely placed on one end of the specimen, and the other end is impacted with a hammer instrumented with a load cell. A specimen can be tested, and the test result can be obtained in less than three minutes (Nazarian, 2003).

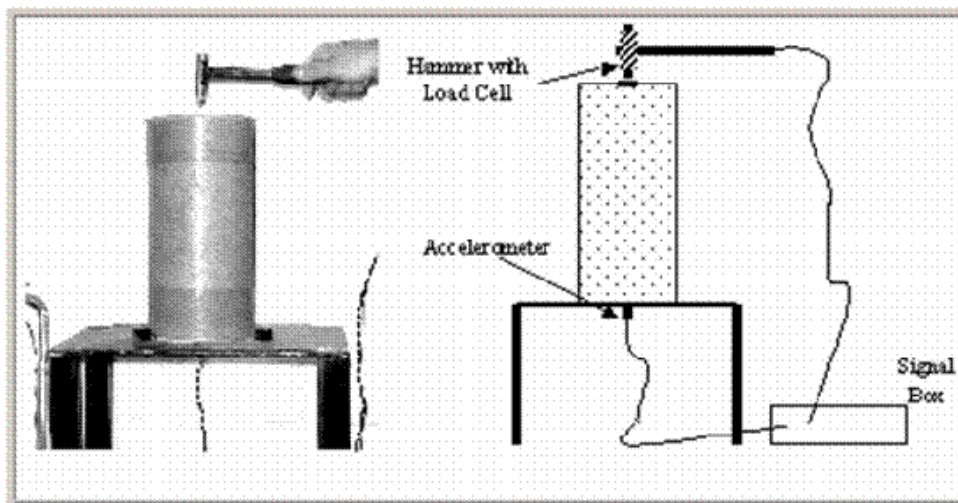


Figure 2.11 – Free-Free Resonant Column System

The fixed-free resonant column test (Figure 2.12) is used for measuring the low-strain properties of soils. The resonant column equipment is used to determine shear wave velocity, shear modulus and damping ratio of soil under different confining pressure, void ratios, shear strain amplitude, number of cycles and time of confinement (Xiaoming and Jing, 2002).

The test subjects solid or hollow cylindrical specimens to torsion or axial loading by an electromagnetic loading system. The soil specimen in fixed-free end conditions is either put to torsion simple shear or in a fundamental torsion mode of vibration. From theory of elasticity and geometric properties of specimen, the shear modulus can be determined. Damping ratio is determined from decaying vibration or hysteresis loop characteristics (Xiaoming and Jing, 2002).

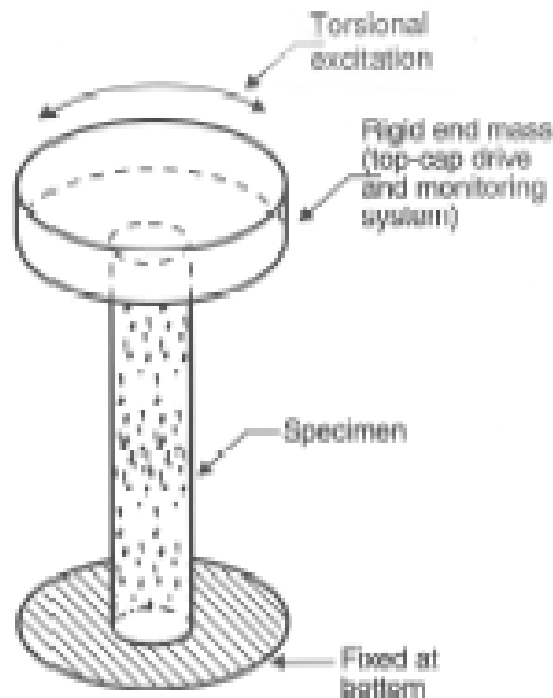


Figure 2.12 – Fixed-Free Resonant Column System

2.6 EFFECT OF MOISTURE VARIATION ON STIFFNESS PROPERTIES OF CLAYS

Numerous efforts have been carried out by the Federal Highway Administration (FHWA), long-term pavement performance (LTPP) and from other programs that can be used to study the impact of moisture on the moduli of different layers (Briggs and Lukanen, 2000). These data have been used to develop trends for determining the variation in modulus with moisture content.

The use of seismic modulus in quantifying the variation in modulus with moisture of pavement materials has been extensively described by Nazarian and Yuan (2003). The moisture-modulus relationship under constant compaction effort can be analyzed. As shown in Figure 2.13, for a fine-grained material the relationship resembles that of a typical moisture-density curve. The maximum modulus occurs at a moisture content that is less than the optimum moisture content.

For moisture contents greater than the value at which the peak modulus occurs, the modulus decreases with an increase in moisture. Also a sharp drop in modulus for moisture contents less than that of the peak modulus is observed.

Pavement subgrades, while usually compacted close to optimum moisture content and maximum dry density during construction, experience seasonal variations in water content. Most fine-grained soils exhibit a decrease in the modulus as the water content is increased. To simulate this condition, Yuan and Nazarian (2003) carry out seismic test on high-PI clay specimens prepared at the optimum moisture content. The specimens were first subjected to four days of drying in a 106^oF (40^oC) oven. Each day the specimen was removed from the oven and tested with the FFRC device to obtain the seismic modulus and weighed to determine the moisture content. After the 4-day drying period, which is associated with the change in the properties of the exposed soil during hot summer days, the specimen was placed in a water bath allowing for it to soak moisture for the next six days, in order for it to complete a 10-day testing cycle. Once again, the specimen was removed from the water bath daily, tested with the FFRC device and weighed. Typical results are shown in Figure 2.14. As the specimen is dried, the modulus significantly increases and the moisture content decreases. However, as soon as the water is introduced, the modulus decreases and the moisture content increases.

The moisture content at compaction affects the strength and stiffness properties of the soil due to the influence of particle orientations during compaction (Seed et al. 1962). For this reason the soil structure is an important factor that impacts the resilient response.

Elfino and Davidson (1989) conducted resilient modulus tests on specimens subjected to water content variations after compaction. They found that clay specimens exhibited a decrease in resilient modulus with an increase in moisture content relative to the conditions at optimum water content.

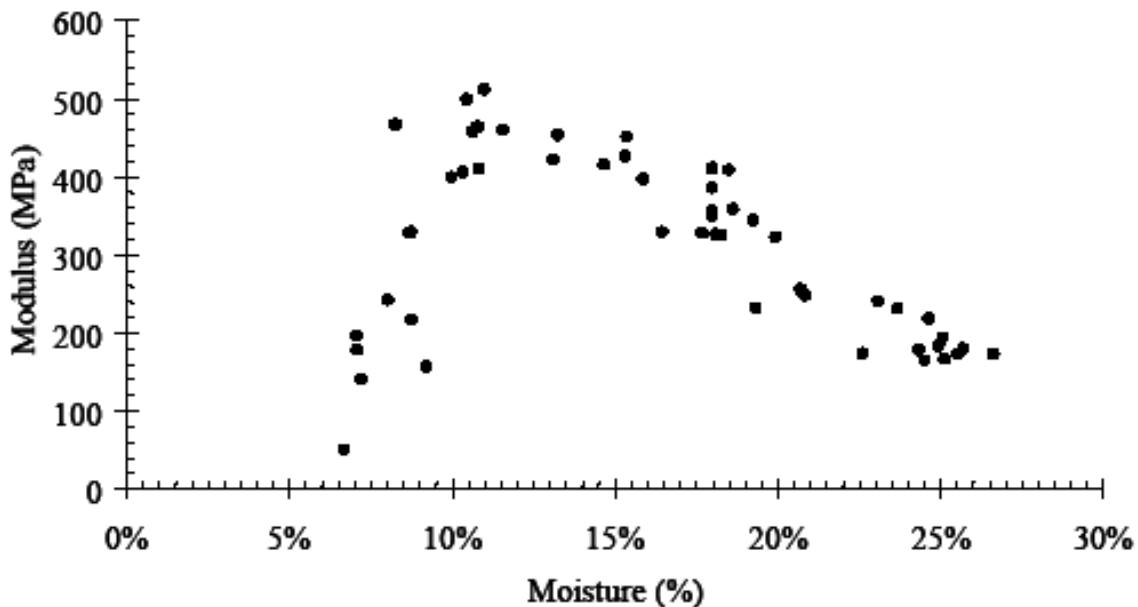


Figure 2.13 – Variation in Seismic Modulus with Moisture Content under Constant Compaction Effort for a Fine-Grained Material (Yuan and Nazarian, 2003)

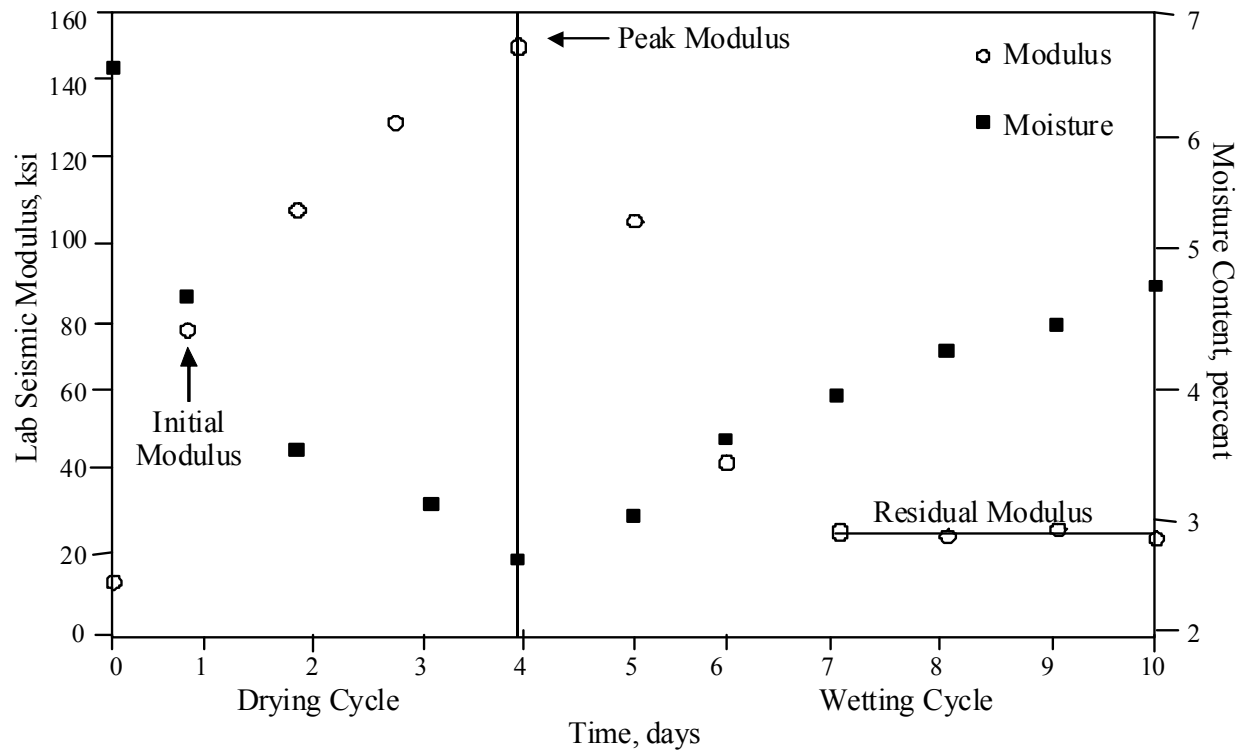


Figure 2.14 – Typical Variations of Modulus and Moisture Content with Time

In a related study, Drumm et al. (1995) evaluated the effect of post-compaction moisture content on the resilient modulus of subgrade soils in Tennessee. Soils from 11 different sites were investigated. Three specimens of each soil, ranging from A-4 to A-7-6 in accordance with AASHTO classification, were compacted at optimum water content and maximum dry density with two of these specimens being saturated. After the saturation process was completed, the specimens were stored in a moist curing room for seven days prior to resilient modulus testing. Figure 2.15 shows a typical reduction in resilient modulus with an increase in the moisture content and the degree of saturation.

Figure 2.16 shows a plot of MR versus moisture content at a given state of stress. All soils exhibited a decrease in resilient modulus with an increase in the degree of saturation. Consequently, Drumm et al. presented a method for correcting the resilient modulus value due to an increase in degree of saturation.

Khoury and Zaman (2004) also determined the influence of moisture change on the resilient modulus (MR) of subgrade soils beneath a pavement. In their study, a clayey soil from Oklahoma was used for laboratory testing in order to establish new procedures for wetting and drying of specimens, and thus, establish a correlation between resilient modulus and moisture variation.

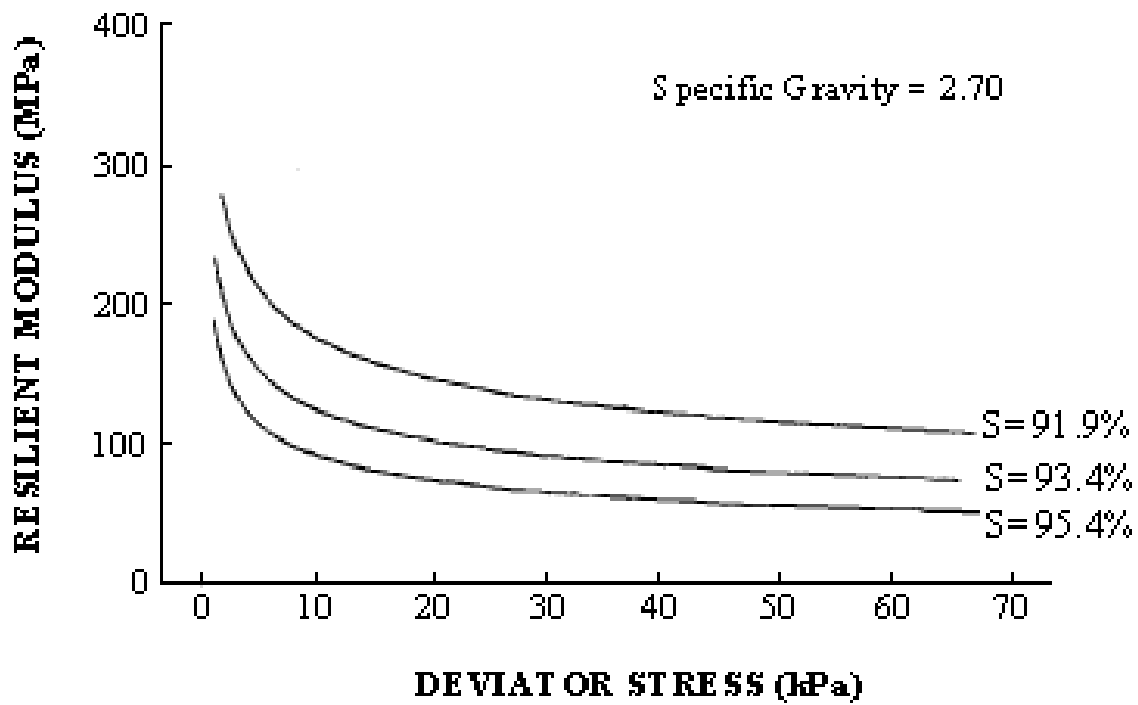


Figure 2.15 – Typical Effect of Post-compaction Saturation on Resilient Responses (Drumm et al, 1997)

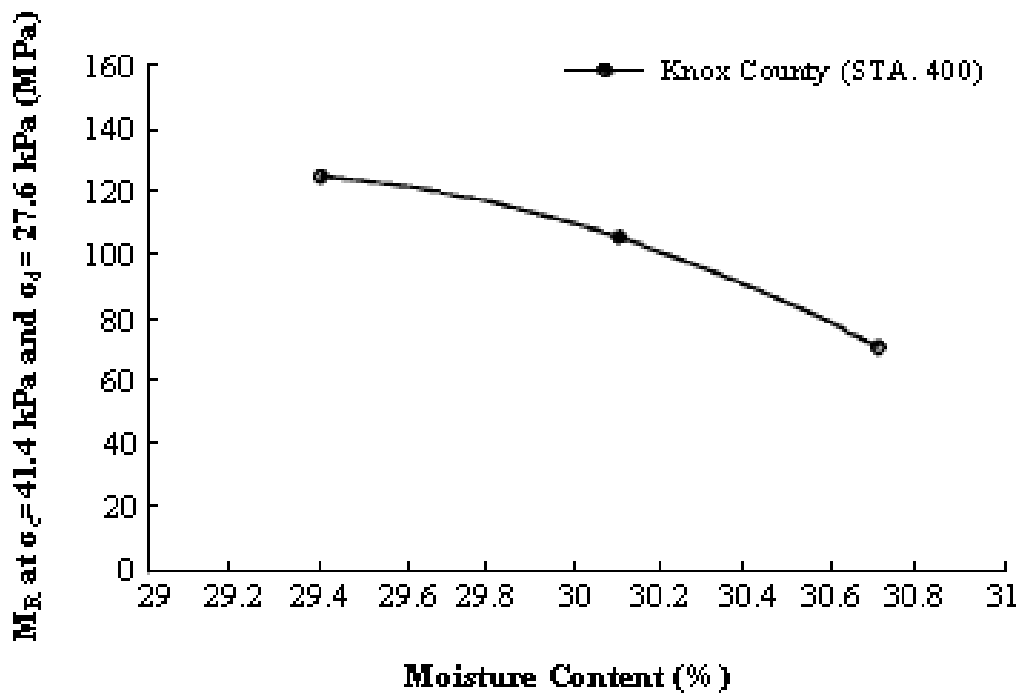


Figure 2.16 – Typical Effect of Post-compaction Moisture Increase on Resilient Modulus (Drumm et al, 1997)

Thirty-four clay specimens were prepared and tested for that study. The specimens were divided into three categories. The first category consisted of 11 specimens subjected to MR tests, of which four were compacted at OMC-4%, four at OMC, and three at OMC+4%. The second category included 16 specimens of which 11 were compacted at OMC-4% and five at OMC. The specimens in this category were wetted and then tested for MR. The third category consisted of seven specimens, of which four were compacted at OMC+4% and three at OMC. These specimens were dried and then tested for MR.

The effects of moisture variations on the resilient modulus were observed by evaluating the changes in MR values at a specific deviatoric stress and confining pressure. Tables 2.1 to 2.3 present the k_1 , k_2 , and k_3 model parameters for all three categories of specimens. Once parameters k_1 , k_2 , and k_3 are obtained, the resilient modulus of the material at any state of stress can be determined.

Khuory and Zaman (2004) then predicted the MR values of the wetted specimens prepared and tested at OMC+4%. A comparison between the predicted MR values of these specimens and the MR values of the specimens having different moisture gradients was made but the same average moisture content (i.e. specimens prepared at OMC-4% and OMC and then wetted till moisture content equals OMC+4%) is illustrated in Figure 2.24. The effect of the moisture gradient on the MR values can be considered negligible.

Khuory and Zaman (2004) indicated that the moisture content of the bulk specimens influences the resilient modulus. For this reason, the moisture content of the bulk specimens was used in establishing a MR-moisture content (MR-MC) relationship for specimens compacted at OMC-4% and OMC, and then wetted to higher moisture contents. The variation in MR values for specimens compacted at OMC-4% and wetted to approximately OMC+4% are represented by curve MrMC-1 in Figure 2.17, while curve MrMC-2 represents the MR-MC relationship for specimens compacted at OMC and then wetted to OMC+4%. Comparatively, for a given moisture content, the MR values from MrMC-1 are lower than corresponding values from MrMC-2 indicating that both the initial moisture content and the extent of wetting are important factors.

The MR-MC relationships for specimens compacted at OMC+4% and OMC and dried to a lower moisture content were established and are presented by curves MrMC-3 and MrMC-4, respectively, in Figure 2.18. For a given moisture content, the modulus from Mr-MC-3 is higher than the MrMC-4 at a moisture content ranging between OMC and OMC-2%. Results show that the percentage increase in the resilient modulus for specimens compacted at OMC+4% and dried to approximately OMC-4% is approximately 200%, while specimens compacted at OMC and dried to OMC-4% exhibited only 80% increase in MR values. From these results it can be concluded that the changes in MR values due to drying is influenced by the initial moisture content of a specimen. For a given moisture content, the MR values are higher for a drying cycle than a wetting cycle (Tinjum et al, 1996).

Table 2.1 – Resilient Modulus Results for Compacted Clay Specimens Tested without Further Conditioning

Sample #	Compaction Moisture Content	Model: $M_r = k_1 \times S_d^{k_2} \times S_v^{k_3}$				R^2	Mr @ $S_d = 4\text{psi}$; & $S_v = 6\text{psi}$
		k_1	k_2	k_3			
1	18.05	11549	-0.075	0.123	0.88	12980	
2	19.03	12300	-0.054	0.087	0.73	13326	
3	19.51	13397	-0.061	0.051	0.69	13492	
4	19.60	10685	-0.006	0.118	0.66	13101	
5	22.72	11044	-0.153	0.065	0.83	10035	
6	23.50	10267	-0.109	0.091	0.82	10397	
7	23.48	11704	-0.195	0.037	0.82	9537	
8	23.50	10019	-0.138	0.087	0.81	9664	
9	26.6	8371	-0.415	0.123	0.80	5865	
10	27.60	8376	-0.425	0.130	0.82	5873	
11	27.50	10850	-0.476	-0.036	0.87	5259	

1 psi = 6.89 kPa

Table 2.2 – Resilient Modulus Results for Compacted Clay Specimens Tested after Moisture Conditioning

Sample #	Moisture Content After Wetting	Model: $M_r = k_1 \times S_d^{k_2} \times S_v^{k_3}$				R^2	Mr @ $S_d = 4\text{psi}$; & $S_v = 6\text{psi}$
		k_1	k_2	k_3			
Specimen compacted at OMC-4% then wetted							
12	22.56	9401	-0.234	0.103	0.93	8169	
13	23.13	9467	-0.275	0.078	0.90	7431	
14	23.35	8483	-0.329	0.075	0.96	6145	
15	23.64	8580	-0.316	0.069	0.96	6257	
16	23.83	7938	-0.243	0.113	0.95	6941	
17	23.89	6842	-0.259	0.133	0.91	6064	
18	24.03	7405	-0.228	0.124	0.93	6740	
19	25.12	6281	-0.207	0.139	0.92	6047	
20	25.51	7288	-0.349	0.083	0.92	5210	
21	26.23	7304	-0.385	0.072	0.93	4878	
22	26.63	6676	-0.431	0.072	0.96	4182	
Specimen compacted at OMC then wetted							
22	25.18	7528	-0.140	0.153	0.93	8154	
23	26.15	7325	-0.188	0.090	0.87	6632	
24	26.63	7096	-0.424	0.150	0.92	5162	
25	26.88	7344	-0.260	0.098	0.89	6103	
26	27.02	5916	-0.401	0.219	0.92	5026	

1 psi = 6.89 kPa

Table 2.3 – Resilient Modulus Results for Compacted Clay Specimens Tested after Drying

Specimen #	Moisture Content After Drying	Model: $Mr = k_1 \times S_d^{k_2} \times S_3^{k_3}$				R^2	Mr @ $S_d = 4\text{psi}$; & $S_3 = 6\text{psi}$
		k_1	k_2	k_3			
Compacted specimens at OMC then dried							
27	19.29	13648	0.061	0.118	0.86	18376	
28	19.2	14513	0.040	0.122	0.84	19072	
29	20.95	12734	-0.001	0.119	0.77	15726	
Compacted specimens at OMC+4% then dried							
30	20.95	14918	-0.026	0.069	0.79	16304	
31	18.41	14906	0.013	0.088	0.82	17759	
32	22.34	11187	-0.077	0.084	0.80	11688	
33	23.42	11075	-0.020	0.097	0.85	12824	

1 psi = 6.89 kPa

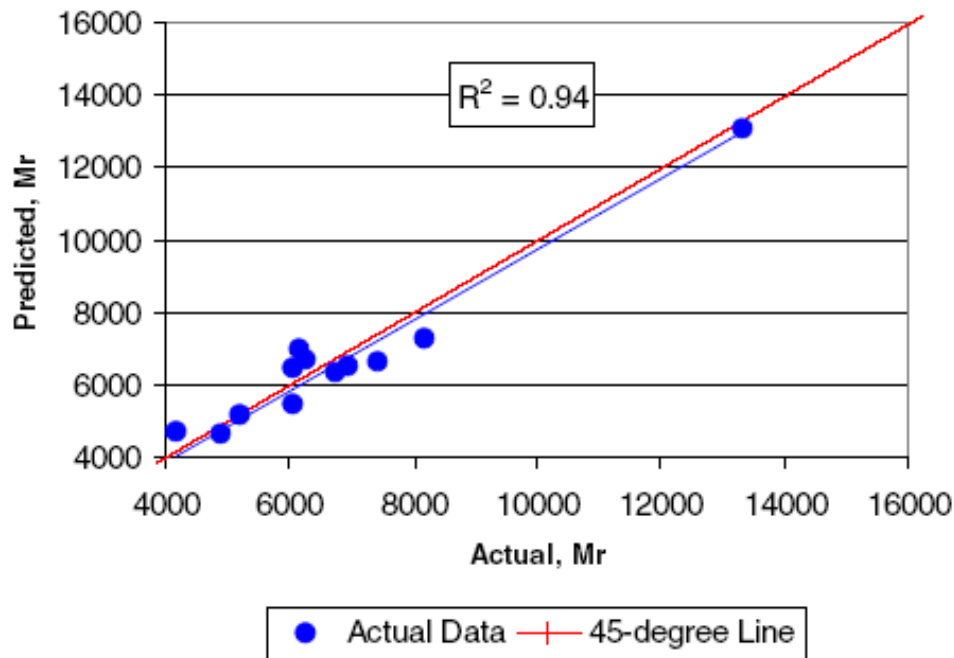


Figure 2.17 – Variation of Actual MR with Predicted MR Values

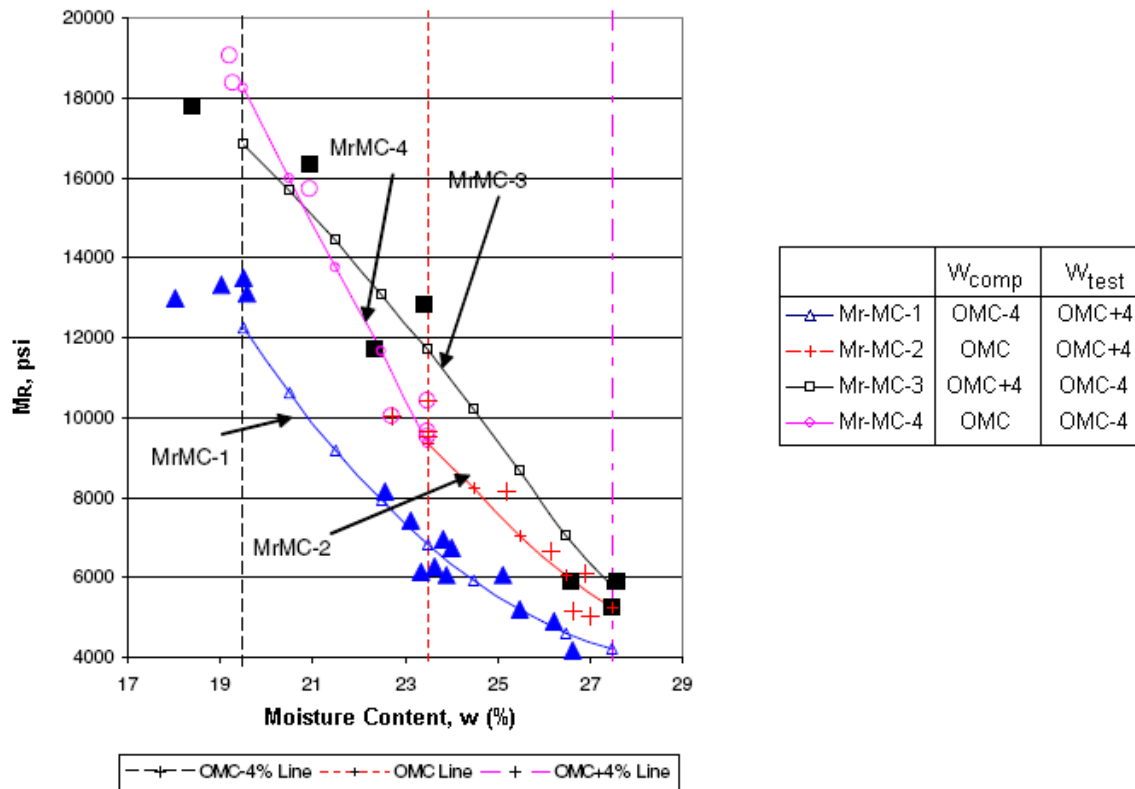


Figure 2.18 – Variation of Resilient Modulus with Moisture Content

Heydinger (2003) also studied general expressions for the seasonal variations and changes of temperature and moisture in a fine-grained subgrade soil at an Ohio test site. An expression for how the resilient modulus changed with seasonal variation was derived. Resilient modulus tests were conducted on the soil at several moisture contents. Seasonal monitoring program (SMP) instrumentation was installed in 18 test sections at the test site. The subgrade soil at the site was an A6 soil by the AASHTO Soil Classification System or CL by the Unified Soil Classification System. Three probes were placed in the upper 18 inches of subgrade soil, since the subgrade soil in that range would have the greatest impact on pavement performance. Heydinger (2003) found that there is no relationship between volumetric moisture content and precipitation for the probes in the subgrade soil and for probes placed in base layers at other test sections.

A closer examination of the volumetric water content data revealed that it varied seasonally similarly to the seasonal variation of soil temperature. The moisture content of the subgrade soil at that site with a high water table increased after construction until it approached the saturated state. Thus, it is concluded that the seasonal variation of subgrade soil moisture can be predicted independent of precipitation. Data from test sections in Ohio showed that there is a seasonal variation of moisture content even at the site where there is a high water table and no drainage. Consequently, a seasonal variation of resilient modulus is prognosticated.

Drumm and Madgett (1997) have shown that resilient modulus is dependent on moisture content and dry density during compaction and on matric suction or moisture content, thereafter.

Drumm and Madgett (1997) also proposed methods for estimating resilient modulus based on soil type and properties. Because of the difficulty in determining relationships between matric suction and moisture content, they recommended to use the seasonal variation of volumetric moisture content for estimating the variation of resilient modulus. Their research showed that it may be appropriate to approximate the seasonal variation in moisture content as a function of day of the year using a sinusoidal curve.

Empirical evidence from other researchers (Drumm and Madgett, 1997; Tian et al., 1998) shows that there is a strong dependence of soil resilient modulus on the moisture condition of the soil. The resilient modulus of a fine-grained soil can be expressed as a function of deviator stress, and is dependent on compaction energy and moisture, changes in moisture after compaction and freeze-thaw effects. The resilient modulus of fine-grained soils does not depend on the confining stress (Thompson et al., 1979).

Research work also have shown that the resilient modulus can vary by as much as a factor of two for a variation in saturation from approximately 85% to 95% which will then lead to a significant variation in required AC pavement thickness or to a significant reduction in pavement life.

Research on the effects of freezing has shown that resilient modulus can be significantly affected by freezing and thawing (Simonsen et al., 2002). The resilient modulus of fine-grained (frost susceptible) soils increases significantly as the temperature decreases to -20°C. The resilient modulus of thawed soils is significantly lower than unfrozen soils.

Li and Selig (1994) described a procedure for predicting resilient modulus as a function of moisture content and compaction effort for fine-grained soils. They recommended a two-parameter power model relating resilient modulus and deviator stress. The first procedure included determination of resilient modulus of soils compacted with different compaction efforts but with the same dry density. The second alternative was described for determining resilient modulus for soils with the same compaction effort but with different moisture contents. They also presented an equation for resilient modulus at the optimum water content as a function of percent clay and plasticity index. Comparisons between predicted and measured values of resilient modulus were excellent.

2.7 CRACKING OF PAVEMENT STRUCTURE

Uzan et al. (1972) investigated the cracking of flexible pavements caused by the shrinkage due to drying of the subgrade. According to Uzan et al. (1972), when clay shrinks it is subjected to tensile stresses while the base course undergoes compressive stresses initiating shear stresses at subgrade-base interface. Cracking starts when tensile stresses in clay equals its strength limit. However, the strength of the clay is dependent on the degree of restraint. If shrinking of clay continues the crack propagates to the base layer and heads towards the asphalt layer. This is mainly because of the bond between the base and the subgrade layer and their low tensile strength. Now if the tensile strength of the asphalt layer is inadequate to resist this cracking, crack will appear on the surface that completes one cracking cycle. Thus, cracking starts at the edges of the asphalt layers and it advances towards the center.

Uzan et al. (1972) prepared a small-scale test specimen, simulating field conditions regarding thickness and layer composition. The subgrade was loaded with the horizontal jack and the cracks formed at the subgrade-base interface were measured using LVDT's. LVDT's were also installed at other layer interfaces to measure the displacements. The subgrade was then unloaded and then displacement in the model were recorded. When no further displacements were observed at the asphalt interface the subgrade was reloaded. Throughout the test the asphalt layer was visually observed for any fine cracks which were detected at the bottom of the granular layer. Uzan et al. (1972) concluded that the following factors affect cracking of asphalt layers:

Small changes in the modulus of clay and base material do not affect the stress in the asphalt layer. Possible reasons for this include, small changes in the degree of restrained, lateral pressure and density and moisture content.

Increase in the modulus of asphalt increases the tensile stress in it.

The thickness of the asphalt and granular layers varies inversely with tensile stresses in subgrade layer. Therefore, the possibility of the asphalt layer cracking due to subgrade shrinkage decreases with increasing thickness. They recommend a minimum pavement thickness of 35 in. including 30 in. of granular material and 4 in. of asphalt to prevent crack reflection.

Shrinkage of drying soils due to loss of moisture forms a network of cracks that are very detrimental for the pavement structure. Two types of growing cracks can be considered in clays: 1) fairly isolated cracks that grow, curve, and branch with negligible influence from other cracks, and 2) cracks that strongly interact with others. Most cracks of first type eventually develop into the second (Chertkov, 2002).

Longitudinal cracks are generally developed in structures when strain energy generated by shrinking or swelling is sufficient enough to break the inter-particle bonds (Raats, 1984). Most of the fracture mechanics models applied to soils do not account for toughness. These models use the techniques based on Griffith's (1920) work on the fracture mechanics of ideal linear elastic materials. Alternatively some researchers have also used the Irwin-Orowan extension to the Griffith's model. However, either approach does not account sufficiently for plasticity in wet soils (Hallett, 1996). So these approaches are applicable for dry brittle soils but when it comes to ductile soils like high PI Clays, plasticity can be a dominant sink to the imposed strain energy.

Chandler (1984) provides a detailed description of crack propagation in soils that considers plasticity. Lawn (1993) came up with an alternative approach which uses crack opening displacement (COD) to understand cracking mechanism. Sture et al. (1999) used this COD approach for stiff soils and found that considerable amount of fracture occurs at a consistent amount of crack opening. But COD approach fails to predict the ductile growth adequately (Turner and Kolednik, 1994). Crack opening displacement can also be used in finite element modeling to characterize the strain dependant fracture of materials (Hallett and Newson, 2001). An ideal testing approach to describe crack growth in soils should account for plasticity, be easy to conduct and provide theoretically sound parameters.

A test set up for measuring the crack propagation was suggested by Hallett and Newton (2005). As shown in Figure 2.19, a rectangular specimen is placed on two pieces of thin glass. To minimize the frictional influence, rollers are provided which allow glass slides to move freely.

An initial crack of appropriate length is often inserted at the center of the specimen which acts as a plane of failure initiation. The specimen is loaded from the top to provide the strain energy to drive crack elongation. During testing, the load point is lowered causing crack mouth to open. Crack opening and elongation are estimated from video images that are captured during the loading of the specimen. Alternatively, strain gauges or extensometers can be used to measure the opening and elongation. Crack opening angle can be measured using following formula:

$$\alpha = \Delta V_{pl} / \Delta a \quad (2.8)$$

where, α = crack tip opening angle (CTOA), ΔV_{pl} = crack mouth opening, and Δa = crack length.

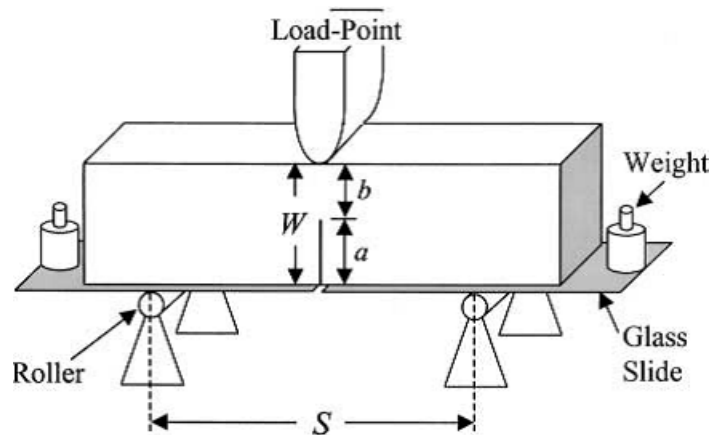


Figure 2.19 – Three Point Bend Test

The 3-point bend test has several drawbacks. In case of ductile soils, excess plastic deformation at the load points may limit the use of 3-point bend test. Specimens which fail under self weight can not be used to test for 3-point bend test. At the beginning of the test, if the length of the crack is not large enough, there is a tendency of the crack to deviate during loading because of the presence of anisotropic stress fields. Turner and Kolednik (1997) suggested inserting a long preformed crack into the specimen to overcome above problems.

The 4-point bend test, as shown in Figure 2.20, can also be used to evaluate the cracking properties of ductile soils. According to Hallett and Newton (2005), this test is more robust than the 3-point bend test. Test specimens are bars measuring about 5.5 in. in length and 1 in. square in the cross-section. Before starting the test, a crack with a length a_0 equals half the specimen thickness is cut into the sample using a razor blade. The test set up is very similar to the 3-point bend test with the exception of the additional two rollers added close to the crack.

Figure 2.21 shows different stages of cracking mechanism in test specimen subjected to four-point bend test. At the beginning of the curve, the relationship between the applied force and the displacement is linear, which is the elastic region of the fracture. At a critical point this elastic behavior is transformed into a plastic behavior (Maugis, 1985). The intersection of a tangent to the applied force is approximately the yield point of the material. Hallett (1996) suggests that

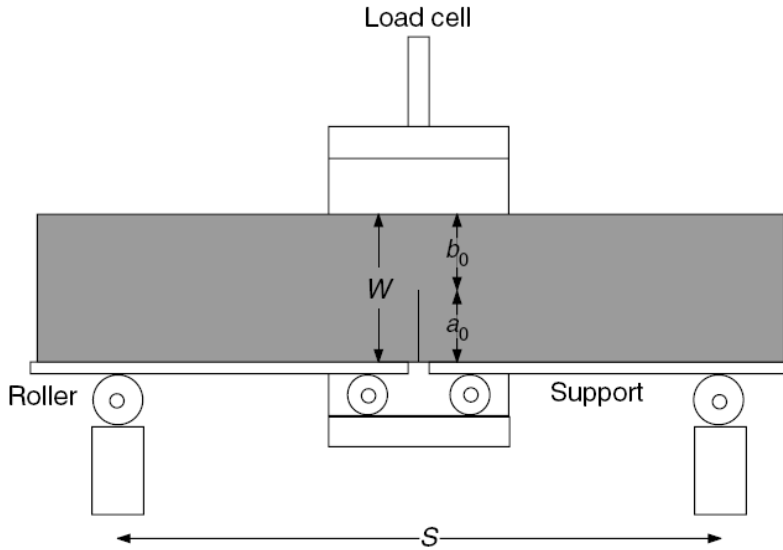


Figure 2.20 – Four Point Bend Test

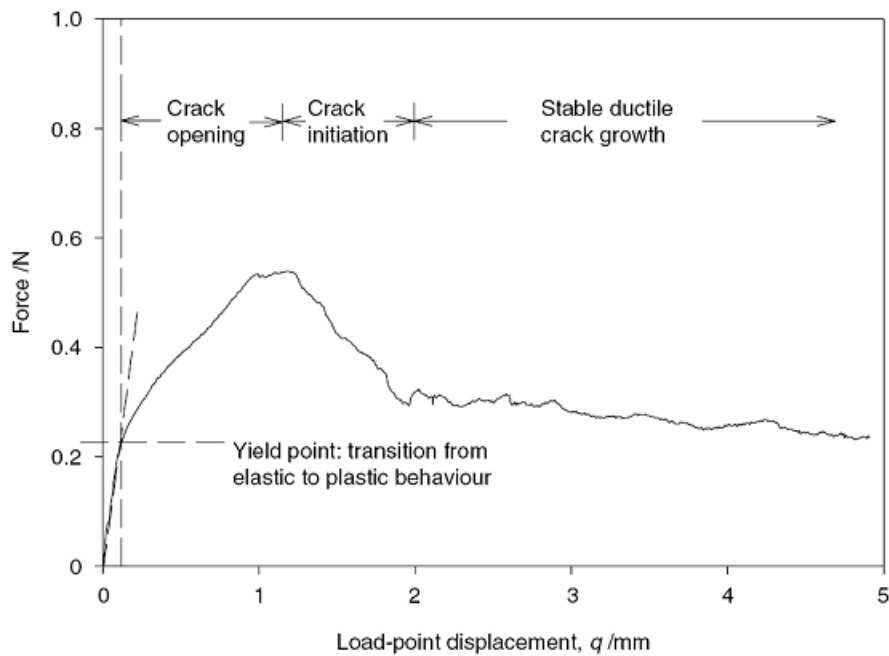


Figure 2.21 – Different Stages of Cracking Mechanism

after the yield point, plastic behavior of the material causes inter-particle bond rupture as particles become reoriented. With the increasing applied force the crack initiates which is marked by decrease in the applied force. At this point stable ductile crack growth occurs which can be described using the crack tip opening angle (CTOA) approach.

Hallett and Newton (2005) performed some deep-notch bend test with data on load transmission, sample bending, crack growth and crack mouth opening collected to assess the crack tip opening

angle (CTOA). They found that the CTOA approach appears to be sensitive to different soil properties and provides a powerful measurement of fracture mechanics of soil samples. Based on the results obtained, they concluded that the increased sand content and salinity decreased CTOA, and that the increased water content decreases the CTOA due to consolidation which increases soil stiffness as particles become more closely packed and the effective stress increases. Groenevelt and Grant (2001) observed that adding sand decreased the CTOA but at the same time it also decreased the shrinkage potential.

Hallett and Newton (2005) indicated that further research needed to be carried out to investigate the relationship between soil fracture mechanics and shrinkage characteristics over a range of moisture content. A combined shrinkage and fracture mechanics model could be developed that would provide a fundamental understanding of soil structure genesis.

CHAPTER 3 - PREPARATION AND CONDITIONING OF SPECIMENS

3.1 INTRODUCTION

First step in any strength or stiffness test is to compact a specimen to a desired moisture content and density and then to carry out appropriate moisture conditioning. The compacted specimen should ideally mimic the condition in the field, and should stay intact during the moisture conditioning, being drying or wetting. A prepared specimen should be easily saturated in optimum time as well as should be dried in oven without generating major cracks. In this chapter, the issues of specimen preparation and moisture conditioning are described and preliminary protocols for executing them are offered.

3.2 TXDOT COMPACTION TECHNIQUE

The current TxDOT practice consists of compacting clayey specimens as per Tex-114-E. In this process, appropriate amount of material is mixed with water and is mellowed. These specimens are nominally 4 in. in diameter by 6 in. in height, and are compacted in four lifts with 25 blows per lift using a 5.5-lb hammer dropping from a height of 12 in. Specimens are then extruded and conditioned as appropriate.

Several problems are observed with this process. During the drying process, the specimens sometimes separate at the interface of the layers. During moisture conditioning using capillary saturation, the water front would sometimes stop at the interface of the compaction lifts. The permeability of the specimens is so low that the middle of the specimens is sometimes dry after ten days of capillary saturation. During triaxial tests, it is not uncommon that the specimens fail at the interface of the lifts. The height of the specimens (6 in.) may be too short for reliable strength and stiffness tests.

3.3 DIFFERENT COMPACTION AND CONDITIONING TECHNIQUES

For the purpose of this project, several laboratory compaction techniques were tried. The compacted specimens were then subjected to moisture conditioning (drying and wetting). The compaction technique that minimized the problems indicated above the most was recommended. Following is a brief description of different compaction techniques tried and problems encountered with each of them.

Method 1

Specimens with dimensions of 4 in. by 8 in. were compacted using a kneading compactor in a plastic mold using the same compaction energy as proposed in Tex-114-E. The plastic molds had perforations at the bottom part which was glued to the mold to allow the intrusion of water.

The conditioning on these specimens is shown in Figure 3.1. The specimens in the plastic molds were placed on porous stones, which were kept in a water bath. The specimens quickly absorbed water, and the bottom one-fourth of the specimen became readily saturated. The waterfront normally never reached above this point. The specimens were weighed every day. After two days of conditioning, the water absorption in the specimens normally stopped.

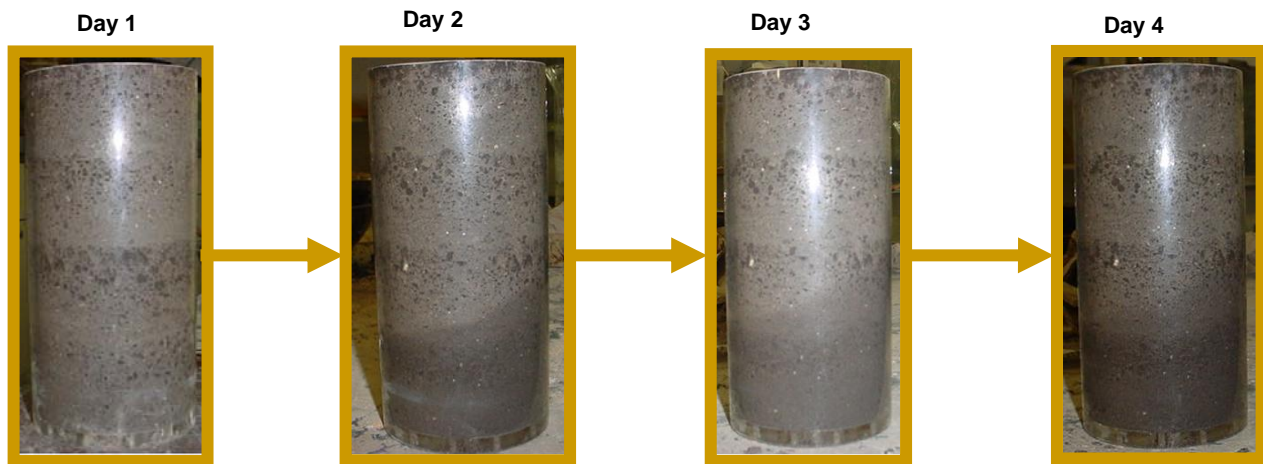


Figure 3.1 – Clay Specimen Subjected To Wetting by *Method 1*

Method 2

One of the concerns with Method 1 was that the fixed plastic base would restrict the access to moisture. As such, the plastic base of the mold was made removable and the conditioning was repeated. Figure 3.2 shows the pictures of a clay specimen subjected to wetting in Method 2. Once again, only the first lift of the specimen normally got saturated and waterfront did not penetrate above that point.

Method 3

Specimens were compacted and subjected to wetting in the same way as explained in Method 2. To accelerate the wetting process, suction was applied to the top of the specimens. After three days, only the first lift of the specimen became saturated. As shown in Figure 3.3, the specimens sometimes became separated between the first and second lifts.

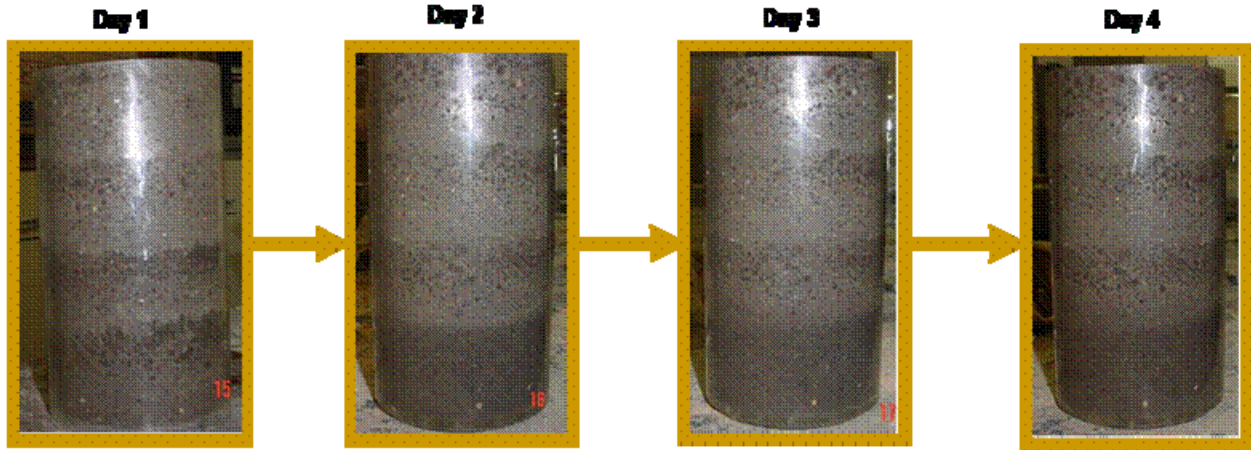


Figure 3.2 – Clay Specimen Subjected To Wetting by *Method 2*



Figure 3.3 – Clay Specimen Subjected To Wetting by *Method 3*

Method 4

Specimens with dimensions of 4 in. by 8 in. were prepared in five lifts using a static compactor (as explained later in this chapter). The specimens were extruded in a rubber membrane, and were subjected to wetting by placing it on top of porous stone and in a water bath. The specimens were weighed and measured regularly for any change in dimensions. The free-free resonant column tests (see Chapter 4 for explanation) were also regularly performed on the specimen. Figure 3.4 shows typical variation in moisture content of these specimens with time. The specimens were reasonably moisture conditioned in seven days, with most of the moisture absorption occurring during the first 120 hours. The modulus, as also shown in Figure 3.4, rapidly dropped in the first 100 hours, and became stable. A 1.5% vertical expansion and a 2% diametrical expansion were observed in the specimen as shown in Figure 3.5.

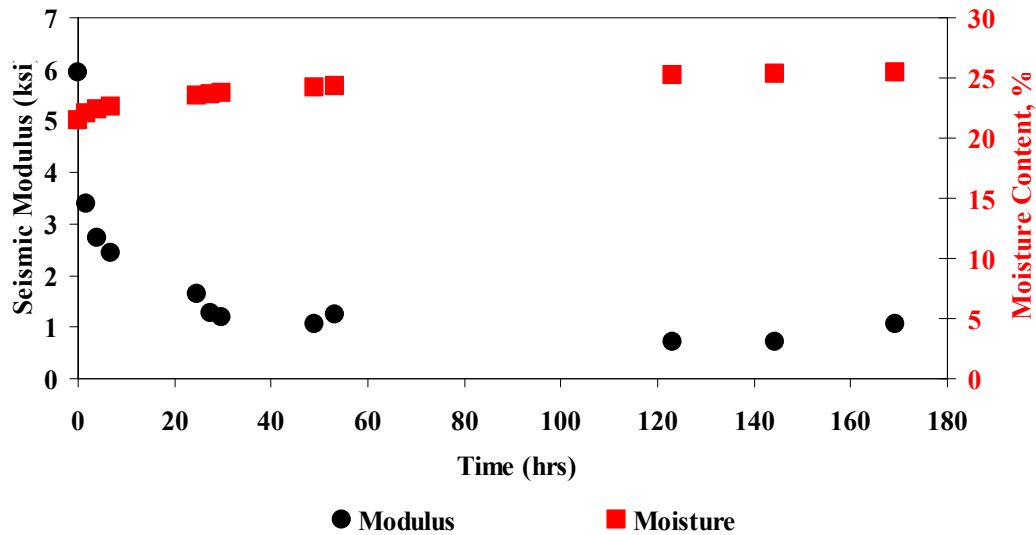


Figure 3.4 – Change in Seismic Modulus and Moisture Content vs. Time

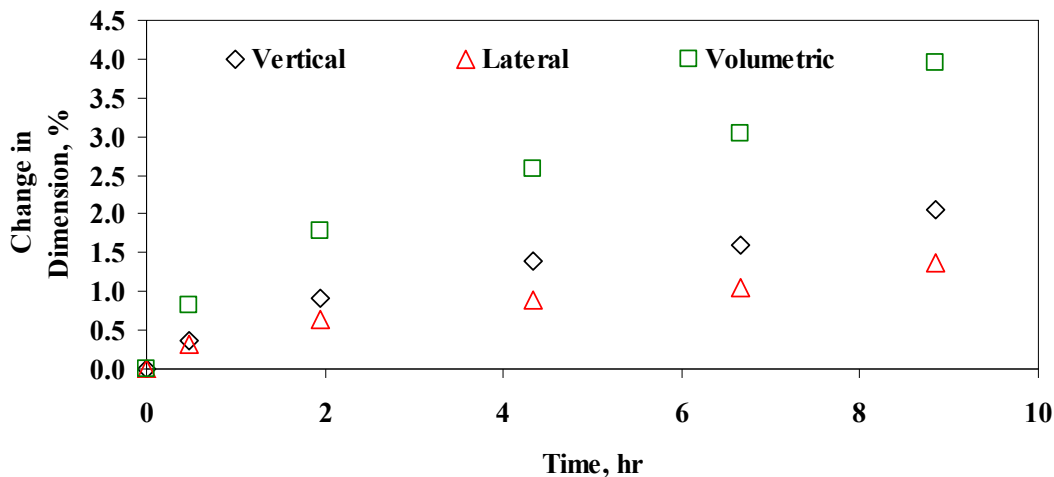


Figure 3.5 – Change in Dimension and Volume vs. Time

Clay specimens prepared in similar way were then subjected to drying in a conventional oven at 104°F (40°C). As shown in Figure 3.6, the specimens badly cracked, especially at the interface of the lifts in just two days.

Method 5

To overcome the problem with the drying of the specimens, 4 in. by 8 in. specimens were prepared in one single lift using a static compactor. The specimens were extruded, covered with cellophane wrap, and subjected from top to bottom saturation as shown in Figure 3.7. Typical change in moisture content with time is shown in Figure 3.8. The entire lengths of the specimens were saturated in less than two days. Changes in the dimensions and weights of the specimens were measured, and the FFRC tests were performed on them until the specimens became saturated throughout.

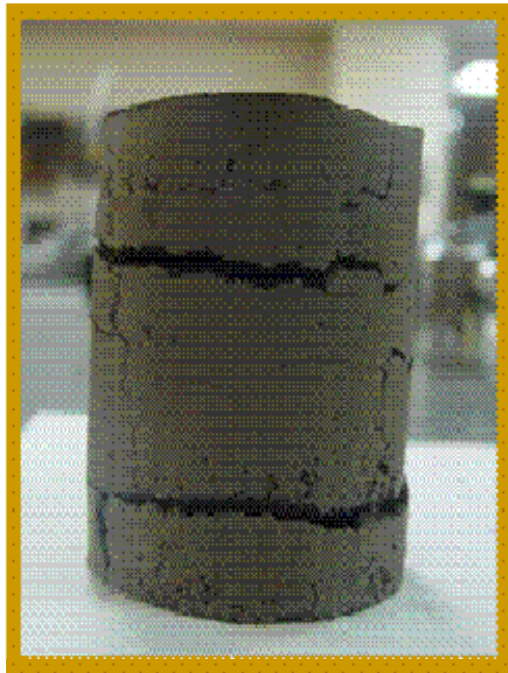


Figure 3.6 – Cracking of the Specimen Compacted by Method – 4 and Subjected to Drying

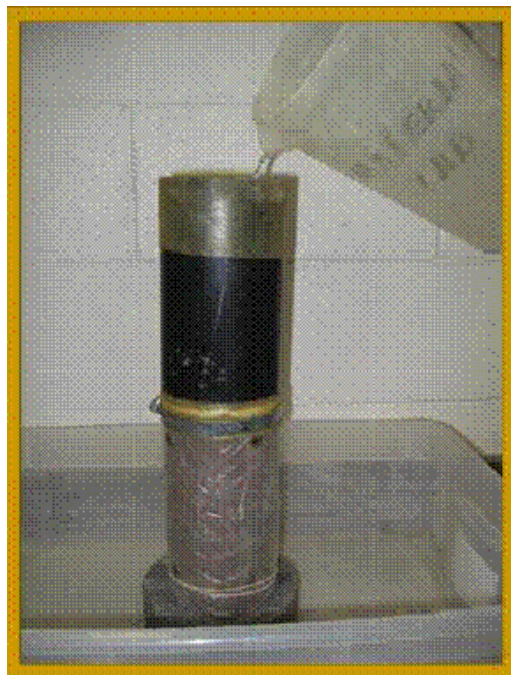


Figure 3.7 – Set-up for Wetting for Specimen Compacted by *Method 5*

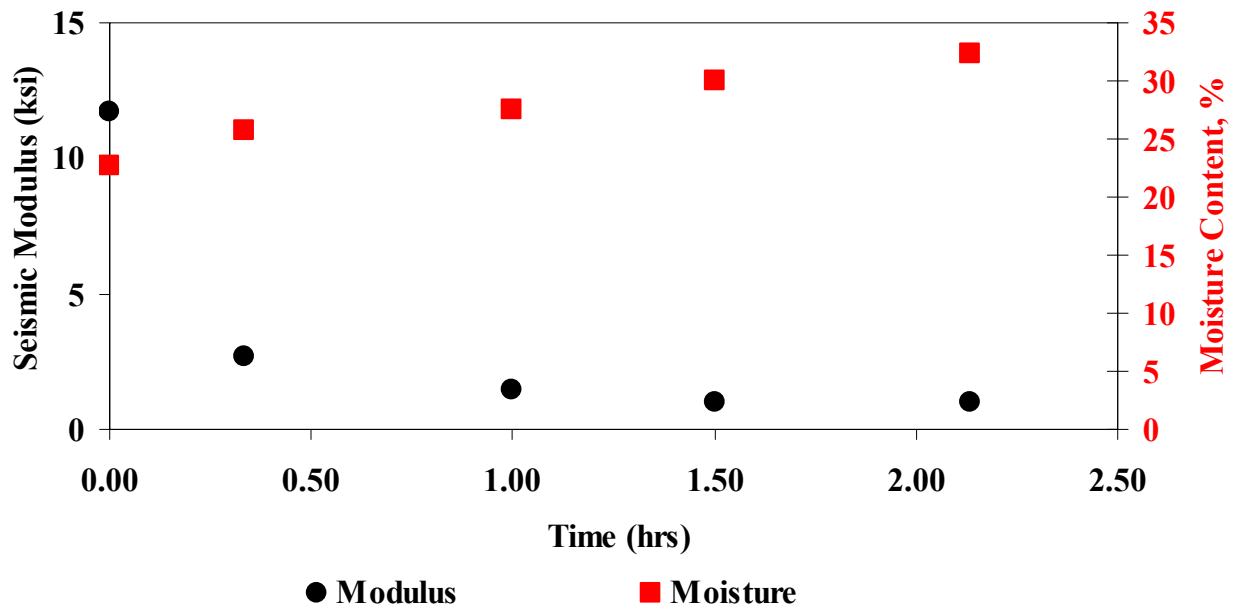


Figure 3.8 – Change in Seismic Modulus and Moisture Content vs. Time during Wetting

When the specimens prepared with Method 5 were subjected to drying in a conventional oven at 104^oF, no major cracks were evident on the specimens (see Figure 3.9). This temperature is lower than the 140^oF normally used by TxDOT. The temperature was reduced to ensure that the specimens would not suffer severe cracking during drying. As shown in Figure 3.10, about three



Figure 3.9 – Completely Dry Specimen Compacted by *Method 5*

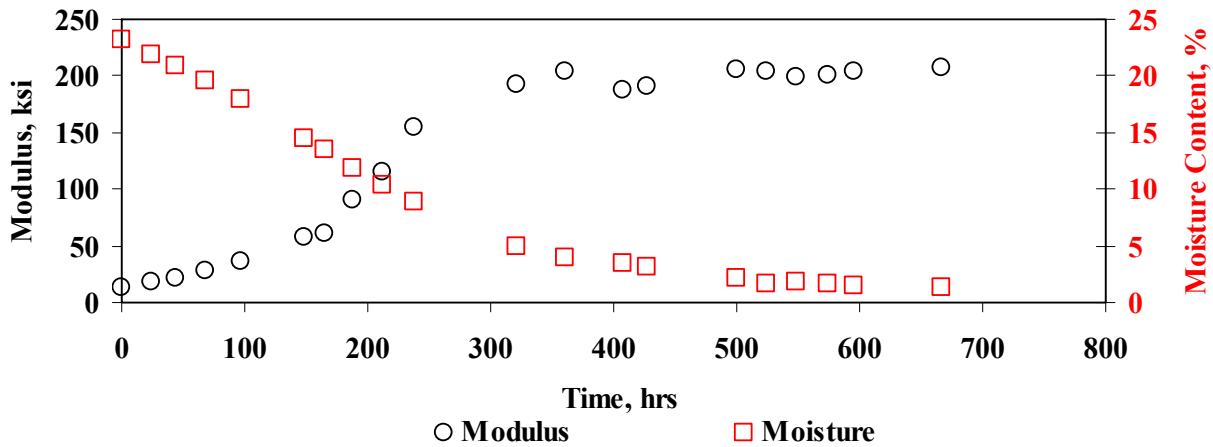


Figure 3.10 – Change in Seismic Modulus and Moisture Content vs. Time during Drying

weeks were necessary to bring the specimens to constant moisture content. Under these conditions, the modulus increased rapidly during the first ten days, but the change in modulus is rather small past that time.

Typical shrinkage of the specimens is shown in Figure 3.11. The changes in diameter and length are more pronounced between 100 hrs and 300 hours, after which the specimen shrinks rather gradually.

Based on this study, Method 5 is recommended for preparing the specimens. This method is discussed in detail in Appendix A.

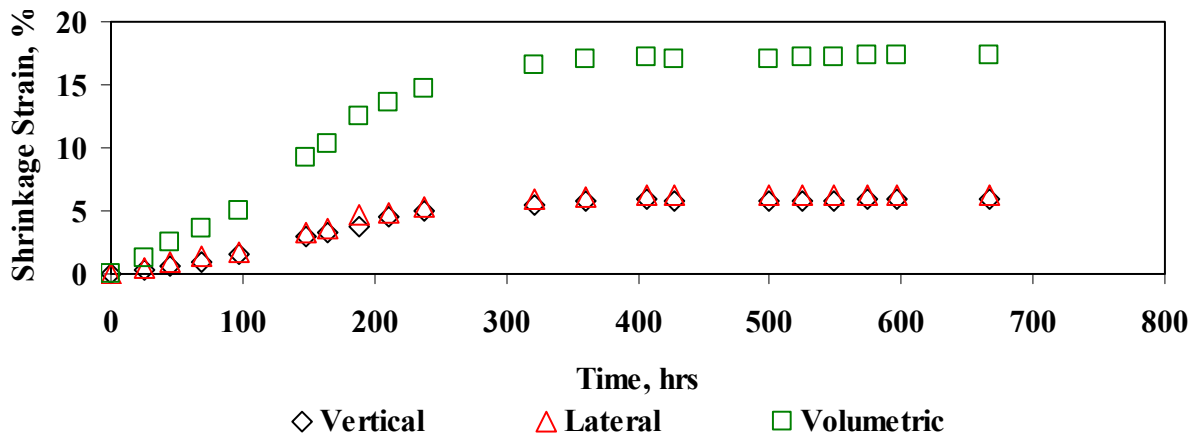


Figure 3.11 – Change in Dimension and Volume vs. Time

3.4 STATIC COMPACTION FOR CYLINDRICAL SPECIMEN

A static compactor is suggested in the AASHTO T-307 for preparing the fine-grained soil specimens. As such, the use of a static compactor instead of a kneading compactor was

investigated. The compaction apparatus consists of one hollow metallic cylinder and three solid metallic blocks. The sizes of the metallic block and hollow cylinder were determined in a way that a specimen can be prepared either in one single lift. Figure 3.12 shows the pictorial representation of specimen preparation using *Method 5*. Step 1 consists of weighing the exact amount of material required for preparing one specimen. As shown in Step 2, a 2.45-in.-long solid metal block is placed at the bottom of the mold. The appropriate amount of soil is placed and spread evenly within the mold (Step 3). As per Step 4, a 5.65-in.-long solid block is placed on top of the material in the mold. The assembly is placed under a common loading system, and the top solid block is axially loaded at a slow rate (see Appendix A) until the top solid block becomes flush with the mold (see Step 5). The assembly is then turned upside down, and a 0.5-in.-long solid block is placed on top of the 2.45-in.-long block (Step 6). As shown in Step 7, an axial load is again applied until the 0.5-in.-long block becomes flush with the mold. The pressure is maintained for 1 minute before the assembly is removed, and the specimen is extracted from the mold (Step 8). Step 9 shows the extruded clay specimen.

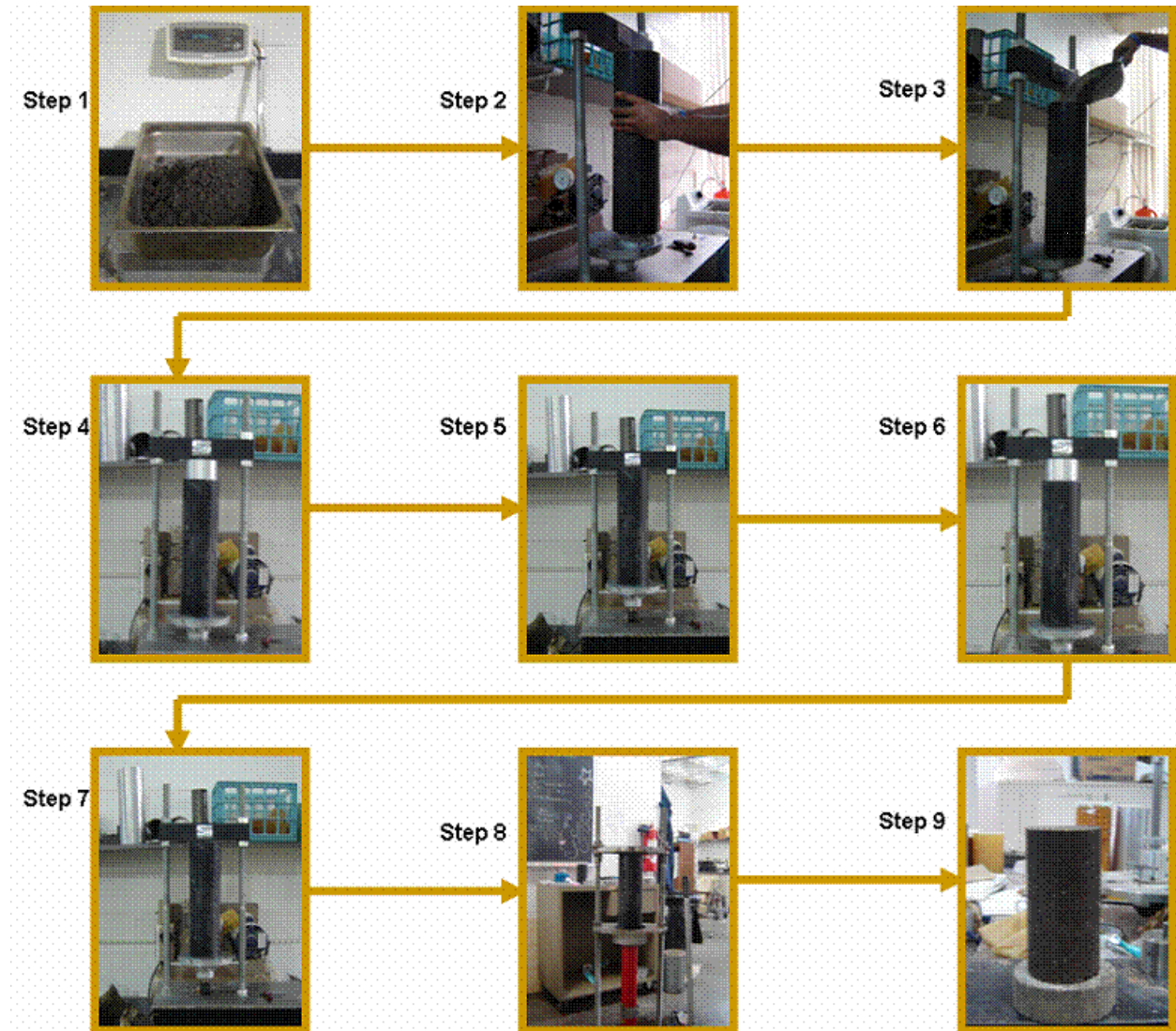


Figure 3.12 – Preparation of Specimen

3.5 PREPARATION OF RECTANGULAR SPECIMEN

To perform four-point bend tests, rectangular clay specimen 1 in. thick, 1 in. wide and 5.6 in. in length were required. For this purpose a special metallic mold and solid blocks were designed and fabricated. Figure 3.13 shows the fabricated mold and solid blocks. Detailed protocol for sample preparation is included in Appendix A. A pictorial representation of preparation of rectangular specimens is shown in Figure 3.13. Step 1 consists of weighing the exact amount of material required for preparing one specimen. As shown in Step 2, a 1.0-in.-thick prismatic solid block is placed at the bottom of the mold. The appropriate amount of mix is placed inside the

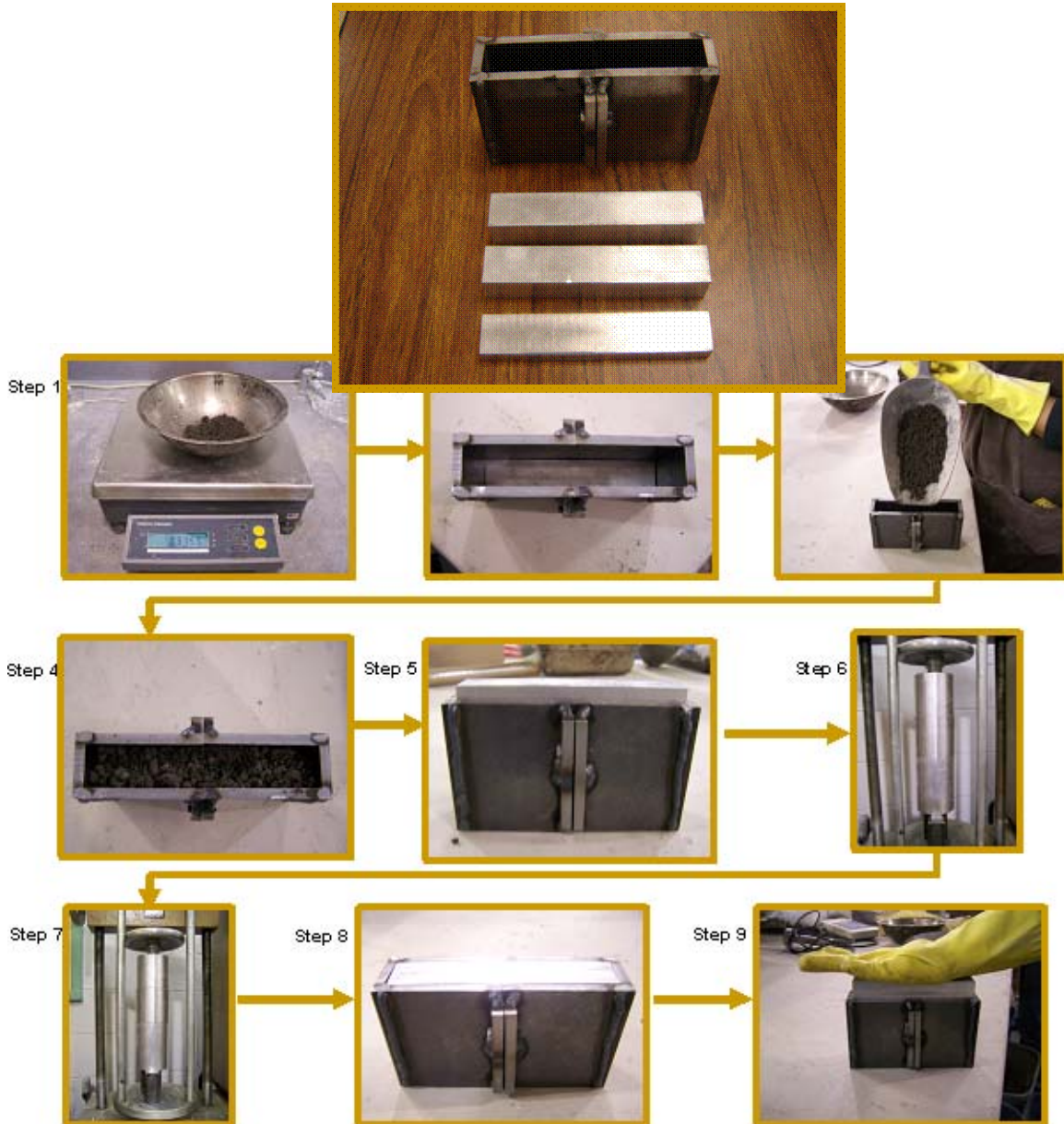


Figure 3.13 - Rectangular Specimen Preparation Using Static Compactor

mold (Step 3). As shown in Step 4, the mix is evenly spread inside the mold. As per Step 5, a second 1.0-in.-thick prismatic solid block is placed on top of the material.

The assembly is placed under a common loading system, and the top solid block is loaded gradually until the top solid block becomes flush with the mold (see Step 6). The assembly is then turned upside down, and a 0.5-in.-thick solid block is placed on top of the 1.0-in.-thick block. As shown in Step 7, the 0.5 in. block is loaded until the 0.5-in.-thick block becomes flush with the mold. The pressure is maintained for 1 minute before the assembly is removed, and the specimen is compacted inside the mold (Step 8). As shown in Step 9, the clay specimen is extruded from the mold by applying pressure from one end.

3.6 DENSITY VARIATION ALONG THE LENGTH OF SPECIMENS

One of the concerns with using static compaction was the variation of density along the length of the specimen. To minimize this density variation, several specimens were compacted by changing the order of solid blocks (as discussed in Section 3.4) used in compaction and the specimens were cut in five layers and density of each layer was measured. Figure 3.14 shows the variation of densities just by changing order of solid blocks in compaction where 1 represents 0.5 in. thick block, 2 is for 2.45 in thick block and 3 for 5.63 in thick block. We recommend using static compaction method used in trial 5 and 6 as it showed least variation in densities along different layers and it was possible to moisture condition the specimens which were later used for different strength and stiffness tests.

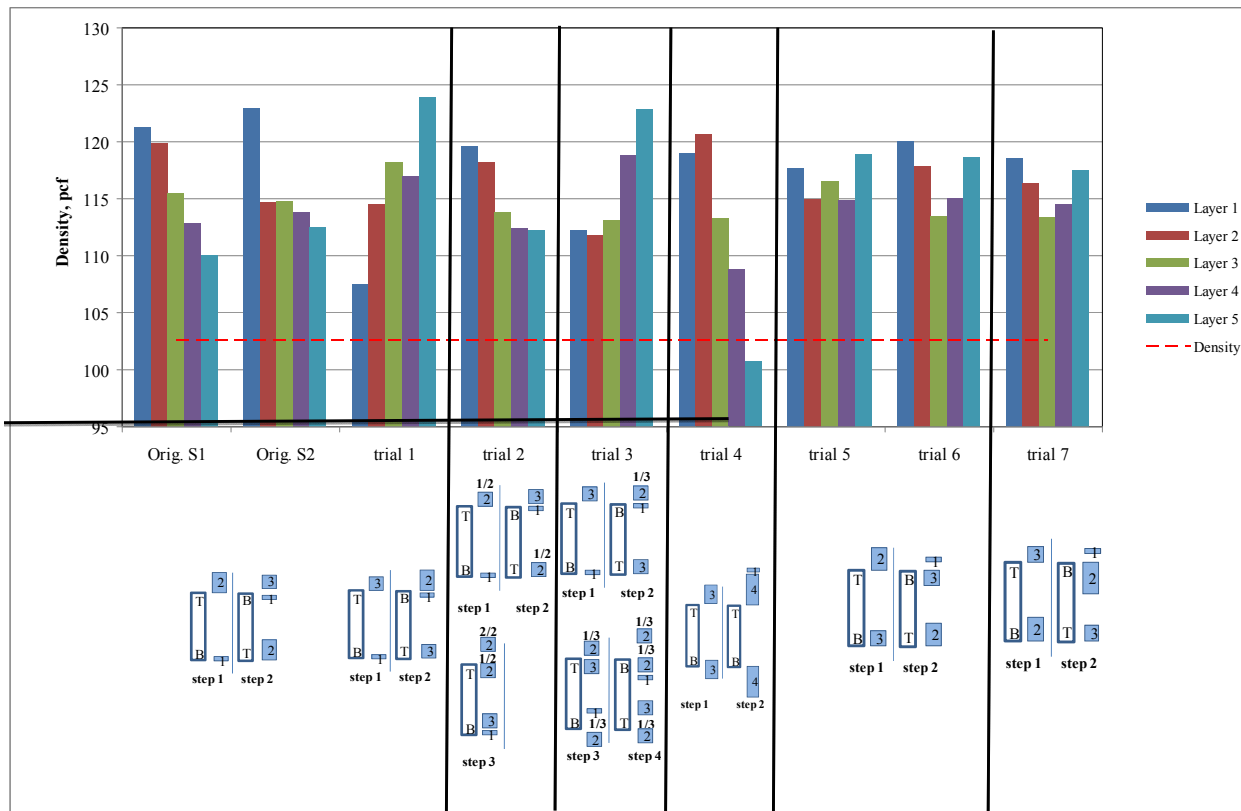


Figure 3.14 –Variation in Density Using Different Compaction Techniques

3.7 CONDITIONING

All clay specimens were prepared in at optimum moisture content and were subjected to moisture conditioning (either drying or wetting). These procedures are discussed below and detailed protocols are included in Appendix A.

3.7.1 Drying Phase

A pictorial representation of the test method for drying is shown in Figure 3.15. A laboratory compacted specimen is shown in Step 1. Immediately after the extrusion, the specimen is wrapped in a cellophane wrap (Step 2). The cellophane wrap covering the specimen is pricked in about a dozen points to allow for the specimen to release the moisture. The drying of the specimen is carried out using a conventional oven at 104°F, as shown in Step 3. After every 24 hours, the specimen is taken out of the oven, the cellophane wrap is removed, the specimen is weighed and the length and diameter are measured. The length is measured at four different sides along the diameter of the specimen (Step 4), and the diameter is measured at top middle and bottom of the specimen using a pi tape (Step 5). The specimen is then tested for modulus with the free-free resonant column device (Step 6), rewrapped and then placed back in the oven. The procedure is repeated until the decrease in weight in two consecutive days is about 0.1%. Figures 3.16 and 3.17 show typical results from drying a specimen. Typically, the variations in dimensions, modulus and moisture become reasonably constant after 10 to 15 days.

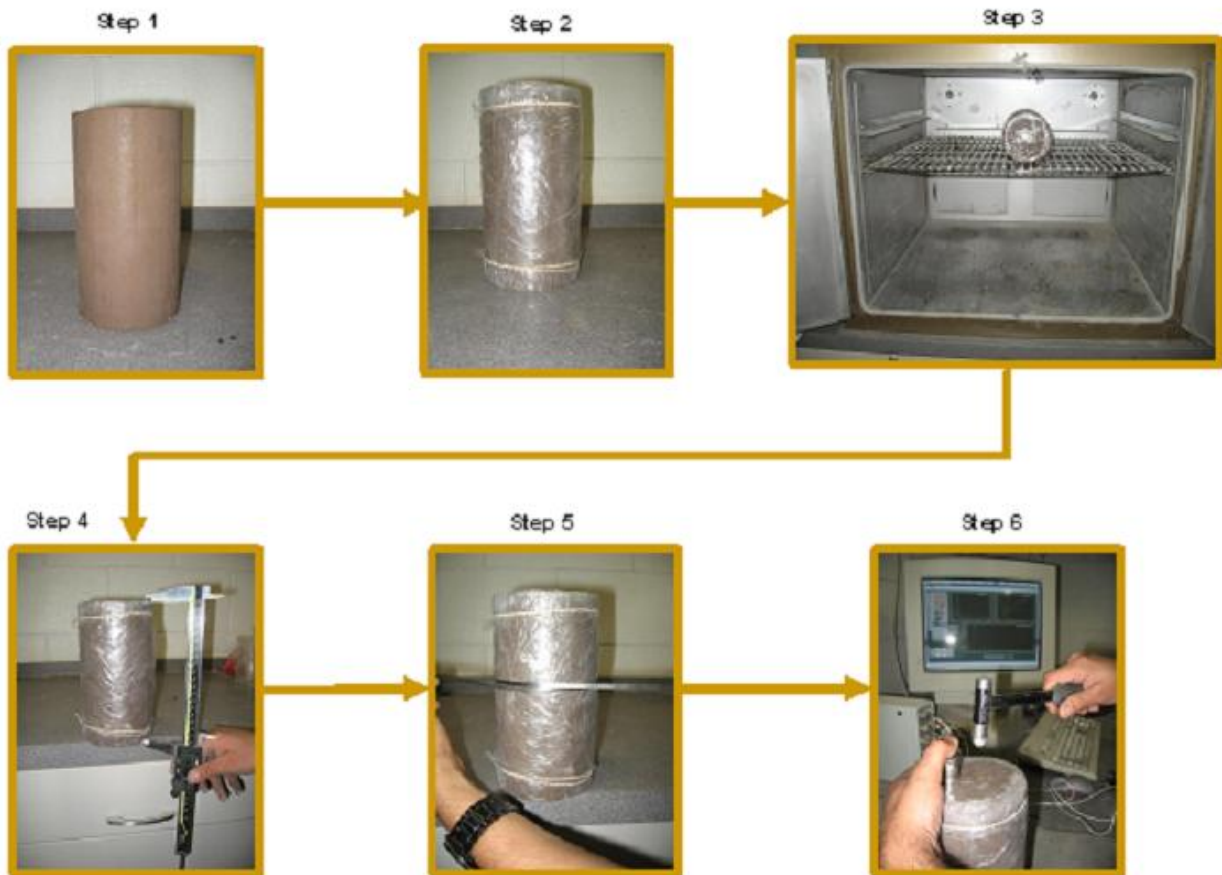


Figure 3.15 – Drying Method for Clay Specimens

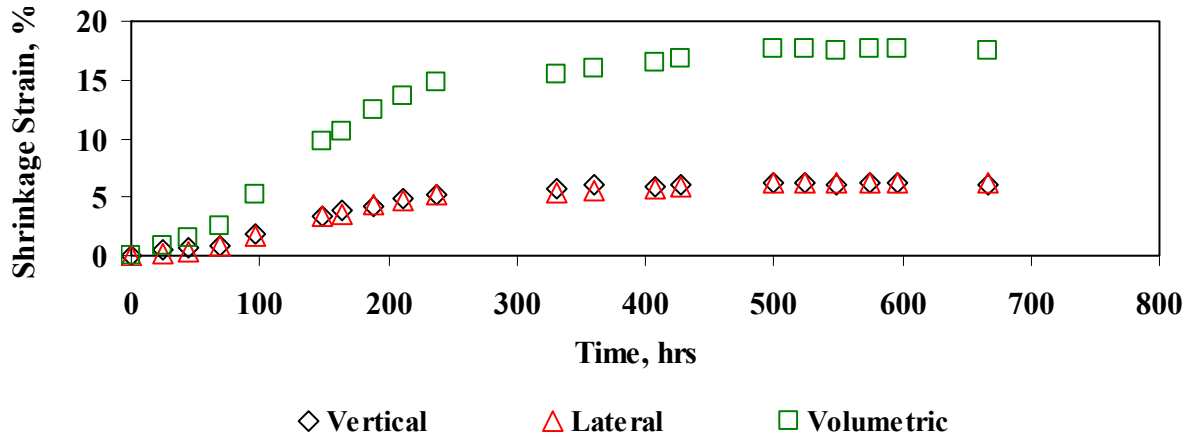


Figure 3.16 – Change in Dimensions and Volume vs. Time

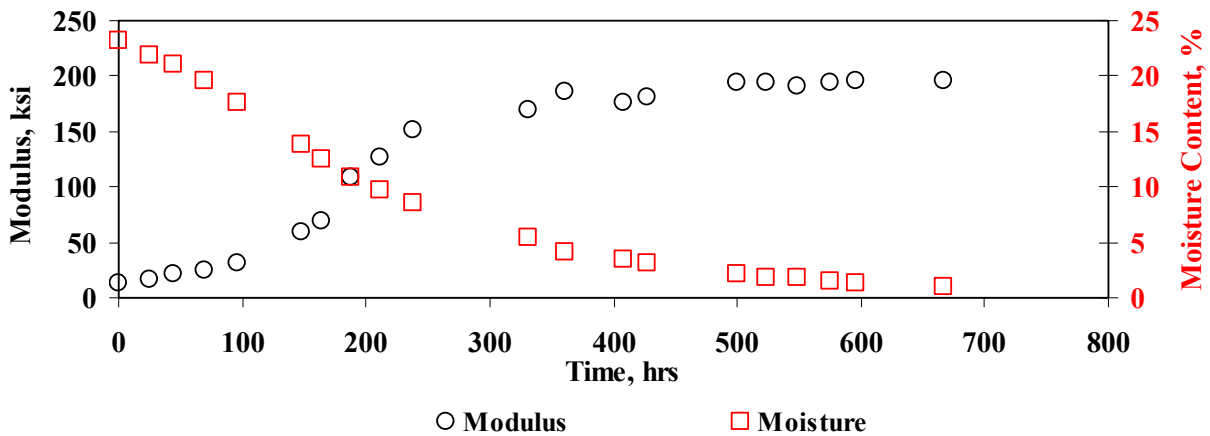


Figure 3.17 – Change in Seismic Modulus and Moisture Content vs. Time

3.7.2 Wetting Phase

A pictorial representation of the test method for moisture conditioning of a specimen is shown in Figure 3.18. A detailed test protocol is included in Appendix A. The specimens are saturated from top to bottom. Step 1 shows a laboratory compacted specimen. Immediately after the extrusion, the specimen is wrapped in a cellophane wrap, and thumb tags are securely placed on the specimen to conveniently measure the length of the specimen (Step 2). A filter paper and a porous stone are placed on top of the specimen in Step 3. A hollow plastic cylinder is securely placed on top of the specimen using a membrane (Step 4). Additionally, a hose clamp is used to ensure that water would not penetrate from the sides (Step 5). The specimen is placed on top of a porous stone, and the plastic mold is filled with water as shown in Step 6. Periodically, the plastic mold is emptied, the specimen is weighed, and the changes in the height and diameter of the specimen are measured until the specimen is saturated. Equation 3.1 is used to estimate the amount of water absorption required by the specimen to become saturated:

$$W_{reqd} = W_{ti} [\gamma_w \{(1 + \omega_i) * D_{ai}\} - 1 / \{(1 + \omega_i) * G_s\} - 1 + 1 / (1 + \omega_i)] \quad (3.1)$$

where W_{reqd} = required additional amount of absorbed water to saturation, W_{ii} = the initial total weight of the specimen, ω_i = initial moisture content of the specimen, D_{ai} = maximum dry density of the clay, and G_s = specific gravity of the clay, γ_w = density of water.

The change in height is measured at four sides along the diameter of the specimen (Step 7). The expansion of the specimen is determined by measuring the distance between thumbtacks. The diameter is measured at the top center and bottom of the specimen using a π -tape (Step 8). After each measurement, the plastic cylinder is again filled with water.

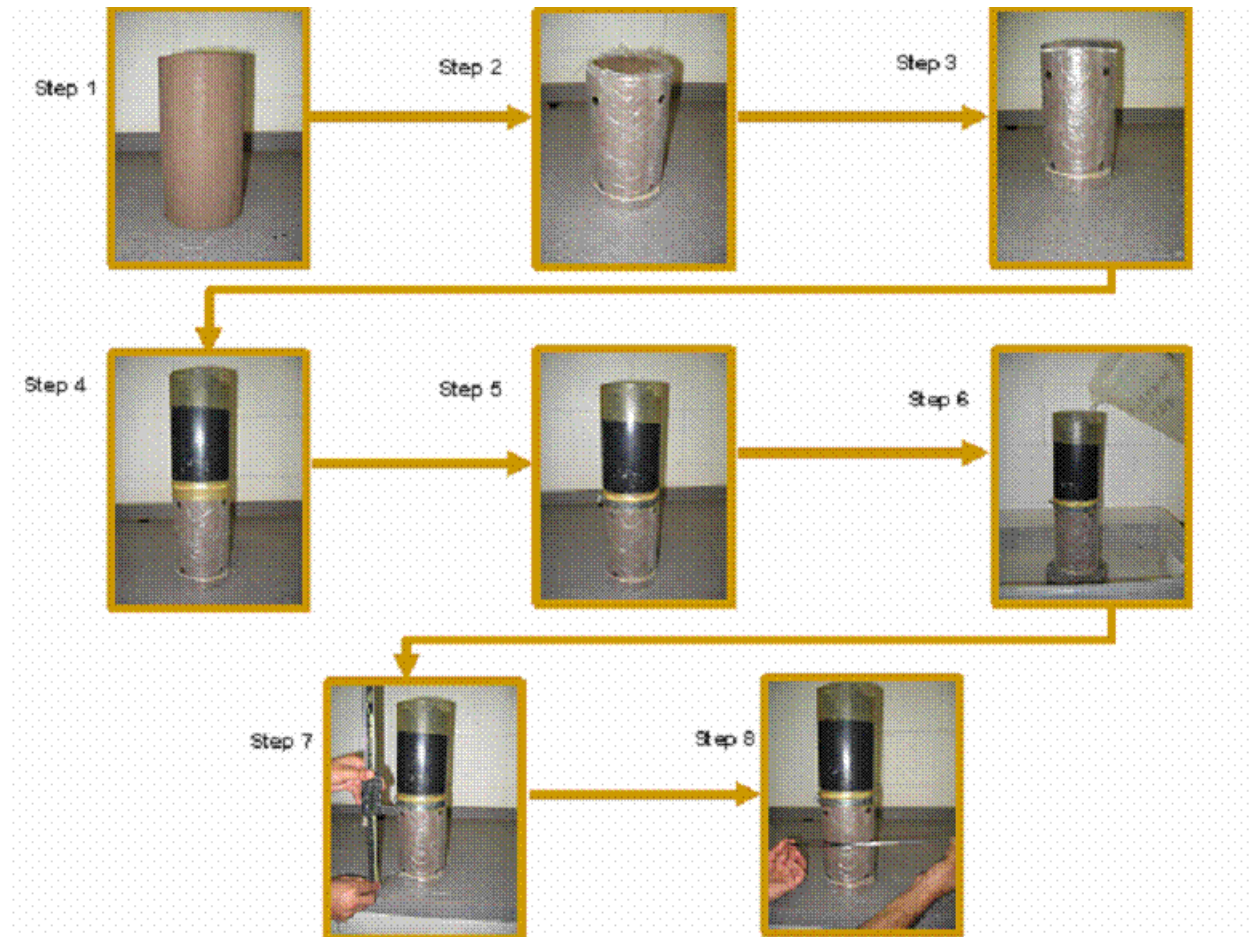


Figure 3.18 – Wetting Method for Clay Specimens

Figures 3.19 and 3.20 show typical results of the wetting phase. As per Figure 3.20, the diametric expansion of the specimen was recorded as 1.2% whereas vertical expansion was 4%. As initially moisture content increases, seismic modulus also increases after which it starts falling down till it becomes almost negligible when the specimen gets saturated. The moisture conditioning of a specimen usually takes two to four days.

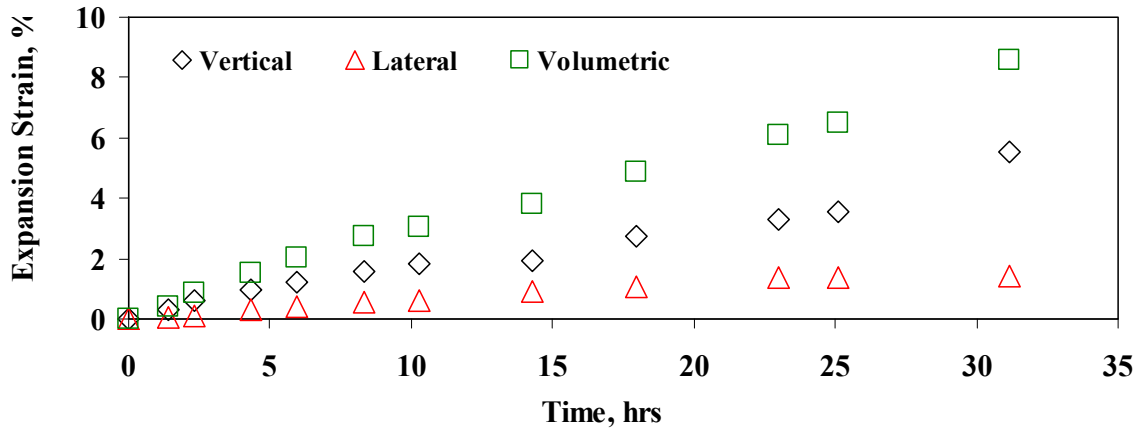


Figure 3.19 – Change in Dimensions and Volume vs. Time

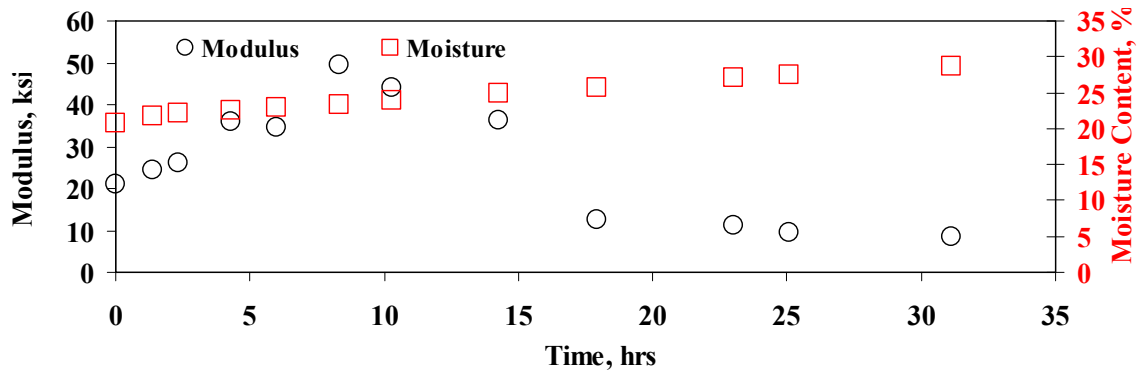


Figure 3.20 – Change in Seismic Modulus and Moisture Content vs. Time

CHAPTER 4 - TESTING METHODOLOGY

4.1 INTRODUCTION

This chapter describes the test program carried out to determine the strength and stiffness properties of several clays at different moisture conditions. Six different clay materials were tested consisting of five high-PI clays (PI greater than 25) and one low-PI clay. The high PI clays were brought from Houston, Forth Worth, San Antonio, Paris and Bryan Districts, whereas the low PI-clay was from El Paso.

The Bryan and El Paso clays were used to develop protocols for all test methods and to validate the feasibility of the proposed testing program. These preliminary tests were very useful to differentiate between behavior of high-PI and low-PI clays with change in moisture content.

4.2 TEST PROGRAM

Several index tests, consisting of hydrometer (Tex-110-E) and Atterberg limits (Tex-104-E and Tex-105-E) were carried out on clay materials. Moisture density tests were also performed on all materials to obtain their optimum moisture contents and maximum dry densities following Tex-114-E.

Several chemical and mineralogical tests were also carried out to better understand the properties of the clays. These include the soluble sulfate content, cation exchange capacity and dominant clay mineralogy.

Strength tests include unconfined compressive strength (UCS) tests and indirect tensile strength tests (IDT, Tex-226-F). A four-point bend test was also performed to study the crack propagation properties of the clays. The free-free resonant column (FFRC, Tex-149-E), resilient modulus (MR, AASHTO-T-307) and permanent deformation (PD) tests were carried out to quantify the stiffness of each clay material. The specimens for stiffness and strength tests were prepared using a static compactor as described in Chapter Three.

A number of volumetric tests, such as volumetric shrinkage, 3-D free swell and swell pressure, were also performed. A series of suction measurements were also carried out.

Specimens were prepared and tested at three different moisture conditions. Table 4.1 demonstrates the tests carried out on each clay and each moisture condition where ‘O’ stands for optimum, ‘D’ for dry and ‘S’ for saturated. In the first set of tests, the specimens were prepared and tested at their corresponding optimum moisture contents. The second moisture conditioning involved drying specimens prepared at their optimum moisture contents to constant weights. The third set of specimens were again prepared at their optimum moisture contents then saturated. Methods used for drying and saturating specimens are described in Chapter Three. The IDT, flexural and RM/PD tests on saturated specimens could not be carried out simply because the specimens were too soft to withstand the loads.

Table 4.1 – Test Matrix Carried Out in This Study

Clay Source	Strength			Stiffness	
	UCS	IDT	Flexural	Seismic	RM/PD
Bryan	O-D-S*	O-D	O-D	O-D-S	O-D
El Paso	O-D-S	O-D	O-D	O-D-S	O-D
Houston	O-D-S	O-D	O-D	O-D-S	O-D
Forth Worth	O-D-S	O-D	O-D	O-D-S	O-D
San Antonio	O-D-S	O-D	O-D	O-D-S	O-D
Paris	O-D-S	O-D	O-D	O-D-S	O-D

* O= Specimen at optimum moisture content, D= Dried specimen, S=Saturated specimen

4.3 CHEMICAL AND MINERALOGICAL TESTS

4.3.1 Determination of Soluble Sulfates Contents

The soluble sulfate content in the soil is an important test property that is known to affect the sulfate heaving process when stabilized with calcium based stabilizers. Hence, it is of importance to determine the sulfate levels of the control soils of both test sites before treatment. A method formulated by Puppala et al. (2002) which is a modified standard gravimetric procedure was used for measuring the amount of soluble sulfates along with a calorimetric based TxDOT method. Further details on the sulfate gravimetric method can be found in Intharasombat (2003) and Wattanasanticharoen (2004).

4.3.2 Cation Exchange Capacity (CEC)

The CEC is the quantity of exchangeable cations required to balance the negative charge on the surface of the clay particles. CEC is expressed in milliequivalents per 100 grams of dry clay. In the test procedure, excess salts in the soil are first removed and absorbed cations are replaced by saturating the soil exchange sites with a know species. The amount of the known cation needed to saturate the exchange sites is determined analytically (Nelson and Miller, 1992).

CEC is related to clay mineralogy. High CEC values indicated a high surface activity. In general, swell potential increases as the CEC increases. Typical values of CEC for the three basic clay minerals are shown in Table 4.2.

Table 4.2 - Typical Values for Three Basic Clay Minerals (Mitchell, 1976).

Clay Mineral	CEC (Meq/100 g)	Basal Spacing (Å)
Kaolinite	3 -15	14.4
Illite	10 – 40	10.0
Montmorillonite	80 – 150	9.6

The measurement of CEC requires detailed and precise testing procedures that are not commonly done in most soil mechanics laboratories. However, this test is routinely performed in many agricultural soils laboratories and is inexpensive (Nelson and Miller, 1992).

4.3.3 Determination of Clay Mineralogy

Clay mineralogy is a fundamental factor controlling expansive soil behavior. Clay minerals can be identified using a variety of techniques. For this research, X-Ray diffraction, the most popular method, has been utilized. The method works on the principle that beams of X-Ray diffracted from crystals are similar to light reflections from the crystal lattice planes. X-Ray analysis is of the same order of magnitude (about 1 Å or 10^{-9} mm) as the atomic plane spacing of these minute crystals. The basal plane spacing is characteristic for each clay mineral group and gives the most intense reflections. Characteristic basal spacing is also tabulated in Table 4.2.

4.4 STRENGTH AND STIFFNESS TESTS

4.4.1 Unconfined Compressive Strength (UCS) Test

The UCS tests were carried out as per a Tex-117-E. Briefly, a 4 in. by 8 in. laboratory compacted specimen is placed in a triaxial chamber, which is then axially loaded until the specimen fails. A typical stress-strain curve is shown in Figure 4.1. The maximum stress at which the specimen fails is called the unconfined compressive strength of the material. The strain at which the strength is determined is an indication of the brittleness of the material. In this research, a SIGMA-1 loading system was used.

4.4.2 Indirect Tensile Strength (IDT) Test

The IDT test was performed as per Tex-226-F. A 4 in. by 8 in. laboratory compacted specimen is first placed in a metal jig and it is then laterally loaded till it fails. An Instron-Satec System with control software of NuVision Partner V5.1E was used to perform indirect tensile strength test. The maximum load at which specimen fails is used to determine the indirect tensile strength of the specimen.

4.4.3 Flexural Test

The flexural test (four point bend test) procedure is detailed in Appendix A. A 1 in. by 5.6 in. prismatic specimen is first prepared in the laboratory as explained in Chapter Three. To control the direction of cracking of the specimen, a cut is made at the center of the specimen just before starting the test. The specimen is placed in a special apparatus and tested in flexure. The crack growth is observed during testing.

Figure 4.1 shows a pictorial representation of steps followed to perform the flexural test. A close up of the test set up is shown in Figure 4.2. Step 1 in Figure 4.1 shows the apparatus used for testing clay specimens for flexural test. A clay specimen supported with two plastic plates is placed on top of the two supports of the apparatus (see Step 2). The spacing between the two supports is 1.2 in. The purpose of the two plastic plates is to cause the frictionless movement of the specimen during testing so that the specimen is not subjected to any external moment. As shown in Step 3, the top plate of the apparatus is brought down in such a way that the top prop just touches the specimen. Since this prop is fixed in that position throughout the test, it does not apply any load to the specimen. The apparatus with the specimen is then attached to the loading device (see Step 4). The actuator is then brought down in such a way that the specimen rests on two outer supports. The spacing between the two outer supports is 4.7 in. As shown in Step 5, two cameras are arranged in such a way that one focuses on the test specimen (to observe the crack growth) while the other on the computer screen that registers the load-deformation curve. These cameras are synchronized so that the initiation of the crack growth can be estimated. Step 6 shows the graph generated during testing.

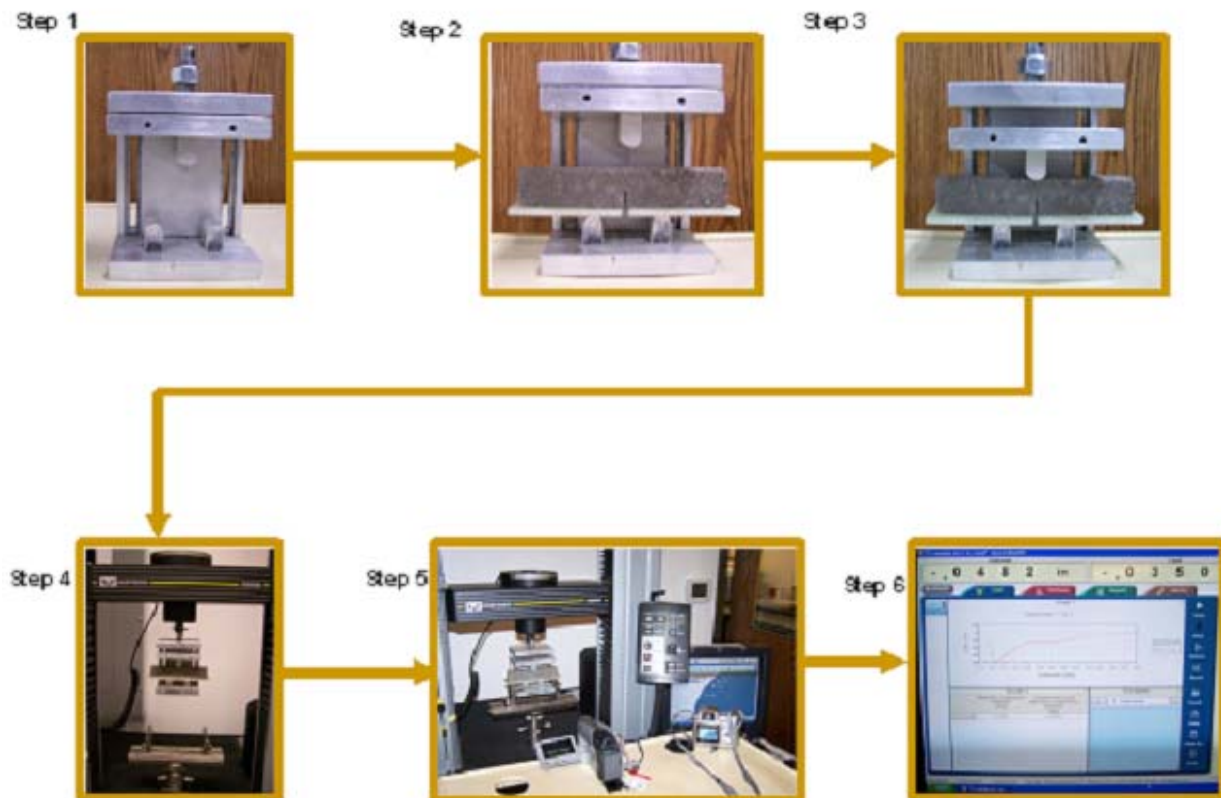


Figure 4.1 – Steps in Flexural Test

Figure 4.3 shows a typical stress-strain curve for a dry specimen. When test is started, the testing apparatus moves down and the specimen is subjected to bending. Initially as shown in Figure 4.3, stress on the specimen (load coming from the middle two supports) increases. This increase in stress is continued until the breakage of the inter-particle bond is initiated (peak stress). Past

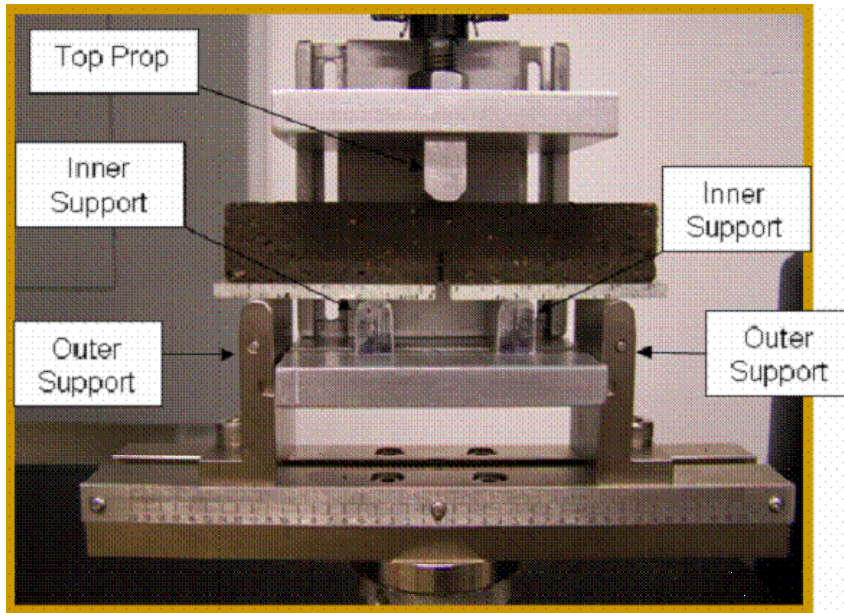


Figure 4.2 – Flexural Test Set-up

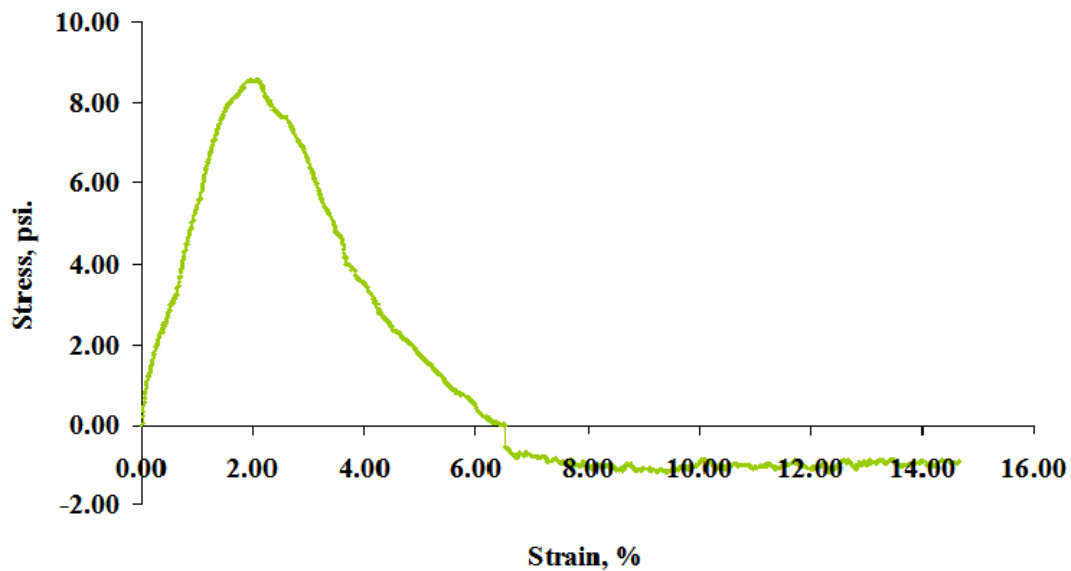


Figure 4.3 – Typical Flexural Test Result

that point, the stress decreases until the stress becomes nil. At this point there is considerable damage inside the specimen by the crack growth in the middle of the specimen. As the specimen fails completely, it cannot even withstand its own weight which is reflected as a negative stress level. As such, the peak stress usually coincides with the initiation of the crack, and the zero crossing to the point where the crack is clearly visible.

4.4.4 Free-Free Resonant Column Test

The free-free resonant column (FFRC) test, performed as per proposed Tex-149-E, is a simple laboratory test for determining the modulus of pavement materials. When a cylindrical specimen is subjected to an impulse load at one end, seismic energy over a large range of frequencies will propagate within the specimen. Depending on the dimensions and the stiffness of the specimen, energy associated with one or more frequencies are trapped and magnified (resonate) as they propagate within the specimen. The goal with this test is to determine these resonant frequencies. Since the dimensions of the specimen are known, if one can determine the frequency (ies) that are resonating (i.e. the resonant frequencies), one can determine the modulus of the specimen.

Figure 4.4 shows typical test results while Figure 4.5 shows the pictorial representation of the test method. A 4 in. by 8 in. clay specimen with a thumbtack at the center is placed on a pedestal. An accelerometer is placed next to the thumbtack. The thumbtack is gently tapped using hammer and a frequency is generated. A computer generated program records the frequency and the data is saved.

4.4.5 Resilient Modulus Test

The resilient modulus test is carried out using a modified version of the AASHTO T-307 test procedure. A detailed test protocol is included in Appendix A. A compacted specimen is placed in a confining chamber and a haversine deviatoric load is applied from the top along with a confining pressure. The load consisted of a 0.1 second pulse followed by a 0.9 second rest period. The test starts with a 1000 cycles of conditioning, followed by a series of tests at different confining pressures and deviatoric stresses.

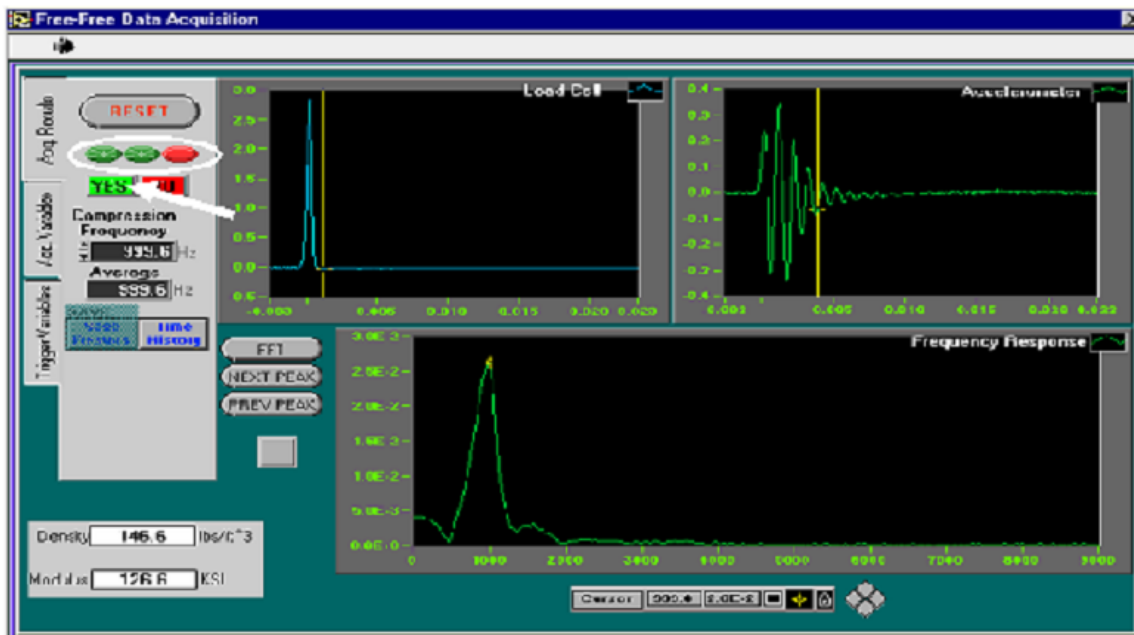


Figure 4.4 – Typical Free-Free Resonant Column Test Results

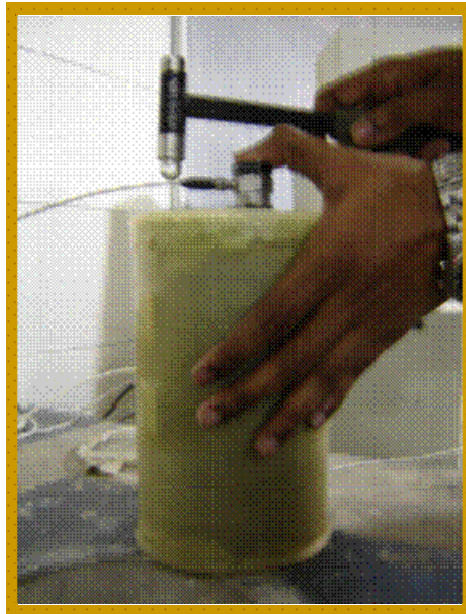


Figure 4.5 – Free-Free Resonant Column Test

The test is carried out using an MTS testing device. Figure 4.6 shows the variation in resilient modulus with deviatoric stress and different confining pressures. A constitutive equation in the form of Equation 4.2 is fitted to the data:

$$M_r = k_1 * \sigma_c^{k_2} * \sigma_d^{k_3} \quad (4.2)$$

where parameters k_1 , k_2 and k_3 are the material constants which are obtained after data reduction. Parameter σ_c is the confining pressure, and σ_d is the deviatoric stress.

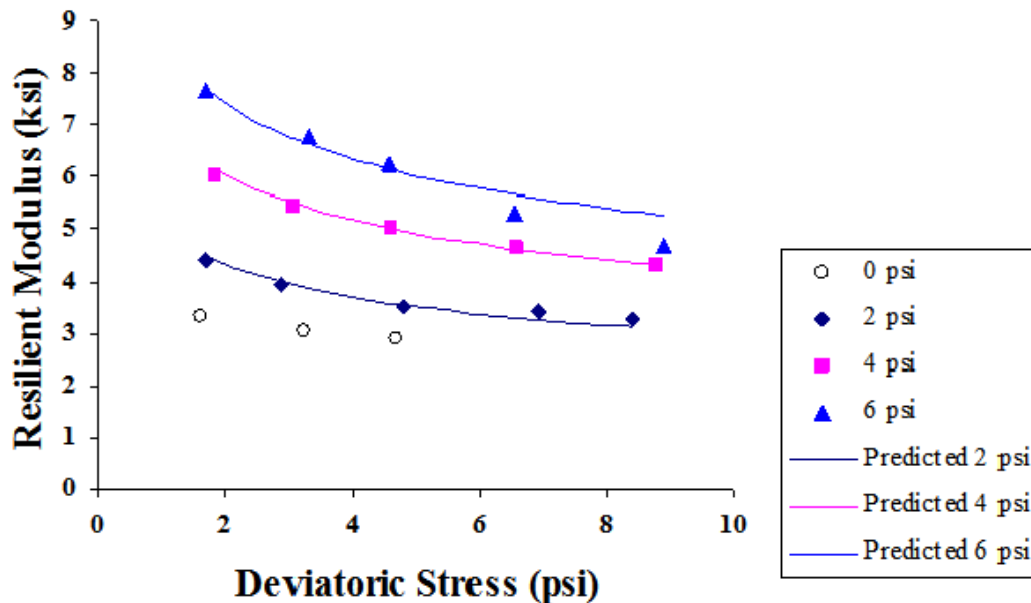


Figure 4.6 – Typical Resilient Modulus Test Results

Figure 4.7 shows a pictorial representation of steps followed for resilient modulus test. The specimen is placed on the bottom platen as shown in Step 1. Using a centering rod, the specimen is carefully centered (Step 2). The confining chamber is then placed around the specimen (Step 3). The top plate is secured to the confining chamber as shown in Step 4. The load cell is then securely attached to the specimen and the actuator (see Step 5). A computer program is then used to perform resilient modulus test following the loading sequence shown in Table 4.3. Step 6 shows the graph of load and deformation variation during testing.

4.4.6 Permanent Deformation Test

Permanent deformation test is carried out according to protocol AASHTO-T-307 to assess the permanent deformation of the specimen. The actual test requires 10,000 cycles of load. For the purpose of this research, the deformation of the specimen during the conditioning cycles for the resilient modulus test was used. The set up is same as for the resilient modulus test. To carry out this test on clays a confining pressure of 6 psi and a deviatoric stress of 4 psi is applied.

A typical test result of permanent deformation test is shown in Figure 4.8. The permanent deformation parameters are determined from intercept (a) and slope (b), from the linear portion of the permanent strain curve. The resilient strain is noted at the 200th cycle while as permanent strain is at 1000th cycle. These parameters are used to calculate rutting parameters (α , μ) using:

$$\mu = (1 - b) \quad (4.3)$$

$$\alpha = (a \times b) / \epsilon_{\text{resilient}} \quad (4.4)$$

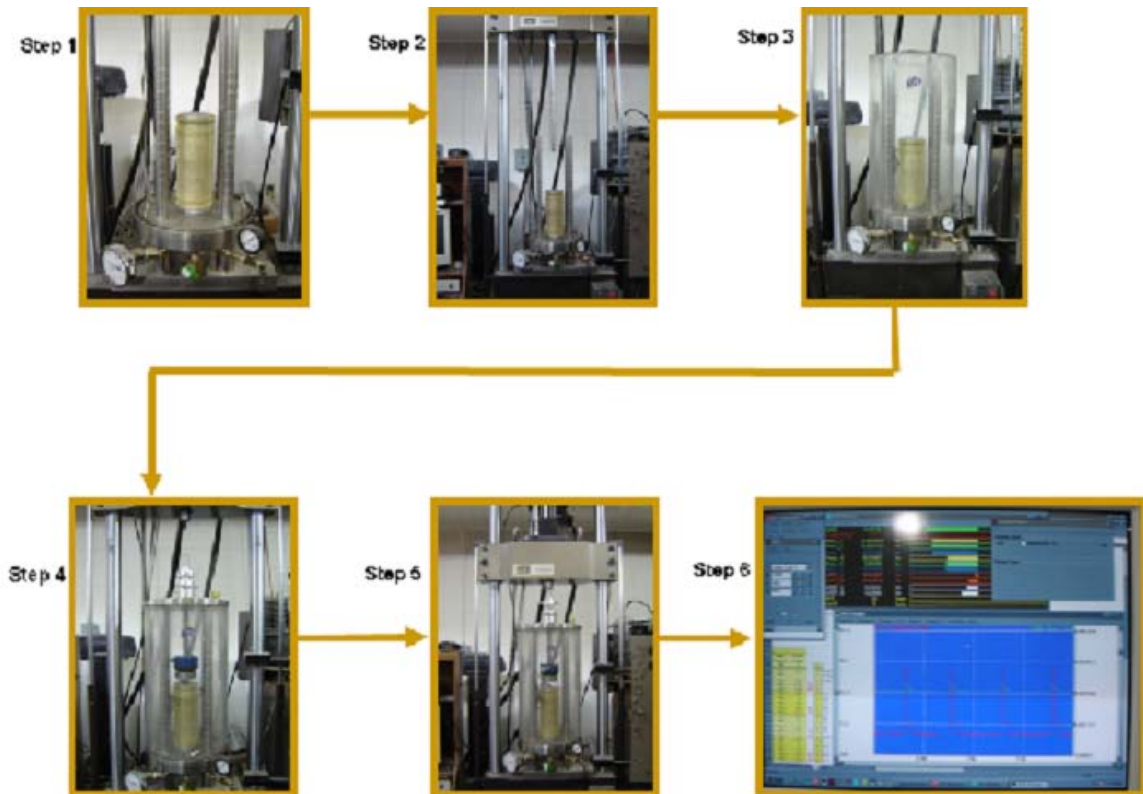


Figure 4.7 – Steps for Resilient Modulus Test

Table 4.3 – Loading Sequence for Resilient Modulus Test

Sequence	Confining pressure, psi	Deviatoric Stress, psi	Number of cycles
Conditioning	6	4	1000
1	6	2	25
2		4	
3		6	
4		8	
5		10	
6	4	2	25
7		4	
8		6	
9		8	
10	2	10	25
11		2	
12		4	
13		6	
14		8	
15		10	

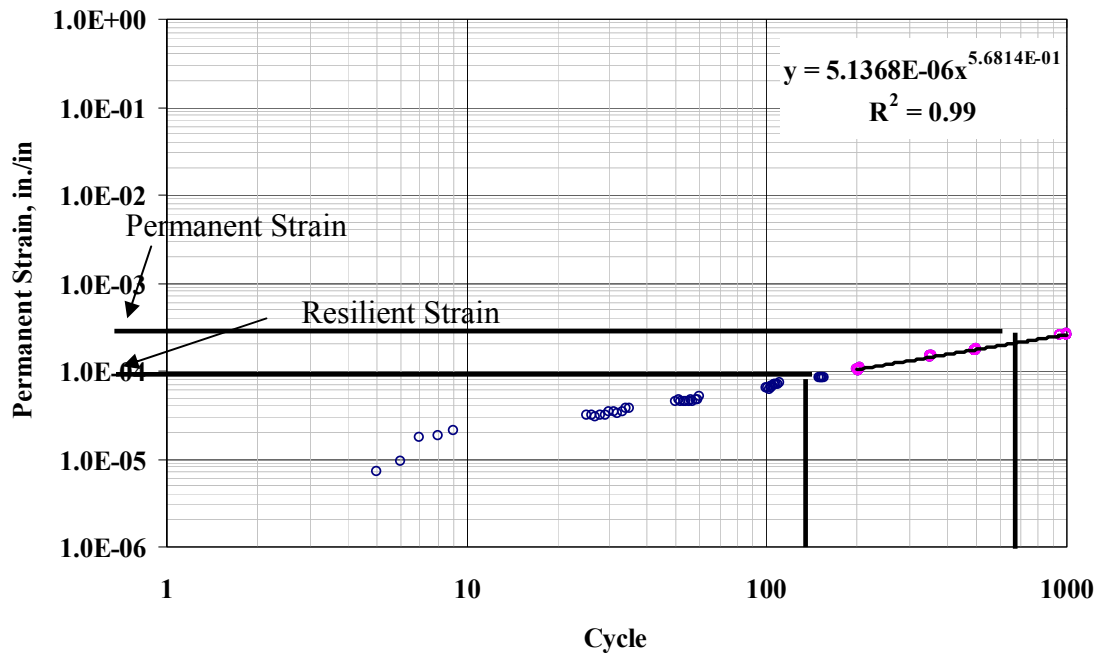


Figure 4.8 – Typical Permanent Deformation Test Result

4.5 VOLUMETRIC TESTS

Volumetric shrinkage test, three-dimension free swell test and pressure swell test were performed as part of this testing program.

4.5.1 Volumetric Shrinkage Test

Volumetric shrinkage tests were conducted to measure the decrease in the total volume of soil specimens due to loss of moisture content from predetermined initial moisture content to a completely dry state. A test method developed by Puppala et al. (2004) was used. A cylindrical compacted soil specimen is subjected to drying process so that the volumetric, axial and radial shrinkage strains using digital imaging technology can be estimated. This test offers several advantages over conventional linear shrinkage bar test such as reduced interference of boundary conditions on shrinkage, larger amount of soil being tested, and simulates compaction states of moisture content - dry density conditions. Linear shrinkage bar test was also conducted to complement the volumetric shrinkage properties and develop correlations between linear and volumetric shrinkage strains.

Three different initial moisture contents (optimum, wet of optimum and dry of optimum) were used. Specimen preparation is performed by mixing the dry clay with appropriate amount of water to achieve the designed water contents, the compaction of the soil specimens in 2.3 in. diameter and 5 in. height mold, and measuring the initial height of the specimen. The specimens are then cured in the mold at room temperature for 12 hours and then transferred to an oven set at a temperature of 220°F for 24 hours (Figure 4.9). The average height and diameter of the shrunk specimens are manually measured. The same specimens are then subjected to digital imaging. The images, as shown in Figure 4.10, are used in the following equation to determine volumetric shrinkage strains.

$$V.S. = \frac{V_i - V_f}{V_i} = 1 - \frac{V_f}{V_i} = 1 - \left[\frac{A_{sf}}{A_{si}} * \frac{A_{cf}}{A_{ci}} * \frac{P_{ci}}{P_{cf}} \right] = 1 - (R_s * R_c * R_p) \quad (3.1)$$



(a) before oven dried



(b) after oven dried

Figure 4.9 - Typical Specimens

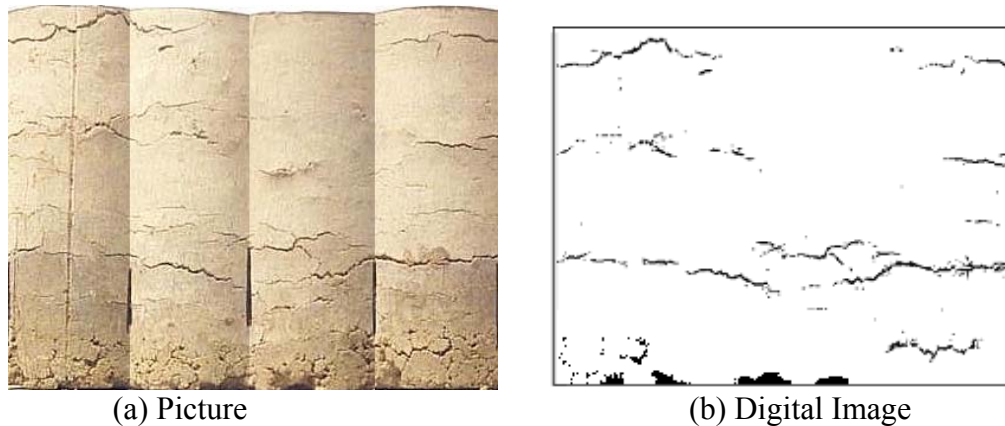


Figure 4.10 - Typical Photograph and Digital Image of a Specimen

where

R_s	=	ratio of surface area of the soil specimen = A_{sf}/A_{si}
R_c	=	ratio of circular cross-section area of soil specimen = A_{cf}/A_{ci}
R_p	=	ratio of the circular perimeter of the soil specimen = P_{cf}/P_{ci}
V_f	=	final volume of the cylindrical specimen
V_i	=	initial volume of the cylindrical specimen
A_{sf}	=	area of the final surface area of specimen after shrinkage in pixels
A_{si}	=	area of initial surface area of specimen before shrinkage in pixels
A_{cf}	=	area of final circular area of specimen after shrinkage in pixels
A_{ci}	=	area of initial circular area of specimen before shrinkage in pixels
P_{cf}	=	perimeter of the final circular area after shrinkage in pixels
P_{ci}	=	perimeter of circular area before shrinkage in pixels

4.5.2 Three-Dimensional Free Swell Testing

The three-dimensional free swell test investigates the maximum vertical, diametric and volumetric swell potentials for soil types. Specimens, 4.0-in. diameter and 4.6 in. high, are prepared at three different moisture conditions (optimum, dry of optimum and wet of optimum) at their corresponding densities. A specimen is placed between two porous stones (Figure 4.11), wrapped in a rubber membrane, and is subjected to soaking by inundating it with water from both ends (Punthutaecha et al., 2003). The vertical and radial swell movements are monitored until there was no further movement is observed. The vertical and radial swell movements are simply measured using a dial gauge and a pi tape (Figure 4.11), respectively. All measurements are conducted at room temperature on three identical specimens.

4.5.3 Swell Pressure Test

The constant swell pressure is defined as the amount of load that should be applied over the expansive soil to resist any volume change in vertical direction. Tests were conducted as per ASTM D-4546 as shown in Figure 4.12. Specimens, compacted in a ring of 2.5 in. in diameter and 1.0 in. in thickness, are fully soaked in a standard consolidation setup. Two porous stones are placed at the top and bottom of the specimen. A dial gauge is used to monitor the specimen's movement. Load is added to maintain the original position. Testing is discontinued when no swell movement is observed for more than two days. The total load applied to the specimen is then used to calculate its swell pressure.



Figure 4.11 - Three-Dimensional Free Swell Test Setup

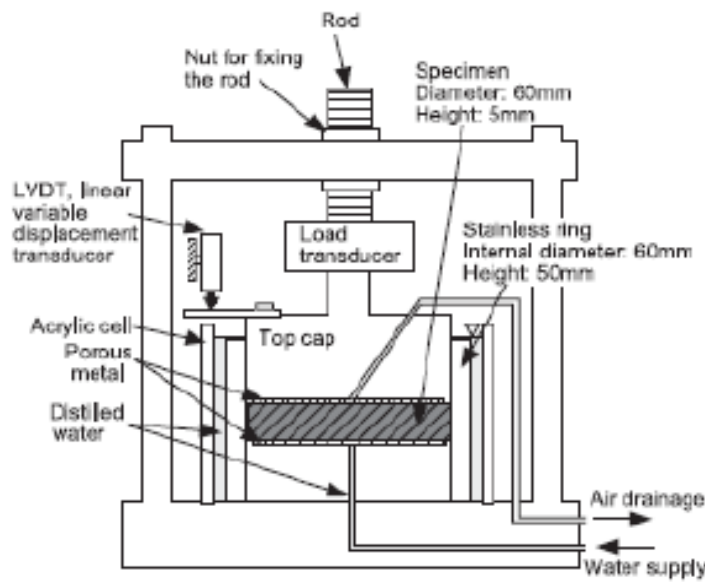


Figure 4.12 - Modified Consolidation Test Setup for Swell Pressure Test

4.6 SUCTION TESTS

Several test methods including filter paper and pressure plate method are commonly used to develop Soil Water Characteristic Curves (SWCCs) of unsaturated soils. The limitation of the current available pressure plate device is that it can measure matric suction up to only 1,000 kPa. Therefore, filter paper method was used to measure soil suction ranging more than 1,000 kPa. Hence, both pressure plate and filter paper methods were employed in the development of a complete SWCC of the present soils.

4.6.1 Pressure Plate Method

Figure 4.13 and 4.14 show a typical pore water extraction testing setup using a pressure plate apparatus. The primary components of the system are a steel plate pressure vessel and a saturated high air entry (HAE) ceramic plate. A small water reservoir is formed beneath the plate using an internal screen and a neoprene diaphragm. The water reservoir is vented to the atmosphere through an outflow tube located on top of the plate, thus allowing the air pressure in the vessel and the water pressure in the reservoir to be separated across the air-water interfaces bridging the saturated pores of the HAE material (Lu and Likos, 2004).

Specimens are initially saturated, typically by applying a partial vacuum to the air chamber to imbibe water from the underlying reservoir through the ceramic disk. Air pressure in the vessel is then increased to some desired level while pore water is allowed to drain from the specimens in pursuit of equilibrium. The outflow of water is monitored until it ceases, the pressure vessel is opened, and the water content of one or more of the specimen is measured, thus generating one point on the soil-water characteristic curve. Subsequent increments in air pressure are applied to generate additional points on the curve using the other specimen.

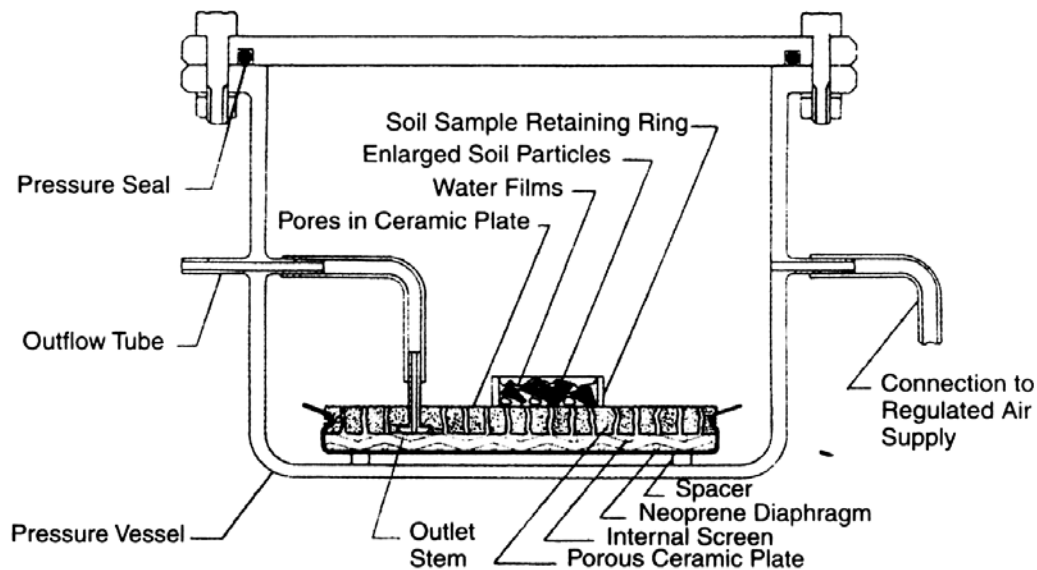


**Figure 4.13 - Schematic Of Pressure Plate Apparatus
(Soil-Moisture Equipment Corp., 2003)**



(a) Initial Setup



(b) Closed Pressure Vessel

Figure 4.14 - Pressure Plate Testing

4.6.2 Filter Paper Method

A filter paper (Schleicher & Schuell No. 589-WH type) is suspended in the headspace above the specimen such that moisture transfer occurs in the vapor phase. The equilibrium amount of water absorbed by the filter paper is a function of the pore-air relative humidity and the corresponding total soil suction. The water content of the filter paper is measured after it reaches equilibrium with the soil through vapor for a period of ten days. The suction is estimated from the filter papers' moisture content using a calibration curve proposed by Bulut, Lytton, and Wray (2001) (Figure 4.15). By measuring at various moisture contents, the soil water characteristic curves are obtained.

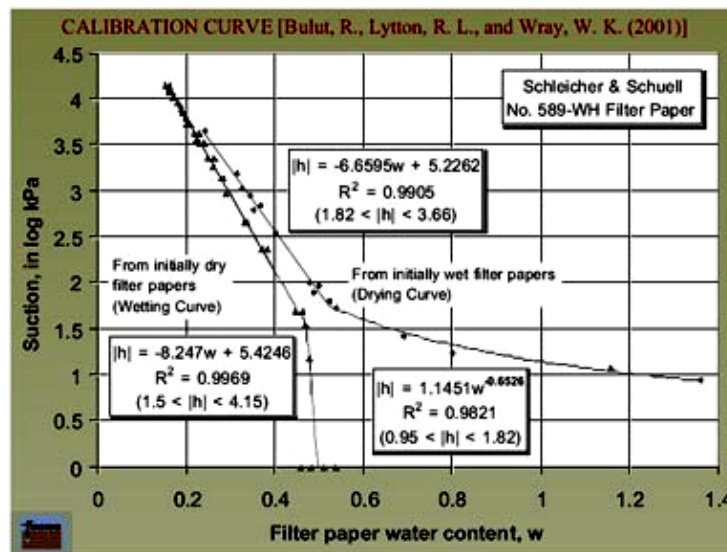


Figure 4.15 - Calibration curves (Bulut, Lytton and Wray, 2001)

CHAPTER 5 - PRESENTATION OF RESULTS

5.1 INTRODUCTION

In this chapter the data collected from different tests are presented. Since some of the tests may be time-consuming or difficult to perform, Chapter 6 is dedicated to relating the results from different tests to more readily-available parameters.

5.2 INDEX PROPERTIES

Table 5.1 presents a summary of various index properties of all soils. Generally, soils that exhibit plastic behavior over wide ranges of moisture content and that have high liquid limits have greater potential for swelling and shrinking. Soils from Fort Worth, San Antonio, Bryan and Paris are considered very high swelling potential, whereas Houston soil is considered as exhibiting high swelling potential. These soils are classified as A-7-6 as per American Association of State Highway and Transportation Officials (AASHTO) Soil Classification System and CH as per Unified Soil Classification System (USCS).

Table 5.1 - Index Properties

Property	Soil Type					
	Fort Worth	San Antonio	Bryan	Paris	Houston	El Paso
Passing #40 (%)	100	100	100	100	100	100
Passing #200 (%)	85	83	78	81	87	88
Assumed Specific Gravity	2.7	2.7	2.7	2.7	2.7	2.7
Liquid Limit (LL, %)	61	58	45	60	54	30
Plastic Limit (PL, %)	24	22	14	23	21	14
Plasticity Index (PI, %)	37	36	31	37	33	16
AASHTO Classification	A-7-6	A-7-6	A-7-6	A-7-6	A-7-6	A-6
USCS Classification	CH	CH	CH	CH	CH	CL

The moisture density properties of the soils are shown in Table 5.2. El Paso clay exhibits the highest dry density which may indicate the quality of this soil in supporting civil infrastructure, whereas Houston clayey soil exhibits the highest value among high PI clay group. Also shown in

the table is the moisture contents associated with a 95% MDD at the wet and dry sides. These moisture contents were used in some of the shrinkage and swell tests.

Table 5.2 - Moisture Density Test Results

Property		Soil Type					
		Fort Worth	San Antonio	Bryan	Paris	Houston	El Paso
Moisture Content (%)	Wet of OMC	33.0	31.8	24	33.0	27.3	20.0
	OMC	24.0	21.7	19.5	23.0	20.1	16.5
	Dry of OMC	15.1	10.5	15.0	13.0	12.9	13.0
Dry Density (pcf)	Wet of OMC	86.9	86.9	102.6	87.5	94.1	106.4
	OMC	91.5	91.5	108.0	92.1	99.1	112.0
	Dry of OMC	86.9	86.9	102.6	87.5	94.1	106.4

5.3 MINERALOGICAL PROPERTIES

Chemical analysis was introduced in this research in order to justify the causes of volume change problems. In many cases, not only the intrinsic properties of soil itself but also soluble sulfate content plays important roles in swell/shrink behaviors. The concentrations of the soluble sulfates are shown in Table 5.3. Soluble sulfates less than 2,000 ppm are considered to be a low value.

Table 5.3 - Chemical Parameters of Soils

Property	Soil Type					
	Fort Worth	San Antonio	Bryan	Paris	Houston	El Paso
Soluble Sulfates (ppm)	358	82	498	136	247	1,201
Cation Exchange Capacity (meq/100 g)	117	96	77	133	76	57
Specific Surface Area (m ² /gm)	314	269	205	431	236	167

Cation Exchange Capacity (CEC) is the quantity of exchangeable cations required to balance the negative charge on the surface of clay particles. High CEC values indicate a high surface activity of the clays (Nelson and Miller, 1992). In general, the swell potential increases as the CEC increases. The CEC and specific surface area values are reported in Table 5.3 as well.

Clay minerals which typically cause soil volume changes are montmorillonites and some mixed layer minerals. Illite can be expansive but generally do not pose significant problem. Kaolinite is normally non-expansive (Nelson and Miller, 1992). The test results for all soils are shown in Table 5.4. Fort Worth, San Antonio, Bryan and Paris clays predominantly contain Montmorillonite, signifying the potential for greater volume change in the field. Although the Houston clay contains less Montmorillonite, the value is still considerable. El Paso clay contains noticeably low amount of Montmorillonite.

Table 5.4 - Mineralogy Characteristics of Soils

Clay Minerals	Soil Types					
	Fort Worth	San Antonio	Bryan	Paris	Houston	El Paso
% Illite	16	18	37	13	26	63
% Kaolinite	34	40	18	17	38	29
% Montmorillonite	50	42	45	70	36	8

5.4 STRENGTH TESTS

As discussed in Chapter 4, the unconfined compressive strength (UCS), indirect tensile strength (IDT) and flexural tests were performed on the clays. The UCS tests were performed on two specimens of each clay type at three different moisture conditions, namely dry, optimum and wet. The average unconfined compressive strengths for the six clays are shown in Table 5.5. The UC strengths of the dry specimens are significantly (4 to 11 times) greater than the corresponding strengths at the optimum moisture contents. As specimens become wet, they lose almost all of their strengths. The maximum wet UCS is 6 psi.

The strains at failure for all tests are summarized in Table 5.5. The strains at failure for wet specimens are on the order of 3% to 6% which are significantly greater than those at optimum (less than 3.5%). On the other hand, the strains at failure of the dry specimens are typically less than 2% indicating that the clays get more brittle as the moisture content decreases.

The indirect tensile strength (IDT) tests were also performed on two specimens of each clay type at the optimum and dry conditions. It was impossible to test the wet specimens because they were too soft. The average IDT strengths are shown in Table 5.6. Once again, the strengths of the dry specimens were anywhere from 5 to 10 times greater than those at optimum. However, the strains at failure for optimum and dry specimens were similar for most of the clay materials.

Flexural tests were performed on two specimens at each optimum and dry conditions. Again, due to loss of strength upon saturation of the clay specimens, it was not possible to test them for flexural strength. As reflected in Table 5.7, the strengths of the dry specimens were 14 to 50 times greater than those of optimum specimens. The strains at peak stress were greater at dry condition as compared to optimum.

5.5 STIFFNESS TESTS

The free-free resonant column (FFRC), resilient modulus and permanent deformation tests were performed to characterize the stiffness parameters of the soils. FFRC tests were performed on all clay specimens during drying and saturation. During drying, the specimens were taken out of the oven and tested daily. As a part of these tests, the changes to the diameters, heights and weight of the specimens were also measured. The changes in the dimensions were used to estimate the shrinkage strains and the change in weight to estimate the change in moisture content.

Table 5.5 - UCS Test Results at Different Moisture Conditions

Material	Optimum		Wet		Dry	
	UCS, psi	Strain at Failure, %	UCS, psi	Strain at Failure, %	UCS, psi	Strain at Failure, %
El Paso PI = 17	30 (4.7)	3.5 (0.0)	4 (0.0)	10.3 (3.4)	140 (17.2)	0.9 (8.3)
San Antonio PI = 26	33 (4.3)	2.2 (9.9)	4 (0.0)	9.5 (14.9)	124 (1.1)	1.3 (10.9)
Forth Worth PI = 29	36 (7.9)	1.8 (20.2)	4 (1.8)	9.0 (3.8)	206 (7.6)	0.8 (17.7)
Bryan PI = 31	31 (34.8)	1.7 (33.3)	3 (13.3)	9.8 (3.6)	328 (6.0)	1.7 (4.3)
Houston PI = 35	60 (2.4)	1.9 (34.4)	5 (31.4)	8.0 (35.4)	264 (1.6)	0.8 (35.4)
Paris PI = 36	28 (20.2)	1.6 (26.5)	6 (9.6)	10.0 (7.1)	199 (24.9)	1.8 (4.0)

Note: Numbers in bracket indicate coefficient of variation

Table 5.6 – Indirect Tensile Strength Test Results at Different Moisture Conditions

Material	Optimum		Dry	
	IDT, psi	Strain at Failure, %	IDT, psi	Strain at Failure, %
El Paso PI = 17	5 (0.0)*	0.4 (20.2)	53 (17.5)	0.6 (38.6)
San Antonio PI = 26	14 (5.2)	0.6 (0.0)	88 (26.7)	1.3 (50.9)
Forth Worth PI = 29	12 (23.6)	0.6 (12.9)	61 (8.2)	0.6 (12.9)
Bryan PI = 31	15 (18.9)	0.8 (0.0)	131 (10.8)	1.2 (6.2)
Houston PI = 35	18 (20.2)	0.8 (17.7)	108 (2.6)	0.7 (20.2)
Paris PI = 36	10 (42.4)	0.9 (8.3)	69 (4.1)	1.0 (22.3)

Note: Numbers in brackets indicate the coefficient of variation

Table 5.7 – Flexural Test Results at Different Moisture Conditions

Material	Optimum		Dry	
	Peak Stress, psi	Strain at Peak Stress, %	Peak Stress, psi	Strain at Peak Stress, %
El Paso PI = 17	Specimens were too soft and failed during test set-up		37(27.6)	1.8 (15.7)
San Antonio PI = 26	4 (4.9)*	1.1 (16.8)	56 (13.8)	2.7 (18.4)
Forth Worth PI = 29	3 (17.5)	1.1 (36.7)	55 (22.7)	3.8 (63.3)
Bryan PI = 31	3 (34.7)	3.5 (33.4)	137 (29.0)	4.1 (22.5)
Houston PI = 35	5 (67.1)	1.5 (48.3)	99 (9.8)	3.6 (14.2)
Paris PI = 36	6 (14.5)	1.6 (79.0)	78 (12.5)	4.1 (7.0)

Note: Numbers in brackets indicate the coefficient of variation

The seismic moduli, moisture contents and maximum shrinkage strains from the drying activity are shown in Table 5.8. The initial moduli were measured as soon as the specimens were prepared, whereas the final moduli are measured at the end of the drying process. In the case of the high-PI clays, the final moduli are 6 to 15 times the corresponding initial moduli, while for the low-PI clay, the final modulus was about 30 times greater than the initial modulus.

The initial moisture contents are the moisture contents at which the specimens were prepared (nominally equal to OMC). The final moisture contents are the moisture contents after the completion of the drying process. The final moisture contents are approximately 85 to 95% less than the corresponding initial moisture contents.

The maximum shrinkage strains are presented in Table 5.8 as well. The high-PI clays shrank drastically more than the low PI clay. The maximum horizontal and vertical shrinkage strains in high PI clays were found to be 5 to 6%, while the corresponding shrinkage in low PI clay was just 1 to 2%.

Three representative specimens were subjected to wetting conditioning as well. As with the drying process, the changes in modulus, dimensions and weight were estimated frequently. It was very difficult to perform seismic tests on specimens when they became close to saturation.

The initial (as soon as the specimens were prepared) and final (upon completion of wetting process) moduli, moisture contents and maximum expansion strains are shown in Table 5.9. The saturated specimens' moduli were less than 6 ksi. The final moisture contents were 1.3 to 1.6 times greater than the OMC. The high PI clays generally expanded more than the low PI clay

Table 5.8 – Summary of Test Results during Drying Process

Material	Seismic Modulus, ksi		Moisture Content,%		Maximum Shrinkage Strain, %		
	Initial	Final	Initial	Final	Vertical	Horizontal	Volumetric
El Paso PI = 17	9 (0.0)*	269 (17.7)	16.5 (0.0)	2.6 (19.6)	1.2 (20.2)	2.0 (2.3)	5.3 (6.1)
San Antonio PI = 26	20 (8.3)	118 (10.3)	20.9 (0.0)	2.9 (26.4)	5.1 (8.2)	5.0 (9.2)	14.3 (8.3)
Forth Worth PI = 29	13 (3.3)	194 (6.9)	23.2 (0.0)	1.2 (23.6)	6.0 (2.1)	6.3 (1.7)	17.5 (1.3)
Bryan PI = 31	21 (14.0)	142 (22.9)	20.2 (0.0)	4.0 (31.3)	5.7 (35.0)	4.9 (16.0)	12.8 (21.5)
Houston PI = 35	19 (12.7)	255 (5.0)	20.7 (0.0)	4.0 (23.4)	5.1 (8.8)	5.7 (6.9)	15.5 (7.1)
Paris PI = 36	21 (15.5)	201 (18.0)	23.3 (0.0)	4.8 (2.1)	6.1 (6.0)	6.4 (5.5)	17.8 (5.2)

Note: Numbers in brackets indicate the coefficient of variation

Table 5.9 – Summary of Test Results during Wetting Process

Material	Seismic Modulus, ksi		Moisture Content,%		Maximum Expansion Strain, %		
	Initial	Final	Initial	Final	Vertical	Horizontal	Volumetric
El Paso PI = 17	9	Not Possible	16.5 (0.0)*	28.5 (2.7)	1.5 (26.4)	0.6 (26.8)	2.6 (3.8)
San Antonio PI = 26	19	11	22.6 (0.0)	34.7 (1.8)	2.7 (66.9)	1.5 (31.8)	5.3 (0.7)
Forth Worth PI = 29	12	1	23.4 (0.0)	34.8 (1.9)	1.7 (26.8)	0.5 (25.9)	2.7 (2.9)
Bryan PI = 31	23	6	21.0 (0.0)	27.5 (0.4)	1.8 (13.9)	0.9 (14.2)	4.1 (14.3)
Houston PI = 35	16	4	20.7 (0.0)	30.3 (0.5)	1.7 (1.8)	0.3 (81.3)	2.3 (44.7)
Paris PI = 36	22	1	23.3 (0.0)	35.1 (1.2)	2.2 (9.8)	1.2 (26.4)	4.7 (6.8)

Note: Numbers in brackets indicate the coefficient of variation

The resilient modulus tests were performed on two specimens of each clay at optimum and dry conditions. The wet specimens were not stable enough to test since they deformed excessively during the conditioning cycles. The resilient modulus stiffness parameters k_1 , k_2 and k_3 are presented in Table 5.10. For specimens tested under the optimum conditions, parameters k_1 are similar for the high-PI clays since they vary between 10 ksi and 15 ksi. Parameters k_2 are quite

Table 5.10 – Resilient Modulus Test Results at Different Moisture Conditions

a) Optimum Condition

Material	Resilient Modulus Model Parameters			Representative Resilient Modulus, ksi	Seismic Modulus, ksi
	k ₁	k ₂	k ₃		
El Paso PI = 16	3 (14.1)*	0.44 (11.8)	-0.22 (-21.3)	4 (5.4)	7 (5.7)
San Antonio PI = 26	11 (0.0)	0.03 (28.3)	-0.11 (-12.9)	10 (1.0)	18 (0.0)
Fort Worth PI = 29	10 (22.3)	0.05 (47.1)	-0.08 (0.0)	9 (19.5)	15 (4.9)
Bryan PI = 31	13 (33.3)	0.14 (15.9)	-0.41 (-5.3)	9 (31.7)	15 (0.0)
Houston PI = 35	14 (0.0)	0.04 (106.1)	-0.12 (-35.4)	13 (11.7)	25 (17.0)
Paris PI = 36	15 (43.9)	0.04 (141.4)	-0.11 (-38.6)	13 (42.1)	28 (2.6)

b) Dry Condition

Material	Resilient Modulus Model Parameters			Representative Resilient Modulus, ksi	Seismic Modulus, ksi
	k ₁	k ₂	k ₃		
El Paso PI = 16	49 (7.4)	0 (assumed)	0 (assumed)	49 (10.4)	191 (3.3)
San Antonio PI = 26	48 (15.3)			48 (4.6)	129 (9.8)
Fort Worth PI = 29	36 (1.84)			36 (8.69)	162 (3.86)
Bryan PI = 31	64 (18.3)			64 (19.4)	134 (8.9)
Houston PI = 35	55 (11.5)			55 (20.3)	242 (6.5)
Paris PI = 36	31 (20.7)			31 (4.6)	120 (1.9)

Note: Numbers in brackets indicate the coefficient of variation

small (less than 0.14) for the high-PI clays, indicating that the moduli are not very dependent on the confining pressures. Parameters k₃ are also rather small (less than 0.11) except for the Bryan clay, indicating that the moduli are weakly impacted by the deviatoric stress (axial strain). The representative resilient moduli, calculated as discussed in Chapter 4, vary between 10 ksi and 13 ksi. As reflected in Table 5.10a, the seismic moduli are 1.6 to 2 times greater than the representative resilient moduli, indicating that the two are reasonably related.

Parameters k_1 , representative moduli and seismic moduli are significantly greater for the dry specimens as compared to specimens tested at the OMC. The dry specimens were very stiff. The representative resilient moduli may be too conservative because of the limitations of the test protocol. In addition, for the dry state, parameters k_2 and k_3 should be close to zero. These two parameters were assumed to be zero as reflected in the table. The representative resilient moduli of dry specimens of the high-PI clays are 2.5 to 7 times greater than the corresponding specimens tested at optimum condition while, this ratio for the low-PI clay was 12. The seismic moduli of the dry specimens were 4 to 12 times greater than the optimum ones.

Permanent deformation parameters of the specimens tested at the optimum and dry conditions are reported in Table 5.11. The wet specimens failed after a few cycles of conditioning. The low-PI El Paso clay exhibited resilient and permanent strains in excess of 2800 μ strain at optimum condition. For the high-PI clays, the permanent and resilient strains were less than 715 μ strain. The resilient and permanent strains of the dry specimens are in most cases less than those from the specimens prepared at optimum. The permanent deformation parameters α for all materials at optimum fell in a narrow range of 0.04 and 0.07 for both moisture conditions. For the five high-PI clays, the parameters μ also tend to fall in a reasonably narrow range for both moisture conditions.

5.6 VOLUMETRIC TESTS

Shrinkage strains in radial and vertical directions were first measured as per the procedure discussed in Chapter 4, and used to determine volumetric shrinkage strains. Volumetric shrinkage strain test is a better test method than linear shrinkage strain test since volumetric strain was evaluated on tests on soil samples of considerable volume. At least three samples were prepared for each moisture condition. The average values are presented in Table 5.12. The highest to the lowest shrinkage strain potentials are attributed to the clays from San Antonio, Paris, Fort Worth, Bryan, Houston, and El Paso, respectively.

Three-Dimensional Free Swell tests were also carried out. Three samples for each moisture condition were compacted at three different moisture contents as per the procedure discussed in Chapter 3. Typical swell characteristic graphs are shown in Figure 5.1. Even though the majority of swell strains occurred within the first eight hours, subsequent swell strains were continuously recorded until no swell movement was observed. Majority of the volumetric swell strains were contributed from vertical swell strains.

Table 5.13 presents the average swell strains. All high-PI soils experienced volumetric swell strains (for OMC condition) in excess of 10%, which is considered as a very high degree of expansion (Chen, 1965). As expected, El Paso clay exhibited the lowest swell strains because of its low plasticity index, low percent of Montmorillonite, low CEC and low specific surface area.

The constant swell pressure tests results are presented in Table 5.14 for all soils at three different moisture conditions. As expected, the swelling pressures for soils tested at wet of optimum exhibited the lowest values and those at dry of optimum provided the highest. This is the reason behind numerous roads on expansive soils experiencing cracking when those soils are exposed to heavy rain falls following long dry periods of high temperatures. Test results revealed the same

Table 5.11 – Permanent Deformation Test Results at Different Moisture Conditions
a) Optimum Condition

Material	Resilient Strain, μ strain	Permanent Strain, μ strain	Permanent Deformation Parameters	
			μ	α
El Paso PI = 17	2801 (48.2)*	3394 (36.2)	0.84 (16.3)	0.05 (66.6)
San Antonio PI = 26	267 (107.5)	490 (83.0)	0.49 (61.2)	0.04 (85.2)
Forth Worth PI = 29	163 (55.7)	383 (68.8)	0.49 (14.2)	0.04 (14.7)
Bryan PI = 31	211 (66.0)	304 (63.9)	0.77 (2.1)	0.07 (2.1)
Houston PI = 35	320	470	0.72	0.06
Paris PI = 36	604 (103.0)	715 (86.9)	0.81 (22.7)	0.05 (19.5)

b) Dry Condition

Material	Resilient Strain, μ strain	Permanent Strain, μ strain	Permanent Deformation Parameters	
			μ	α
El Paso PI = 17	125 (132.9)	164 (131.2)	0.82 (10.5)	0.07 (44.5)
San Antonio PI = 26	162 (23.7)	271 (19.4)	0.68 (6.9)	0.06 (17.7)
Forth Worth PI = 29	175 (71.0)	257 (45.7)	0.78 (16.9)	0.07 (7.7)
Bryan PI = 31	66 (29.7)	136 (61.5)	0.56 (28.8)	0.04 (30.7)
Houston PI = 35	198 (30.2)	317 (68.2)	0.78 (35.5)	0.03 (54.8)
Paris PI = 36	1.04 (5.1)	2.56 (29.4)	0.43 (38.8)	0.03 (58.2)

Note: Numbers in brackets indicate the coefficient of variation

Table 5.12 - Volumetric Shrinkage Strain Results

Moisture Condition	Parameter	Shrinkage Strain (%)					
		Fort Worth	San Antonio	Bryan	Paris	Houston	El Paso
Wet of OMC	Vertical	8.43 (17.4)	9.91 (20.0)	7.85 (15.2)	8.78 (27.6)	5.11 (5.1)	4.28 (31.4)
	Radial	8.87 (6.9)	9.66 (4.5)	8.56 (3.7)	9.45 (4.9)	7.37 (2.5)	3.55 (16.4)
	Volumetric	23.59 (3.6)	26.68 (3.6)	21.58 (4.5)	24.66 (8.8)	18.58 (2.7)	10.97 (5.7)
OMC	Vertical	5.29 (13.6)	6.98 (11.0)	3.59 (8.5)	4.92 (8.2)	2.25 (8.3)	1.86 (23.9)
	Radial	2.47 (9.9)	5.33 (5.2)	3.59 (7.2)	4.91 (10.1)	4.57 (6.9)	1.77 (23.0)
	Volumetric	12.51 (4.6)	18.08 (5.3)	13.9 (6.6)	14.04 (6.3)	10.97 (9.3)	5.30 (16.6)
Dry of OMC	Vertical	2.17 (4.3)	2.81 (8.6)	1.89 (5.1)	2.41 (4.5)	1.44 (6.7)	0.36 (20.0)
	Radial	0.97 (9.3)	2.13 (3.5)	2.01 (4.5)	1.46 (7.1)	1.75 (11.8)	1.50 (10.6)
	Volumetric	5.22 (3.6)	7.55 (1.2)	6.04 (3.3)	6.15 (4.0)	4.85 (1.5)	3.33 (11.8)

Note: Numbers in brackets indicate the coefficient of variation

Table 5.13 - Volumetric Swell Strain Tests Results

Moisture Condition	Parameter	Swell Strain (%)					
		Fort Worth	San Antonio	Bryan	Paris	Houston	El Paso
Wet of OMC	Vertical	3.63 (6.2)	2.99 (7.0)	3.72 (7.2)	1.43 (5.7)	4.14 (13.7)	1.47 (10.6)
	Radial	1.95 (5.4)	1.95 (5.1)	1.93 (6.1)	1.51 (7.8)	1.63 (4.7)	0.81 (13.8)
	Volumetric	7.71 (1.9)	7.04 (1.5)	7.76 (2.0)	7.50 (2.4)	7.56 (3.7)	3.11 (10.6)
OMC	Vertical	9.28 (8.8)	6.98 (5.1)	6.92 (6.5)	7.37 (9.2)	6.71 (13.8)	2.43 (19.7)
	Radial	3.46 (11.1)	3.80 (7.8)	3.83 (8.3)	3.60 (8.2)	3.81 (10.6)	1.27 (22.0)
	Volumetric	16.97 (3.5)	15.27 (2.6)	14.84 (2.8)	15.25 (2.8)	14.99 (6.5)	5.04 (5.2)
Dry of OMC	Vertical	14.13 (15.3)	14.92 (17.8)	13.25 (16.4)	14.35 (14.3)	11.44 (18.4)	4.51 (29.2)
	Radial	4.26 (19.7)	5.93 (8.0)	5.42 (16.5)	5.36 (14.6)	4.49 (20.3)	1.76 (22.0)
	Volumetric	24.07 (4.8)	28.95 (5.9)	23.59 (8.2)	26.93 (5.2)	21.69 (11.7)	8.23 (14.1)

Note: Numbers in brackets indicate the coefficient of variation

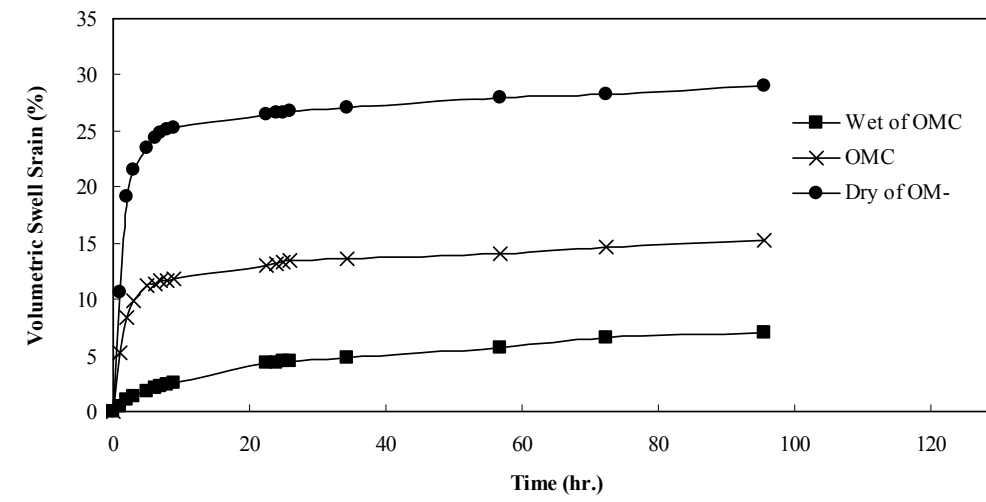
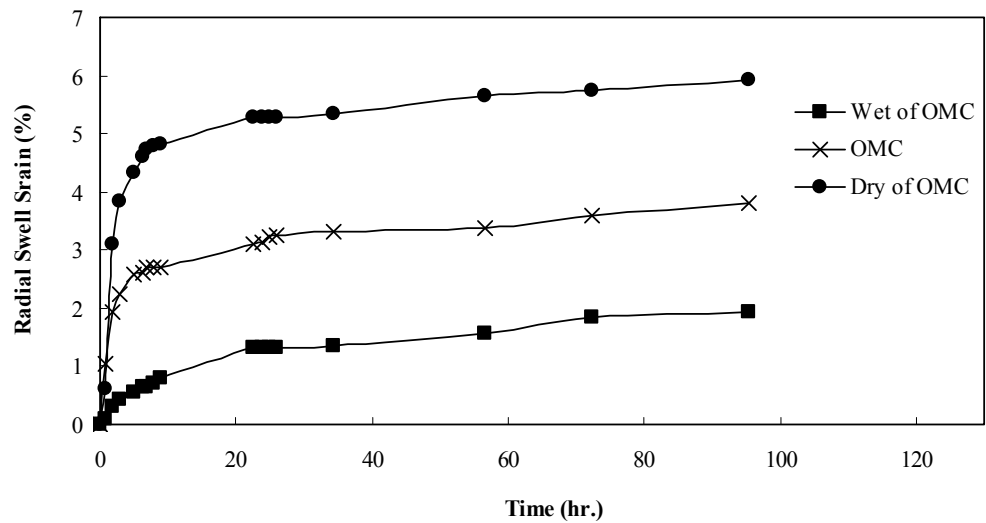
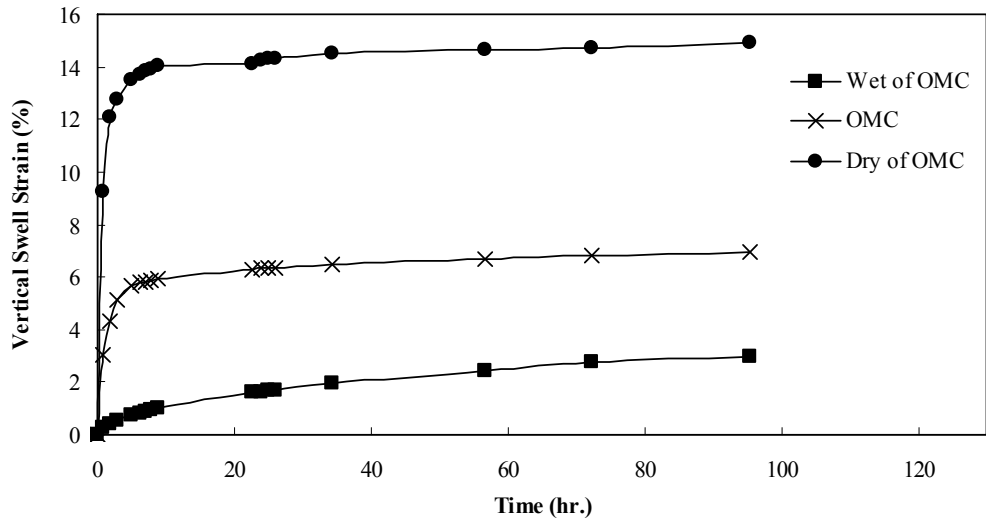


Figure 5.1 - Typical Swell Strains from 3-D Swell Tests for Different Moisture Contents

Table 5.14 - Swell Pressure Test Results

Moisture Condition	Swell Pressure (ksf)					
	Fort Worth	San Antonio	Bryan	Paris	Houston	El Paso
Wet of OMC	1.55	1.44	1.45	1.51	1.26	0.23
OMC	2.67	2.32	2.52	3.47	1.65	0.54
Dry of OMC	3.10	2.89	2.97	3.98	2.47	0.78

trend as other test results, with El Paso clay exhibiting the lowest swell pressure values than other clays, and Houston clay providing the lowest values among the high-PI clays. Still, the swell values measured for the Houston clay are considerable to pose the problem under field conditions.

As indicated before, the pressure plate method was used to measure soil matric suctions up to 1000 kPa and the filter paper method were then used for the ranges more than 1000 kPa. Although, filter paper method can evaluate both matric and total suctions (total suction is a summation of matric suction and osmotic suction), only the total suctions were measured with this approach. The measured total suction is considered as matric suction because, at high total suction levels (over 150 psi), the measured values are minutely affected by osmotic suction especially since the soils considered in this study contain very low amounts of salts or soluble sulfates (as shown in Table 5.3). The combined test results from pressure plate and filter paper methods are presented in the form of SWCCs in Figure 5.2 for all soils. The SWCCs of the high PI soils exhibited similar characteristics. The only noticeable difference is the saturated moisture content (at zero suction) for Houston clay, which is much lower than the other soils. This lower value indicates less ability to hold up water or moisture, which mean that they do not undergo large swelling when hydrated.

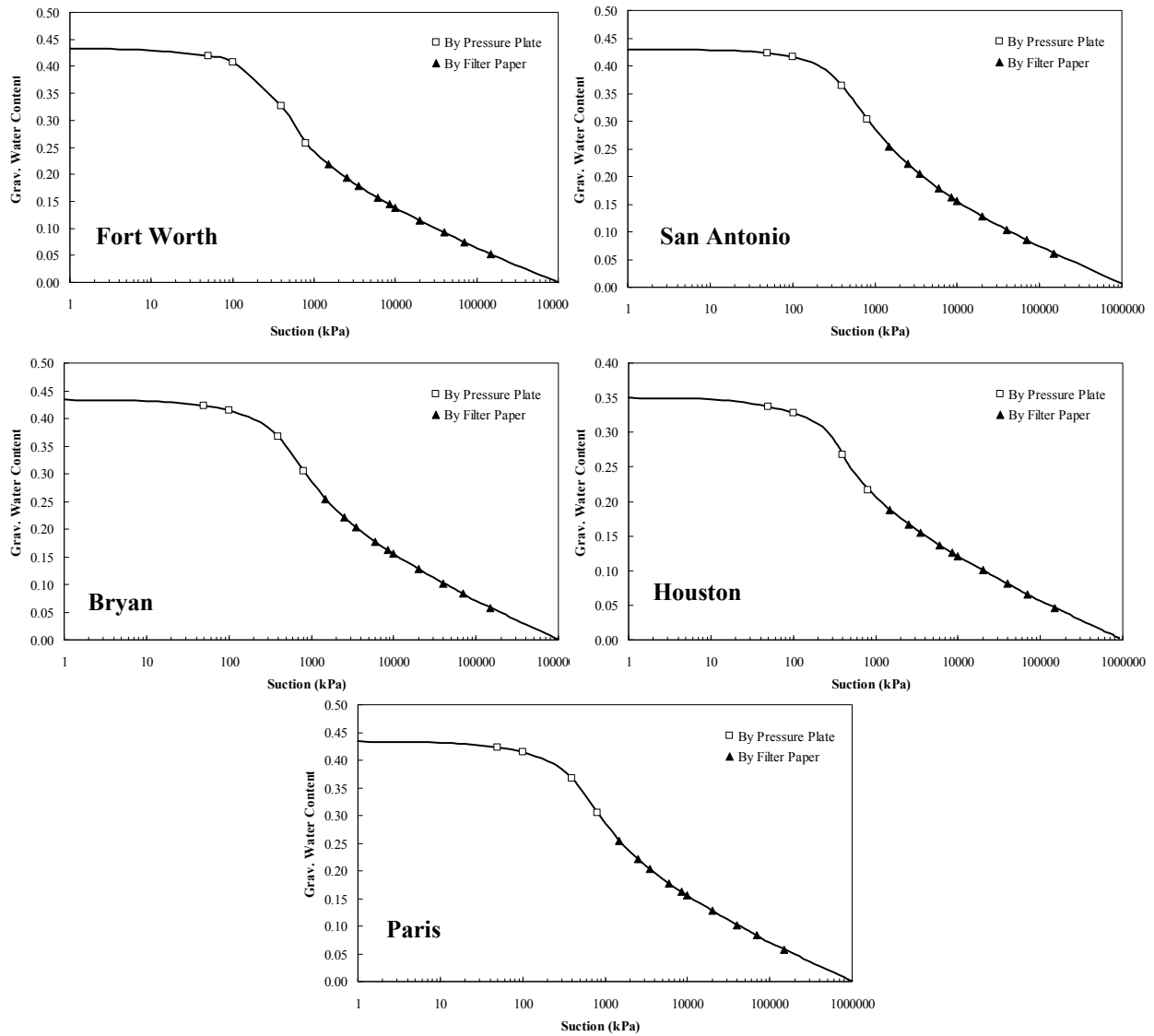


Figure 5.2 - Soil Water Characteristic Curves of Soils

CHAPTER 6 – DEVELOPMENT OF RELATIONSHIPS

6.1 INTRODUCTION

A number of parameters were measured with different moisture conditioning processes. These parameters were used to develop trends, relationships and models for estimating the changes in modulus and strains with moisture. The trends, relationships and models are discussed in this section. The process of developing models started with developing relationships among different measured parameters of clay materials, which is discussed through an example using the test data of clay material from Paris District. The detailed results can be found in the appendices for all soils. The developed relationships were then related to common soil properties such as, Plasticity Index, Liquid Limit, etc. The process was ultimately expanded to develop models that predict strain and modulus at different moisture content based on index properties. Each step in this procedure is explained next.

The main parameters used in establishing relationships are moisture content, seismic modulus and shrinkage and expansion strains. The relationships are presented for three different moisture conditioning processes represented in Figure 6.1. In the first process (called Dry-from-optimum, DFO), specimens were compacted at their corresponding optimum moisture contents and then subjected to drying. In the second process (saturated-from-optimum, SFO), specimens prepared at their optimum moisture contents were subjected to moisture conditioning to saturation. The third process (dry-from-saturated, DFS) consisted of moisture conditioning specimens prepared at their corresponding optimum moisture contents to saturation first and then drying the saturated specimens.

In Figure 6.1, the origin represents the optimum moisture content (OMC) and zero strain. As specimen is moisture conditioned, its moisture content increases with increase in expansion strain, which is represented as the SFO model. As specimen is subjected to drying process its moisture content decreases and shrinkage strain increases, which is represented as the DFO model. Drying after moisture conditioning process is also shown as the DFS model.

While developing the appropriate relationships, the moisture contents and moduli were first normalized, in order to generalize these relationships for different types of clay materials. Modulus was normalized by dividing the individual modulus by the modulus at OMC. Three different approaches were followed to normalize the moisture content. For the DFO process, the moisture contents were normalized by dividing the individual moisture content by the OMC

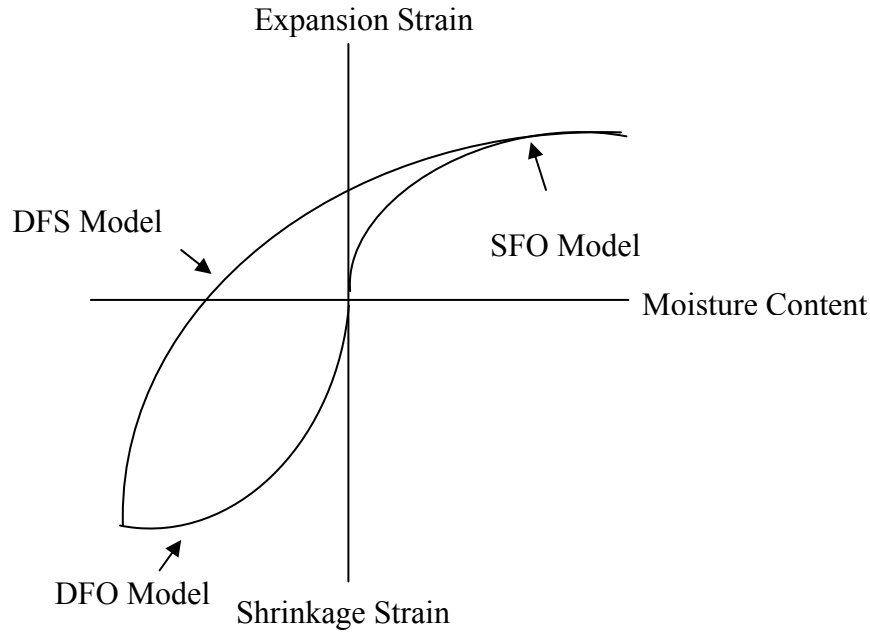


Figure 6.1 – Three Conditioning Processes

(Equation 6.1); whereas, for the SFO process the OMC values were subtracted from the individual moisture contents and then divided by the OMC (Equation 6.2). Similar approach was followed for the DFS process as employed for the SFO process. However, a factor of 1 was added to the normalized values to make sure that all values were positive (Equation 6.3) for ease in model development.

$$NMC_{DFO} = \frac{\text{Individual Moisture Content}}{OMC} \quad (6.1)$$

$$NMC_{SFO} = \frac{(\text{Individual Moisture Content} - OMC)}{OMC} \quad (6.2)$$

$$NMC_{DFS} = \frac{(\text{Individual Moisture Content} - OMC)}{OMC} + 1 \quad (6.3)$$

6.2 DRY FROM OPTIMUM PROCESS (DFO)

Typical variations in moisture content and modulus with time for one specimen are shown in Figure 6.2. The moisture content decreased for the first 400 hrs and then leveled off passed that time to 5% for this case. The modulus also increased for the first 400 hrs, after which it leveled off to a constant value of about 220 ksi. These trends are observed for all clay materials.

The variations in the vertical, lateral and volumetric shrinkage strains with time measured on the same specimen are shown in Figure 6.3. The patterns associated with the three strains are quite similar to that of the modulus in Figure 6.2. In this case, the specimen shrunk equally in lateral and vertical direction with the maximum shrinkage of 5%. The volumetric strain had a maximum value of 18%.

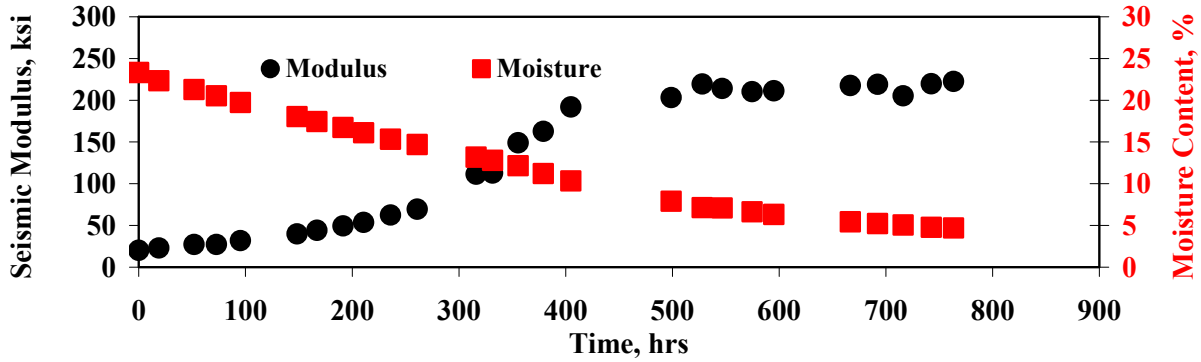


Figure 6.2 – Typical Variations in Moisture Content and Modulus with Time

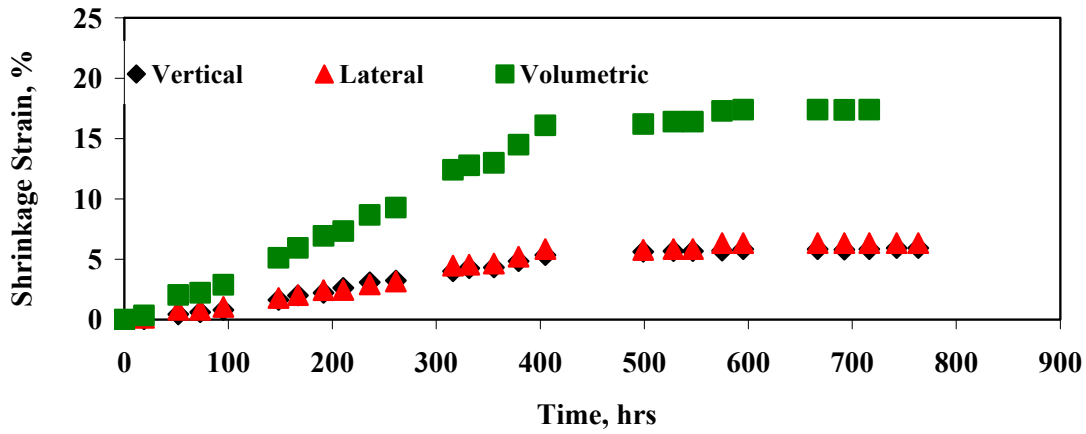


Figure 6.3 – Typical Variations in Shrinkage Strains with Time

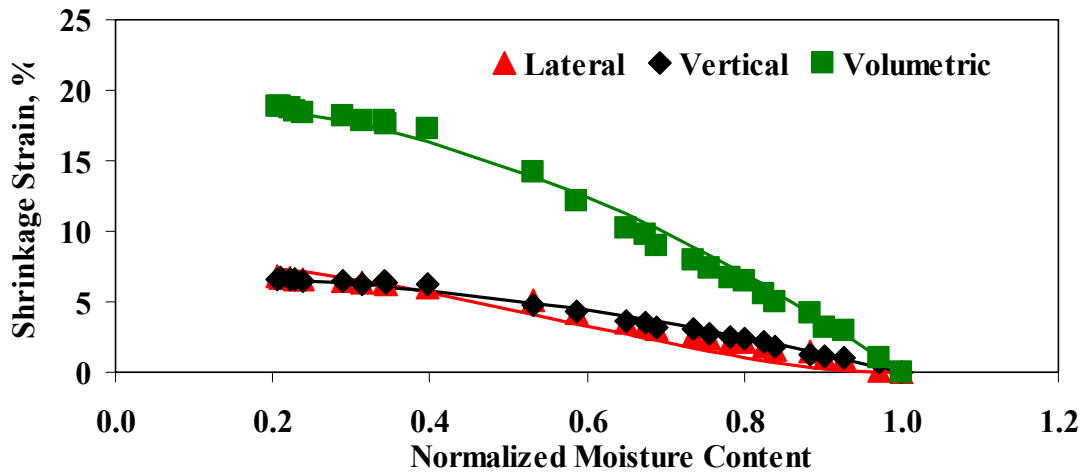


Figure 6.4 – Typical Variations in Shrinkage Strains with Normalized Moisture Content

The shrinkage strains are related to the NMC_{DFO} in Figure 6.4. The shrinkage strains and moisture content seem well correlated. A NMC_{DFO} of unity corresponds to OMC, and theoretically a NMC_{DFO} of zero corresponds to a completely dry soil. Shrinkage strains increase rapidly until NMC_{DFO} is decreased to 0.4 after which, it is almost constant.

A number of mathematical relationships can describe the relationships between the three shrinkage strains and the NMC_{DFO} . Based on extensive curve fitting analysis a relationship in the form of was selected

$$e_s = [A(1 - NMC_{DFO}^2)]^n \quad (6.4)$$

where e_s = shrinkage strain, and A is the parameter obtained from curve fitting. Figure 6.4 also shows the best fit curves obtained using Equation 6.4. The best fit curves follow the measured data quite well. The values of A for the three shrinkage strains are summarized in Table 6.1. All three modes of shrinkages correlated well with the NMC_{DFO} since the R^2 values were close to 1.

The variation in normalized modulus with NMC_{DFO} is shown in Figure 6.5 The normalized modulus increases till the NMC_{DFO} decreases to 0.4; after which it is almost a constant. In this case, the maximum normalized modulus at a “dry condition” was approximately 9, which indicates that upon the drying process modulus increased 9 times as compared to its value at the OMC. A relationship in the following form was selected

$$E_n = (B + (-C) \times NMC_{DFO}^2) \quad (6.5)$$

where E_n = normalized modulus, and B and C are the parameters obtained from curve fitting. The values of B and C for are summarized in Table 6.2.

Table 6.1 – Typical Best Fit Parameters for Shrinkage Strain vs. Normalized Moisture Content, NMC_{DFO}

Mode of Shrinkage	Parameter A	R^2
Vertical	6.89	0.98
Lateral	2.83	0.96
Volumetric	19.41	0.99

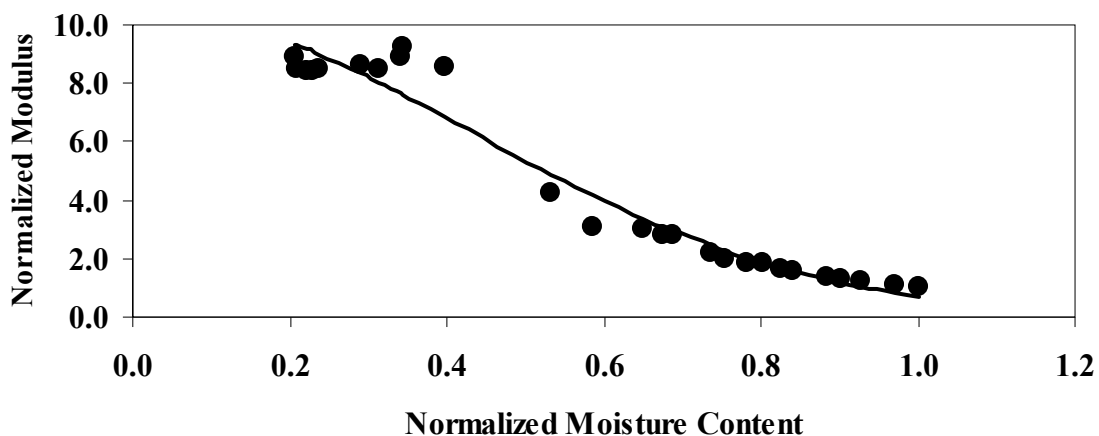


Figure 6.5 – Typical Variation in Modulus with Moisture Content (DFO Process)

Table 6.2 – Typical Best Fit Parameters between Normalized Modulus and Normalized Moisture Content (DFO)

Parameter B	Parameter C	R ²
2.35	2.69	0.94

The normalized modulus and the three shrinkage strains are related as shown in Figure 6.6. The normalized modulus increases until the lateral and vertical shrinkage strain reaches 6%; after which it is almost constant. The model in the form of Equation 6.6 was used to develop this relationship.

$$E_n = \text{EXP}(D * e_s) \quad (6.6)$$

where D is the empirical best-fit parameter and e_s is shrinkage strain. The values of D for the three shrinkage strains are summarized in Table 6.3. The normalized modulus was well correlated to all three modes of shrinkage strains with R² values were more than 0.99.

6.3 SATURATED FROM OPTIMUM PROCESS (SFO)

Typical variation in seismic modulus and moisture content with time for one specimen is shown in Figure 6.7. The moisture content increases from 24% to 39% in less than 8 hours. The modulus initially increases from 12 ksi to 37 ksi in about four hours and after which it starts decreasing and becomes less than 10 ksi after about 6 hours. These trends are observed for most of the materials.

The variations in the vertical, lateral and volumetric expansion strains with time measured on the same specimens are shown in Figure 6.8. The maximum lateral expansion strain of this clay was about 1.5% whereas; the vertical expansion was about 6%. The maximum volumetric expansion strain reported for this specimen was about 7%.

The relationships of expansion strains and the normalized moisture content parameter NMC_{SFO} (as defined in Equation 6.2) are shown in Figure 6.9. The NMC_{SFO} of zero corresponds to OMC. For this particular specimen the NMC_{SFO} of 0.5 corresponds to a saturated specimen. With increase in the moisture content, the vertical and volumetric expansion strains also increased substantially to 4% and 7% respectively. The appropriate relationship found for estimating the expansion strain is in the form of

$$e_e = [E * \text{NMC}_{\text{SFO}} (1 - \text{NMC}_{\text{SFO}})]^2 \quad (6.7)$$

where e_e is the expansion strain and E is the parameter obtained from curve fitting. Figure 6.9 also shows the best fit curves obtained using Equation 6.7. The best fit curves follow the measured data quite well. The values of E for the three expansion strains are summarized in Table 6.4. All three expansion strains correlated moderately well with the NMC_{SFO} since the R² values were more than 0.78.

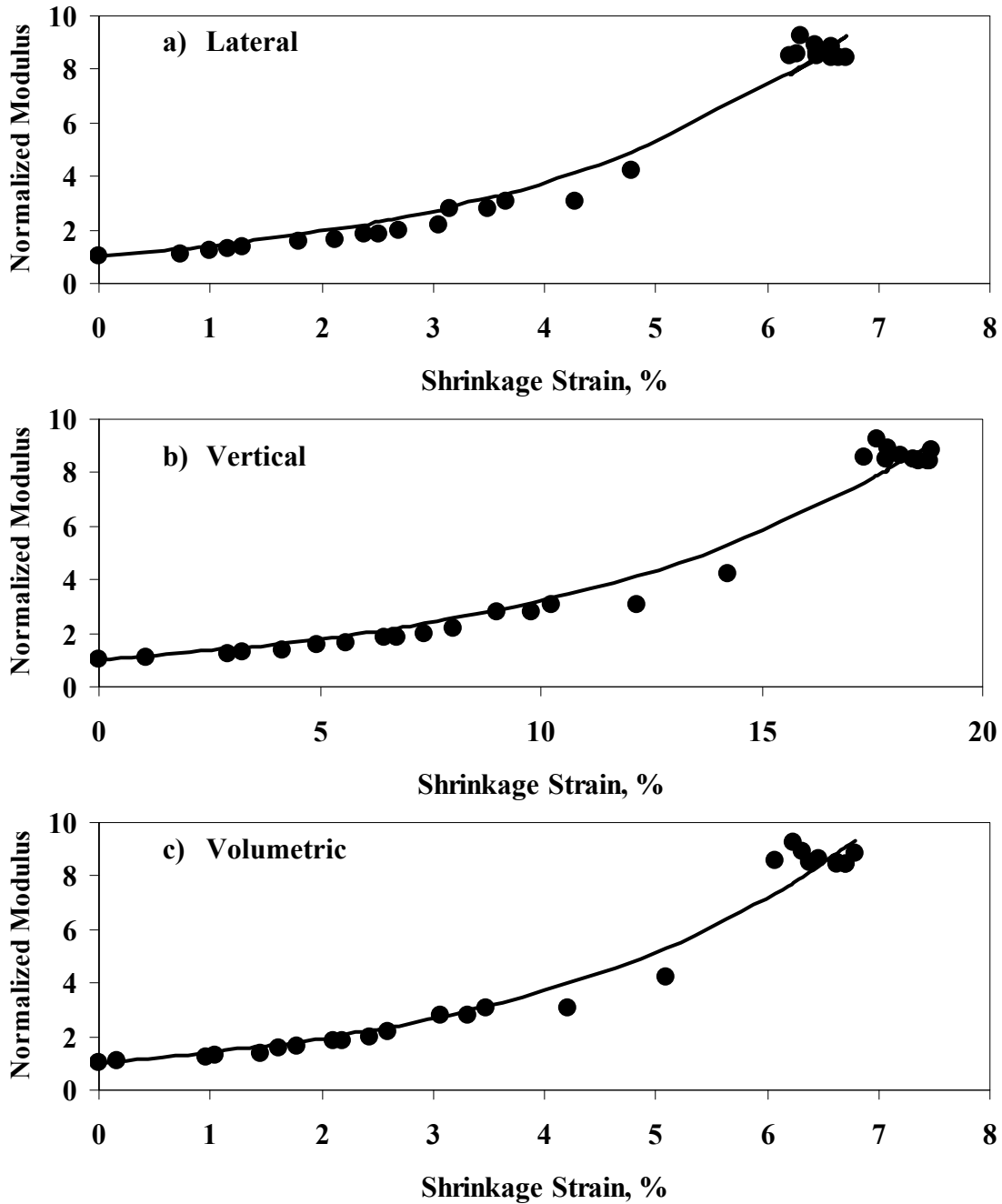


Figure 6.6 – Typical Variations in Modulus with Shrinkage Strains

Table 6.3 – Typical Best Fit parameters between Normalized Modulus and Shrinkage Strains

Mode of Shrinkage	Parameter D	R ²
Vertical	0.35	0.992
Lateral	0.36	0.992
Volumetric	0.12	0.994

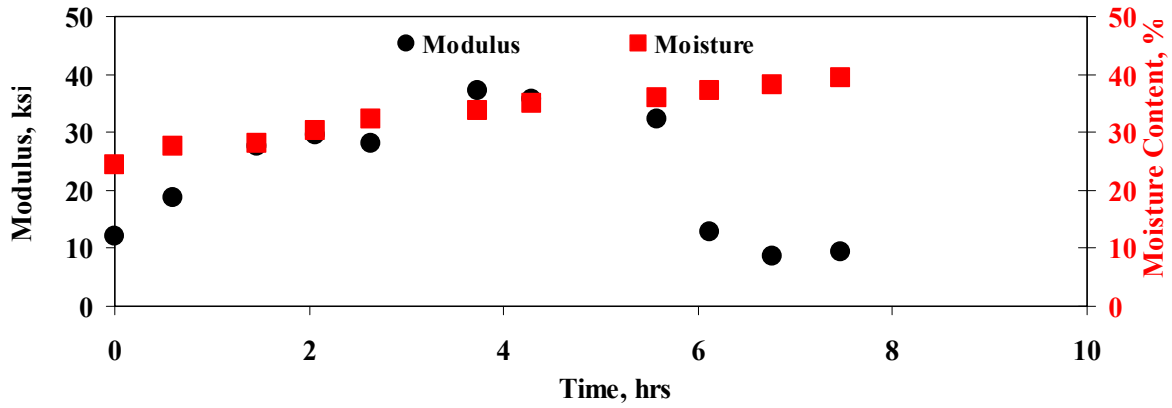


Figure 6.7 – Typical Variations in Moisture Content and Modulus with Time (Wetting Process)

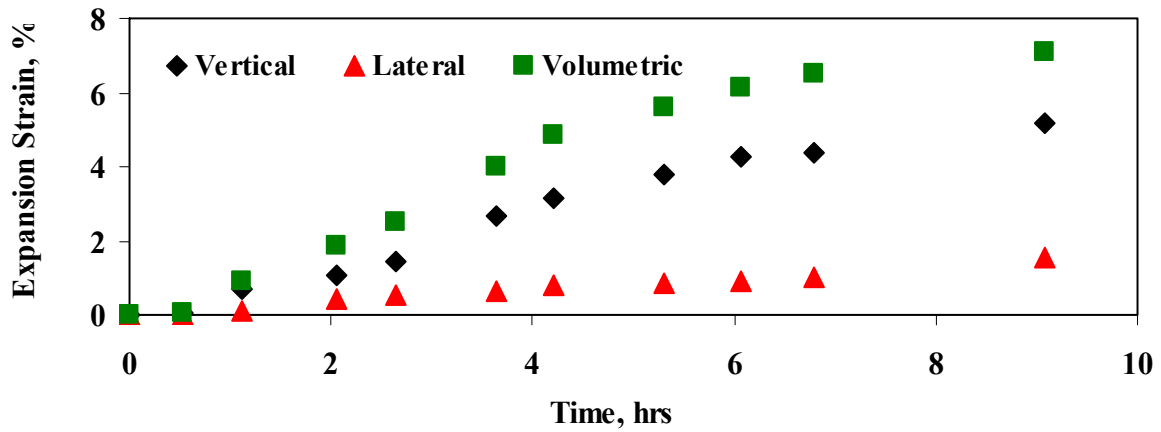


Figure 6.8 – Typical Variations in Expansion Strains with Time

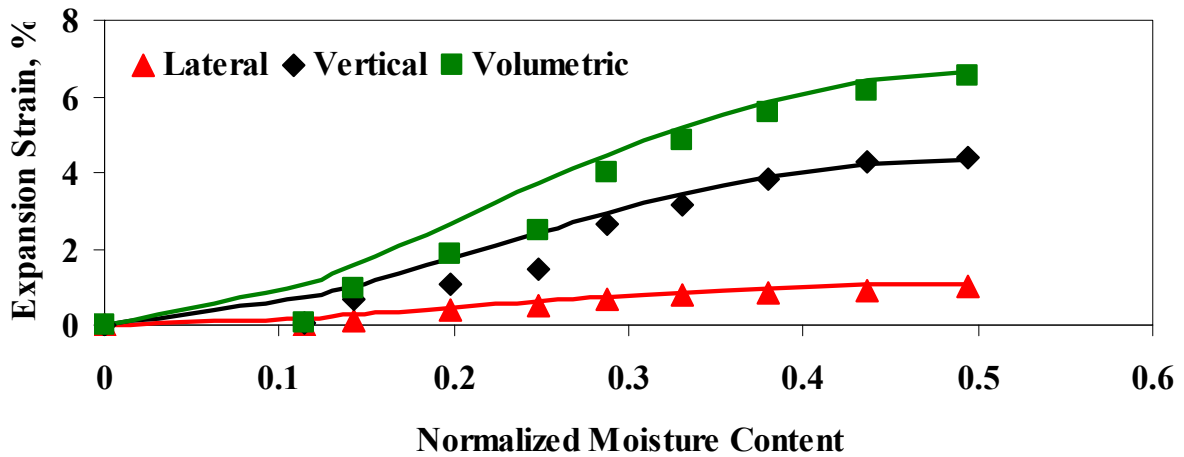


Figure 6.9 – Typical Variations in Expansion Strains with Normalized Moisture Content (NMC_{SFO})

Table 6.4 – Typical Best Fit Parameters (Expansion Strain vs. Normalized Moisture Content, NMC_{SFO})

Mode of Expansion	Parameter E	R^2
Vertical	9.09	0.86
Lateral	4.13	0.78
Volumetric	10.89	0.84

The variation in normalized modulus with NMC_{SFO} is shown in Figure 6.10. The normalized modulus initially increases till the NMC_{SFO} increases to 0.4, after which the normalized modulus starts decreasing until it almost becomes close to 0.5 at a NMC_{SFO} of about 0.65. An inverse polynomial (Equation 6.8) was finally selected to describe this relationship.

$$E_n = \frac{1}{(1 + (-F) \times NMC_{SFO}^{1.5} + G \times NMC_{SFO}^{2.5})} \quad (6.8)$$

where parameters F and G are obtained from curve fitting. The values of F and G are summarized in Table 6.5. The best fit curve as shown in Figure 6.10 describes the measured data moderately well.

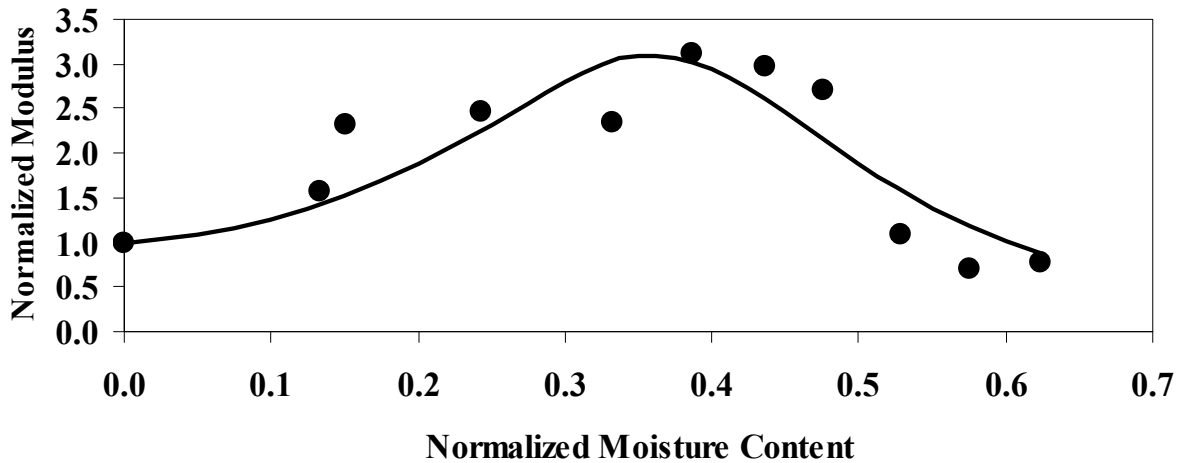


Figure 6.10 – Typical Variation in Seismic Modulus with Normalized Moisture Content (NMC_{SFO})

Table 6.5 – Typical Best Fit Parameters between Normalized Modulus and Normalized Moisture Content (NMC_{SFO})

Parameter F	Parameter G	R^2
7.80	12.97	0.75

The normalized modulus and the three expansion strains are well related as shown in Figure 6.11. With increase in the expansion strain, the normalized modulus initially increases, reaches a peak value and then starts decreasing again. The normalized modulus, E_n , was related to the Expansion strains, ϵ_s , using a model in the form of

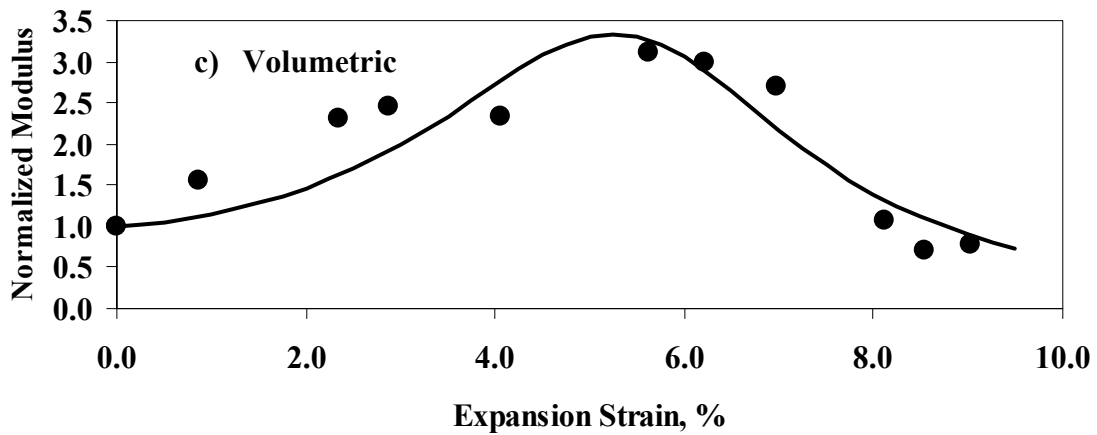
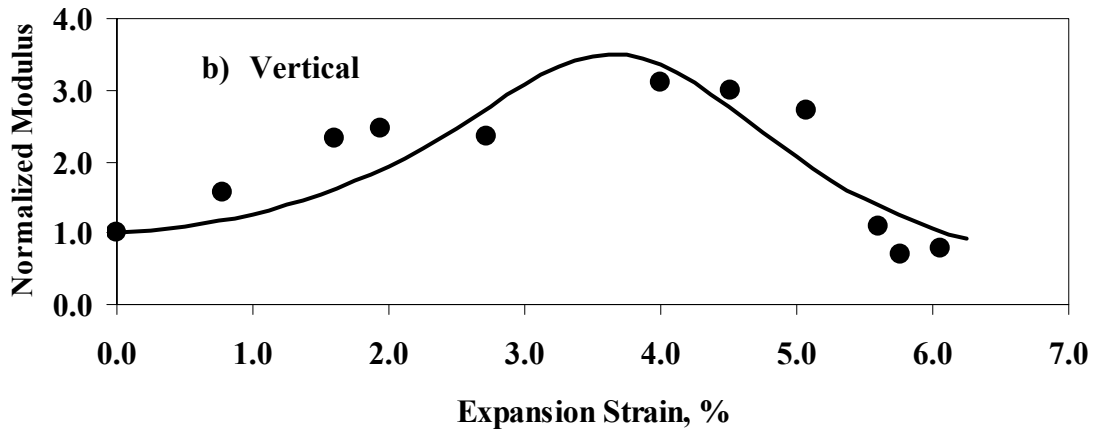
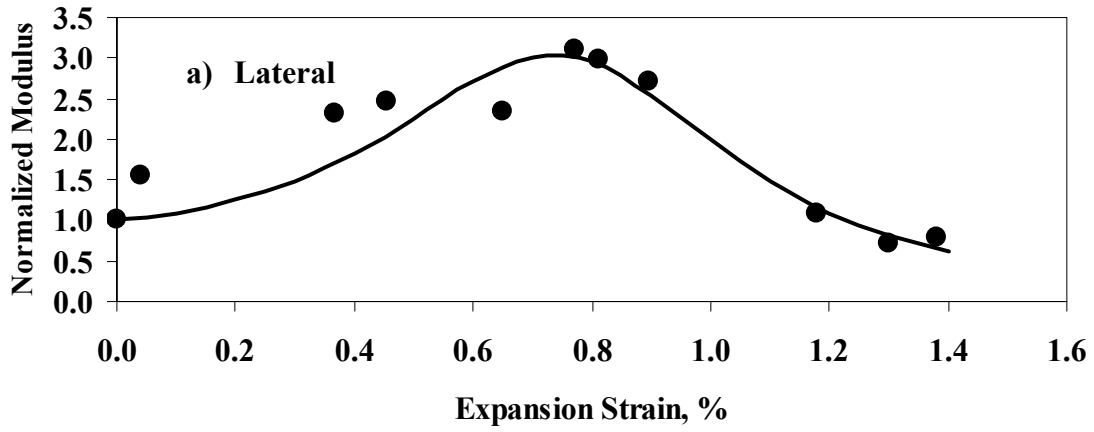


Figure 6.11 – Typical Variations in Modulus with Expansion Strains

$$E_n = \frac{1}{(1 + (-H) \times e^{1.5} + I \times e^{2.5})} \quad (6.9)$$

where H and I are the empirical best-fit parameters. The values of H and I for the three expansion strains are summarized in Table 6.6. The normalized modulus is moderately well correlated to all three modes of expansion strains with R² values are more than 0.75, and as reflected in Figure 6.11.

Table 6.6 – Typical Best Fit parameters between Normalized Modulus and Expansion Strains

Mode of Expansion	Parameter H	Parameter I	R ²
Vertical	0.26	0.04	0.75
Lateral	2.64	2.15	0.88
Volumetric	0.15	0.02	0.81

6.4 DRY FROM SATURATION PROCESS (DFS)

Typical variation in seismic modulus and moisture content with time for one specimen is shown in Figure 6.12. Time zero corresponds to the time that the drying of the specimen begun after saturation. The moisture content rapidly decreases from 40% to 12% in the first 200 hours after that it steadily decreases to 0.6% in the next 400 hours. The modulus initially increases slowly from 10 ksi to 20 ksi in about 400 hours and after which it rapidly increases to 35ksi and remains constant even after 550 hours. These trends are observed for most of the materials.

The variations in the vertical, lateral and volumetric shrinkage strains with time measured on the same specimens are shown in Figure 6.13. The lateral and vertical shrinkage strains of this clay were about 12%, whereas the volumetric shrinkage was up to 30% at the end of 550 hours.

The relationships of shrinkage strains and NMC_{DFS} (as described in Equation 6.3) are shown in Figure 6.14. The shrinkage strain initially increases rapidly and then becomes almost constant as the specimen gets completely dried. The following relationship was selected to relate these two parameters

$$e_s = \text{EXP}[J(1 - \text{NMC}_{\text{DFS}}^3)] \quad (6.10)$$

where e_s is the shrinkage strain and J is the parameter obtained from curve fitting. Figure 6.14 also shows the best fit curves obtained using Equation 6.10. The best fit curves follow the measured data quite well. The values of J for the three shrinkage strains are summarized in Table 6.7. All three modes of shrinkage correlated well with the NMC_{DFS} since the R² values were close to 1.

The variation in normalized modulus with NMC_{DFS} is shown in Figure 6.15. The normalized modulus initially decreases rapidly till the NMC_{DFS} becomes 0.5 after which the change is quite gradual.

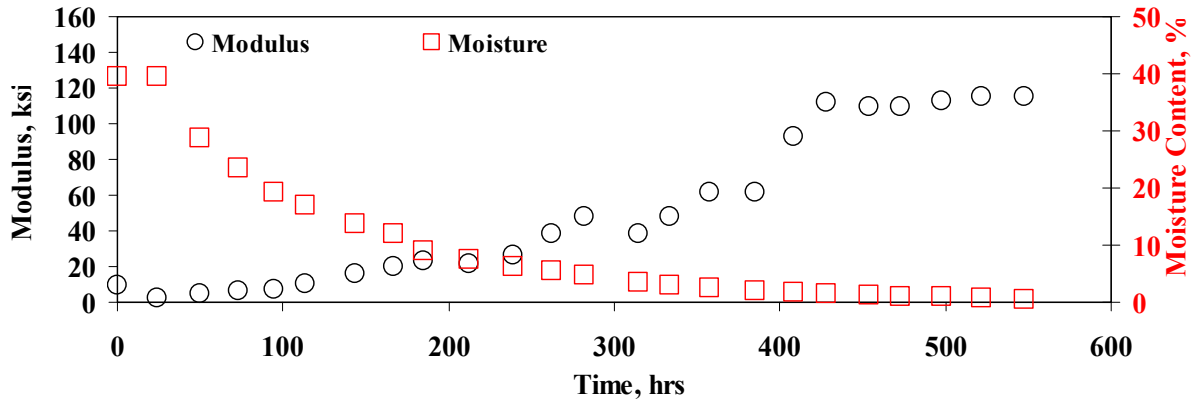


Figure 6.12 – Typical Variations in Moisture Content and Modulus with Time

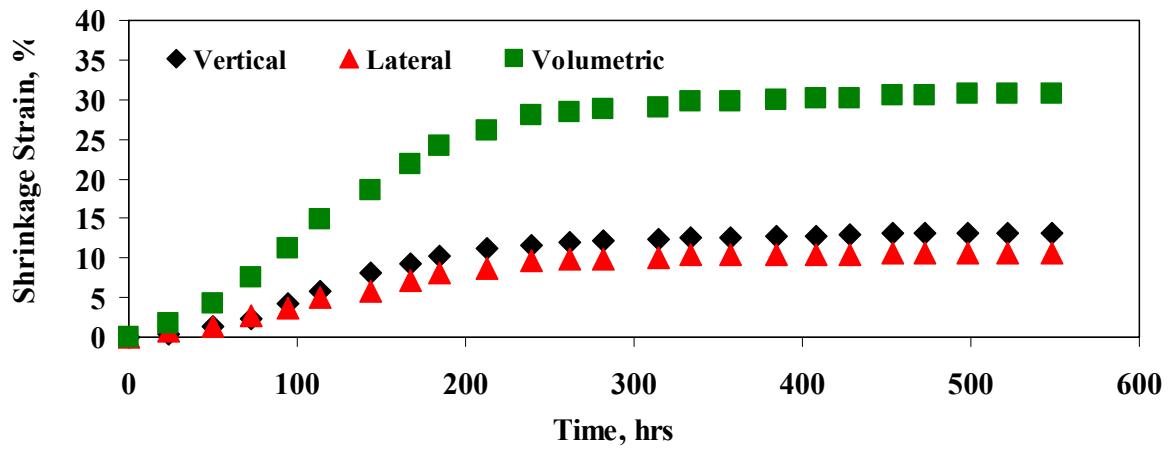


Figure 6.13 – Typical Variations in Expansion Strains with Time

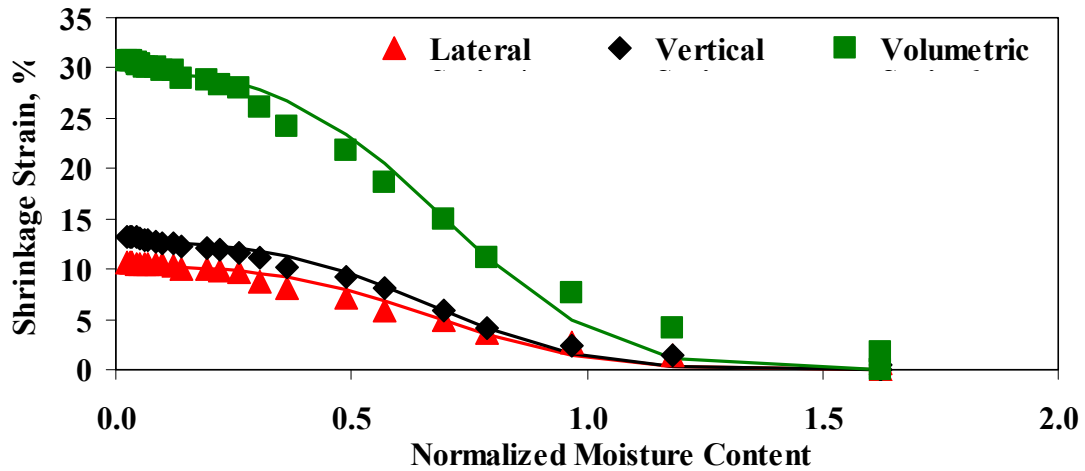


Figure 6.14 – Typical Variations in Shrinkage Strains with Normalized Moisture Content (NMC_{DFS})

Table 6.7 – Typical Best Fit Parameters between Shrinkage Strain and Normalized Moisture Content (DFS)

Mode of Shrinkage	Parameter J	R ²
Vertical	2.60	0.98
Lateral	2.38	0.99
Volumetric	3.47	0.94

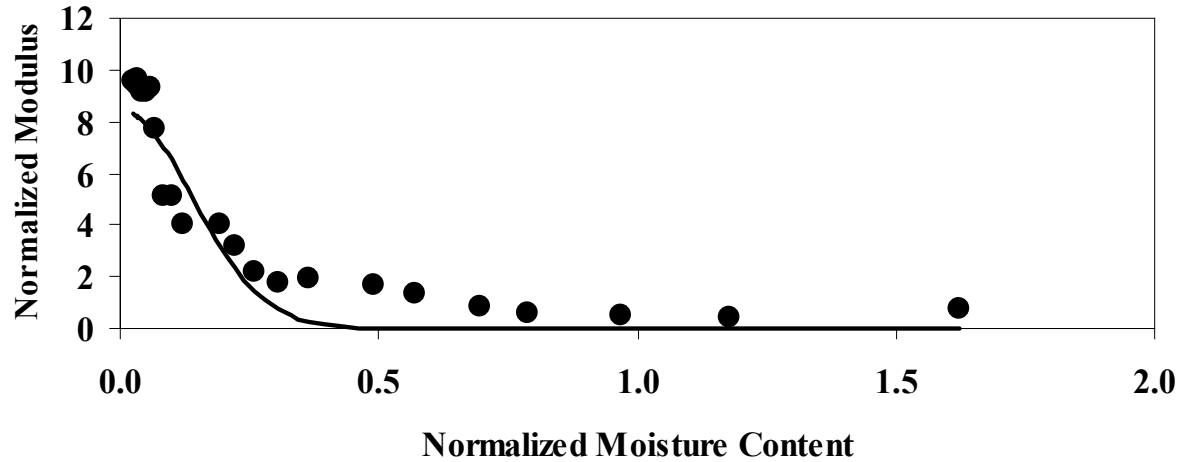


Figure 6.15 – Typical Variation in Normalized Modulus with Normalized Moisture Content (NMCDFS)

The relationship that was selected is in the form of

$$E_n = \text{EXP}(K + (-L) \text{NMC}_{\text{DFS}}^2) \quad (6.11)$$

where K and L are the parameters obtained from curve fitting. The values of K and L for are summarized in Table 6.8.

Table 6.8 – Typical Best Fit Parameters between Normalized Modulus and Normalized Moisture Content

Parameter K	Parameter L	R ²
2.13	26.01	0.88

The normalized modulus and the three shrinkage strains are also related as shown in Figure 6.16. The normalized modulus initially increases slowly with increase in shrinkage strain. A rapid increase in normalized modulus was recorded for last couple of percent increase in shrinkage strain. The same trend was observed for all clay materials. The normalized modulus, E_n , was then related to the Expansion strains, ϵ_s , using a model in the form of

$$E_n = \text{EXP}((-M) + N * \epsilon_s^2) \quad (6.12)$$

where M and N are the empirical best-fit parameters. The values of M and N for the three shrinkage strains are summarized in Table 6.9. The R² values were greater than 0.87.

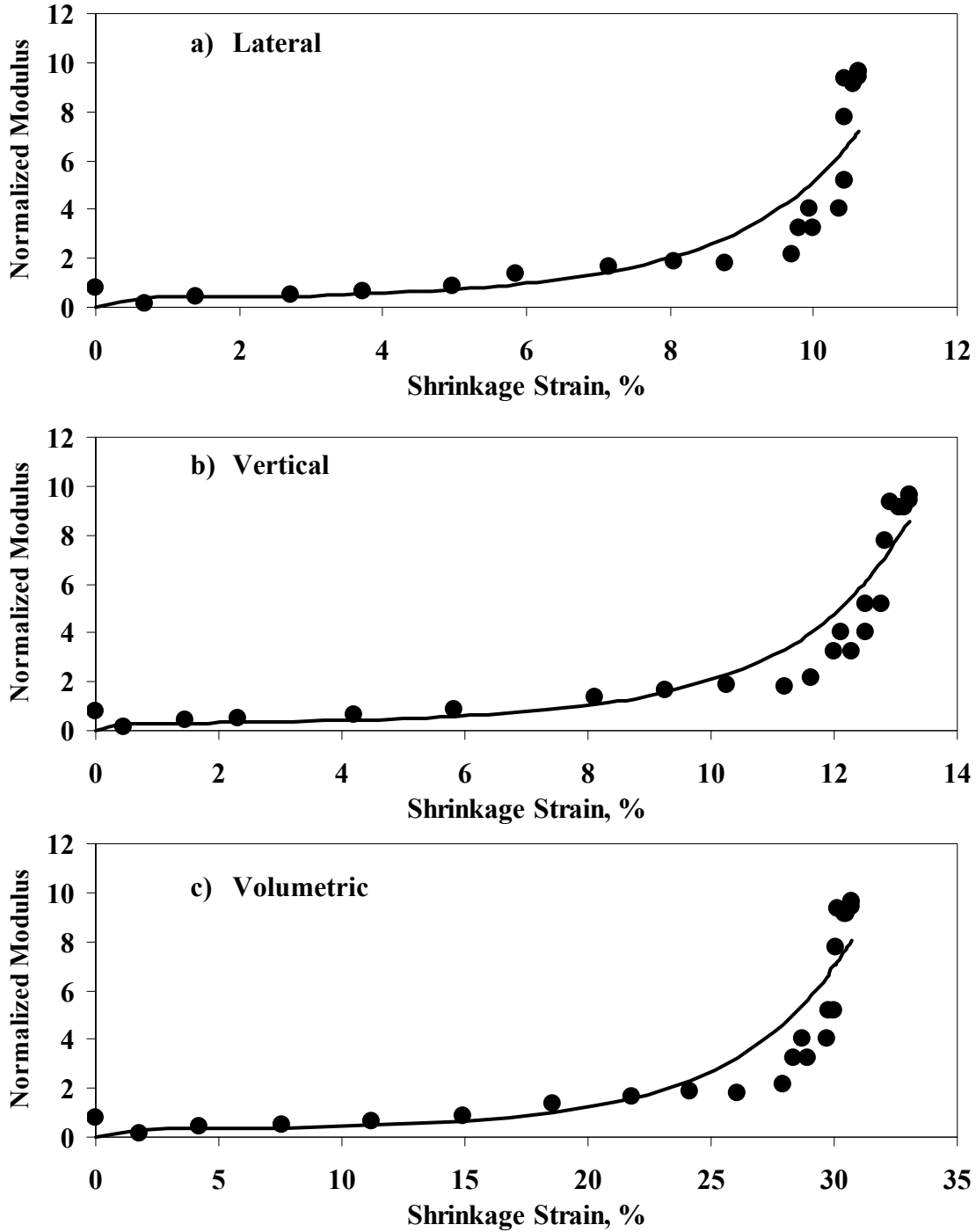


Figure 6.16 – Typical Variations in Modulus with Expansion Strains

Table 6.9 – Typical Best Fit parameters between Normalized Modulus and Expansion Strains

Mode of Shrinkage	Parameter M	Parameter N	R ²
Vertical	3.76	0.03	0.93
Lateral	5.34	0.07	0.87
Volumetric	5.85	0.01	0.91

To summarize all the results, the equations used to describe all relationships are presented in Table 6.10. The equations highlighted in gray are further used to develop models predicting strain and modulus values. After establishing relationships for all tested specimens, the parameters of equations are summarized in Tables 6.11 to 6.19. Each table provides the parameters for the equations in Table 6.17 for all soil types tested. Also, the R^2 values reported in all tables are typically greater than 0.95, indicating that relationships introduced in Equation 6.4 through 6.12 are appropriate. Detailed description of development of models is presented in following section.

Table 6.10 – Summary of Equations Used to Establish Relationships

Moisture condition	Clay Parameters			Curve-fit Equation
	Y-Axis		X-Axis	
DFO	Shrinkage Strain	Lat.	Normalized Moisture Content	$e_s=[A(1-NMC_{DFO}^2)]^2$
		Ver.		$e_s=[A(1-NMC_{DFO}^2)]$
		Vol.		$e_s=[A(1-NMC_{DFO}^2)]$
	Normalized Modulus		Normalized Moisture Content	$E_n = EXP[B+ (-C)*NMC_{DFO}^2]$
	Normalized Modulus		Lat Ver. Vol.	Shrinkage Strain
SFO	Expansion Strain	Lat	Normalized Moisture Content	$e_e=[E*NMC_{SFO}(1-NMC_{SFO})]^2$
		Ver.		
		Vol.		
Normalized Modulus		Normalized Moisture Content	$E_n = \frac{1}{(1+(-F) \times NMC_{SFO}^{1.5} + G \times NMC_{SFO}^{2.5})}$	
Normalized Modulus		Lat Ver. Vol.	Expansion Strain	$\left[E_n = \frac{1}{(1 + (-H) \times e_e^{1.5} + I \times e_e^{2.5})} \right]$
DFS	Shrinkage Strain	Lat	Normalized Moisture Content	$e_s=EXP[J(1-NMC_{DFS}^3)]$
		Ver.		
		Vol.		
Normalized Modulus		Normalized Moisture Content	$E_n=EXP(K+(-L)NMC_{DFS}^2)$	
Normalized Modulus		Lat Ver. Vol.	Shrinkage Strain	$E_n=EXP((-M)+Ne_s^2)$

Table 6.11 –Best Fit Parameters (Shrinkage Strains vs. NMC_{DFO})

Material	Vertical		Lateral		Volumetric	
	A	R ²	A	R ²	A	R ²
El Paso PI = 16	0.87	0.92	1.53	0.87	5.09	0.97
	1.21	0.92	1.53	0.89	5.39	0.99
	1.63	0.91	1.56	0.94	5.81	0.99
San Antonio PI = 26	4.76	0.99	2.33	0.98	13.76	0.98
	4.78	0.97	2.25	0.97	13.27	0.98
	5.16	0.99	2.37	0.99	14.49	0.97
Fort Worth PI = 29	5.72	0.99	2.57	0.98	17.08	0.99
	5.99	0.98	2.52	0.97	16.86	0.99
	5.80	0.97	2.51	0.99	16.71	0.98
Bryan PI = 31	4.27	0.92	2.29	0.97	13.02	0.97
	4.79	0.95	2.38	0.92	13.73	0.99
	6.28	0.85	2.43	0.91	15.90	0.98
Houston PI = 35	5.14	0.98	2.56	0.92	15.63	0.99
	5.25	0.97	2.64	0.92	16.53	0.99
	5.41	0.96	2.59	0.96	16.60	0.98
Paris PI = 36	6.89	0.98	2.83	0.96	19.41	0.99
	6.02	0.96	2.75	0.98	17.86	0.96
	5.96	0.97	2.68	0.93	17.28	0.98

Table 6.12 –Best Fit Parameters (Normalized Modulus and NMC_{DFO})

Material	B	C	R ²
El Paso PI = 16	3.56	6.89	0.97
	3.57	5.90	0.98
	0.04	0.73	0.99
San Antonio PI = 26	1.76	1.91	0.99
	1.86	1.97	0.96
	1.78	2.00	0.97
Fort Worth PI = 29	2.74	2.97	0.99
	2.68	2.94	0.98
	2.65	3.11	0.97
Bryan PI = 31	2.07	2.12	0.91
	2.30	3.07	0.92
	2.16	2.93	0.94
Houston PI = 35	2.61	2.73	0.95
	2.76	3.78	0.97
	2.89	3.53	0.97
Paris PI = 36	2.35	2.69	0.94
	2.56	2.75	0.92
	2.33	2.50	0.82

Table 6.13 –Best Fit Parameters (Normalized Modulus vs. Shrinkage Strains after DFO Process)

Material	Vertical		Lateral		Volumetric	
	D	R ²	D	R ²	D	R ²
El Paso PI = 16	3.64	0.97	1.57	0.70	0.662	0.82
	2.66	0.85	1.61	0.84	0.629	0.85
	1.97	0.73	1.46	0.94	0.546	0.93
San Antonio PI = 26	0.36	0.99	0.35	0.98	0.123	0.99
	0.38	0.96	0.40	0.97	0.138	0.97
	0.33	0.97	0.33	0.94	0.116	0.96
Fort Worth PI = 29	0.47	0.99	0.44	0.99	0.158	0.99
	0.44	0.98	0.43	0.99	0.154	1.00
	0.44	0.99	0.42	0.99	0.153	0.99
Bryan PI = 31	0.46	0.90	0.43	0.84	0.154	0.87
	0.43	0.93	0.46	0.87	0.157	0.90
	0.33	0.98	0.42	0.87	0.140	0.95
Houston PI = 35	0.54	0.98	0.45	0.95	0.17	0.97
	0.49	0.98	0.44	0.91	0.16	0.93
	0.51	0.99	0.46	0.96	0.17	0.97
Paris PI = 36	0.33	0.97	0.33	0.95	0.117	0.96
	0.41	0.97	0.38	1.00	0.139	1.00
	0.37	0.78	0.37	0.82	0.130	0.81

Table 6.14 –Best Fit Parameters (Expansion Strain and NMC_{SFO})

Material	Vertical		Lateral		Volumetric	
	E	R ²	E	R ²	E	R ²
El Paso PI = 16	1.40	0.55	2.35	0.90	5.06	0.91
	3.68	0.97	1.30	0.77	4.12	0.99
	4.80	0.97	3.10	0.93	6.51	0.99
San Antonio PI = 26	8.74	0.43	3.61	0.52	10.18	0.45
	8.87	0.82	3.07	0.75	9.92	0.80
	9.34	0.19	4.70	0.19	11.57	0.19
Fort Worth PI = 29	6.70	0.84	3.62	0.97	8.62	0.95
	6.97	0.77	3.75	0.94	8.98	0.89
	6.35	0.90	4.12	0.97	8.77	0.98
Bryan PI = 31	7.62	0.98	4.90	0.98	10.38	0.99
	9.23	0.94	5.42	0.97	12.10	0.98
	9.96	0.93	5.56	0.97	12.78	0.95
Houston PI = 35	8.23	0.96	4.26	0.90	10.27	0.95
	7.51	0.58	4.03	0.69	9.50	0.62
	8.42	0.96	4.30	0.89	10.47	0.95
Paris PI = 36	9.09	0.86	4.13	0.78	10.89	0.84
	8.35	0.88	4.18	0.76	10.30	0.85
	9.68	0.87	4.35	0.81	11.57	0.86

Table 6.15 –Best Fit Parameters (Normalized Modulus and NMC_{SFO})

Material	F	G	R²
El Paso PI = 16	25.04	91.45	0.87
	34.83	143.12	0.80
	43.23	216.13	0.77
San Antonio PI = 26	6.77	10.61	0.89
	7.53	12.85	0.92
	5.29	7.20	0.90
Fort Worth PI = 29	9.14	20.36	1.00
	9.93	22.92	0.85
	9.55	29.31	0.95
Bryan PI = 31	12.78	42.05	0.59
	24.89	104.62	0.92
	22.55	84.42	0.97
Houston PI = 35	14.46	43.31	0.97
	10.43	24.54	0.98
	11.56	31.37	0.95
Paris PI = 36	7.80	12.97	0.75
	8.40	14.82	0.92
	8.46	14.67	0.80

Table 6.16 –Best Fit Parameters (Normalized Modulus and Expansion Strain after SFO Process)

Material	Vertical			Lateral			Volumetric		
	H	I	R²	H	I	R²	H	I	R²
El Paso PI = 16	143.78	1525.27	0.09	51.77	256.58	0.79	4.20	4.27	0.78
	13.47	30.84	0.39	195.62	2578.67	0.58	10.61	20.31	0.50
	8.83	15.08	0.55	52.75	298.95	0.88	4.20	4.41	0.71
San Antonio PI = 26	0.27	0.05	0.68	3.90	4.27	0.83	0.18	0.02	0.76
	0.28	0.05	0.90	6.65	10.42	0.77	0.20	0.03	0.89
	0.20	0.03	0.83	1.79	1.11	0.78	0.11	0.01	0.81
Fort Worth PI = 29	0.68	0.26	0.92	4.74	5.94	0.92	0.35	0.08	0.95
	0.55	0.19	0.84	3.83	4.78	0.89	0.28	0.06	0.87
	8.49	24.47	0.93	3.77	4.41	0.79	0.35	0.10	1.00
Bryan PI = 31	0.70	0.28	0.91	3.50	4.25	0.81	0.31	0.07	0.87
	0.69	0.27	0.93	2.80	2.67	0.92	0.29	0.06	0.95
	0.51	0.14	0.92	2.95	2.75	0.90	0.24	0.04	0.91
Houston PI = 35	0.61	0.22	0.92	5.15	7.56	0.96	0.34	0.08	0.95
	0.84	0.35	0.89	4.36	5.73	0.79	0.37	0.09	0.85
	0.41	0.12	0.85	3.49	4.32	0.91	0.22	0.04	0.88
Paris PI = 36	0.26	0.04	0.74	2.64	2.15	0.88	0.15	0.02	0.81
	0.32	0.06	0.82	2.69	2.23	0.84	0.18	0.02	0.88
	0.24	0.04	0.81	2.75	2.19	0.80	0.14	0.02	0.82

Table 6.17 –Best Fit Parameters (Shrinkage Strain and NMC_{DFS})

Material	Vertical		Lateral		Volumetric	
	J	R ²	J	R ²	J	R ²
El Paso PI = 16	0.44	0.71	0.88	0.98	1.71	0.97
	0.53	0.78	1.38	0.93	2.24	0.94
	0.37	0.84	1.60	0.94	1.90	0.97
San Antonio PI = 26	2.21	1.00	2.25	0.96	3.25	0.95
	2.23	0.99	2.02	1.00	3.13	0.98
	2.26	0.98	2.17	0.98	3.25	0.94
Fort Worth PI = 29	2.32	0.99	2.30	0.97	3.33	0.93
	2.22	1.00	2.15	0.99	3.21	0.96
	2.12	0.99	2.28	0.97	3.25	0.95
Bryan PI = 31	2.23	1.00	2.12	1.00	3.20	0.98
	2.23	1.00	2.11	1.00	3.21	0.97
	2.19	0.98	2.17	0.99	3.20	0.99
Houston PI = 35	2.26	0.99	2.14	0.99	3.21	0.99
	2.06	0.95	2.04	0.97	3.15	1.00
	2.29	1.00	2.14	1.00	3.22	0.97
Paris PI = 36	2.54	0.99	2.32	0.98	3.41	0.98
	2.59	0.99	2.37	0.99	3.48	0.96
	2.43	0.99	2.30	0.98	3.38	0.93

Table 6.18 –Best Fit Parameters (Normalized Modulus and NMC_{DFS})

Material	K	L	R ²
El Paso PI = 16	4.79	11.28	0.99
	5.27	12.34	0.99
	5.76	27.92	0.96
San Antonio PI = 26	1.87	12.68	0.95
	1.82	8.86	0.91
	2.08	9.65	0.98
Fort Worth PI = 29	2.04	2.07	0.97
	1.80	1.58	0.86
	2.15	2.17	0.93
Bryan PI = 31	2.85	3.82	0.94
	2.50	3.27	0.99
	2.89	4.82	0.90
Houston PI = 35	1.66	5.42	0.99
	1.46	1.37	0.87
	2.16	4.13	0.96
Paris PI = 36	2.13	8.90	0.77
	2.41	7.60	0.98
	2.37	6.46	0.95

Table 6.19 – Best Fit Parameters (Normalized Modulus and Shrinkage Strain after DFS Process)

Material	Vertical			Lateral			Volumetric		
	M	N	R ²	M	N	R ²	M	N	R ²
El Paso PI = 16	0.00	5.04	0.62	3.47	3.33	0.92	0.86	0.97	0.89
	0.00	2.78	0.82	18.09	5.90	0.89	7.33	1.33	0.96
	0.00	3.12	0.66	26.08	6.55	0.72	7.07	1.15	0.85
San Antonio PI = 26	6.46	0.89	0.92	12.95	1.57	0.91	11.48	0.52	0.92
	4.76	0.68	0.92	8.69	1.38	0.90	7.78	0.42	0.92
	7.46	0.98	0.94	18.00	2.34	0.93	14.87	0.69	0.95
Fort Worth PI = 29	0.29	0.23	0.97	0.82	0.29	0.97	0.78	0.10	0.97
	0.10	0.21	0.87	0.23	0.24	0.84	0.26	0.09	0.86
	0.00	0.25	0.91	0.93	0.32	0.94	0.57	0.11	0.94
Bryan PI = 31	0.38	0.34	0.94	1.14	0.47	0.94	1.09	0.16	0.95
	0.80	0.35	0.99	0.99	0.42	0.98	1.12	0.15	0.99
	0.58	0.38	0.94	1.40	0.48	0.87	1.59	0.18	0.90
Houston PI = 35	2.33	0.40	0.98	2.71	0.50	0.98	2.95	0.18	0.98
	0.00	0.17	0.65	0.00	0.18	0.68	0.00	0.06	0.69
	2.12	0.43	0.97	3.32	0.64	0.96	3.78	0.24	0.97
Paris PI = 36	9.49	0.89	0.93	12.87	1.42	0.87	13.73	0.52	0.91
	3.26	0.41	0.95	4.30	0.61	0.97	4.56	0.22	0.97
	2.73	0.43	0.88	5.64	0.81	0.96	4.93	0.26	0.94

6.5 DEVELOPMENT OF RELATIONSHIP WITH INDEX PARAMETERS

In this section, models developed to estimate the fit parameters from index properties of the soils are presented. To help explain the process, the development of shrinkage strain and moisture content model for the dry-from-optimum (DFO) process is described in detail followed by its sensitivity and validation analysis. A summary table of relationships between fit parameters and index properties of clays is provided at the end of this section.

The development process started with a correlation analysis among the index properties and the fit parameters of the equations presented in the previous section. Equation 6.4 was proposed to estimate the shrinkage strains at a particular moisture contents for the DFO process. The results of the correlation analysis between the fit parameter A and the index properties of all clay materials except Houston are shown in Table 6.20. The results from the Houston clay were excluded for validation purposes, since it is not appropriate to validate a model with data used in the development of the model.

In Table 6.20, the correlation coefficients can range between -1 and 1. The values close to zero represent no correlation; whereas values close to -1 or 1 represent perfect correlation. The negative values are for inverse correlation and positive values are for direct correlation. In this study, an index parameter was considered correlated when the absolute value of the correlation coefficient (CC) was between 0.8 and 1.0. When the CC was between 0.6 and 0.8, the two parameters were considered marginally correlated. All fit parameters A are correlated or

marginally correlated to the plasticity index (PI), liquid limit (LL), optimum moisture content (OMC) and dry unit weight (DUW), whereas the plastic limit (PL) and seismic modulus at OMC are poorly or marginally correlated to Parameter A. As such, only the PI, LL, OMC and DUW were further considered in the development of the models.

Table 6.20 –Correlation Analysis between Parameter A from Equation 6.4 and Index Properties of Clays

Shrinkage Mode	Plasticity Index	Liquid Limit	Plastic Limit	Optimum Moisture Content	Dry Unit Weight	Seismic Modulus at OMC
Vertical	0.82	0.79	0.31	0.84	0.57	0.56
Lateral	0.92	0.85	0.36	0.87	0.68	0.64
Volumetric	0.85	0.83	0.33	0.89	0.62	0.51

Figure 6.17 provides a flowchart of the three steps of using the index properties and moisture content in an equation to predict the shrinkage strain. In this case, Equation 6.4 is used as an example for predicting the shrinkage strain. In Step 1, the fit Parameter A in Table 6.11 is predicted from the index properties of clays such as plasticity index, liquid limit, etc. The graph presented in Step 1 is detailed in Figure 6.18. As an example, the PI is used as input in a graph that presents the relationship between the variations of parameter A for the vertical shrinkage strain with PI. A line describes the relationship well. The R^2 is 0.84 in this particular case. The best fit line describes the relationship quite well.

Since Parameter A can be predicted from the PI directly, it can then be used as input to Equation 6.4 for predicting the shrinkage strain (Step 2) knowing the moisture content (Step 3). In that manner, the variations in shrinkage of these soils as well as the change in their moduli can be predicted just by knowing the index properties.

The process presented in Figure 6.17 can be replicated for all other index properties considered. The slope, intercept and R^2 for each set of parameters are shown in Table 6.21. In general, the OMC and PI are the two parameters that most favorably correlate with parameter A. Please note that the term parameter A is used as a general representation of the fit parameters in all the equations presented in Table 6.10 for simplification.

Since PI, LL, DUW and OMC are commonly known, a model was developed to combine the information from all these parameters. To make the model versatile so that it can be used with any missing data. The R^2 value from each of the relationships in Table 6.21 was used as a weighting multiplication factor, F. If the R^2 value was equal to or greater than 0.8, it was multiplied by an F of 4. Similarly, the R^2 values between 0.6 and 0.8 were multiplied by an F of 2. For the R^2 value less than 0.6, a multiplication factor of unity was used. The weighting multiplication factors (F's) for all relationships are also included in Table 6.21. Finally, the contribution factor, G, was obtained by multiplying the R^2 values and the weighting multiplication factors as reflected in Table 6.21.

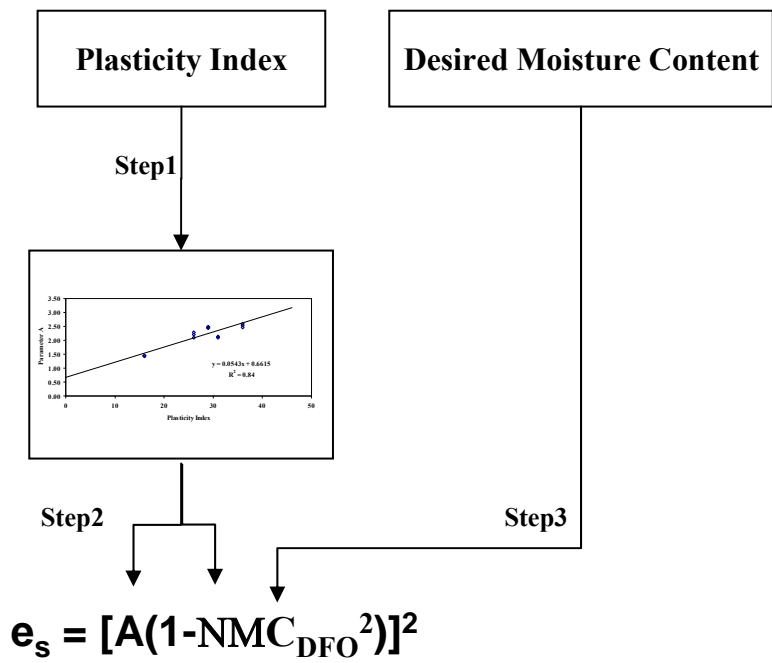


Figure 6.17 – Process in Predicting Shrinkage Strain

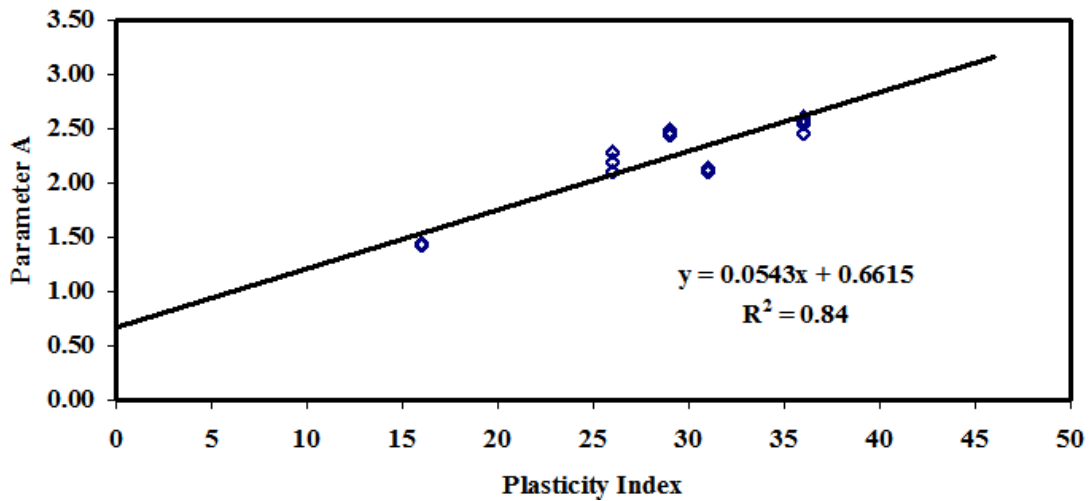


Figure 6.18 –Typical Trend Line for Parameter A with Plasticity Index

Table 6.21 –Relationships between Parameter and Index Properties of Soils

Index Property	Mode of Shrinkage	Parameter A				
		Intercept	Slope	R ²	F	G
Plasticity Index	Vertical	0.25	-2.46	0.82	4	3.29
	Lateral	0.06	0.55	0.92	4	3.70
	Volumetric	0.58	-3.16	0.85	4	3.41
Liquid Limit	Vertical	0.13	-2.24	0.79	2	1.59
	Lateral	0.03	0.65	0.85	4	3.42
	Volumetric	0.30	-2.45	0.83	4	3.31
Optimum Moisture Content	Vertical	0.48	-5.43	0.84	4	3.35
	Lateral	0.14	-0.58	0.87	4	3.49
	Volumetric	1.12	-9.96	0.89	4	3.58
Dry Unit Weight	Vertical	-0.15	19.45	0.57	1	0.57
	Lateral	-0.04	6.32	0.68	2	1.36
	Volumetric	-0.35	48.25	0.62	2	1.23

The weighting factor for each of the index parameters, W_i , were then calculated using

$$W_i = \frac{G_i}{\sum G_i} \quad (6.13)$$

If all the four index parameters are available, the weighted average parameter A, A^* is then calculated from

$$A^* = \frac{(A_{PI} \times W_{A-PI} + A_{LL} \times W_{A-LL} + A_{OMC} \times W_{A-OMC} + A_{DUW} \times W_{A-DUW})}{(W_{A-PI} + W_{A-LL} + W_{A-OMC} + W_{A-DUW})} \quad (6.14)$$

Where, A_{PI} = Parameter A from PI relationship in Table 6.21, A_{LL} = Parameter A from LL relationship, A_{OMC} = Parameter A from OMC relationship and A_{DUW} = Parameter A from DUW, W_{A-PI} = Weight factor for PI parameter, W_{A-LL} = Weight factor for LL parameter, W_{A-OMC} = Weight factor for OMC parameter and W_{A-DUW} = Weight factor for DUW parameter.

This global A^* can then be used in the original formula to calculate shrinkage strains as

$$\varepsilon_s = [A(1 - NMC_{DFO})^2]^n \quad (6.15)$$

The process described above is quite flexible since any or all of the four soil index parameters can be used to estimate the shrinkage strains. If one or more of the index properties are not available, their corresponding term in Equation 6.14 can be simply omitted.

Consider the following example for the San Antonio clay where the four index parameters are reflected in the first column of Table 6.22. Based on the contribution factors (G_i 's) reflected in Table 6.22, the weighting factors (W_i 's) are obtained when all four index parameters are used. The weighting functions for the parameter A of the vertical shrinkage strain model (column 2) for the PI and OMC index parameters are much greater than the other functions, indicating that PI and OMC can more accurately estimate parameter A. In the contrary, considering the weighting factors for lateral and volumetric shrinkage (column 3 and 4), the PI, LL and OMC parameters can equally estimate parameter A; whereas, the DUW is the least desirable parameter for estimating that parameter since W_{DUW} is much less than the weighting factors of the other three parameters.

**Table 6.22 – Weighting Functions for Each Index Parameter of San Antonio Clay
(See Equation 6.13)**

Index Property	Vertical Shrinkage	Lateral Shrinkage	Volumetric Shrinkage
	Strain	Strain	Strain
W_{PI}	0.35	0.31	0.30
W_{LL}	0.17	0.29	0.27
W_{OMC}	0.36	0.29	0.31
W_{DUW}	0.06	0.11	0.12

The composite parameter A, A^* , from Equations 6.13 and 6.14 are reflected in Table 6.23 and the corresponding estimated shrinkage strains in Table 6.24 for a moisture content of 14% (a normalized moisture content of 21%). The estimated and measured strains compare favorably in Table 6.31 especially for vertical strain.

Table 6.23 – Estimated A^* Parameter for Different Shrinkage Types Using all five Index Parameters for San Antonio Clay

Parameter	Vertical	Lateral	Volumetric
A^*	4.48	2.15	13.05

Table 6.24 – Shrinkage Strains at 14% Moisture Content for San Antonio Clay

Shrinkage Type	Shrinkage Strain, %	
	Estimated	Measured
Lateral	1.4	2.1
Vertical	2.5	2.2
Volumetric	7.2	6.3

To illustrate the flexibility of the model, one, two or three of the index parameters were eliminated in estimating A^* (note that OMC is always required). The results are summarized in Figure 6.19, where the solid line indicates the calculated shrinkage strain using all index properties. The estimated strains are normally within 10% to 15% of the measured strains. This indicates that even though it is desirable to use all the index parameters, the impact of eliminating one or two of the index parameters is small.

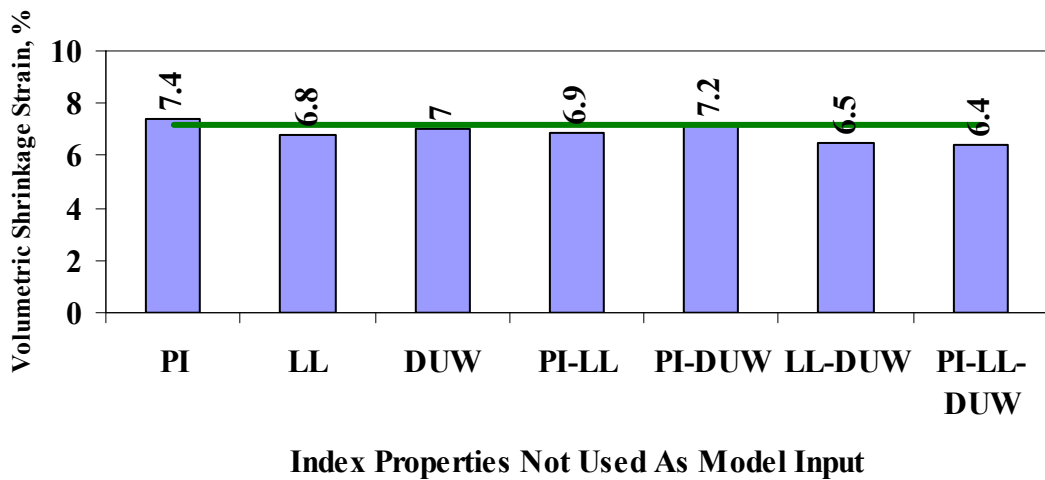
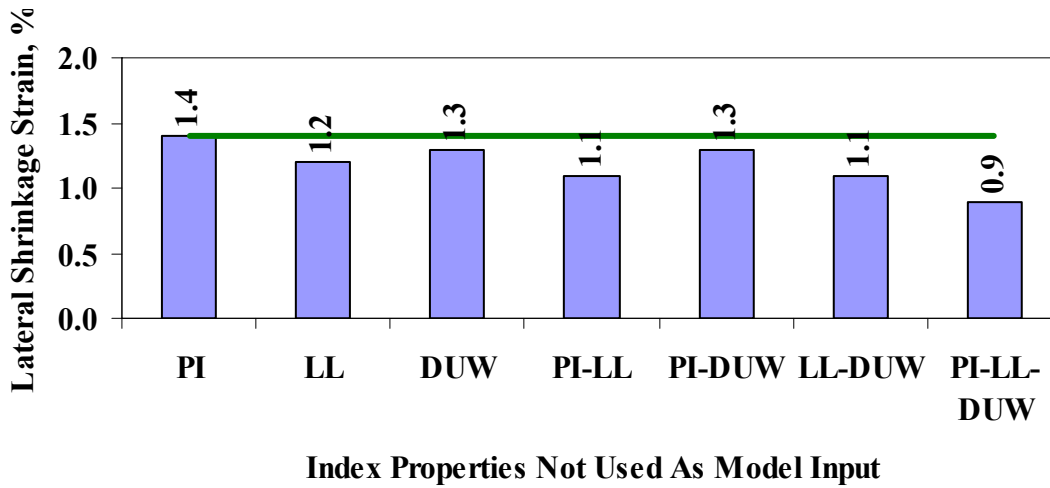
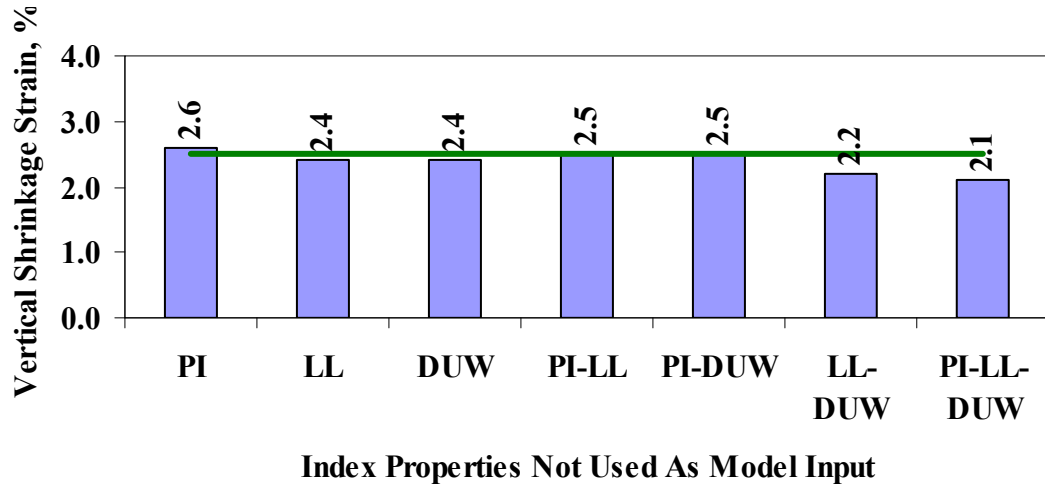


Figure 6.19 – Results of Sensitivity Study on the Shrinkage Models

The clay material from Houston, which was not used to develop the model, was used to validate the lateral, vertical and volumetric shrinkage strain models. The variations in measured and estimated shrinkage strain with moisture content are compared in Figure 6.20. The trends between the estimated and measured strains are similar for all three models of shrinkage. To quantify the differences between the estimated and measured values, the histograms of the errors are shown in Figure 6.21. The error in this case is defined as:

$$\text{Error} = \text{abs}\left(\frac{(\text{Estimated Strain} - \text{Measured Strain})}{\text{Measured Strain}}\right) \times 100\% \quad (6.16)$$

Approximately, 90%, 70% and 75% of the values are estimated with a margin of error of less than 20%.

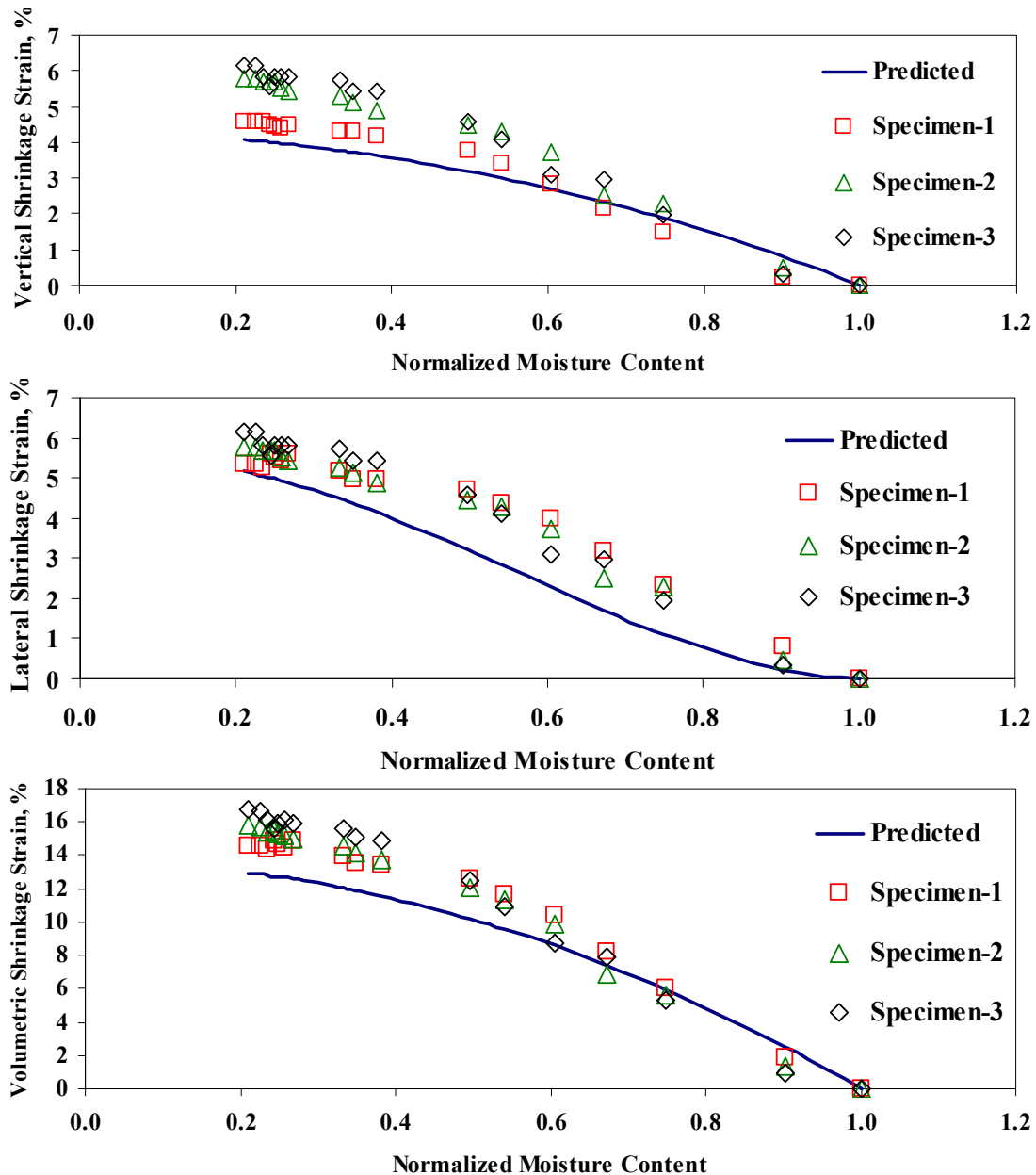


Figure 6.20 - Comparison of Measured and Predicted Shrinkage Strain Data and Moisture Content for Three Specimen of the Houston Clay Material

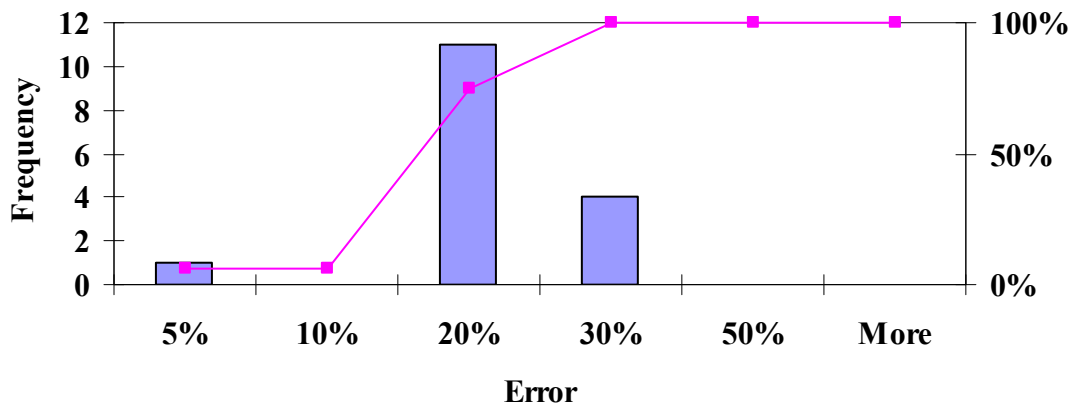
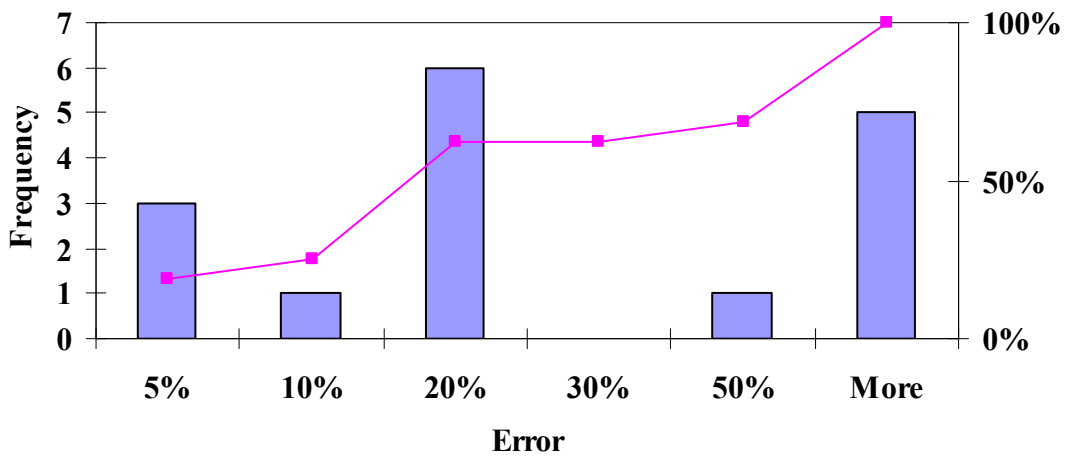
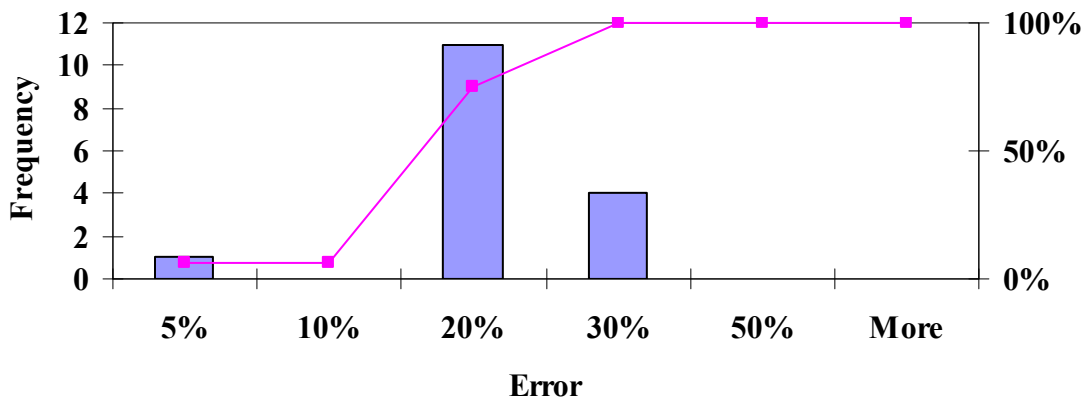


Figure 6.21 –Histograms of Differences between Measured and Estimated Strains

6.6 APPLICATION OF MODELS

Figure 6.22 is a flowchart to explain how the models are utilized for estimating the strains and modulus of a soil at certain moisture content. This procedure, for illustrative purposes is based

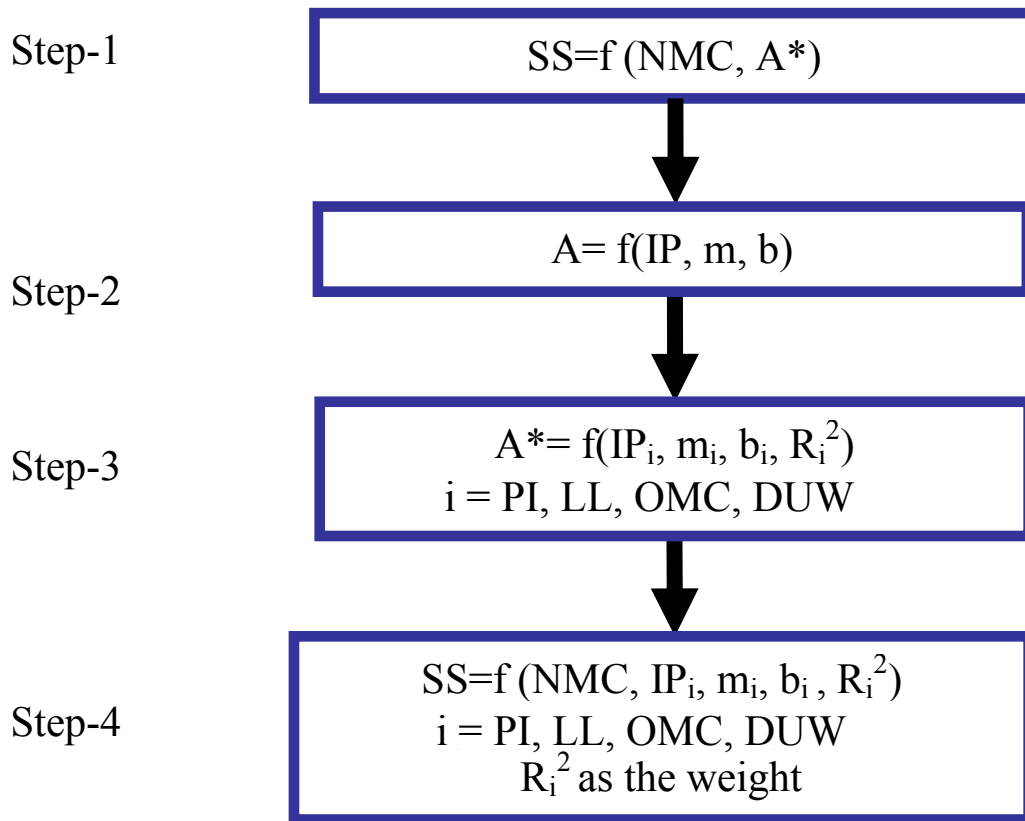


Figure 6.22 – Application of Model

on estimating the shrinkage strain after DFO process. However, the same process can be followed for predicting the modulus or the expansion strain. In Step 1, the shrinkage strain is shown as a function of the NMC and A^* . NMC (or more specific NMC_{DFO}) is the normalized moisture content defined as the moisture content at which the shrinkage strain needs to be estimated divided by the optimum moisture content of the soil of interest.

Step-2 shows that parameter A is determined by measuring the index property of a soil, and knowing the slope and intercept denoted by m and b (an example of the relationship is shown previously in Figure 6.18). Therefore, we can determine parameter A from the slope and intercept, m and b based on a value of a particular index property. If only one index property is known, then Parameter A can be determined and substituted into the model for A^* and the shrinkage strain is determined. However, if the value of several index properties is known, parameter A for each index property needs to be determined. The results of all parameter $A(s)$ are then combined based on Equation 6.14 to determine A^* .

Step-3 defines the process where A^* is a function IP_i, m_i, b_i, R_i^2 . IP_i is the index property for any i where, i is either of PI, LL, OMC or DUW. The remaining three parameters can be determined from a lookup table such as those presented in the appendices. Again, parameters m_i and b_i are the slope and intercept of the line that relates any index property to its respective

parameter A. Last of the three parameters is the R_i^2 values which is described previously as the goodness of fit parameter between an index property and its respective parameter A (best fit of Equation 6.4). This parameter is used as the weighing factor into the model since the shrinkage strain can be estimated from any of the index properties.

Finally, Step-4 provides a summary of the overall model showing that based on the moisture content and parameters generated from empirical relations, the shrinkage strain can be estimated.

The models for estimating the strain or modulus are simple and versatile. Tables 6.25 and 6.26 provide a summary of all developed models.

CHAPTER 7 - SUMMARY CONCLUSIONS

To understand the behavior of the high PI clays with changing moisture content, a number of laboratory tests were carried out on six clay materials, consisting of five high PI clays and one low PI clay. The High PI clays were brought from Bryan, Paris, San Antonio, Fort Worth and Houston districts while the low PI clay was from El Paso.

Several different laboratory techniques to compact clay specimens were evaluated. Static compaction in one lift was found to be the most practical procedure.

The variations in modulus and shrinkage/expansion strains with moisture under a number of different moisture conditioning procedures were evaluated. The moisture conditioning procedures used were a) drying the specimens from the optimum moisture content (DFO), b) saturating the specimens from the optimum moisture content (SFO) and c) drying after saturating the specimen prepared at the optimum moisture content (DFS). For each moisture conditioning process, models were developed to estimate the variations in the modulus and shrinkage/expansion strains with moisture. Finally the fit parameters of those models were correlated to the index properties of the clays so that they can be readily used in practice. The significance of these models is that for the first time, the moduli and shrinkage strains are related to moisture content (as opposed to suction) which can be measured with ease

The developed models in this research project were implemented in the assessment of the pavement performance in Research Report 5430-2.

REFERENCES

- Aubeny, C., and Lytton, R. (2002). "Properties of High-Plasticity Clays," 0-2100, Texas Transportation Institute, College Station, Texas.
- Aubeny, C., and Lytton, R. (2002). "Estimating Strength Versus Location and Time in High-Plasticity Clays," P1-2100, Texas Transportation Institute, College Station, Texas.
- Briggs, R. C., and Lukanen, E. O. (2000). "Variation in Backcalculated Pavement Layer Moduli in LTPP SMP Sites,," STP – 1384, American Society for Testing and Materials, West Conshohocken, PA, 113-128.
- Chandler, H. W. (1984). "The Use of Non-linear Fracture Mechanics to Study the Fracture Properties of Soils." *Journal of Agricultural Engineering Research*, 29, 321-327.
- Chertkov, V. Y. (2002). "Modeling Cracking Stages of Saturated Soils as They Dry and Shrink." *European Journal of Soil Science*, 53, 105-118.
- Coduto (1998). *Geotechnical engineering - Principles and Practices*. Prentice Hall, NJ.
- CRD-C (1995). *Specification for Plate Bearing Test*.
- Drumm, E. C., and Madgett, M. R. (1997). "Subgrade Resilient Modulus Correction for Saturation Effects." *Journal of Geotechnical and Geo-environmental Engineering*, 7 (123), 663-670.
- Drumm, E. C., Boateng-Poku, Y., and Johnson, P. T. (1995). "Estimation of Subgrade Resilient Modulus from Standard Tests." *Journal of Geotechnical Engineering*, 5(116), 774-789.
- Elfino, M. K., and Davidson, J. L. (1989). "Modeling Field Moisture in Resilient Moduli Testing." *American Society of Civil Engineering*, New York, NY., 24, 31-51.
- EI-Sohby, M. A., and Mazen, S. O. (1987). "The Prediction of Swelling Pressure and Deformational Behavior of Expansive Soils." *Regional Conference for Africa on Soil Mechanics and Foundation Engineering*, 1, 129-133.

Engineering Manual (1984). "Pavement Design for Seasonal Frost Conditions Mobilization Construction." US Army Corps of Engineers, 1110, 3-138.

Griffith, A. A. (1920). "The Phenomena of Rupture and Flow in Solids." Royal Society publishing, London, A-221, 163–198.

Groenevelt, P. H., and Grant, C. D. (2001). "Re-evaluation of Structural Properties of Some British Swelling Soils." *European Journal of Soil Science*, 52, 469–477.

Hallett, P. D. (1996). "Fracture Mechanics of Soil and Agglomerated Solids in Relation to Microstructure," thesis, presented to University of Birmingham, Birmingham, in partial fulfillment of the requirements for the degree of Doctor of Philosophy.

Hallett, P. D., and Newson, T. A. (2001). "A Simple Fracture Mechanics Approach for Assessing Ductile Crack Growth in Soil." *Soil Science Society of America*, 65, 1083–1088.

Hallett, P. D., and Newson, T. A. (2005). "Describing Soil Crack Formation using Elastic-Plastic Fracture Mechanism." *European Journal of Soil Science*, 56, 31-38.

Heydinger, A. G. (2003). "Evaluation of Seasonal Effects on Subgrade Soils." *Transportation Research Record*, 1821, 47-55.

Holtz, R. D., and Kovacs, W. D. (1981). *An Introduction to Geotechnical Engineering*, Prentice Hall, Englewood Cliffs, NJ.

Hossain, D., Matsah, M. I., and Sadaqah, B. (1997). "Swelling Characteristics of Madinah Clays." *Quarterly Journal of Engineering Geology*, 30, 205-220.

Khoury and Zaman (2004). "Correlation Between Resilient Modulus, Moisture Variation and Soil Suction for Subgrade Soils." *Transportation Research Record*, 1874, 99-107.

Komornik, A., and David, D. (1969). "Prediction of Swelling Pressure of Clays." *Journal of Soil Mechanics and Foundation Division*, 95(SM1), 209–225.

Krohn, J. P., and Slosson, J. E. (1980). "Assessment of Expansive Soils in the United States." *Fourth International Conference on Expansive soils*, Denver, CO., 596-608.

Ladd, C. C. (1960). "Mechanism of Swelling by Compacted Clay." *Highway Research Board*, 245, 10-26.

Lawn, B. R. (1993). *Fracture of Brittle Solids – Second Edition*. Cambridge University Press, Cambridge, MA.

Li, Dingqing, Selig, and Ernest, T. (1994). "Resilient Modulus for Fine-Grained Subgrade Soils." *Journal of Geotechnical Engineering*, 6(120), 939-957.

- Liao, S. S. C., and Whitman, R. V. (1986). "Overburden Correction Factors for SPT in Sand." *Journal of Geotechnical Engineering, A.S.C.E.*, 3(112), 373-377.
- Matthew, F. W., Paul R. F, Christopher, D. F. R (2004). "Cyclic Triaxial Tests on Clay Subgrades for Analytical Pavement Design." *Journal of Transportation Engineering*, 3(130), 378-386.
- Maugis, D. (1985). "Review: Subcritical Crack Growth, Surface Energy, Fracture Toughness, Stick-slip and Embrittlement." *Journal of Materials Science*, 20, 3041-3073.
- Nayak, N. V., and Christensen, R. W. (1971). "Swelling Characteristics of Compacted Expansive Soils." *Clays and clay minerals*, Pergamon press, (19), 251-261, Lawrence, KS.
- Nazarian, S., and Yuan, D. (1997). "Evaluation and Improvement of Seismic Pavement Analyzer." Research Project 7-2936, The Center for Highway Materials Research, The University of Texas at El Paso, El Paso, TX.
- Nazarian, S., Yuan D., Tandon, V., and Arellano, M. (2002). "Quality Management of Flexible Pavement Layers with Seismic Methods." Research Report 1735-3F, Center for Highway Materials Research, The University of Texas at El Paso, TX.
- Nazarian, S., and Yuan, D. (2003). "Comprehensive Mechanistic-based Quality Control of Flexible Pavements with NDT Methods." *Non-Destructive Testing in Civil Engineering 2003*, Center for Highway Materials Research, The University of Texas at El Paso.
- Nwaiwu, C. M. O., and Nuhu, I. (2006). "Evaluation and Prediction of the Swelling Characteristics of Nigerian Black Clays." *Geotechnical and Geological Engineering*, 1 (24), 45-56.
- Pengelly, A., and Addison, M. (2001). "In-Situ Modification of Active Clays for Shallow Foundation Remediation, in Expansive Clay Soils and Vegetative Influence on Shallow Foundations." *American Society of Civil Engineers*, 115, 192-214.
- Puppala, A. J., Mohammad, L. N., and A. A. (1999). "Permanent Deformation Characterization of Subgrade Soils from RLT Test." *Journal of Materials in Civil Engineering, ASCE*, 11(4), 274-282.
- Raats, P. A. C. (1984). "Mechanics of Cracking Soils." *International Institute for Land Reclamation and Improvement, Wageningen, The Netherlands*, 27-31.
- Saarenketo, T., and Scullion, T. (1997). "Using Suction and Dielectric Measurements as Performance Indicators for Aggregate Base Materials." *Transportation Research Record*, 1577, 37-44.

- Seed, H. B., Woodward, R. J., and Lundgren, R. (1962). "Prediction of Swelling Potential for Compacted Clays." *Journal of the Soil Mechanics and Foundations Division, ASCE*, 88(SM3), 53-87.
- Simonsen, E., Janoo, V. C., and Isacsson, U. (2002). "Resilient Properties of Unbound Road Materials during Seasonal Frost Conditions." *Journal of Cold Regions Engineering*, 16(1), 28-50.
- Skempton, A. W. (1986). "Standard Penetration Test Procedures and the Effects in Sands of Overburden Pressure, Relative Density, Particle Size, Aging and Overconsolidation." *Geotechnique*, 3 (36), 425-447.
- Sture, S., Alqasabi, A., and Ayari, M. (1999). "Fracture and Size Effect Characters of Cemented Sands." *International Journal of Fracture*, 95, 405-433.
- Thompson, M. R. and Elliott, R. P. (1985). "ILLI-PAVE-Based Response Algorithms for Design of Conventional Flexible Pavements." *Transportation Research Board*, 1043, 50-57.
- Thompson, M. R. and Robnett, Q. L. (1979). "Resilient Properties of Subgrade Soils." *Transportation Engineering Journal, ASCE*, 105(TE1), 71-89.
- Thompson, M. R., and Smith, K. L. (1990). "Repeated Triaxial Characterization of Granular Bases," *Transportation Research Record*, 1278, 7-17.
- Tian, P., Zaman, M. M., and Laguros, J. G. (1998). "Variation of Resilient Modulus of Aggregate Base and Its Influence on Pavement Performance." *Journal of Testing and Evaluation*, 26 (4), 329-335.
- Tinjum, J. M., Benson, C. H., and Blotz, L. R. (1996). "Soil-Wager Characteristic Curves for Compacted Clays." *Journal of Geotechnical and Geo-environmental Engineering*, 6 (123).
- Turner, C. E., and Kolednik, O. (1997). "A Simple Test Method for Energy Dissipation Rate, CTOA and the Study of Size and Transferability Effects for Large Amounts of Ductile Crack Growth." *Fatigue and Fracture of Engineering Materials and Structures (UK)*, 11 (20), 1507-1528.
- Turner, C. E., and Kolednik, O. (1994). "Application of Energy Dissipation Rate Arguments to Stable Crack Growth." *Fatigue and fracture of engineering materials and structures (UK)*, 10 (17), 1109-1127.
- Uzan, J., Moshe V., and Elisha, S. (1972). "Cracking Mechanism of Flexible Pavement." *Transportation Engineering Journal*, 17-35.
- Xiao-ming, Y., and Sun Jing, (2000). "Laboratory Experimental Study on Dynamic Shear Modulus Ratio and Damping Ratio of Soil." *Earthquake Engineering and Engineering Vibration*, 4 (20), 133-139.

APPENDIX A - Protocols

Laboratory Compaction of Clay Specimens

Section 1

Overview

Use this method to compact clay specimens in laboratory.

To perform test, a clay specimen is prepared in laboratory using static compactor and in one single layer. For strength and stiffness tests, specimen measures 8 in. (200 mm) in height and 4 in. (100 mm) in diameter while for the four point bend test a rectangular specimen is prepared measuring 1 in. (13 mm) by 1 in. (13 mm) by 5.6 in. (142 mm).

Part-1 of this protocol describes preparation of cylindrical specimen while part-2 deals with the rectangular specimen.

Units of Measurement

The values given in parentheses (if provided) are not standard and may not be exact mathematical conversions. Use each system of units separately. Combining values from the two systems may result in nonconformance with the standard.

Section 2

Apparatus

The following apparatus are required:

- A hollow metallic mold 16.6 in. (400mm) in height and 4.1 in. (103 mm) inner diameter
- Three solid metallic blocks 4.0 in. (100 mm) in diameter and 5.7 in. (140 mm), 2.45 in. (62 mm) and 0.50 in. (13 mm) high respectively
- Static compactor
- Balance, with a minimum capacity of 35 lbs (15 kg), accurate and readable to 0.001 lb (0.5 g) or 0.1% of the test mass, whichever is greater
- Hydraulic press and a metal ring to extrude molded specimens
- Drying oven, maintained at 230 ± 9 °F (110 ± 5 °C)
- Drying oven, maintained at 140 ± 9 °F (60 ± 5 °C)
- Metal pans, wide and shallow for mixing and drying materials
- No. 4 (4.75 mm) sieve

Section 3

Laboratory Compaction of Clay Specimen

This part uses a static compactor to prepare a 4 in. (100 mm) by 8 in. (200 mm) cylindrical and 1 in. (25 mm) by 1 in. (25 mm) by 5.6 in. (140 mm) rectangular clay specimen. The clay passing through No. 4 sieve is used to prepare clay specimens.

Part 1: Preparation of Cylindrical Specimen

Preparation of Material

Follow the steps below to prepare material for compaction:

Material Preparation for Compaction	
Step	Action
1	Crush clay material fine enough so that it passes through No. 4 sieve. Crush enough material to prepare several specimens (Approximately 50 lbs (22 Kg)).
2	Sieve crushed material through No. 4 sieve. Use the material passing through No. 4 sieve and discard the remaining material.
3	Dry sieved material in oven at 230 ± 9 °F (110 ± 5 °C) for no less than 24 hours.
4	Cool the material and measure approximately 7.5 lbs of material per specimen in a container.
5	Calculate the mass of the water to be added based on the air-dry mass of the material. (e.g. if you wish to prepare specimen at 20% moisture content then add $7.5 * 0.20 = 1.50$ lbs of water).
6	Weigh out this amount of water into a tared sprinkling jar.
7	Sprinkle water onto the soil during mixing, in increments.
8	Thoroughly mix each specimen to ensure even distribution of water throughout specimen.
9	Cover the mixed sample and allow sample to stand and cure for at least 12 hours before compacting. When the PI is less than 12, the curing time may be reduced to not less than 3 hours. Cure split or referee samples for the full 12 hours.
10	Cover the mix properly so that there is no moisture loss and allow it to stand and cure for at least 12 hours before compacting.

Preparation of Specimen

Follow the steps below to prepare specimen for testing:

Specimen Preparation for Testing	
Step	Action
1	Measure the amount of material required based on its dry density, degree of compaction and the moisture content at which the specimen is to be prepared. (e.g. if dry density = 112 pcf, degree of compaction = 95% and the moisture content = 20%, then the amount of material required to prepare one specimen = $112 * 0.95 * \pi / 4 * 4^2 * 8 / 12^3 * (1 + 0.20) = 7.428$ lbs)
2	Place the 2.45 in. (62 mm) thick solid block at the bottom of the mold and pour the weighed material inside the mold.
3	Place the 5.65 in. (140 mm) thick solid block on top of the poured material and place this assembly in static compactor.
4	Compact the specimen until the top plate of compactor moves down and the top block becomes flush with the mold (the compaction speed should be approximately 2 in./min).
5	Wait one minute and then start the compactor again to move the top plate up.
6	Flip the mold so that 2.45 in. (62 mm) thick block is facing top.
7	Place the 0.50 in (13 mm) thick metal block on top of 2.45 in. (62 mm) solid block.
8	Start the static compactor again and move the top plate down so that 0.50 in (13 mm) thick solid block gets flushed with the mold.
9	Wait for one minute and then start the compactor again to move the top plate up.
10	Take out the mold and remove the metal blocks from it.
11	Center the mold on top of hydraulic jack and extract the specimen from the mold.
12	Cover the specimen with a rubber membrane.

Note:

- Just before preparing specimen the mix should be weighed. The mix should weigh the same as it was initially prepared, if not add additional water in it to make up for the moisture loss.
- Average the moisture contents just before and after preparing the specimen to make sure the exact moisture content of the specimen prepared.

Part 2: Preparation of Rectangular Specimen

Preparation of Material

Material is prepared as described in part-1 of “Tex 1BB Specimen Preparation Protocol”.

Preparation of Specimen

Follow the steps below to prepare specimen for testing.

Specimen Preparation for Testing	
Step	Action
1	Measure the amount of material required based on its dry density, degree of compaction and the moisture content at which the specimen is to be prepared. (e.g. if dry density = 112 pcf, degree of compaction = 95% and the moisture content = 20%, then the amount of material required to prepare a 1 in. by 1 in. by 5.6 in. specimen = $112 * 0.95 * 1 * 1 * 5.6 / 12^3 * (1 + 0.20) = 0.414$ lbs)
2	Place the 0.50 in (13 mm) thick metal block at the bottom of the rectangular mold and pour the weighed material inside the mold.
3	Place the 1.0 in. (25 mm) thick solid block on top of the poured material and place this assembly in static compactor.
4	Compact the specimen until the bottom plate of compactor moves up and the top block becomes flush with the mold (the compaction speed should be approximately 2 in./min).
5	Wait one minute and then start the compactor again to move the bottom plate down.
6	Flip the mold so that 0.50 in. (13 mm) thick bottom block is facing top.
7	Place other 0.5 in. (13 mm) thick solid block on top of 0.50 in. (13 mm) solid block.
8	Start the static compactor again and move the bottom plate up so that 0.5 in (13 mm) thick solid block gets flushed with the mold.
9	Wait for one minute and then start the compactor again to move the bottom plate down.
10	Take out the mold and remove the metal blocks from it.
11	Place the solid blocks from one side and push them down so that specimen comes out from the other side.
12	Cover the specimen with a cellophane wrap.

Calculations

Use the following formula to calculate the weight of the material required for preparing one specimen:

$$W = DD \times C \times V \times (1 + MC)$$

where,

W = Weight of the material required for preparing one specimen in lbs

DD = Dry density of the material in pcf

C = Degree of compaction

V = Volume of the specimen in ft³

MC = Required moisture content of the specimen

Drying and Wetting Method for Clay Specimen

Contents:

Section 1 — Overview	2
Section 2 — Definitions.....	3
Section 3 — Apparatus	4
Section 4 — Part 1: Drying Method.....	5
Part 2: Wetting Method.....	6

Section 1 Overview

This procedure is used to determine the volumetric change due to variation in moisture content. Use this procedure for drying and saturating clay specimens.

The dried and saturated specimens are tested for strength and stiffness properties.

Units of Measurement

The values given in parentheses (if provided) are not standard and may not be exact mathematical conversions. Use each system of units separately. Combining values from the two systems may result in nonconformance with the standard.

Section 2 Definitions

The following terms and definitions are referenced in this test method:

- Dry cycle: The process a specimen undergoes such that there is no weight loss in consecutive days weight readings
- Wet cycle: The process the specimen undergoes to reach complete saturation.
- Saturation: The process in which all air voids are filled with water.

Section 3 Apparatus

The following apparatus are required:

- Balance, with a minimum capacity of 35 lbs (15 kg), accurate and readable to 0.001 lb (0.5 g) or 0.1% of the test mass, whichever is greater
- Equipment to measure the deformation of specimen, accurate to 0.001 in. (0.025 mm) such as caliper
 - Circumference measuring device, accurate to 0.05 in. (1.0 mm) such as pi-tape

- 8 thumb tacks
- Cellophane paper
- Rubber bands
- Vacuum grease
- Filter paper
- 4 in. (100 mm) diameter by 0.253 in. (6.42 mm) thickness porous stone
- 4 in. (100 mm) diameter rubber membrane
- 4 in. (100 mm) diameter hollow plastic cylindrical mold and approximate 6 in. (150 mm) in height
- 2- 4 in. (100 mm) diameter O-Rings
- A conventional oven at 104 °F (40 °C)

Section 4

Drying and Wetting Method for Clay Specimen

This part explains the steps followed to dry and saturate a laboratory compacted clay specimen.

Preparation of Specimen

The specimen is prepared as per the “Tex-1-BB: Laboratory Compaction of Clay Specimen”.

Part 1: Drying Method

Follow the steps below to dry laboratory compacted specimen:

Drying Method	
Step	Action
1	Cover the cylindrical surface of laboratory compacted specimen with cellophane paper, cut excess paper at ends so that the top and bottom are exposed.
2	Use a thumb tack to make tiny holes in the cellophane paper so that water can escape.
3	Using caliper and pi-tape measure and record the height and diameter of the specimen respectively.
4	Perform FFRC Test on it (Follow Protocol Tex-147-E: Determining Modulus of Base and Subgrade Materials with Free-Free Resonant Column).
5	Keep the specimen in conventional oven at 104 °F (40 °C).
6	Each 24 hours take out the specimen from oven and repeat Step 3, 4 and 5 until drying cycle is complete. The dry cycle is complete when the change in moisture content in two consecutive days is less than 1%.

Part 2: Wetting Method

Wetting Method	
Step	Action
1	Using caliper and pi-tape measure and record the original height and diameter of the specimen (the height will be proportional to the thumb tacks height mentioned on step 10).
2	Determine and record the mass of a rubber membrane, plastic mold, saturated porous stone, and two o-rings to the nearest 0.001 lb (0.5 g).
3	Use 8 thumb tacks as targets to get the readings for height. Evenly distribute 4 thumb tacks around the top side of the specimen approximately 1 in. (25 mm) from top. Aligned with the top thumb tacks, use 4 thumbtacks around the bottom side of the specimen approximately 0.5 in. (12.5 mm) from bottom of the specimen. (Refer to Fig 1).
4	Cover laboratory compacted specimen using cellophane paper. Cover the bottom of the specimen using extra cellophane paper and secure it with a rubber band.
5	Fold the excess cellophane paper out at the top of the specimen so that we leave the top exposed. Apply vacuum grease to the folded cellophane paper. Cover the top of the specimen with a porous stone using a filter paper as a membrane.
6	Using the rubber membrane cover the inside of the plastic mold. Pull the rubber membrane to cover the top 0.75 in. (62.5 mm) of the specimen. Place the two o-rings over the rubber membrane to secure the specimen and prevent water migration from sides of the specimen. (Refer to Fig 1).
7	Based on the calculation provided in this section, determine the amount of water required to fully saturate the specimen. Divide the total amount of water needed by ten. This allows for ten data points before the specimen is fully saturated.
8	Determine and record the mass of the specimen to the nearest 0.001 lb (0.5 g)
9	Using caliper and pi-tape measure and record diameter of the specimen and the height from the top to bottom thumb tacks for each of the 4 sets.
10	Lay down specimen horizontally and perform FFRC test from bottom (Follow Protocol Tex-147-E: Determining Modulus of Base and Subgrade Materials with Free-Free Resonant Column).
11	Fill the plastic mold with water up to 4 in. (100 mm) and allow the specimen to saturate.
12	The rate of moisture absorption varies with the type of material. Therefore, weigh the specimen continuously until 1/10 of the water required to reach full saturation is absorbed by the specimen.
13	Determine the total amount of time for the specimen to absorb 1/10 of the water required to full saturation. Use this time as a gauge for Step 11.
14	Repeat Steps 8 to 11 until the specimen is fully saturated.

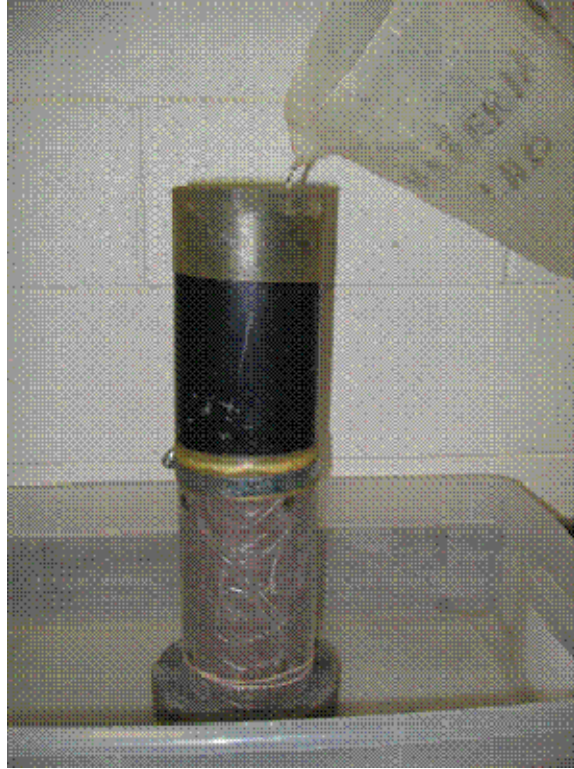


Figure 1: Specimen set up for wetting method

Calculation

- Use the following equation to determine the weight gain required in order to completely saturate the specimen.

$$W_{\text{reqd}} = W_{\text{ti}} \left[\frac{62.4}{(1 + \omega_i) D_{\text{ai}}} - \frac{1}{(1 + \omega_i) G_s} - 1 + \frac{1}{(1 + \omega_i)} \right]$$

where,

W_{reqd} = Weight of water required to fully saturate the specimen

W_{ti} = Total Initial weight of the specimen

ω_i = Water content of the specimen

D_{ai} = Dry unit weight of the material

G_s = Specific gravity of soil (Assume 2.67 if not known)

- Percent change in dimensions = $\{(D - D_0) / D_0\} * 100$

where,

D = Current dimension

D_0 = Initial dimension

- Percent change in volume = $\{(V - V_0) / V_0\} * 100$

where,

V = Current volume

V_0 = Initial volume

- Percent Moisture Content
 $\omega = (M_w/M_s) * 100$

Graphs

Drying method:

- Plot the lateral and vertical shrinkage of the specimen along with the volumetric shrinkage with respect to time as shown in Figure 2.

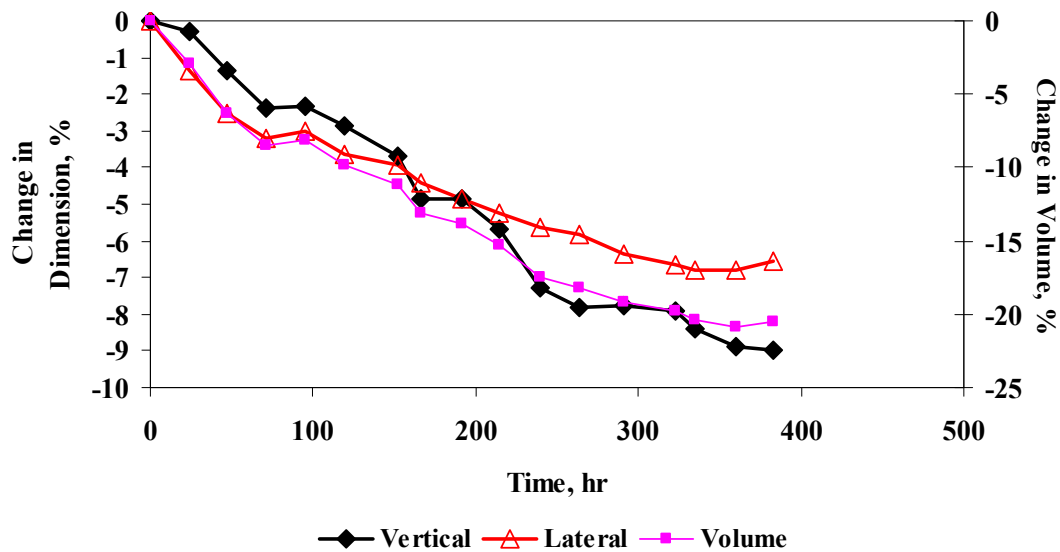


Figure 2: Plot of Change in Dimensions vs. Time

- Plot the variation of moisture content and seismic modulus of the specimen with respect to time as shown in Figure 3.

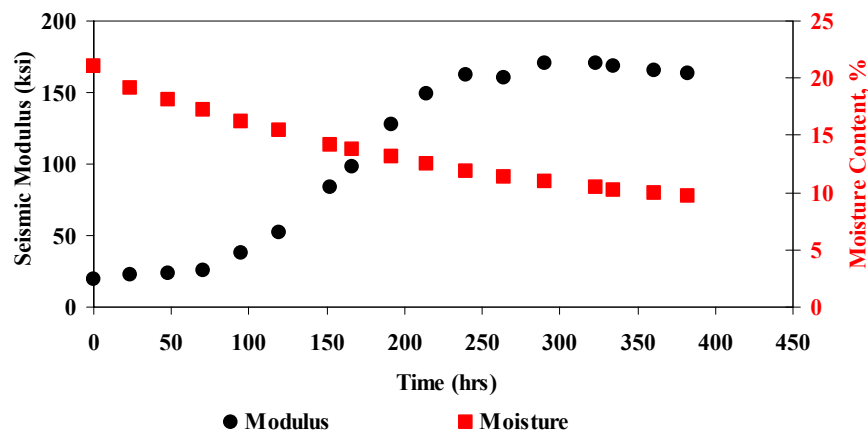


Figure 3: Plot of Seismic modulus and moisture content vs. Time

Wetting method:

- Plot the variation in moisture content and seismic modulus of the specimen with respect to time as it becomes saturated as shown in Figure 4.

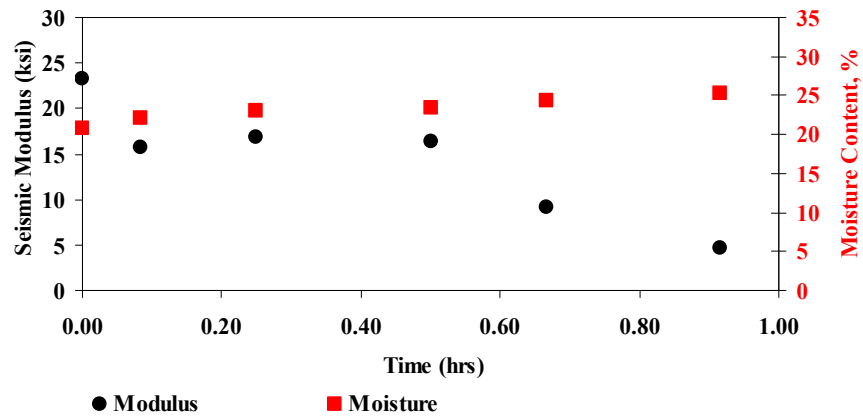


Figure 4: Plot of Seismic modulus and Moisture content vs. Time

APPENDIX B - Static Compactor Apparatus Design

Figure A: Metallic hollow mold

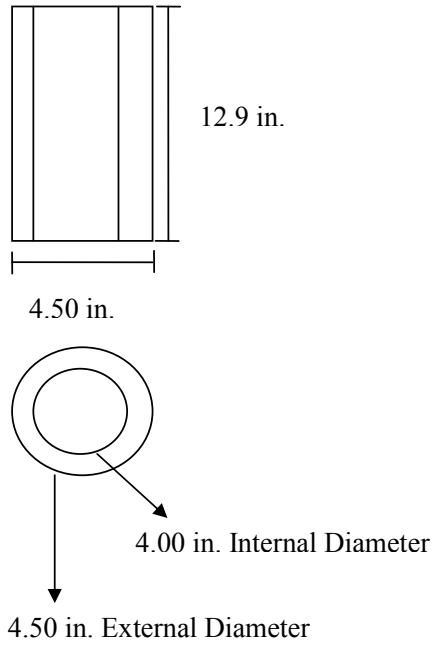


Figure B: Solid metallic blocks *

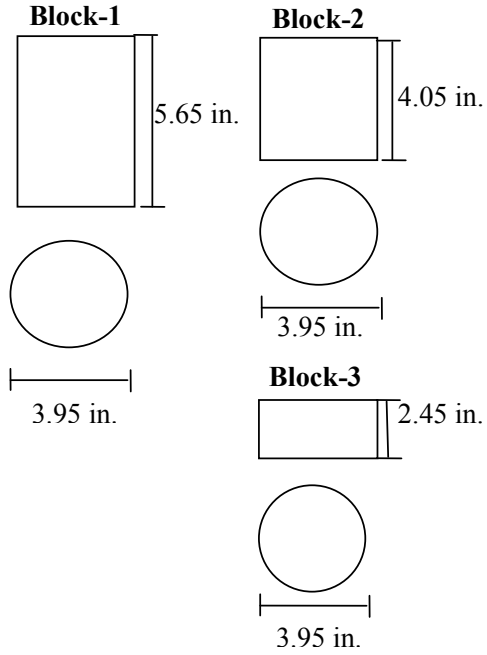


Figure B-1 – Static Compactor Apparatus Design to Prepare Specimen in Five Lifts

Figure A: Metallic hollow mold

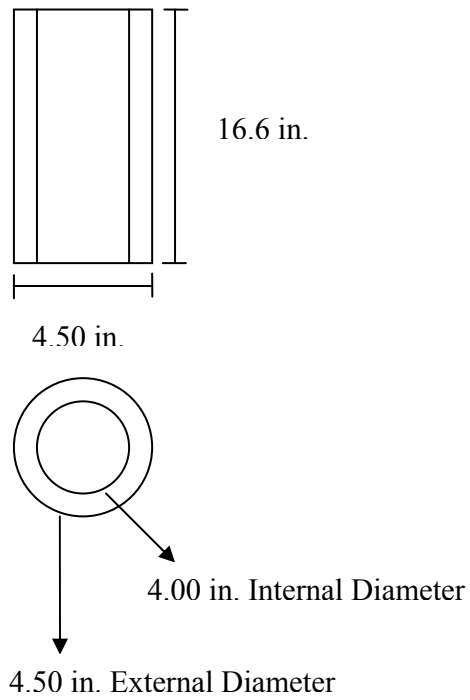


Figure B: Solid metallic blocks

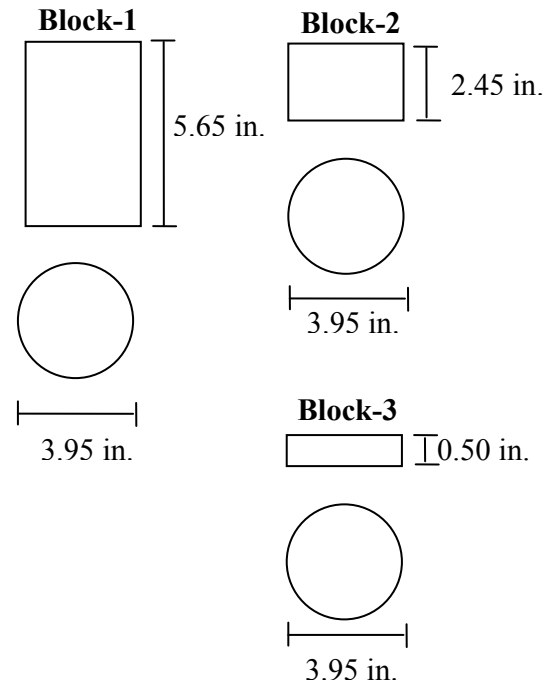
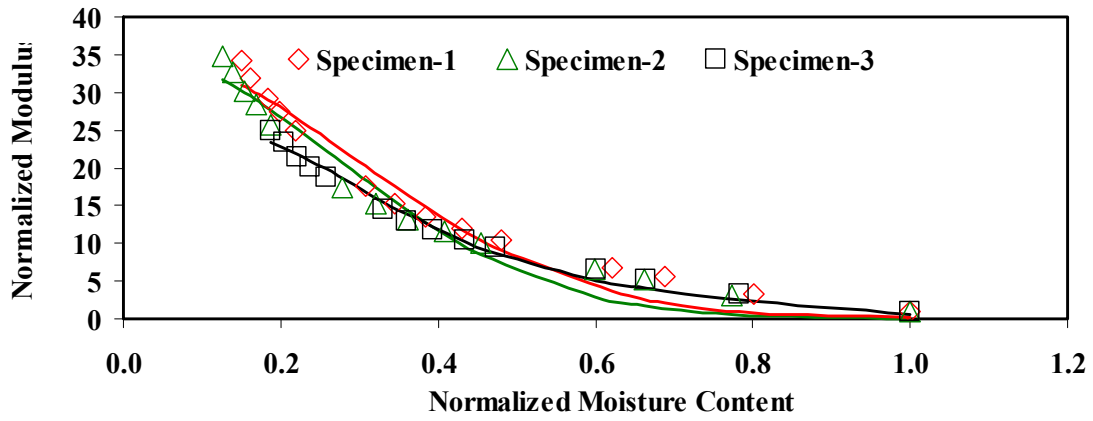


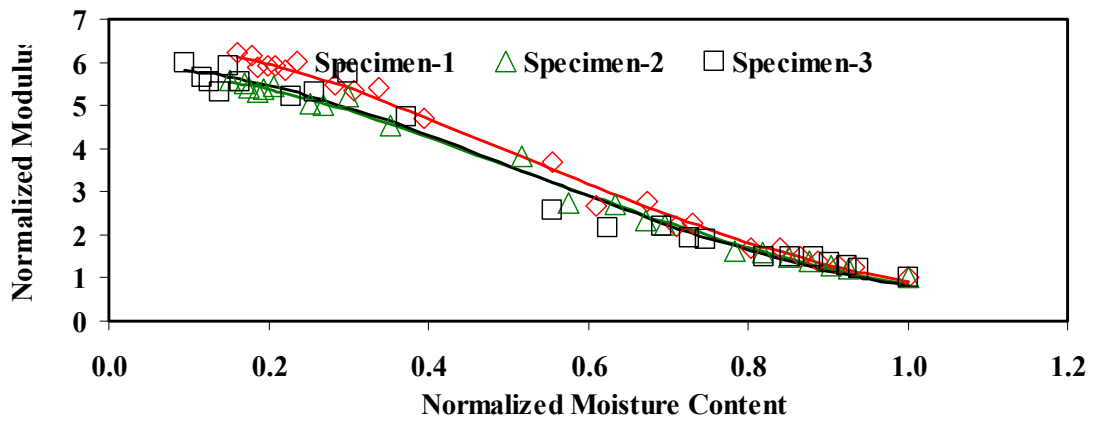
Figure B-2 – Static Compactor Apparatus Design to Prepare Specimen in One Single Lift

APPENDIX C - Normalized Modulus VS Normalized Moisture Content – DFO Results

a) El Paso



b) San Antonio



c) Fort Worth

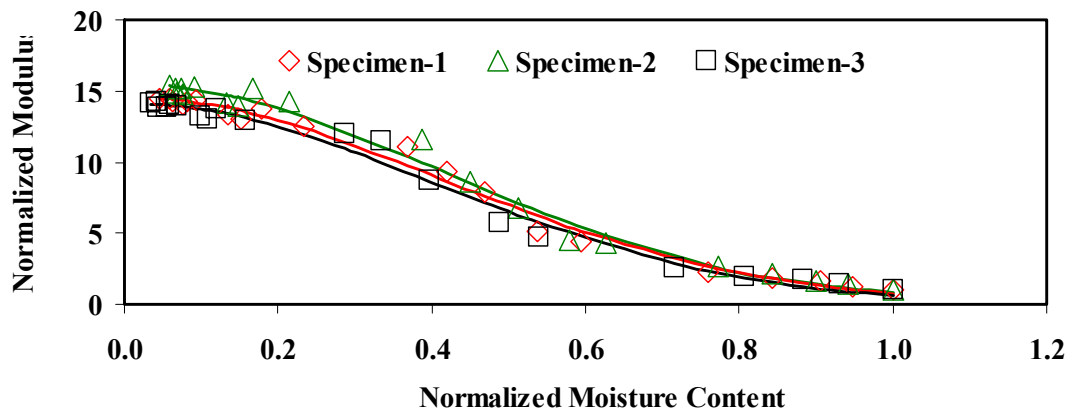
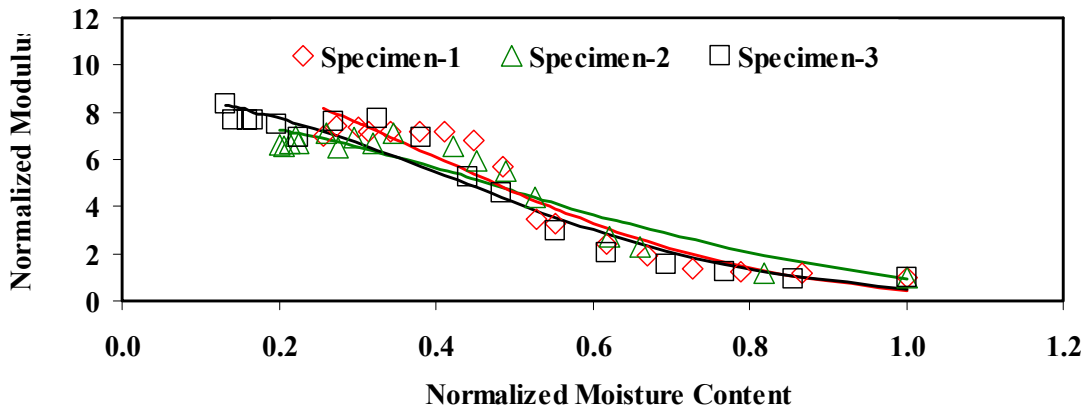
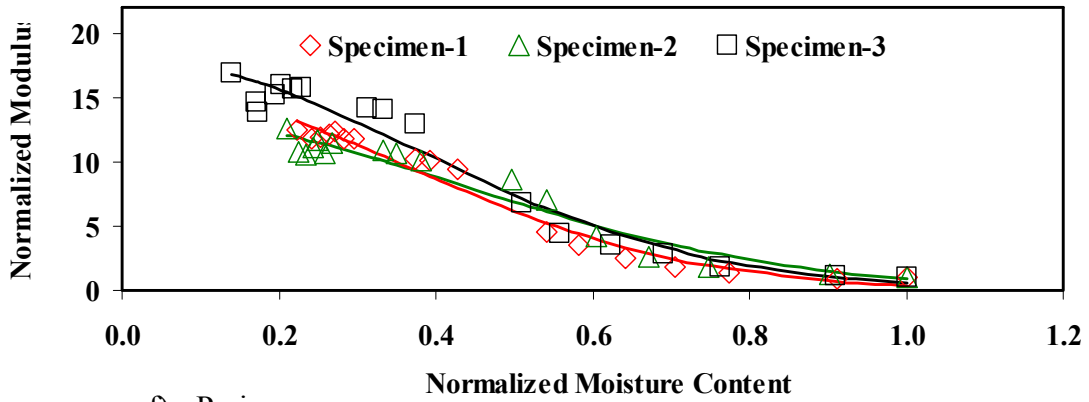


Figure C.1 Typical Variations in Normalized Modulus and NMC

d) Bryan



e) Houston



f) Paris

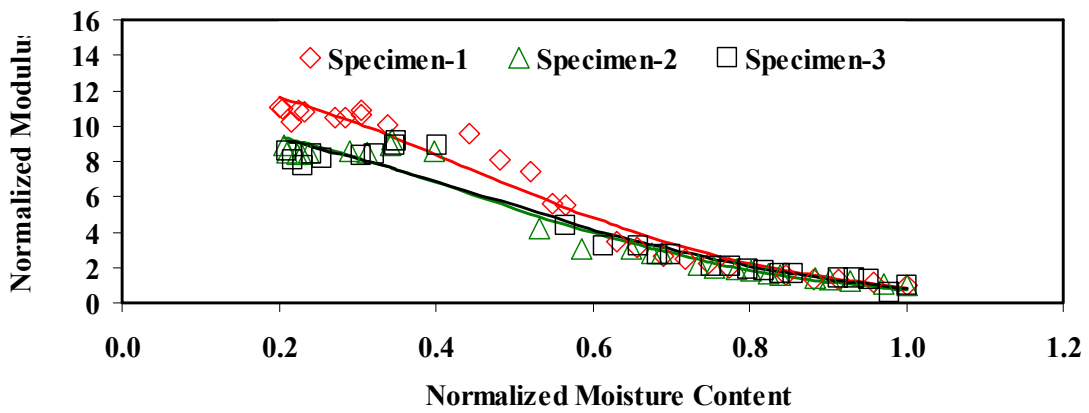


Figure C.2 Typical Variations in Normalized Modulus and NMC

**APPENDIX D - Normalized Modulus
VS Shrinkage Strain – DFO Results**

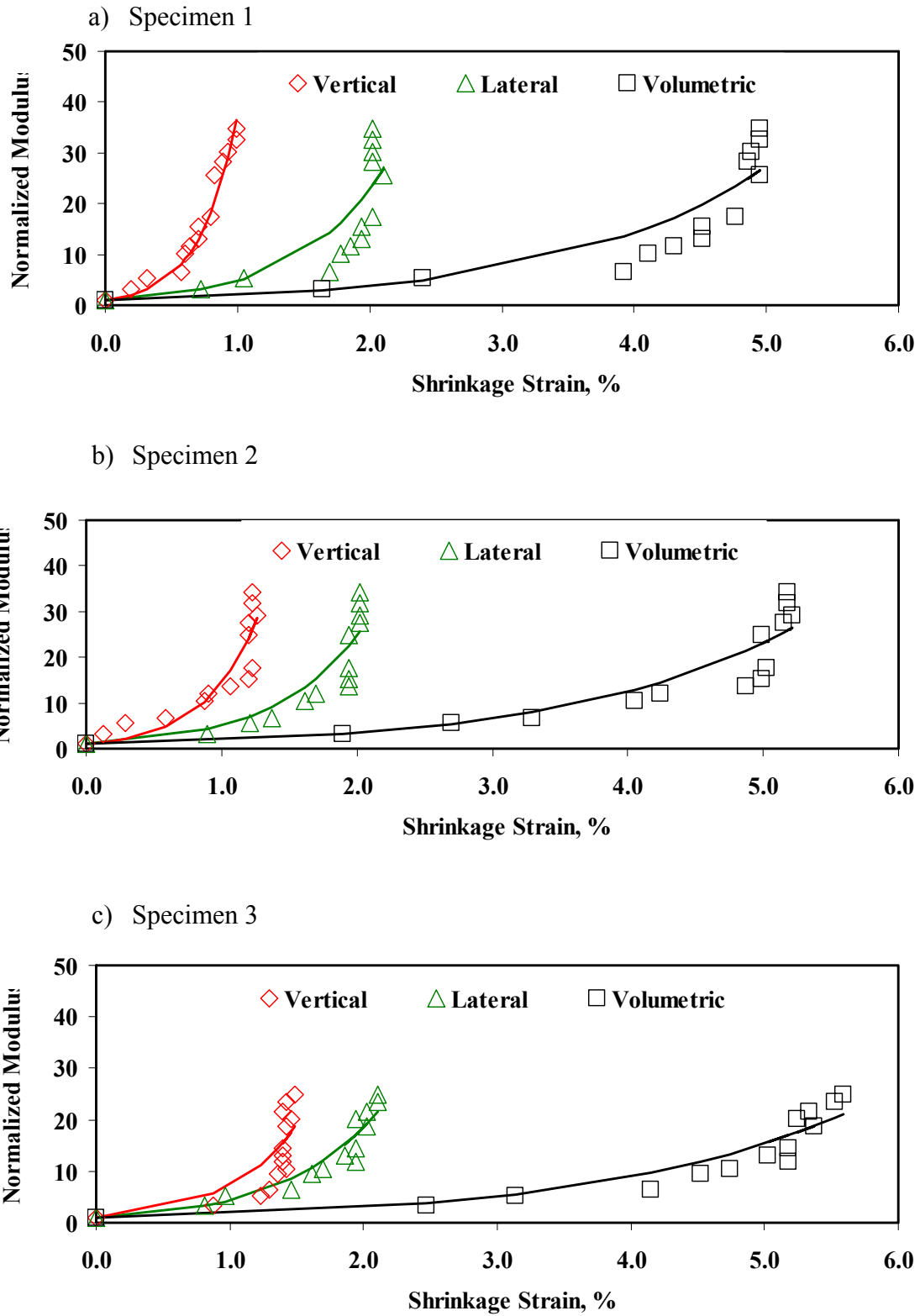


Figure D.1 Typical Variations in Shrinkage Strain and NMC for Clay from El Paso District

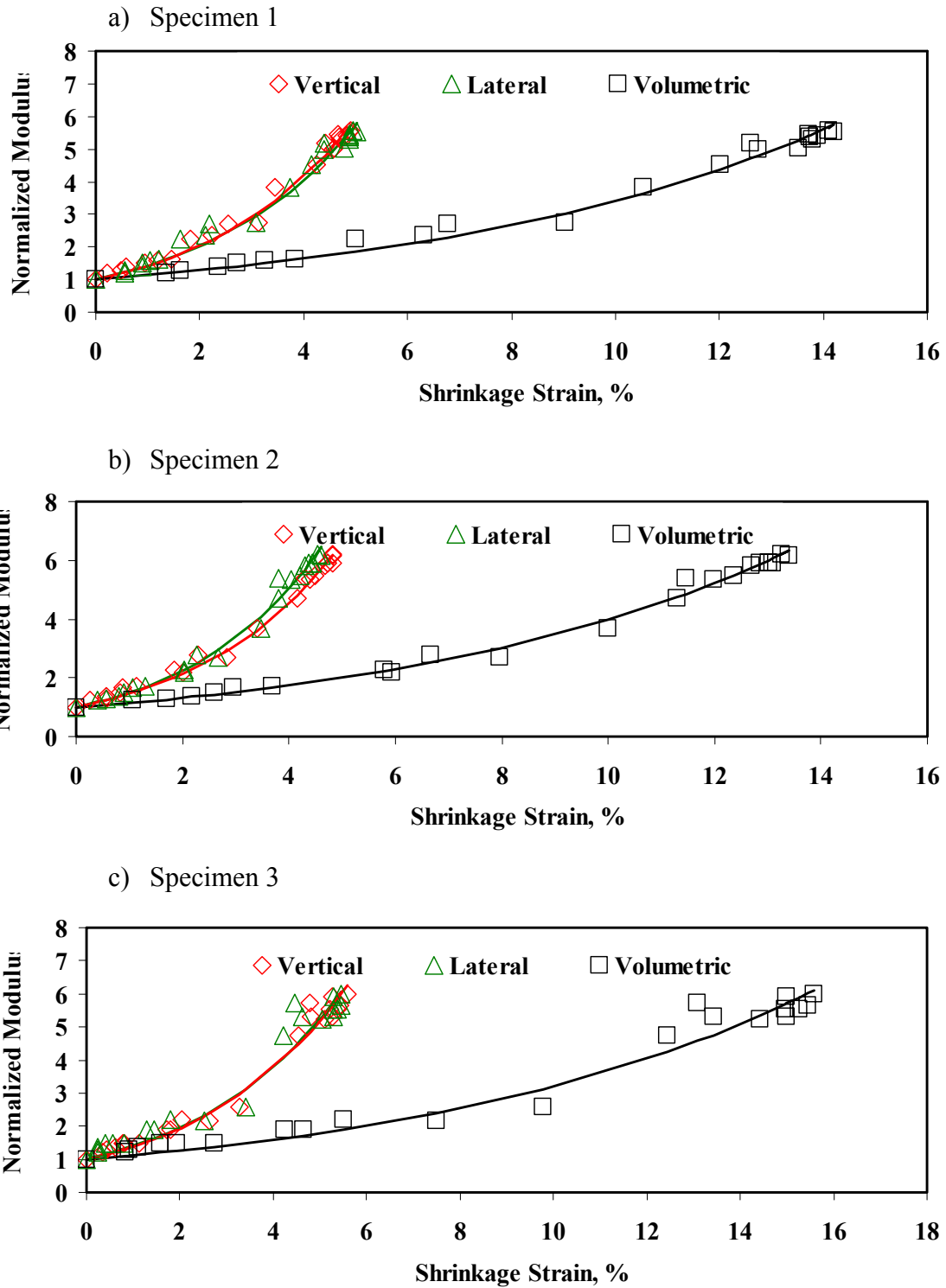


Figure D.2 Typical Variations in Shrinkage Strain and NMC for Clay from San Antonio District

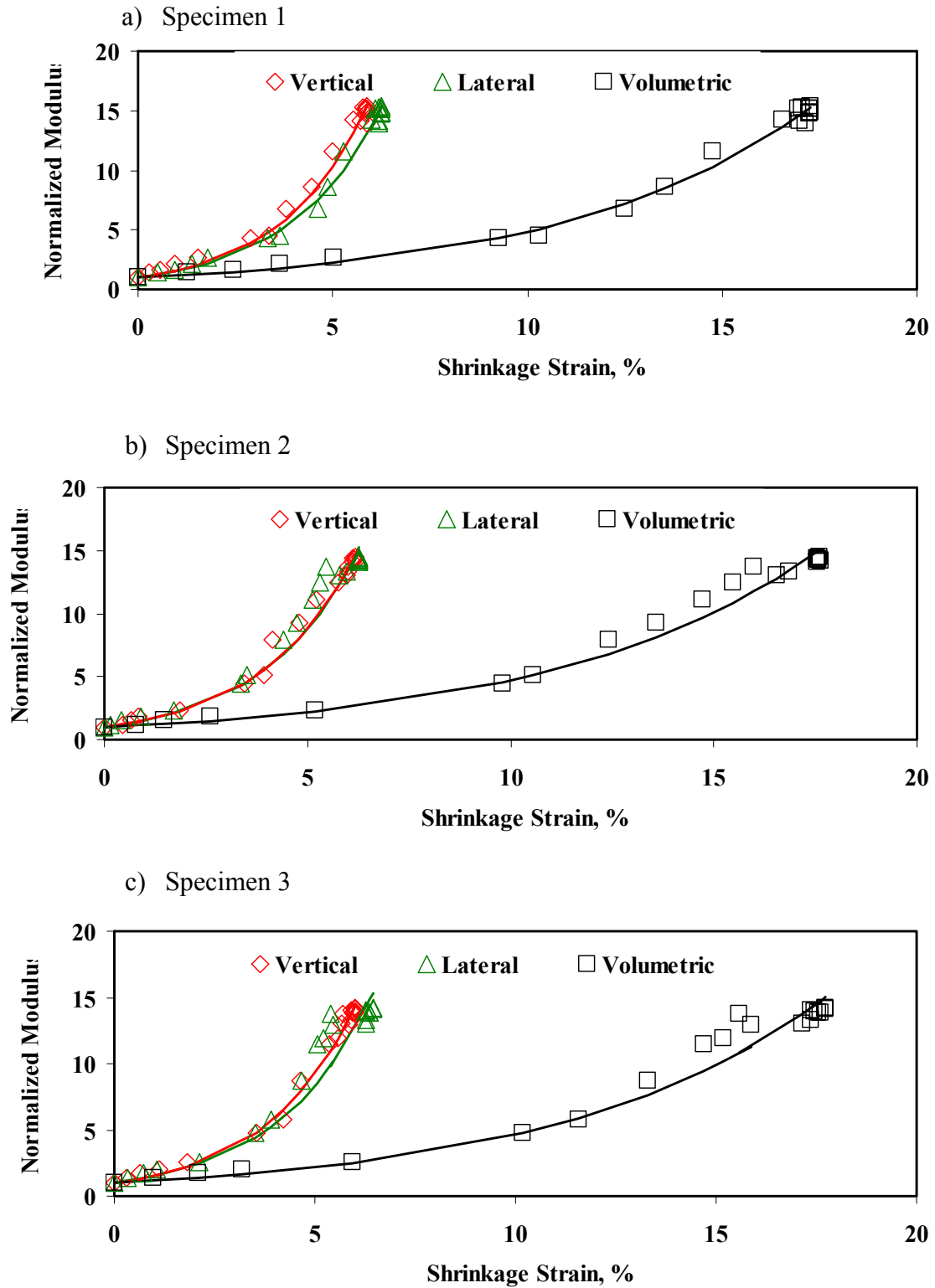


Figure D.3 Typical Variations in Shrinkage Strain and NMC for Clay from Fort Worth District

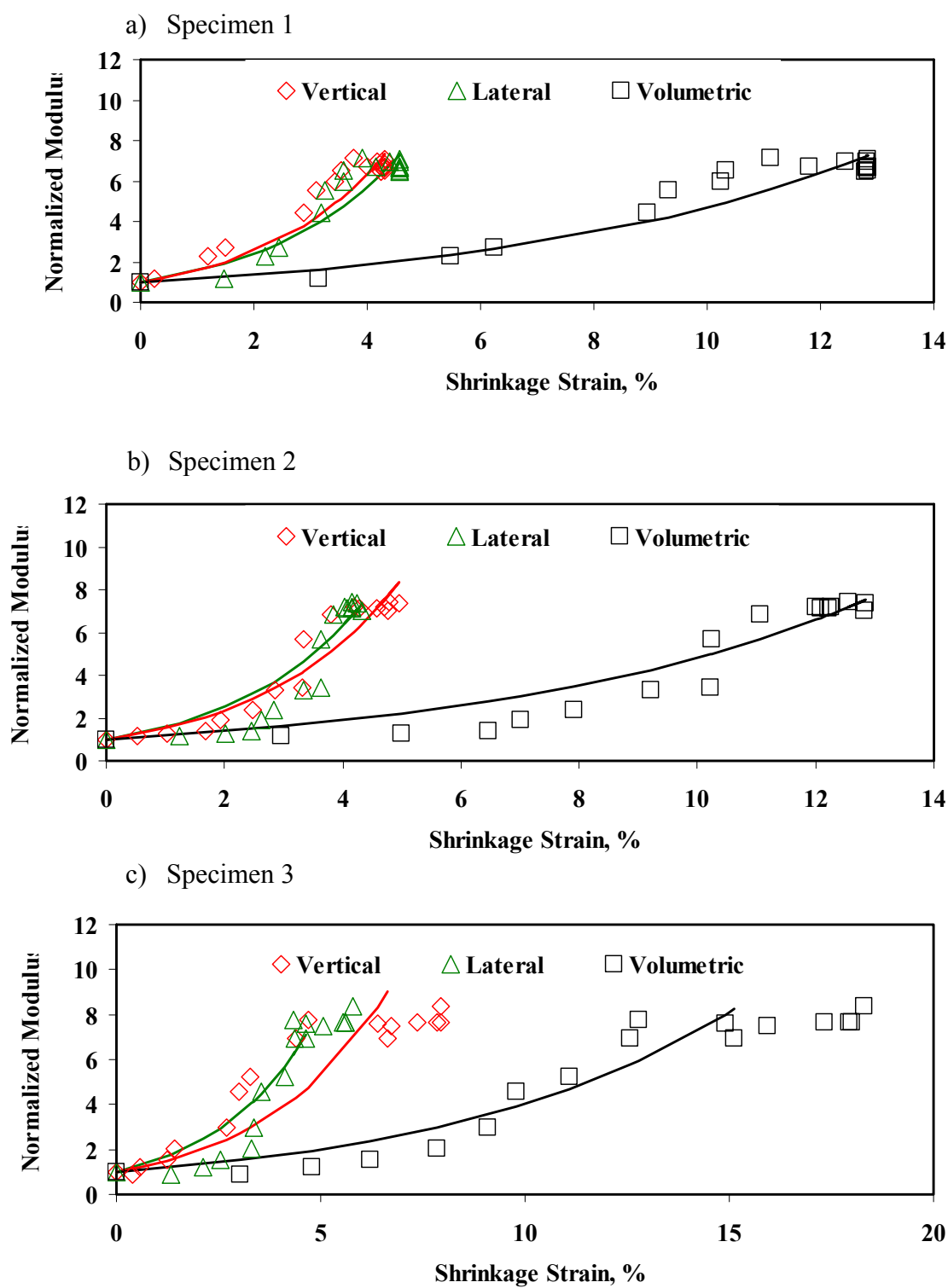


Figure D.4 Typical Variations in Shrinkage Strain and NMC for Clay from Bryan District

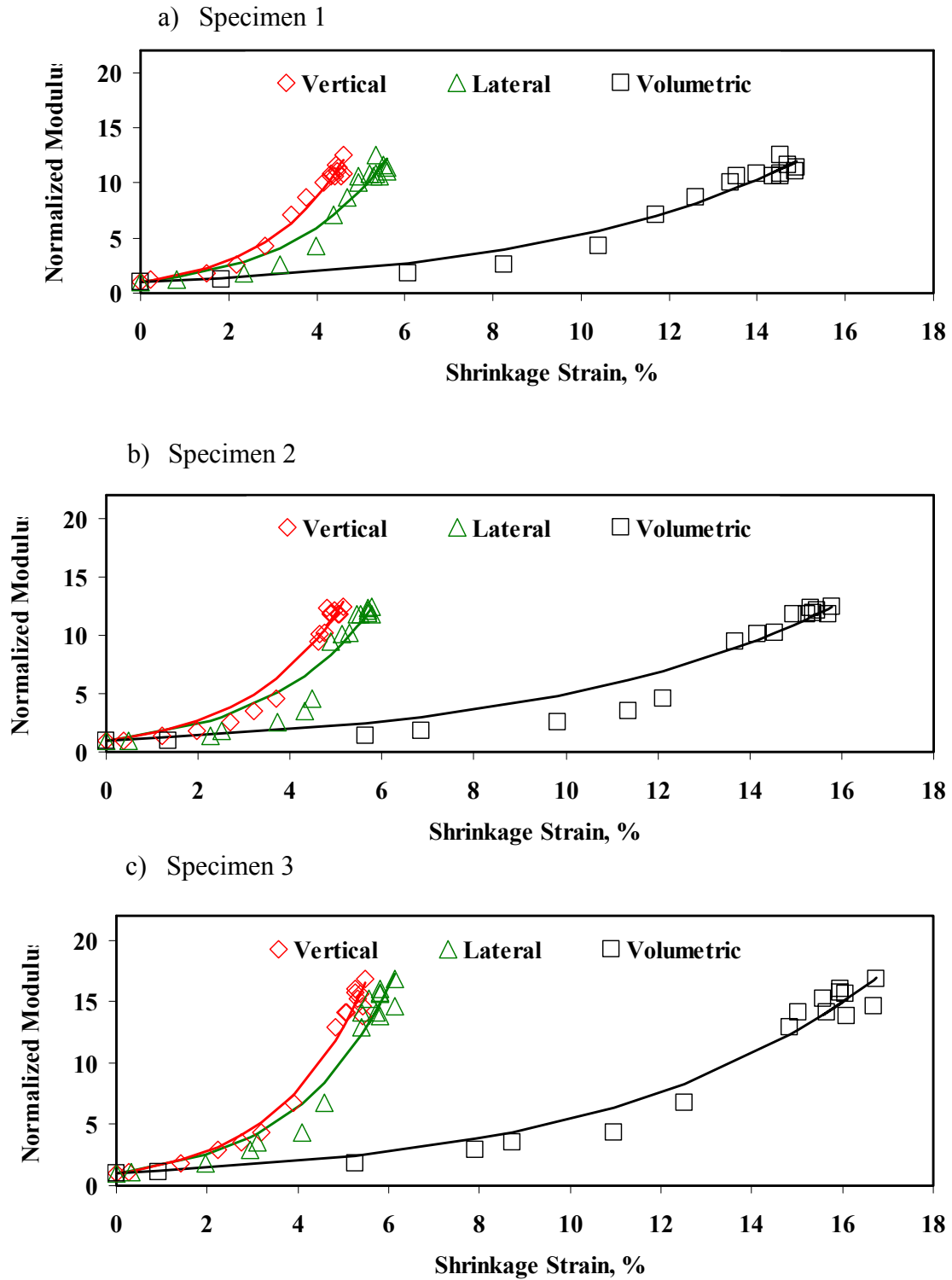
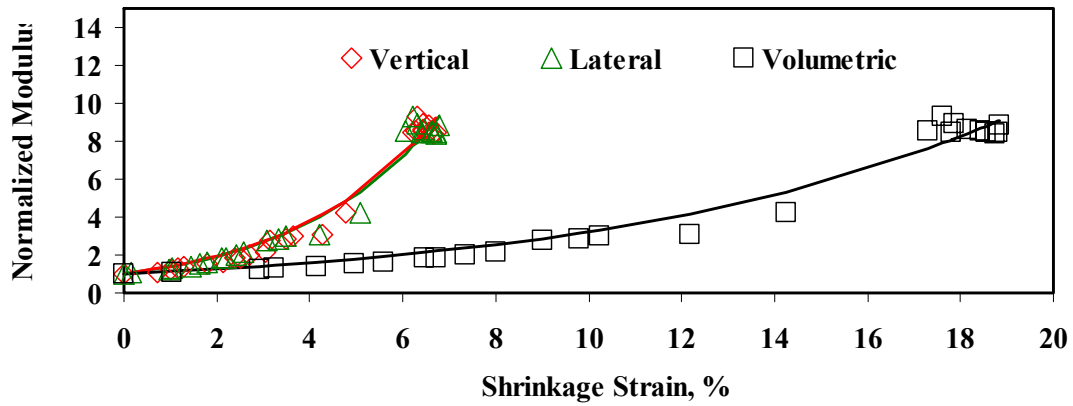
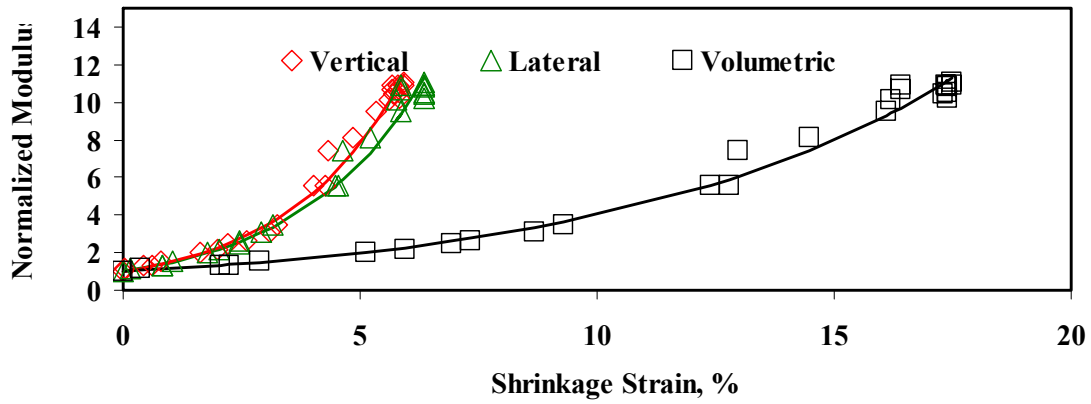


Figure D.5 Typical Variations in Shrinkage Strain and NMC for Clay from Houston District

a) Specimen 1



b) Specimen 2



c) Specimen 3

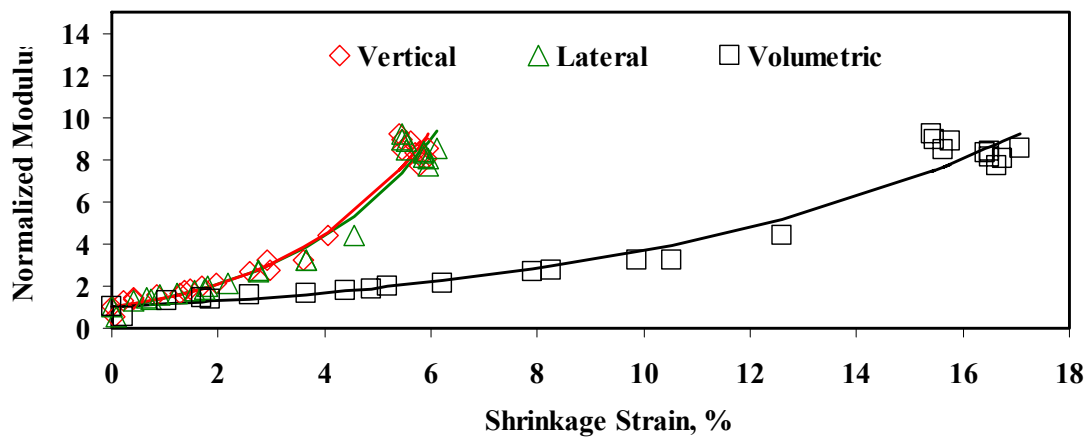


Figure D.6 Typical Variations in Shrinkage Strain and NMC for Clay from Paris District

**APPENDIX E - Expansion Strain VS Normalized
Moisture Content – SFO Results**

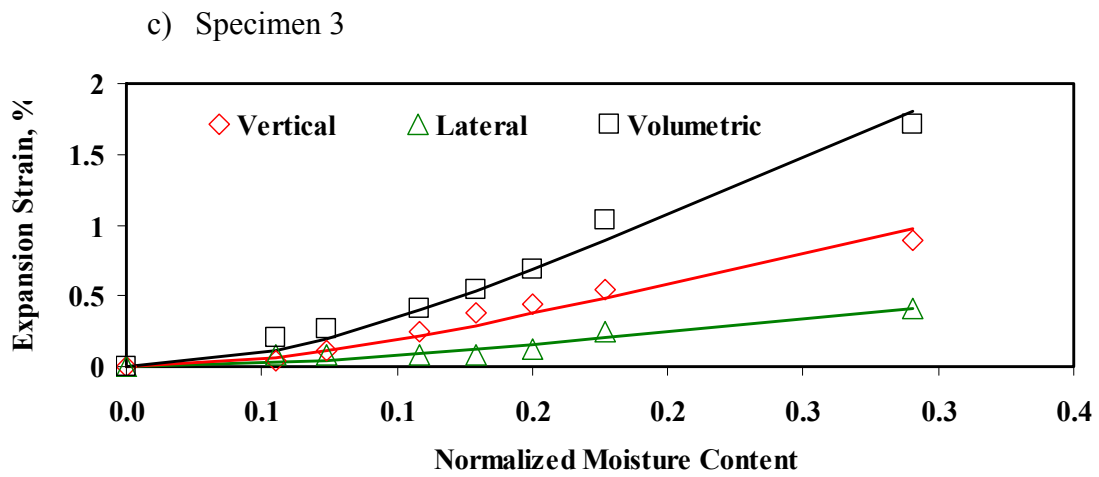
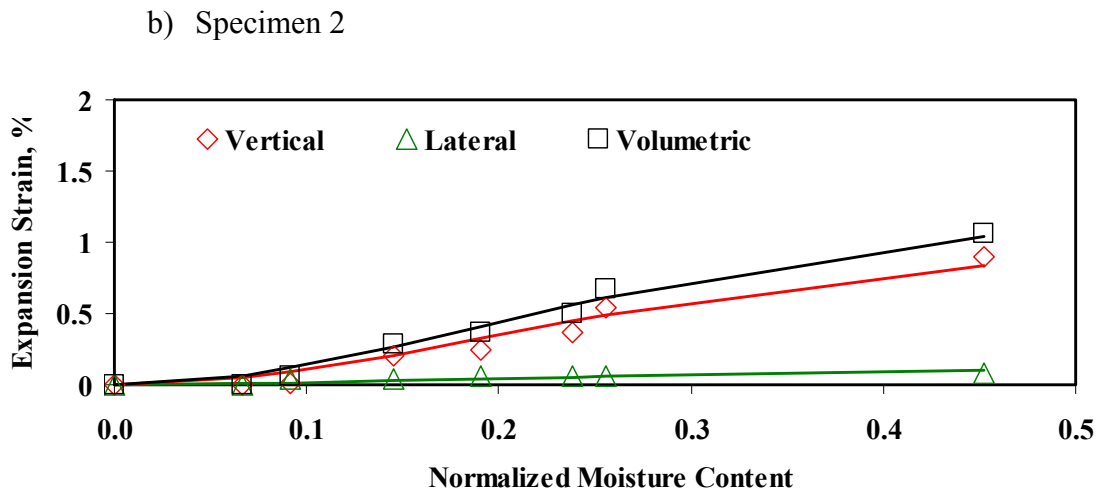
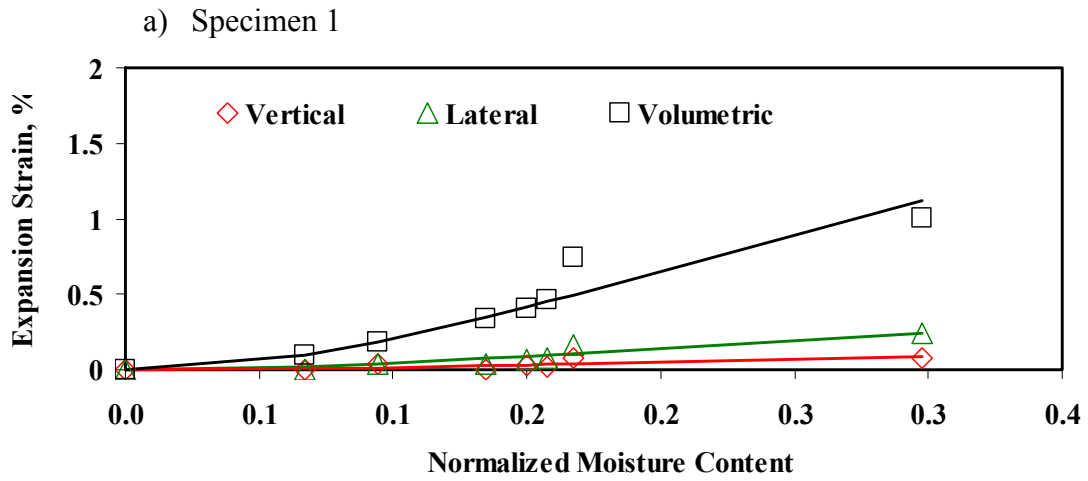


Figure E.1 Typical Variations in Expansion Strain and NMC for Clay from El Paso District

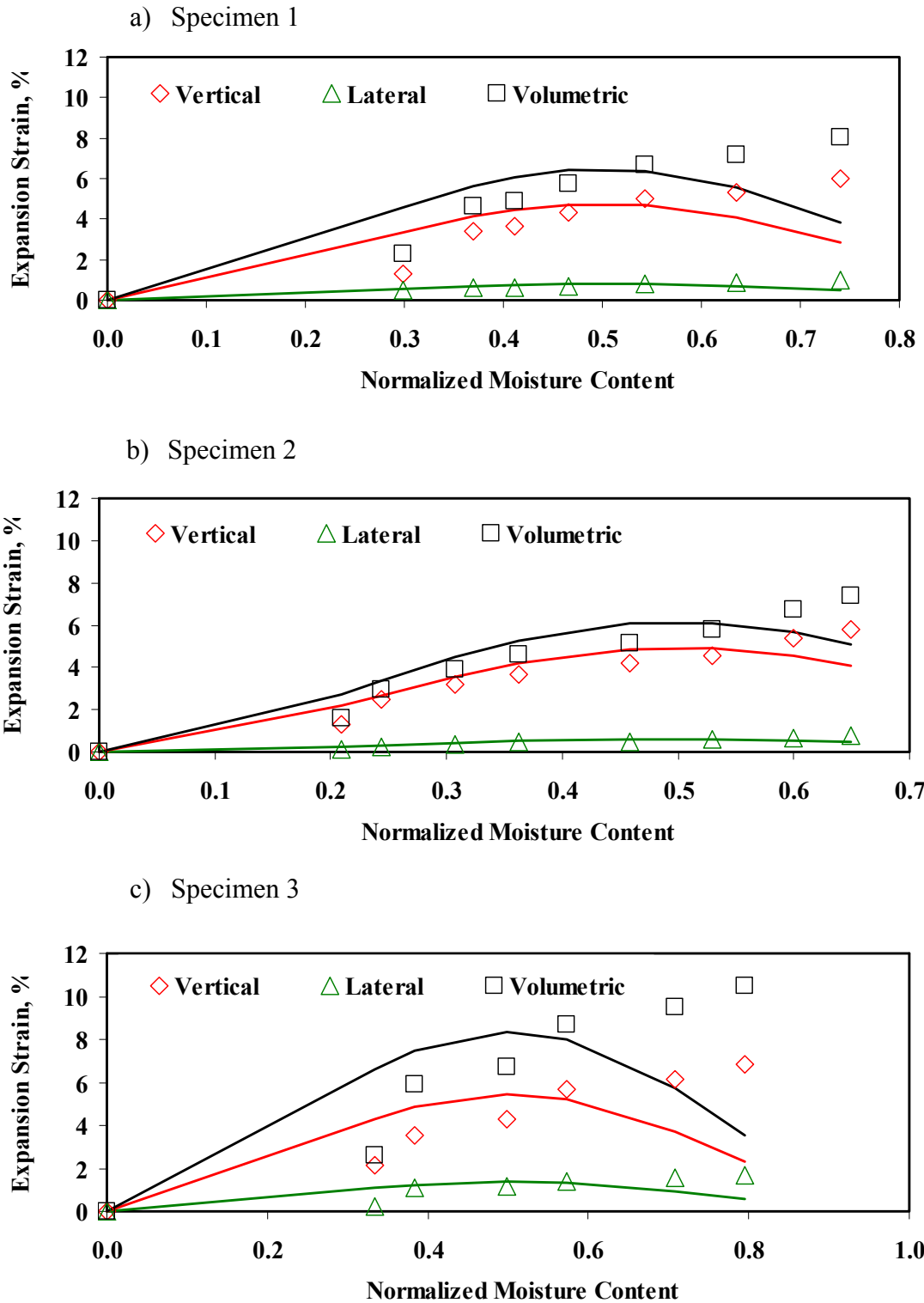


Figure E.2 Typical Variations in Expansion Strain and NMC for Clay from San Antonio District

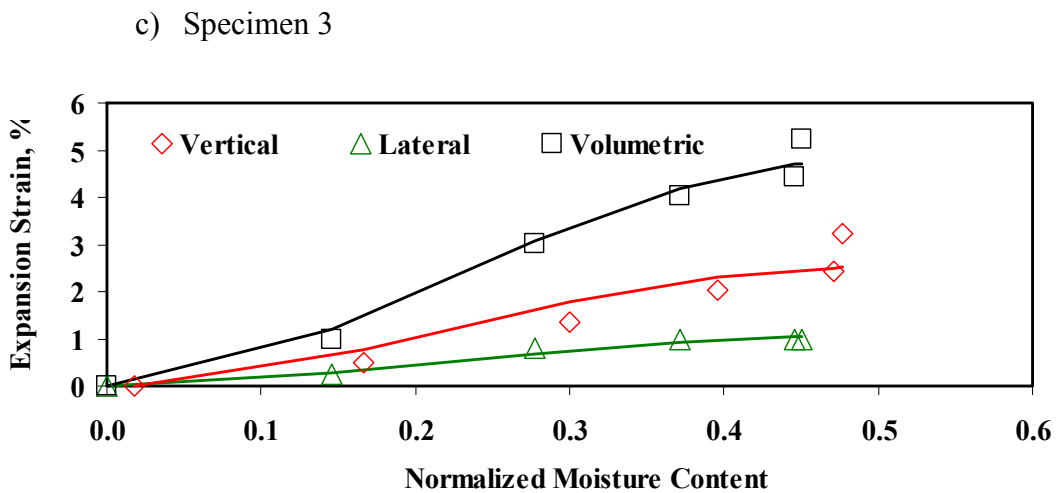
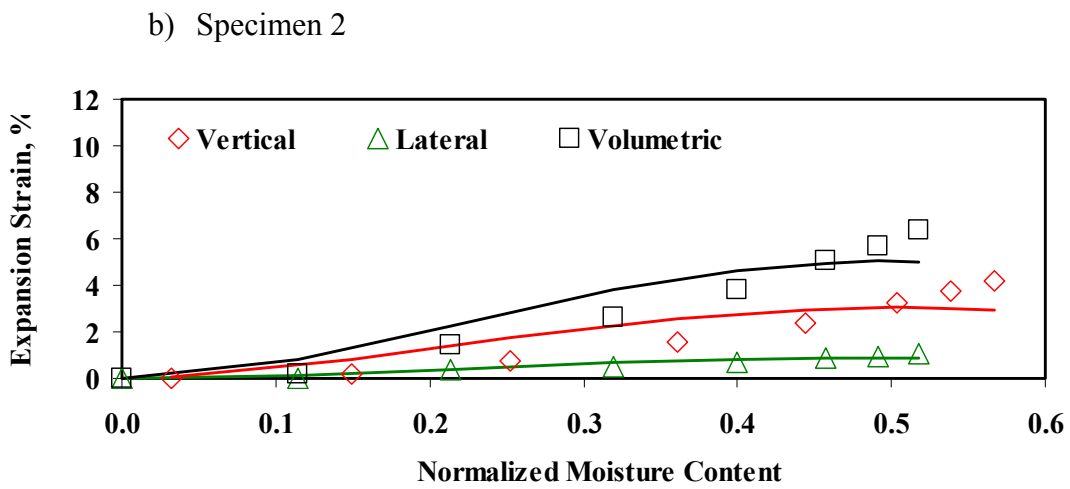
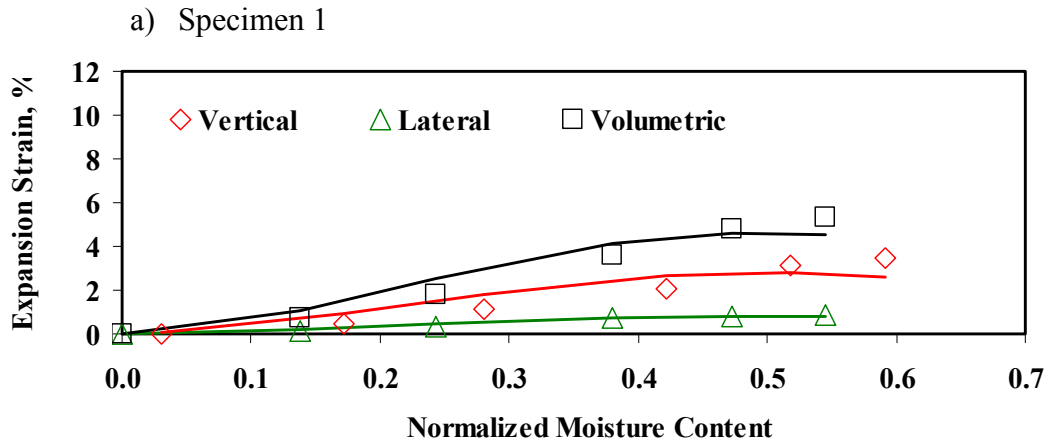


Figure E.3 Typical Variations in Expansion Strain and NMC for Clay from Fort Worth District

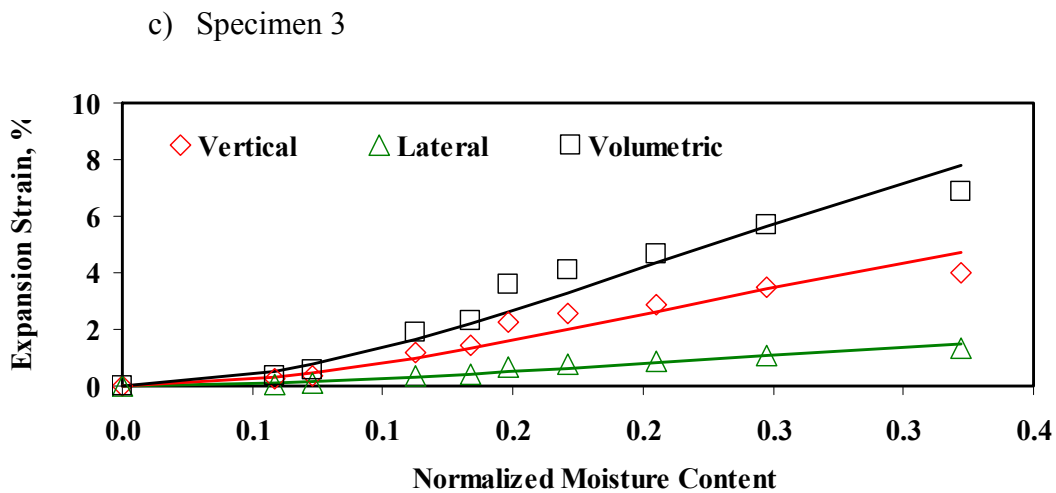
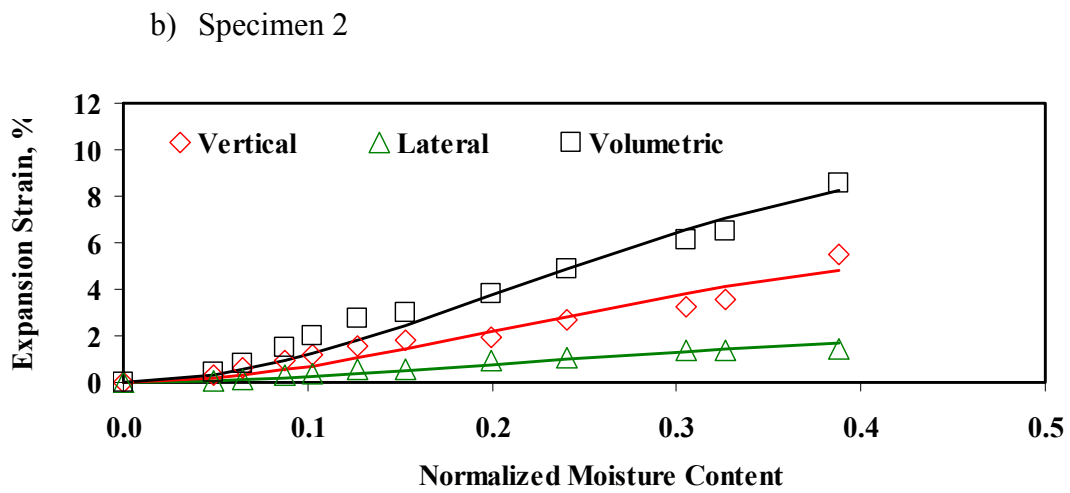
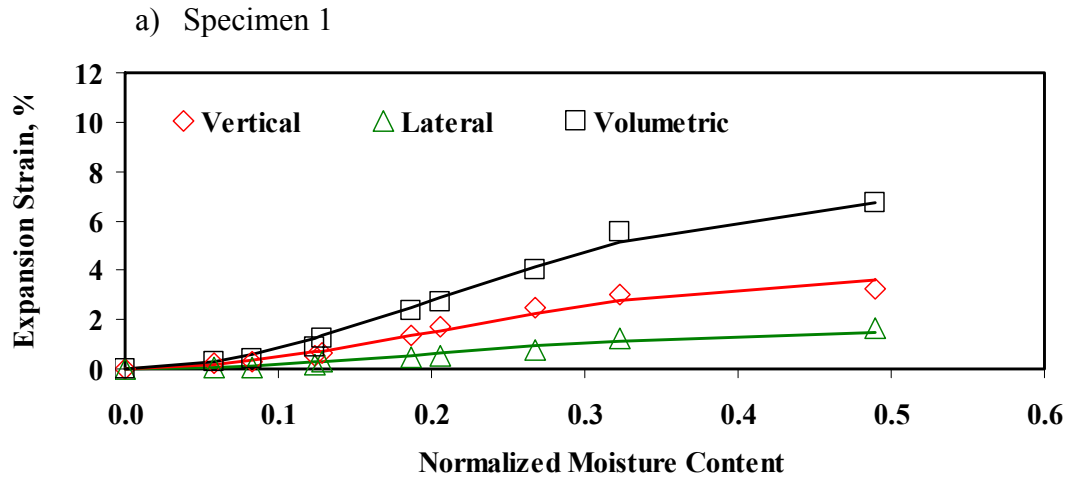
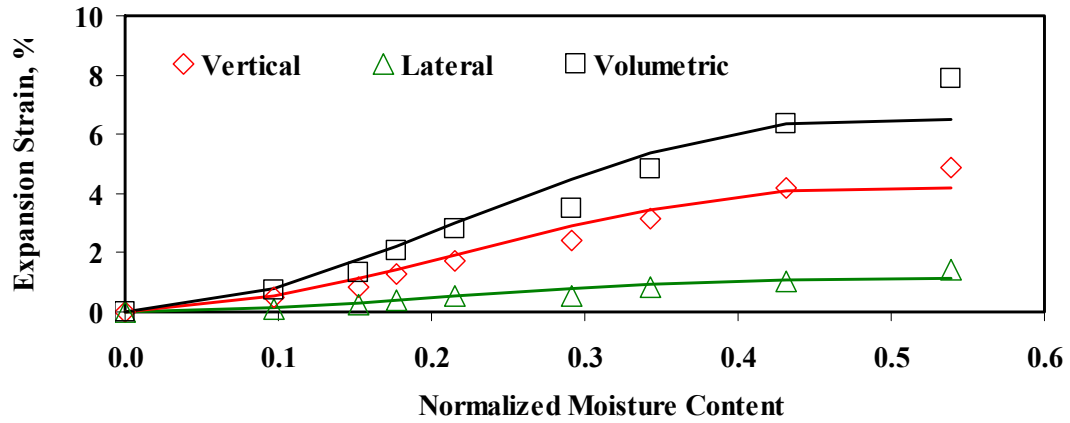
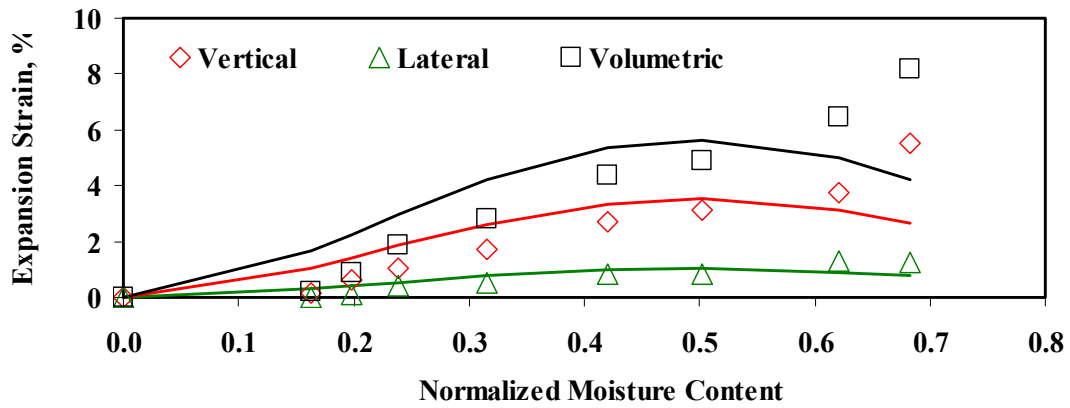


Figure E.4 Typical Variations in Expansion Strain and NMC for Clay from Bryan District

a) Specimen 1



b) Specimen 2



c) Specimen 3

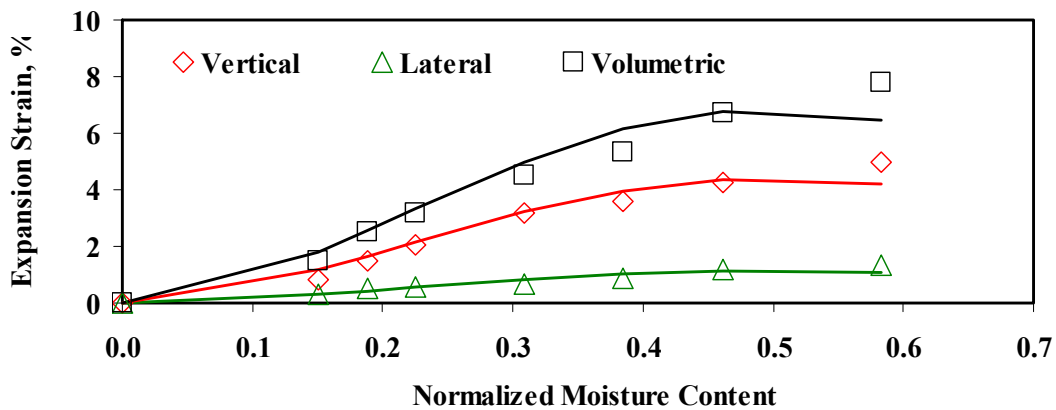


Figure E.5 Typical Variations in Expansion Strain and NMC for Clay from Houston District

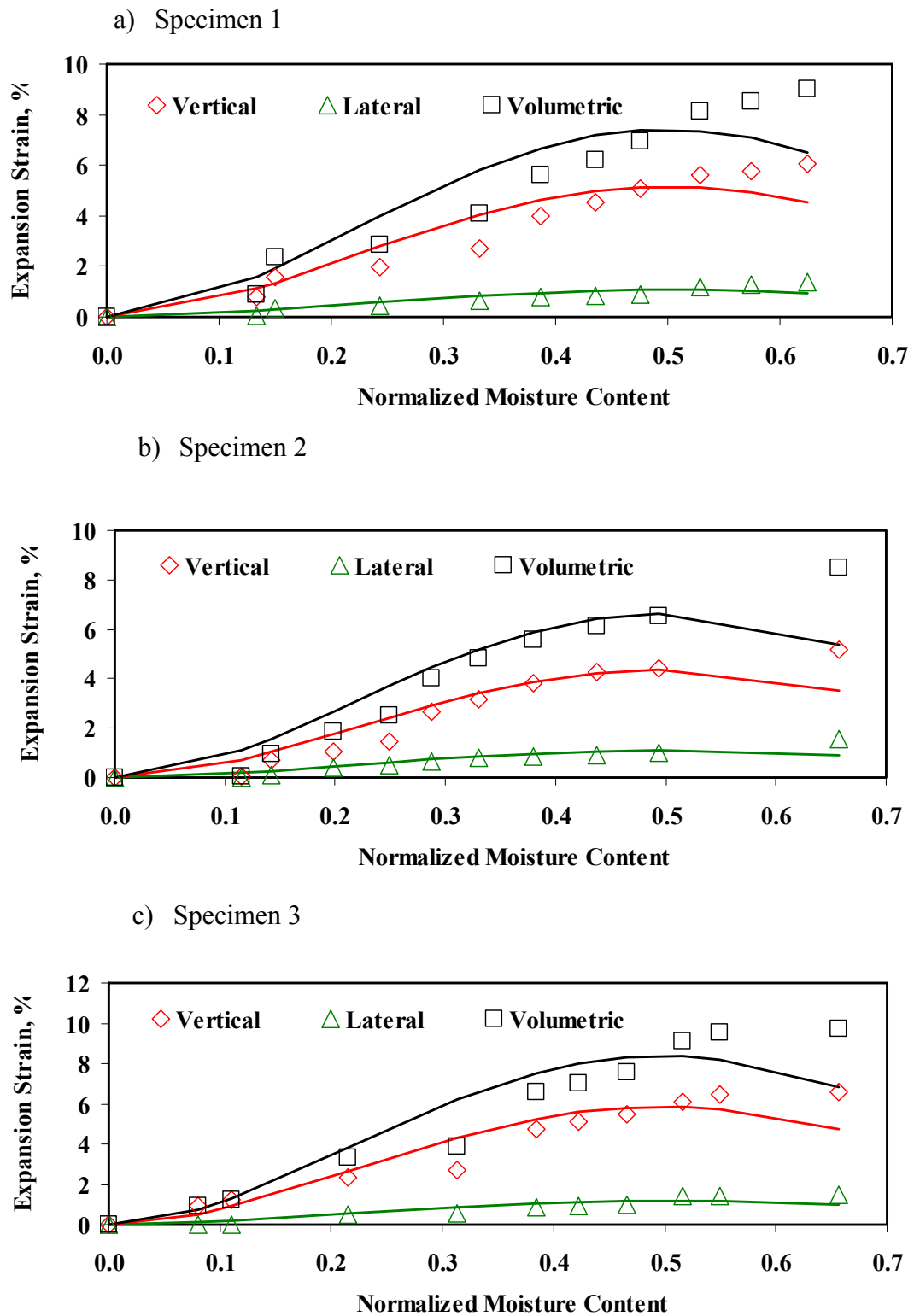
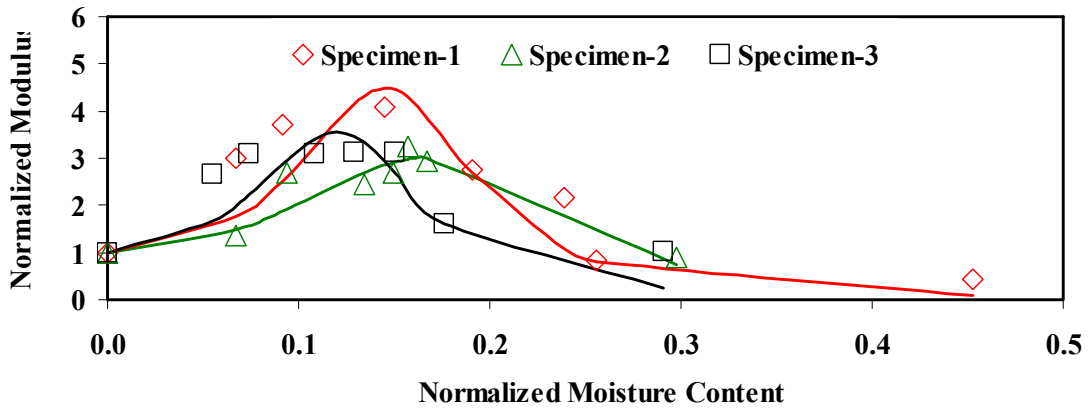


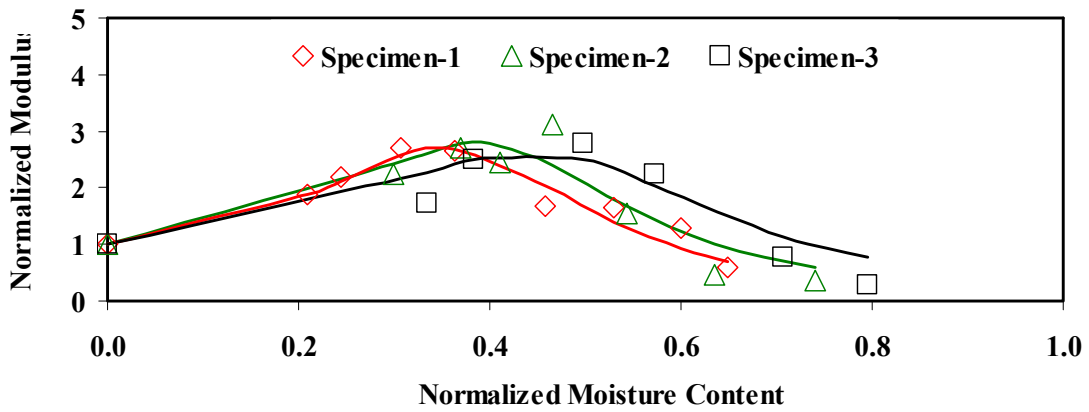
Figure E.6 Typical Variations in Expansion Strain and NMC for Clay from Paris District

**APPENDIX F - Normalized Modulus VS Normalized
Moisture Content – SFO Results**

a) El Paso



b) San Antonio



c) Fort Worth

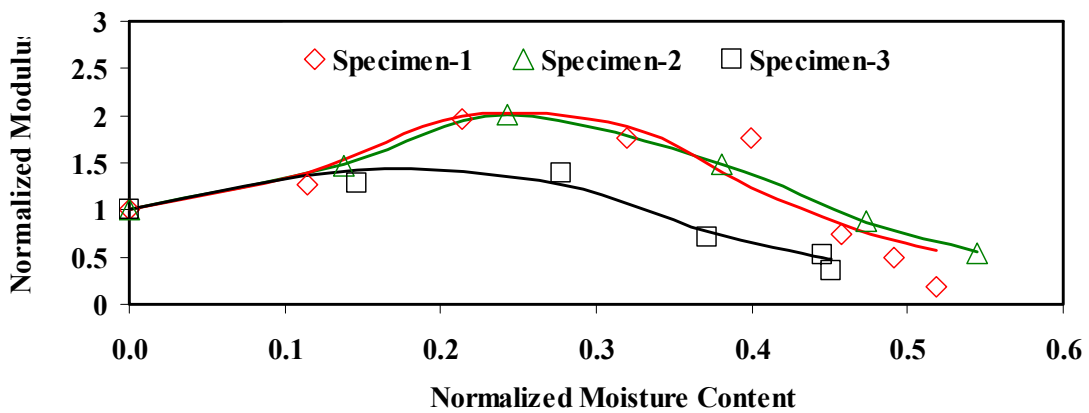
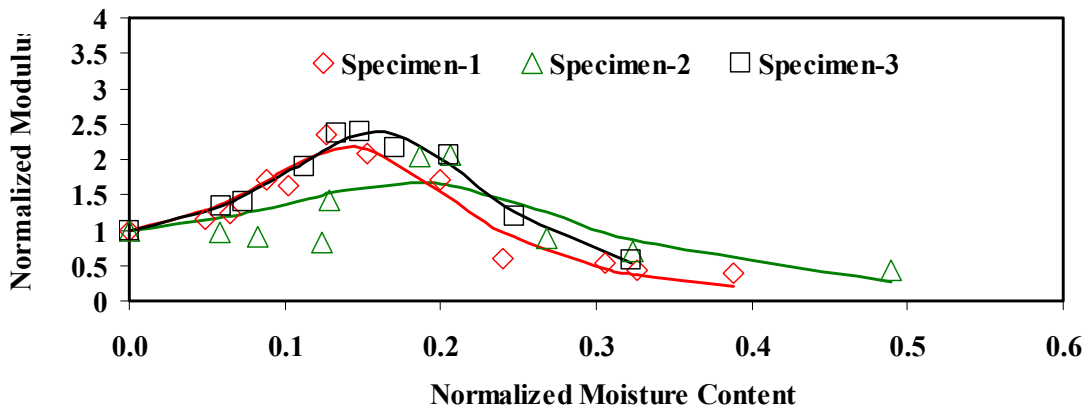
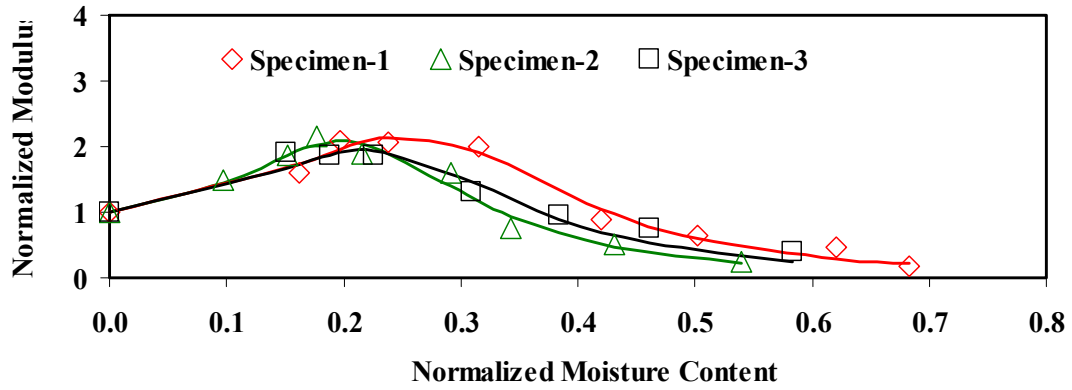


Figure F.1 Typical Variations in Normalized Modulus and NMC

a) Bryan



b) Houston



c) Paris

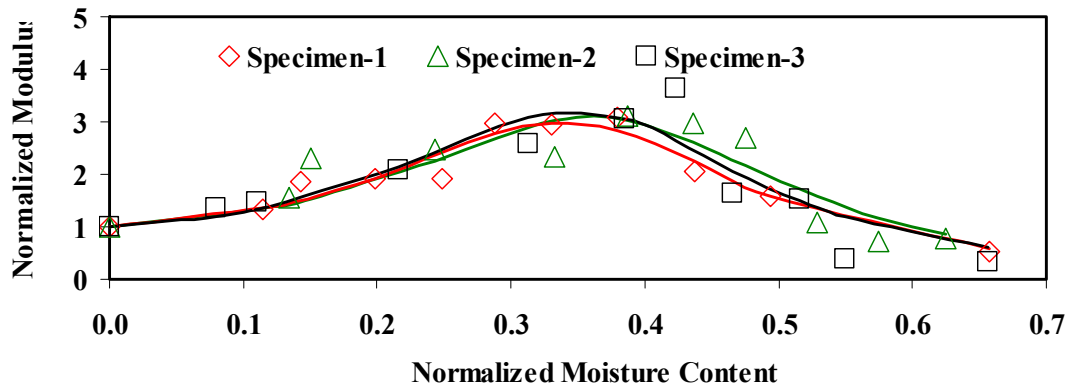
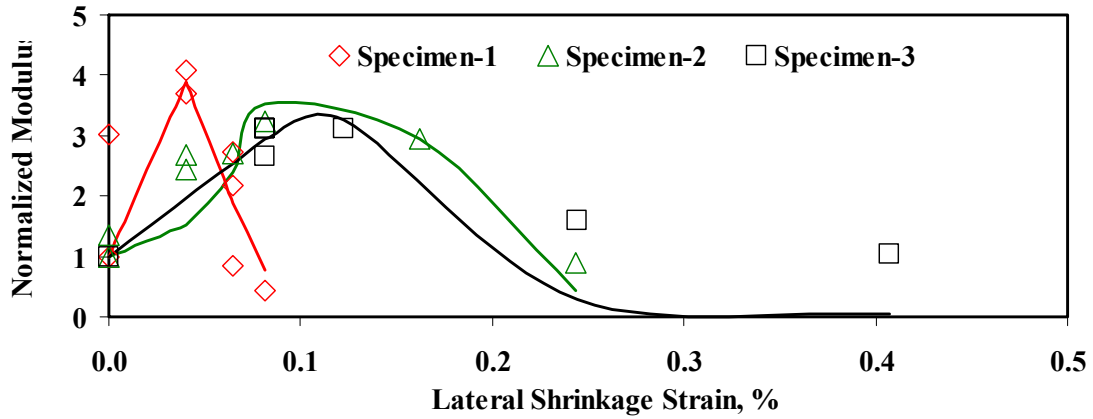


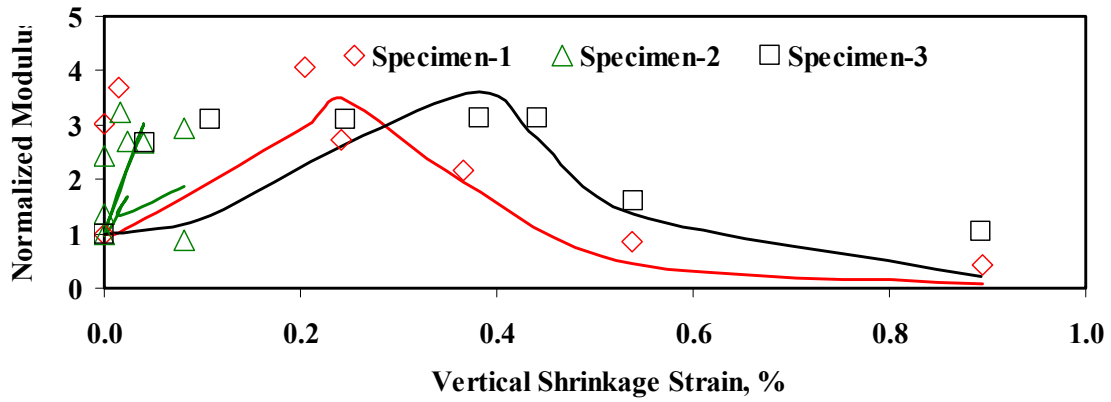
Figure F.2 Typical Variations in Normalized Modulus and NMC

**APPENDIX G - Normalized Modulus
VS Expansion Strain – SFO Results**

a) Specimen 1



b) Specimen 2



c) Specimen 3

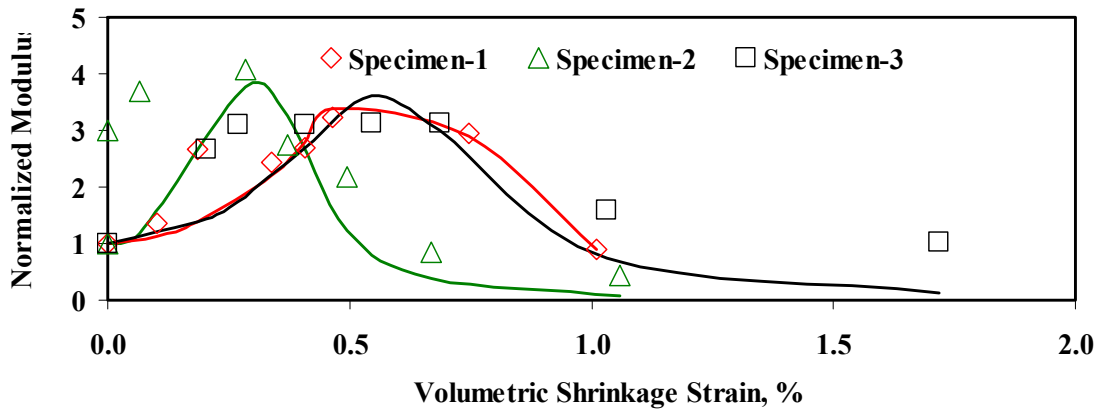


Figure G.1 Typical Variations in Normalized Modulus and Expansion Strain for Clay from El Paso District

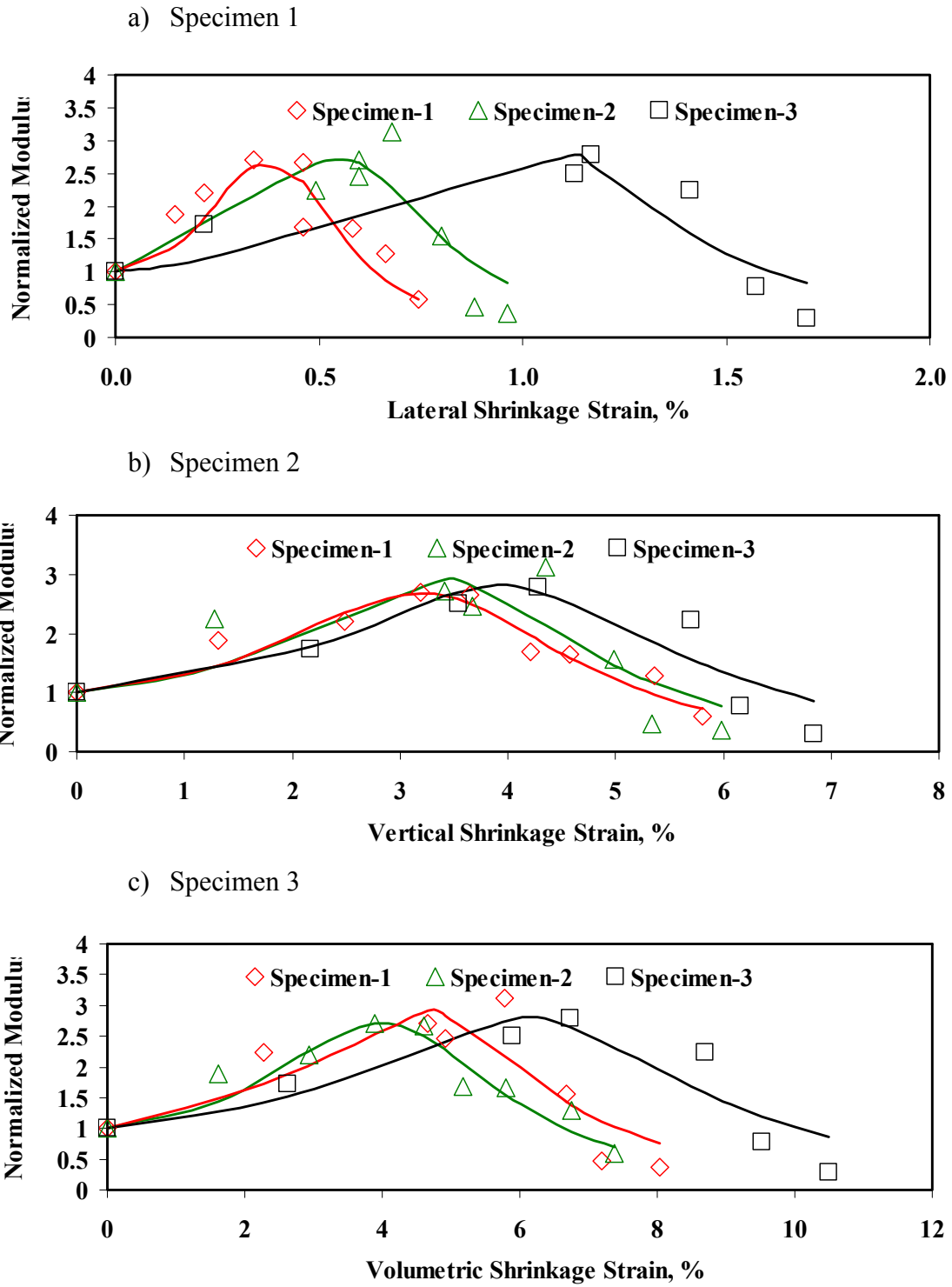


Figure G.2 Typical Variations in Modulus and Expansion Strain for Clay from San Antonio District

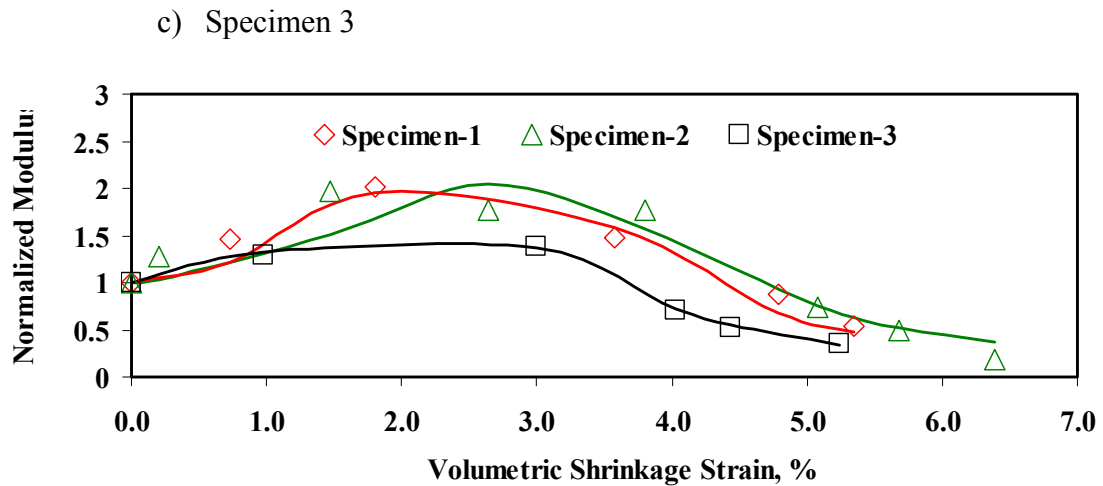
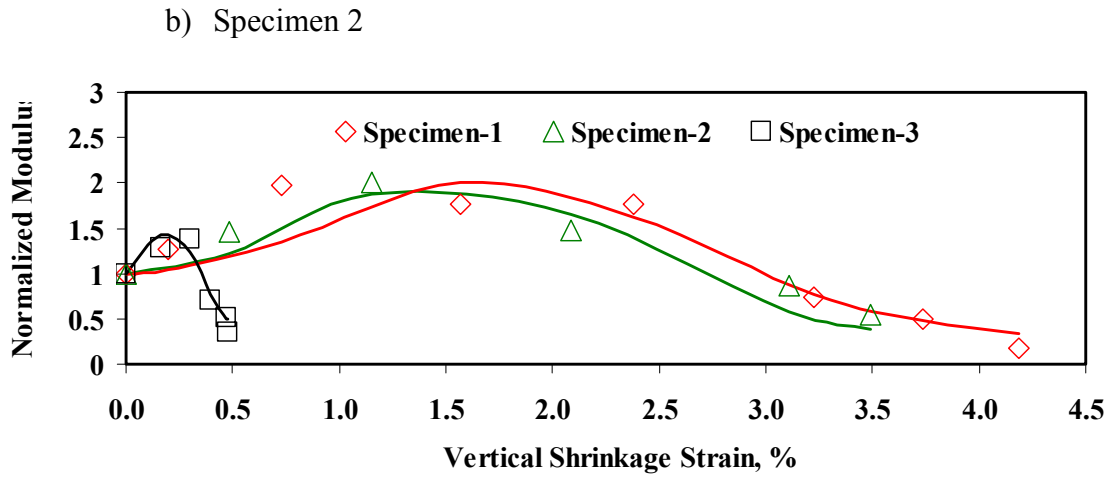
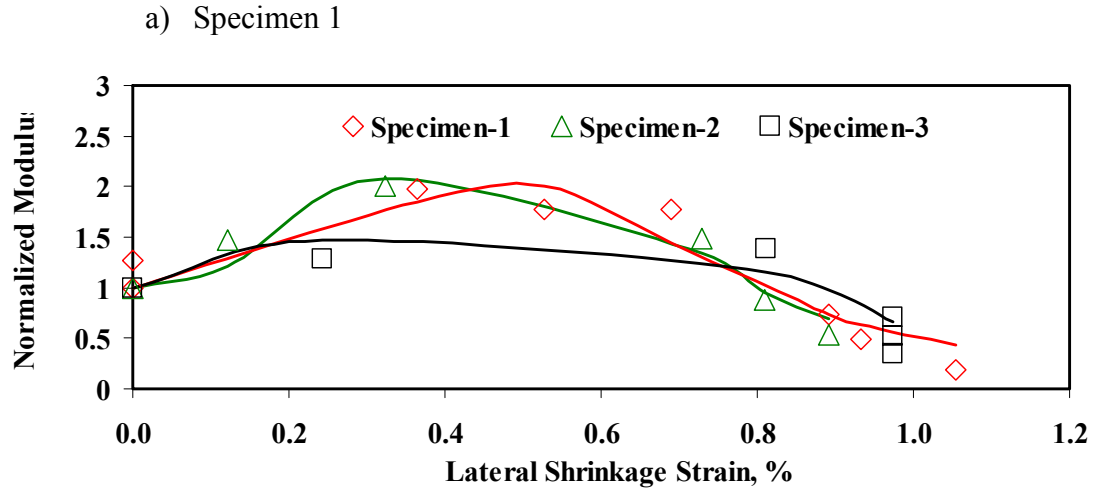
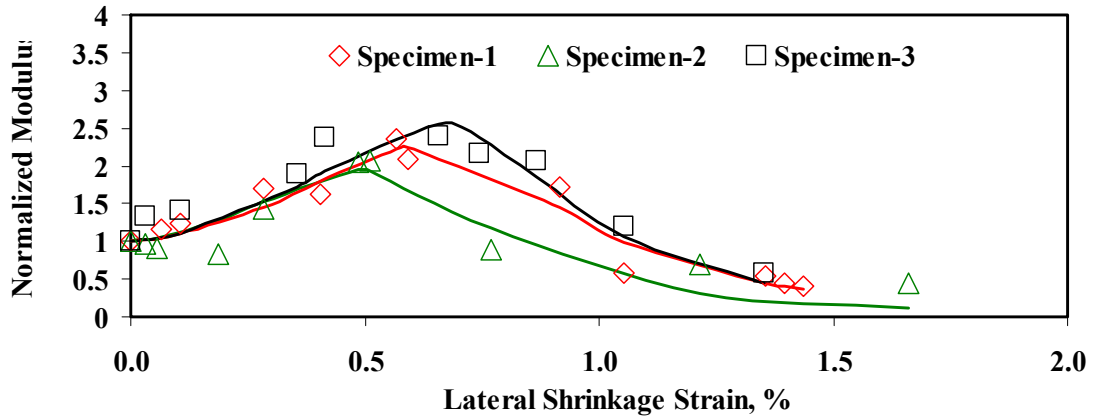
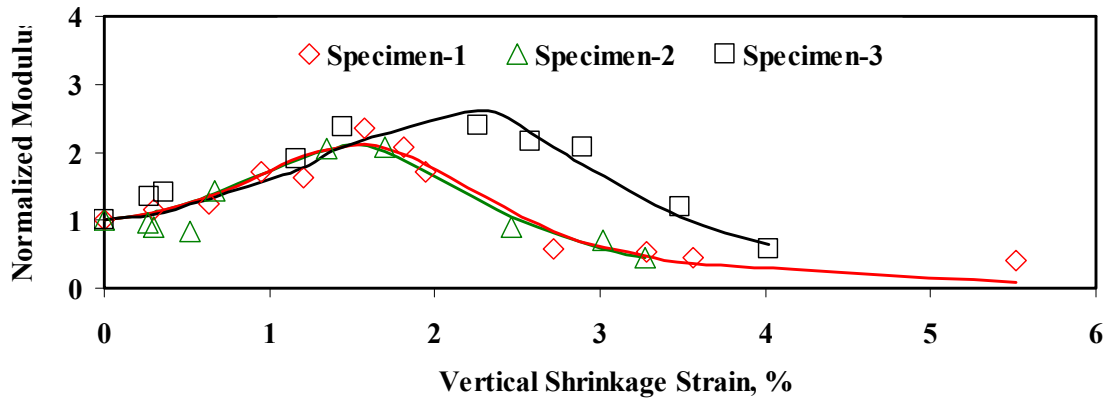


Figure G.3 Typical Variations in Shrinkage Modulus and Expansion Strain for Clay from Fort Worth District

a) Specimen 1



b) Specimen 2



c) Specimen 3

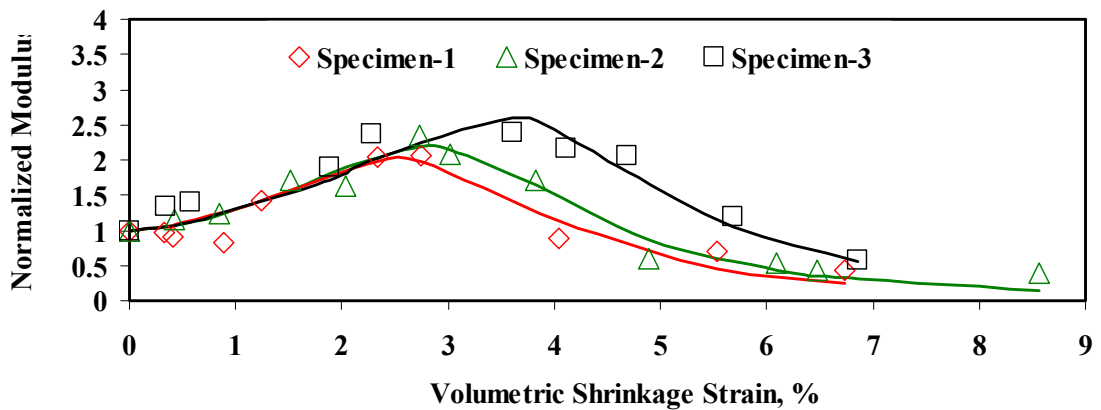
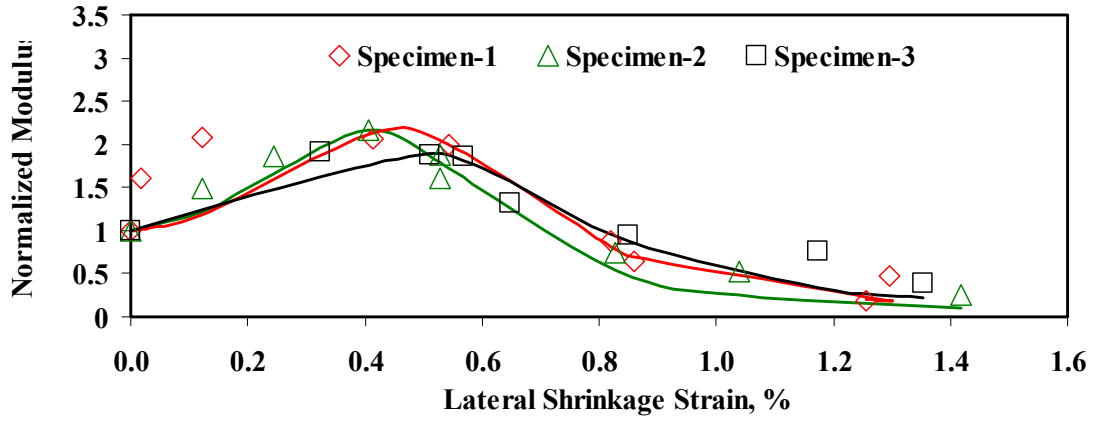
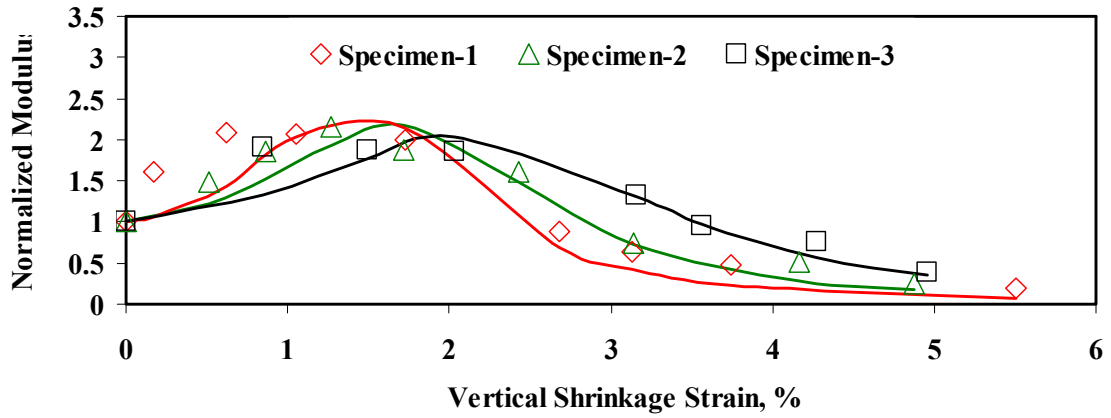


Figure G.4 Typical Variations in Modulus and Expansion Strain for Clay from Bryan District

a) Specimen 1



b) Specimen 2



c) Specimen 3

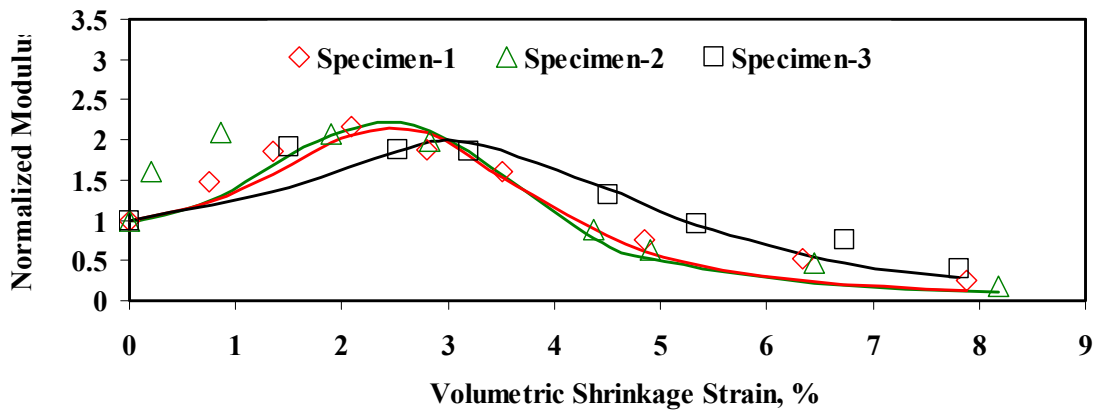
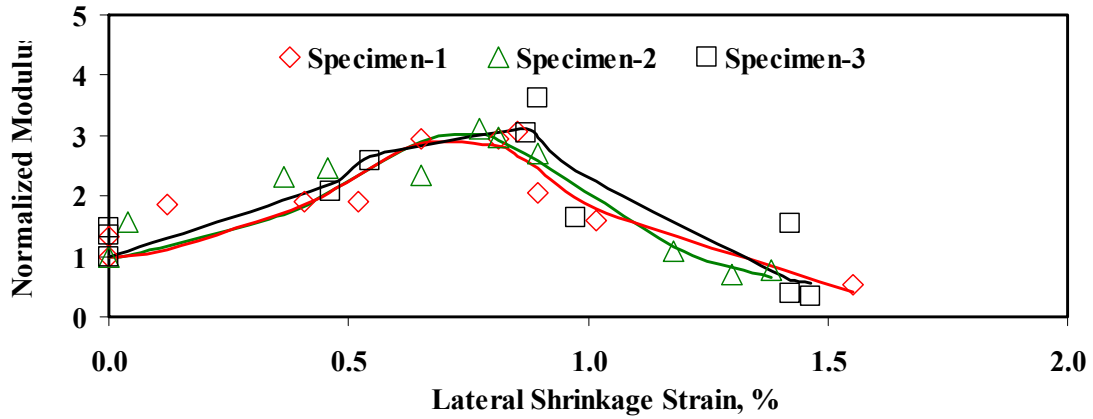
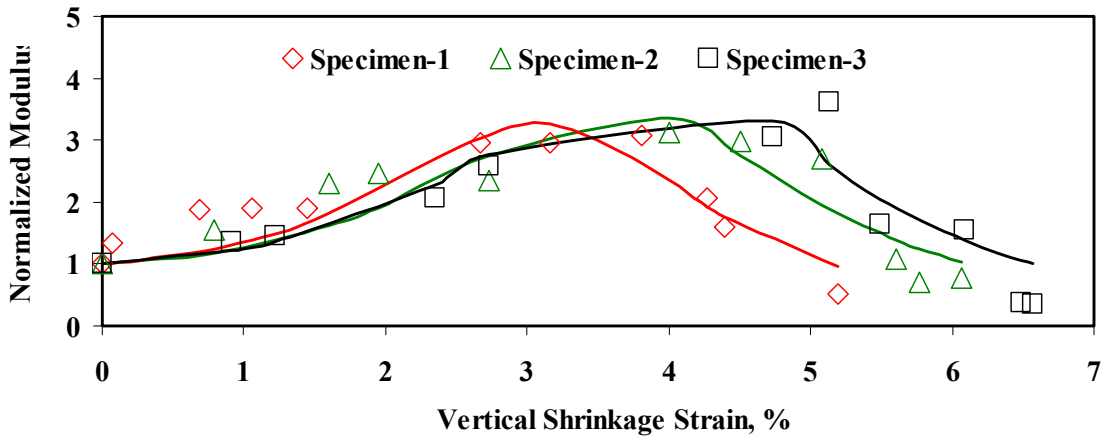


Figure G.5 Typical Variations in Modulus and Expansion Strain for Clay from Houston District

a) Specimen 1



b) Specimen 2



c) Specimen 3

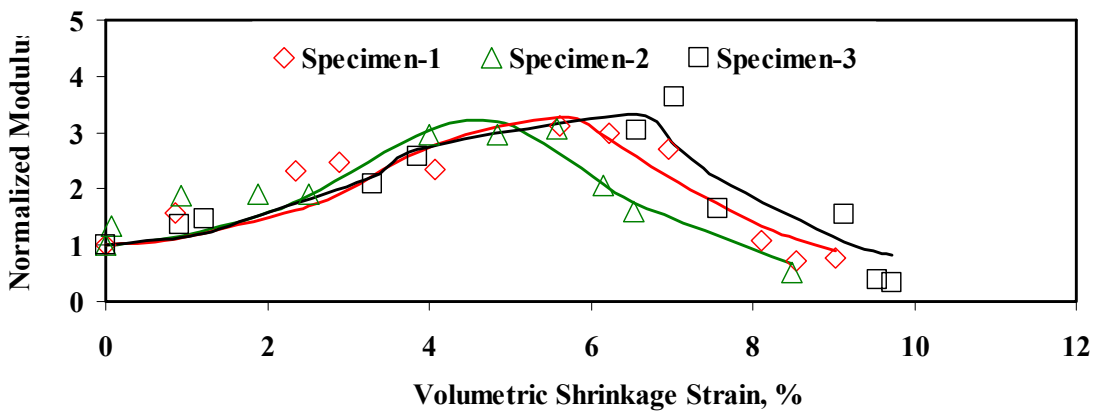


Figure G.6 Typical Variations in Modulus and Expansion Strain for Clay from Paris District

APPENDIX H - Shrinkage Strain VS Normalized Moisture Content – DFS Results

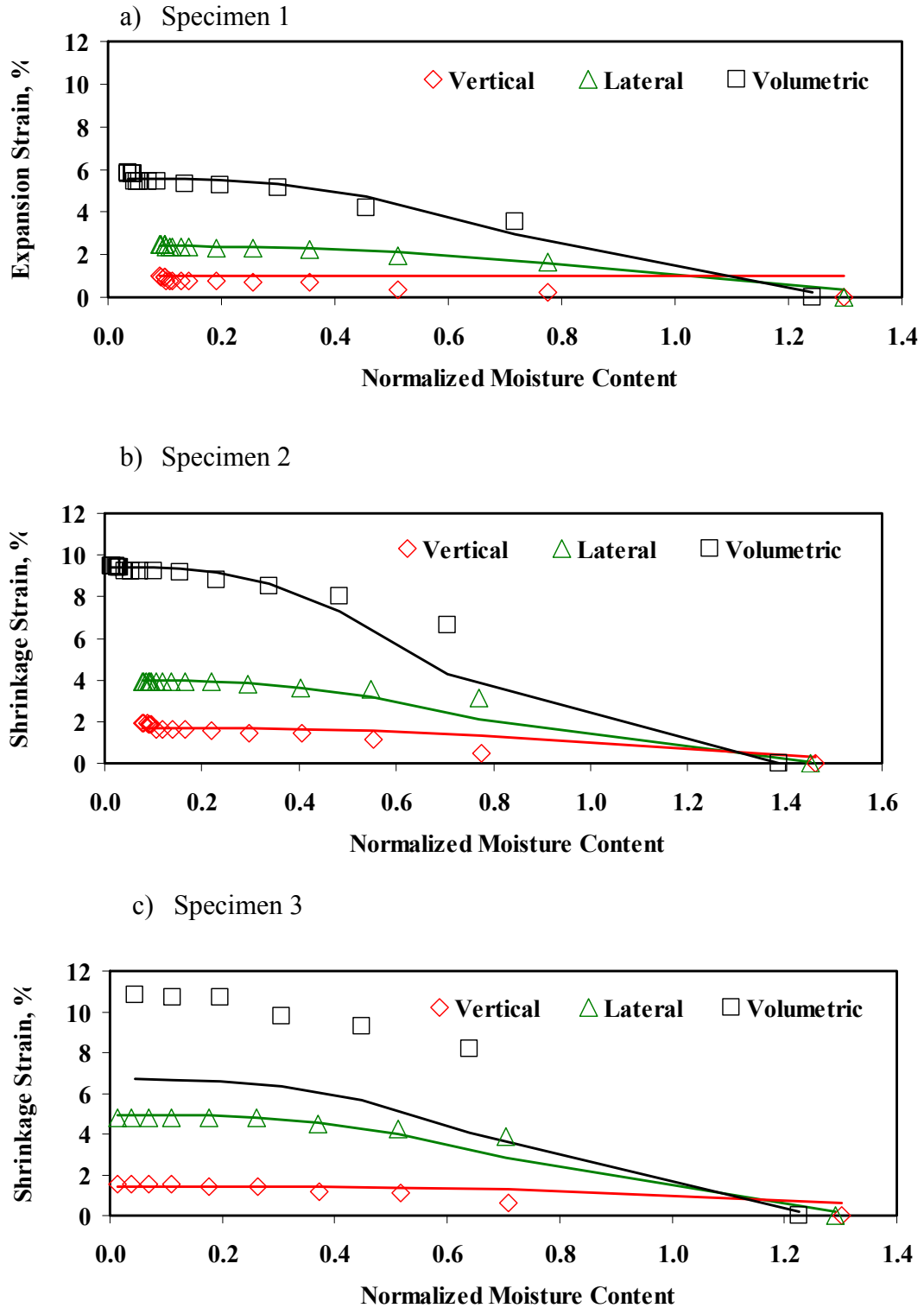


Figure H.1 Typical Variations in Shrinkage Strain and NMC for Clay from El Paso District

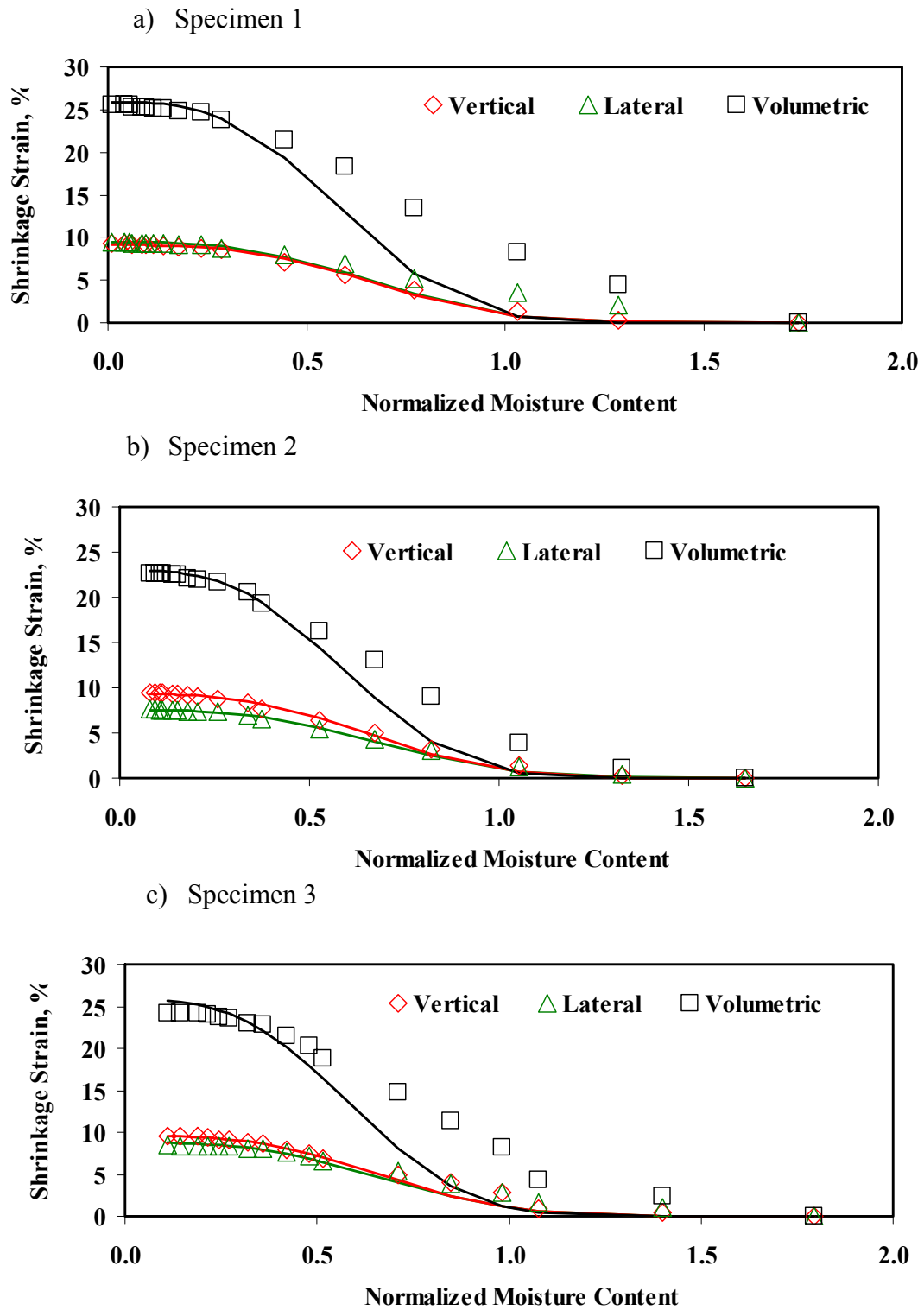
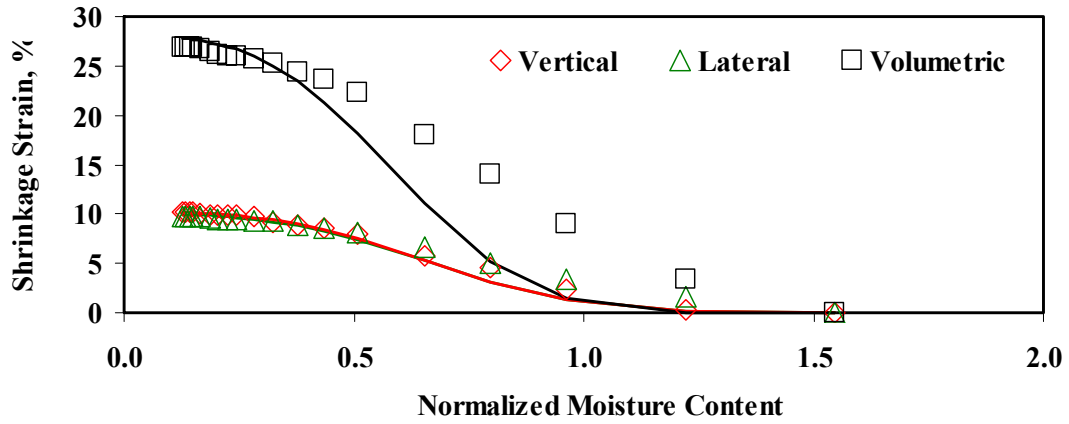
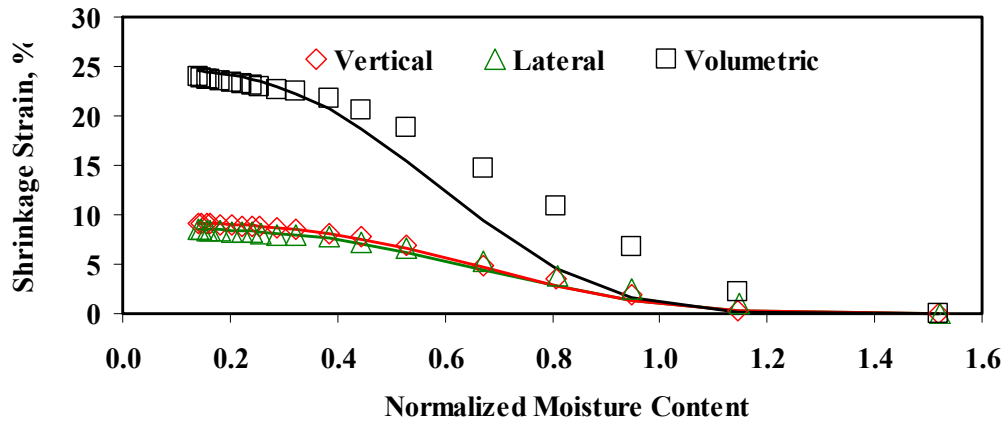


Figure H.2 Typical Variations in Shrinkage Strain and NMC for Clay from San Antonio District

a) Specimen 1



b) Specimen 2



c) Specimen 3

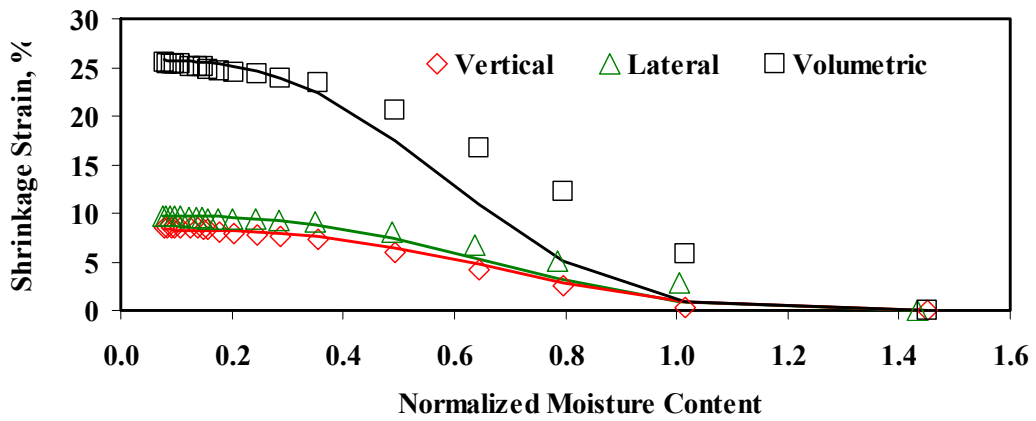
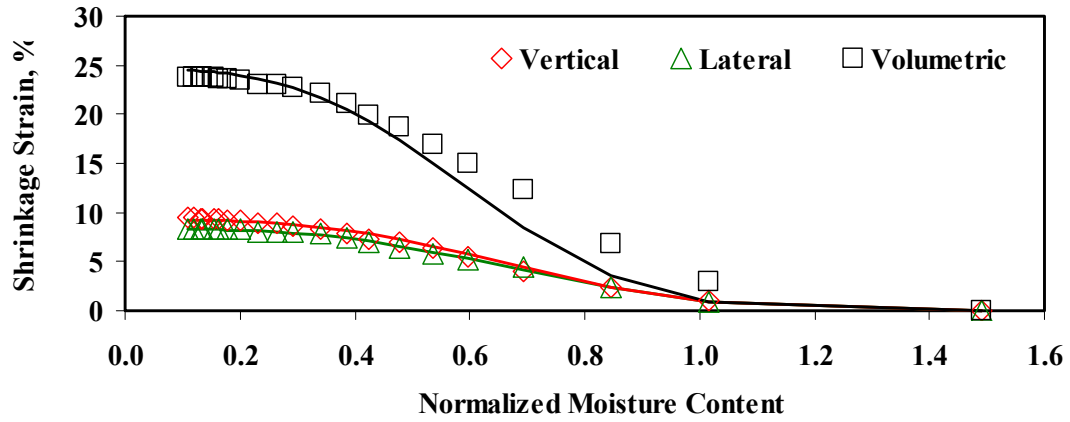
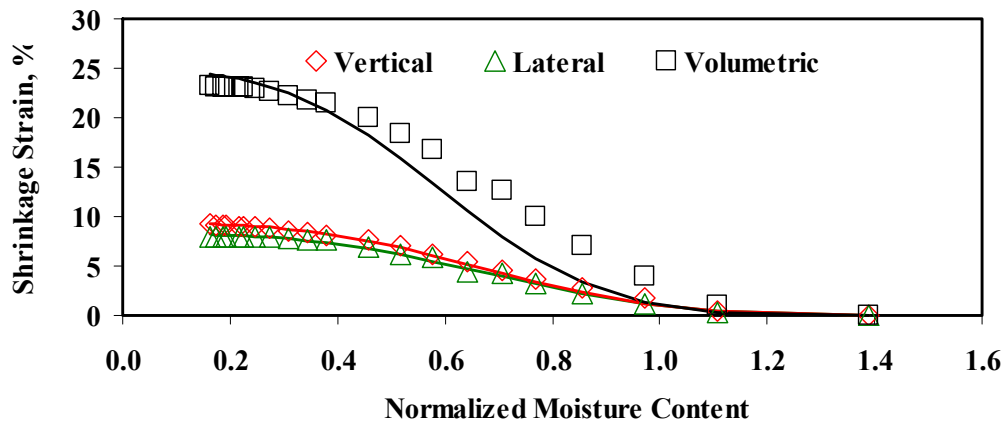


Figure H.3 Typical Variations in Shrinkage Strain and NMC for Clay from Fort Worth District

a) Specimen 1



b) Specimen 2



c) Specimen 3

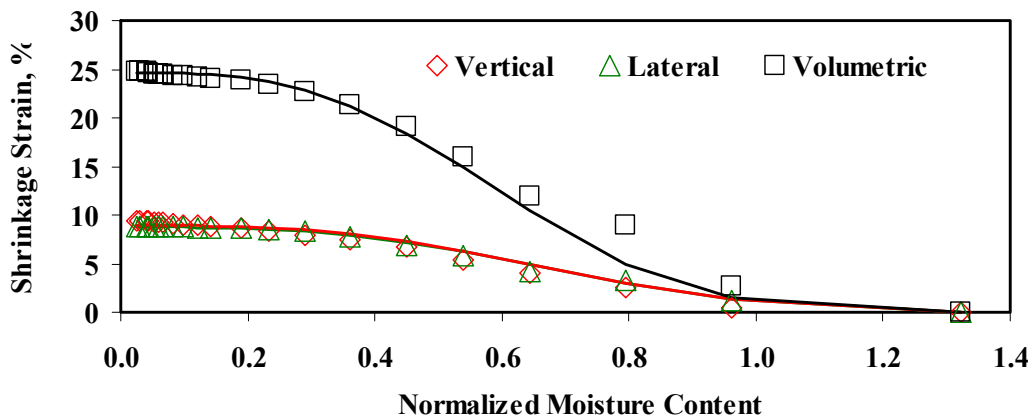


Figure H.4 Typical Variations in Shrinkage Strain and NMC for Clay from Bryan District

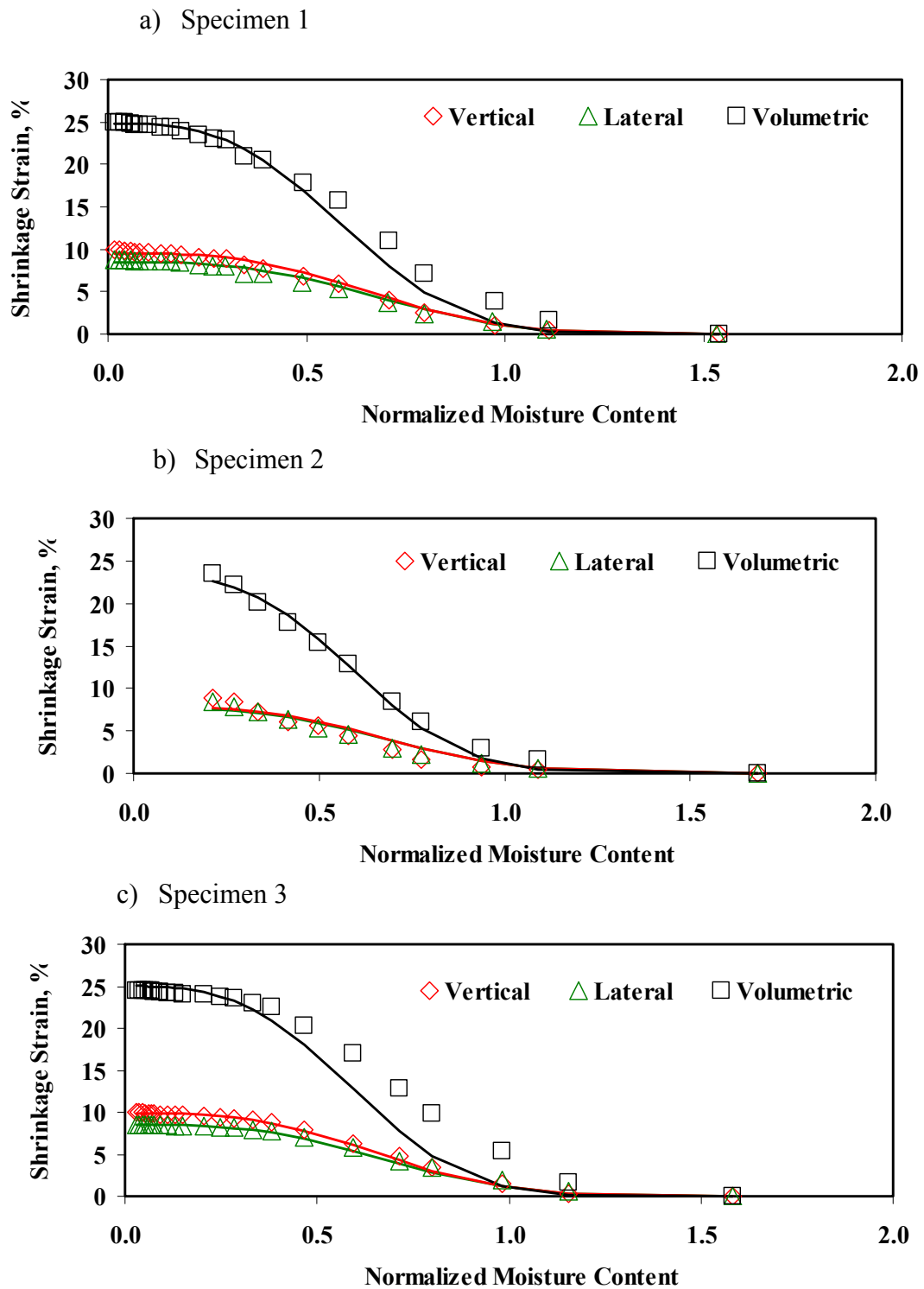
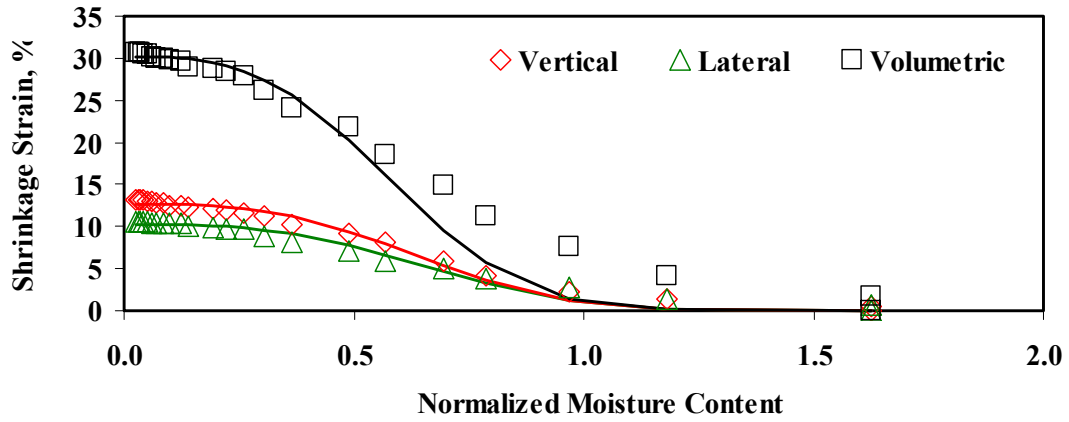
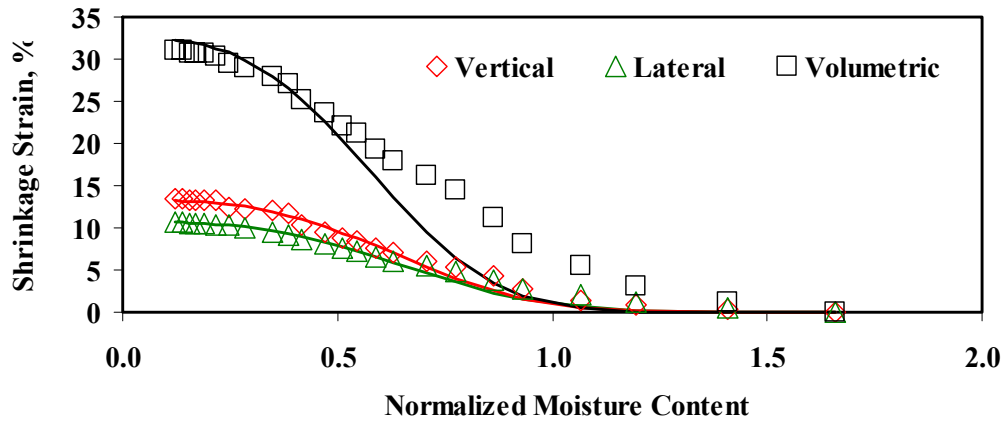


Figure H.5 Typical Variations in Shrinkage Strain and NMC for Clay from Houston District

a) Specimen 1



b) Specimen 2



c) Specimen 3

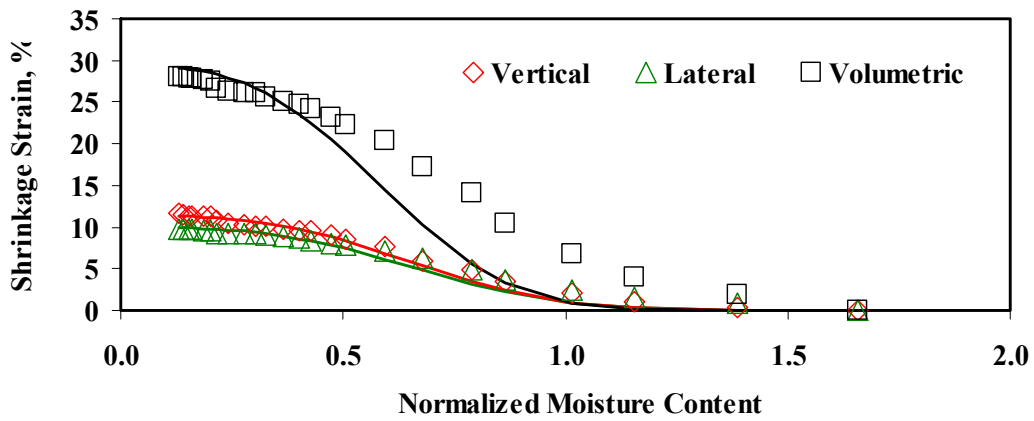
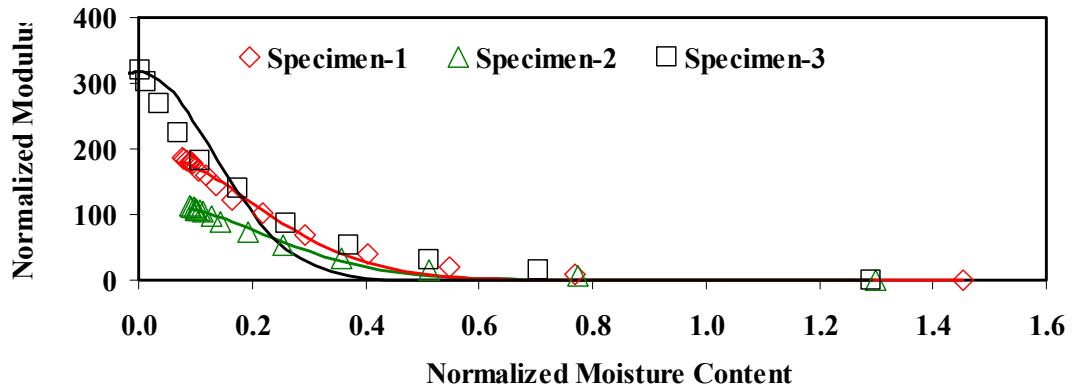


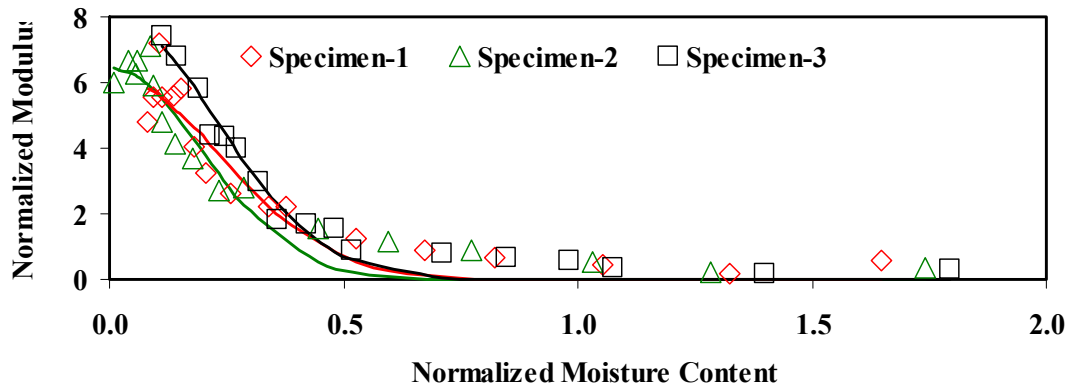
Figure H.6 Typical Variations in Shrinkage Strain and NMC for Clay from Paris District

**APPENDIX I - Normalized Modulus VS Normalized
Moisture Content – DFS Results**

a) El Paso



b) San Antonio



c) Fort Worth

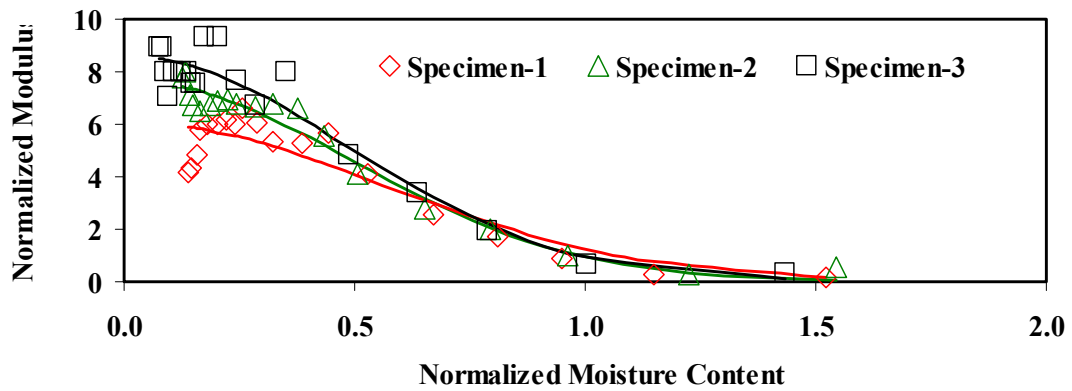
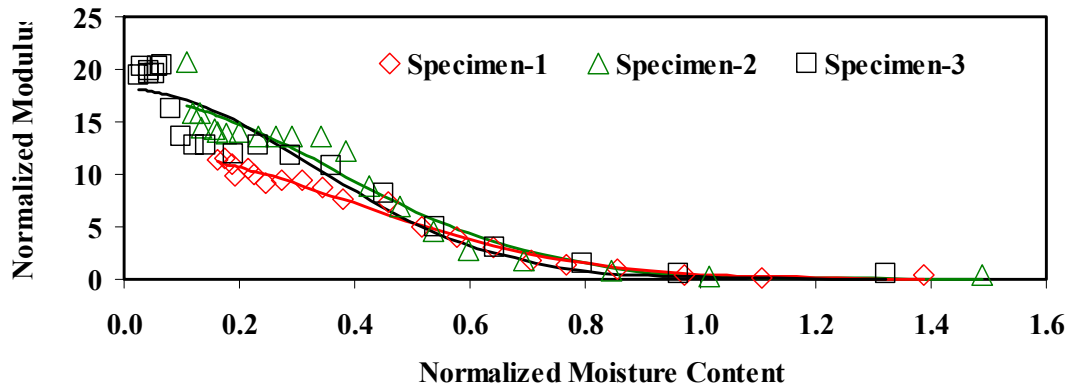
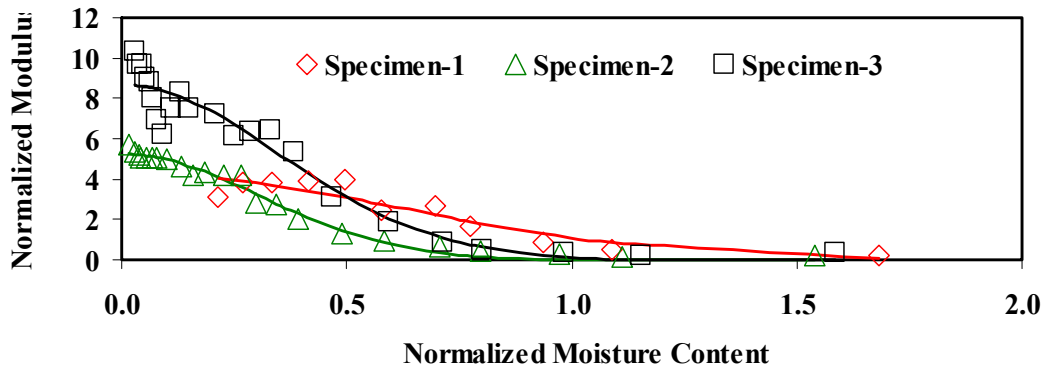


Figure I.1 Typical Variations in Normalized Modulus and NMC

a) Bryan



b) Houston



c) Paris

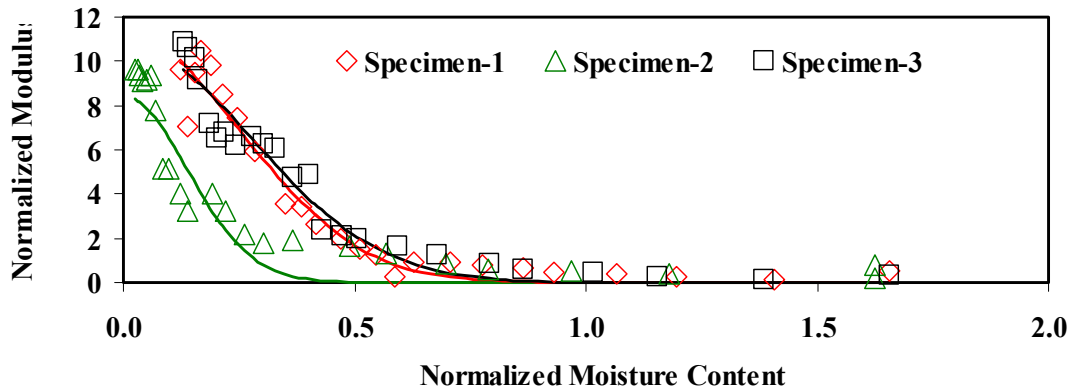


Figure I.2 Typical Variations in Normalized Modulus and NMC

**APPENDIX J - Normalized Modulus
VS Shrinkage Strain – DFS Results**

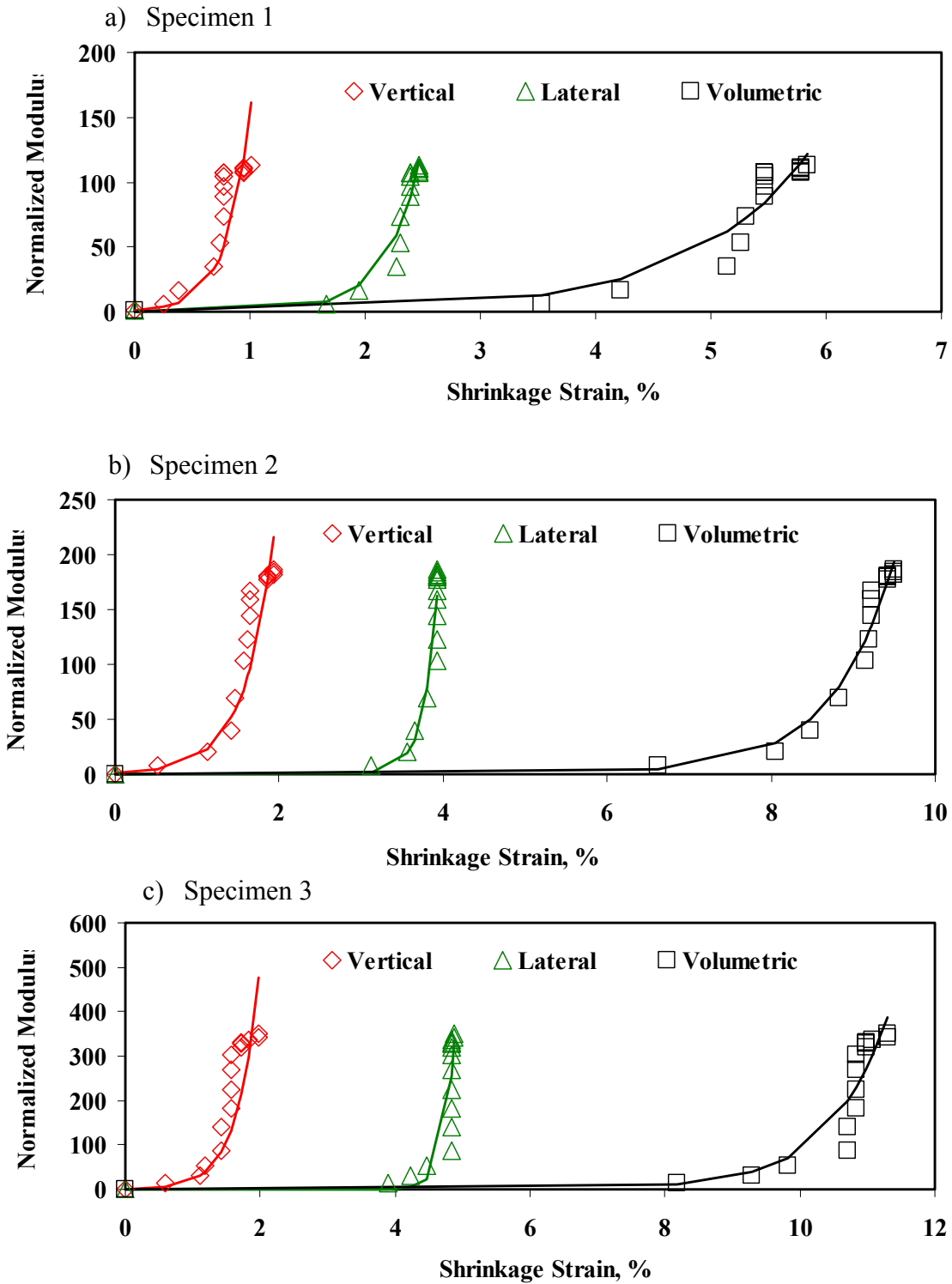


Figure J.1 Typical Variations in Shrinkage Strain and NMC for Clay from El Paso District

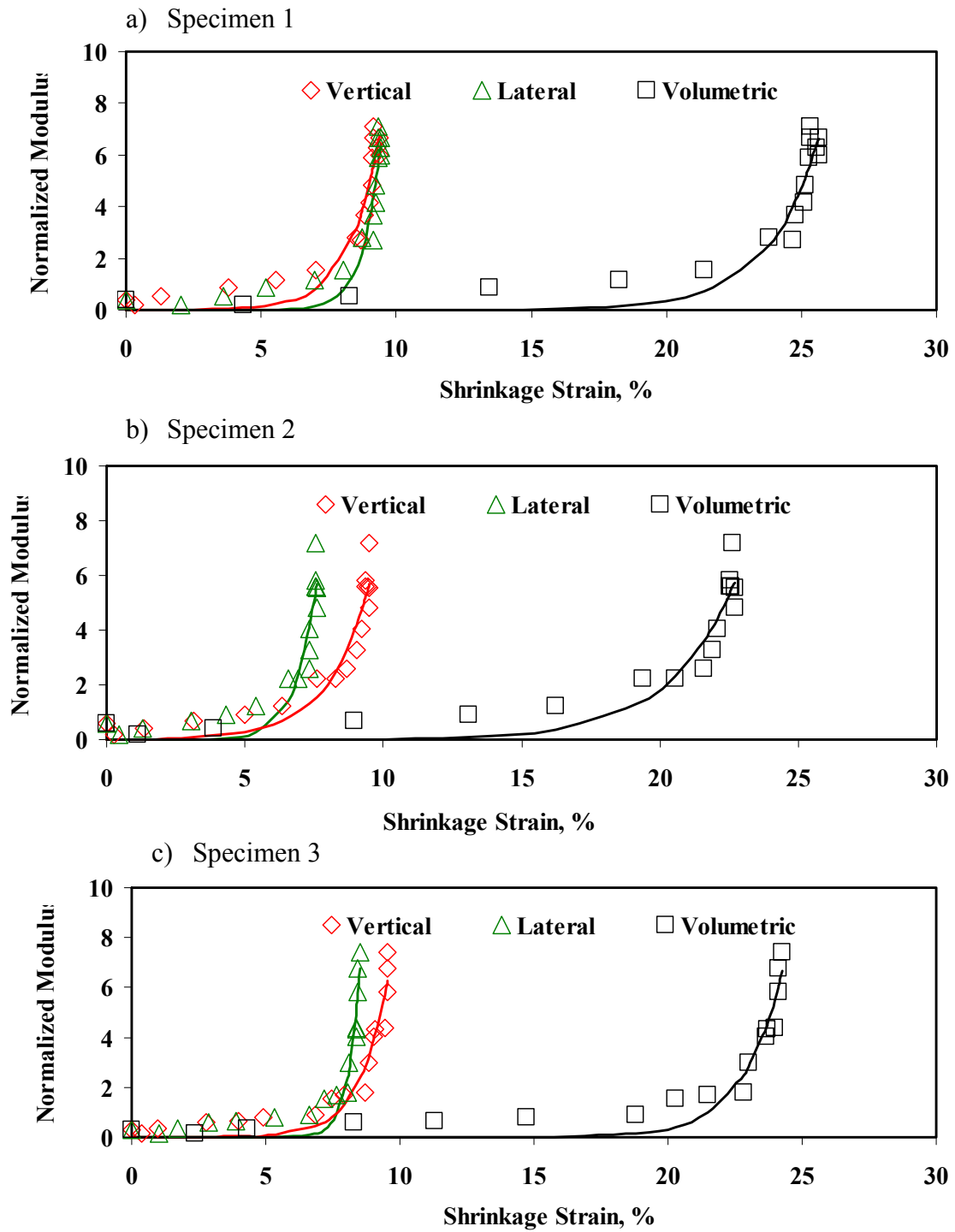


Figure J.2 Typical Variations in Shrinkage Strain and NMC for Clay from San Antonio District

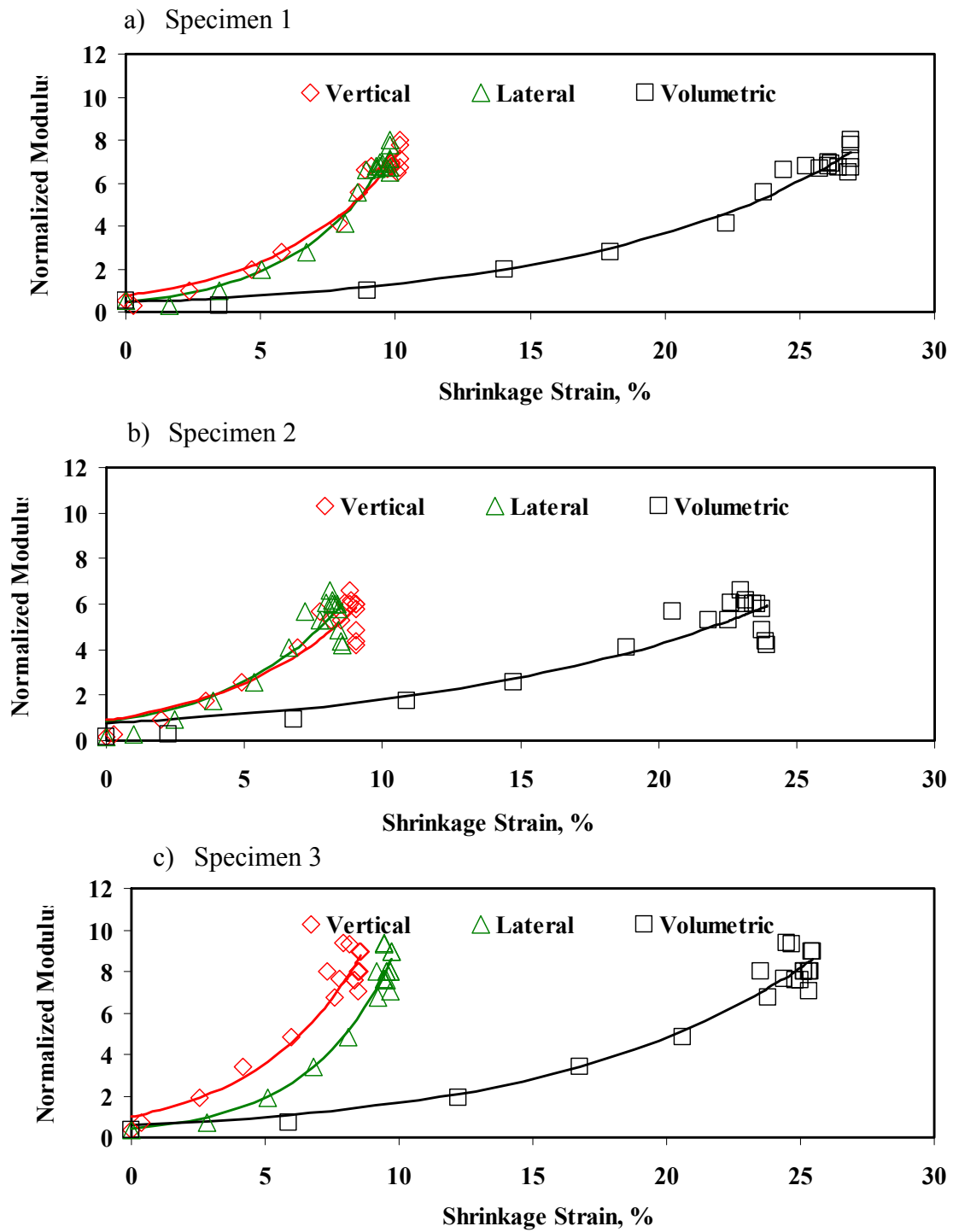


Figure J.3 Typical Variations in Shrinkage Strain and NMC for Clay from Fort Worth District

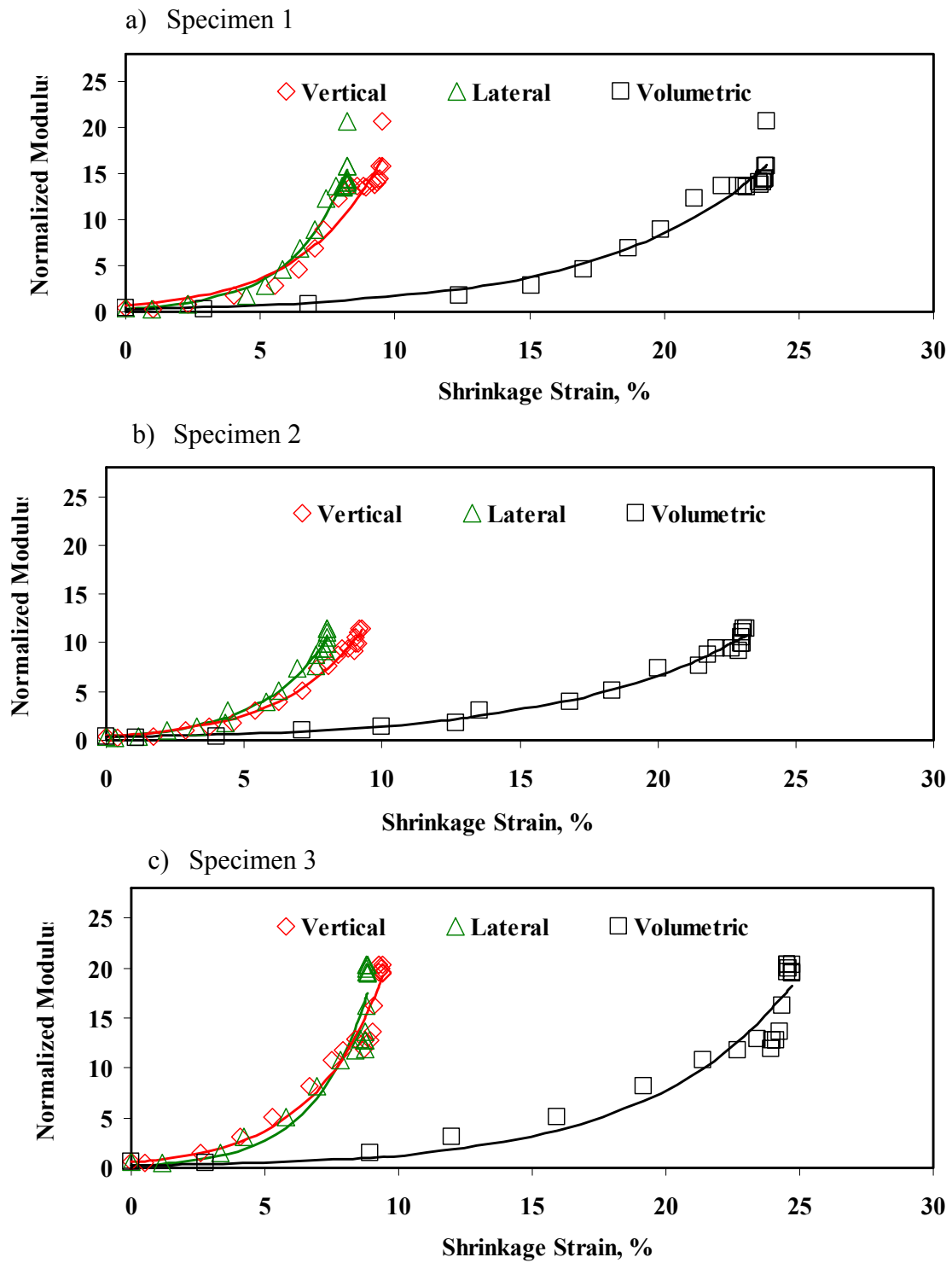


Figure J.4 Typical Variations in Shrinkage Strain and NMC for Clay from Bryan District

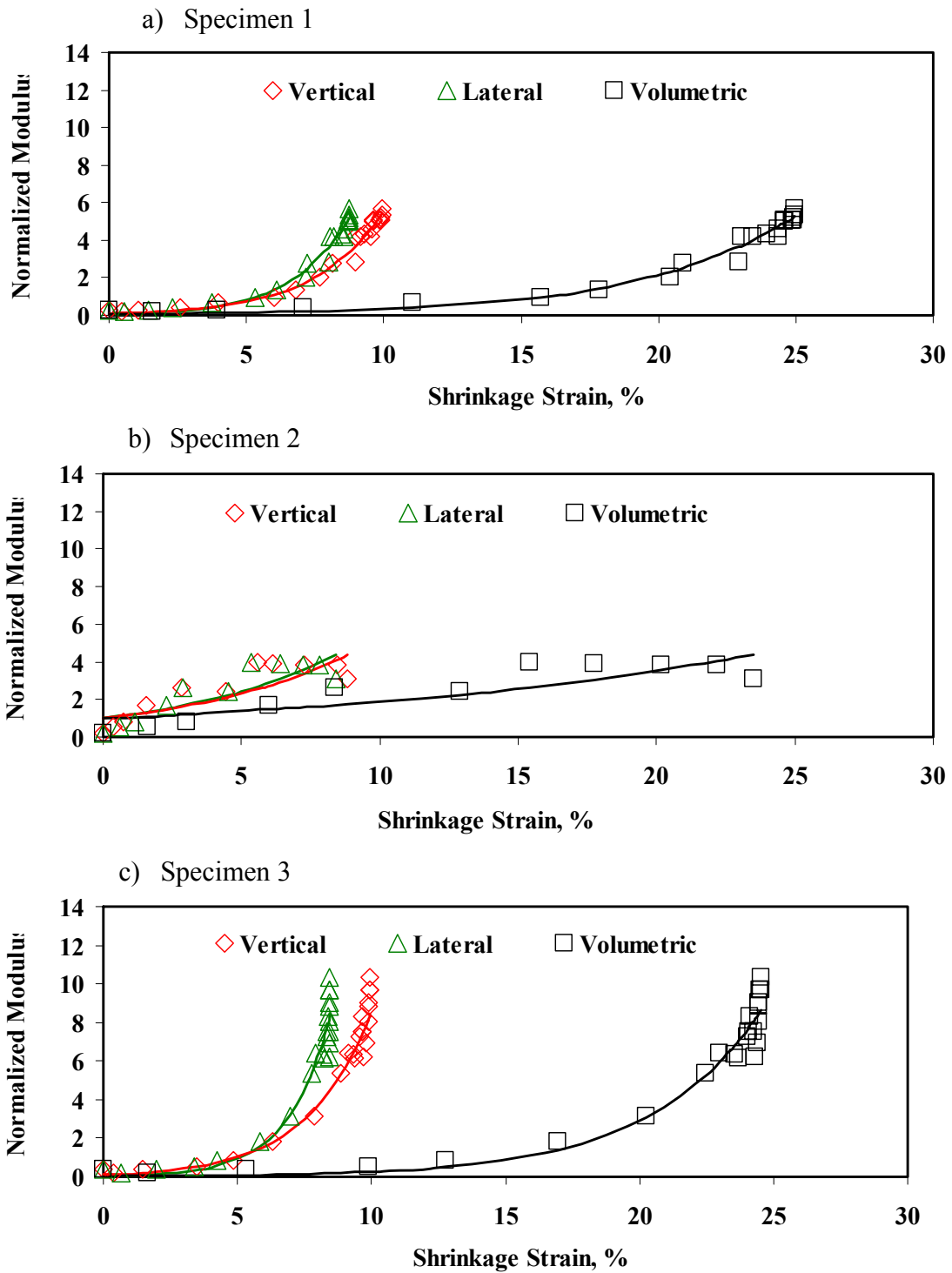


Figure J.5 Typical Variations in Shrinkage Strain and NMC for Clay from Houston District

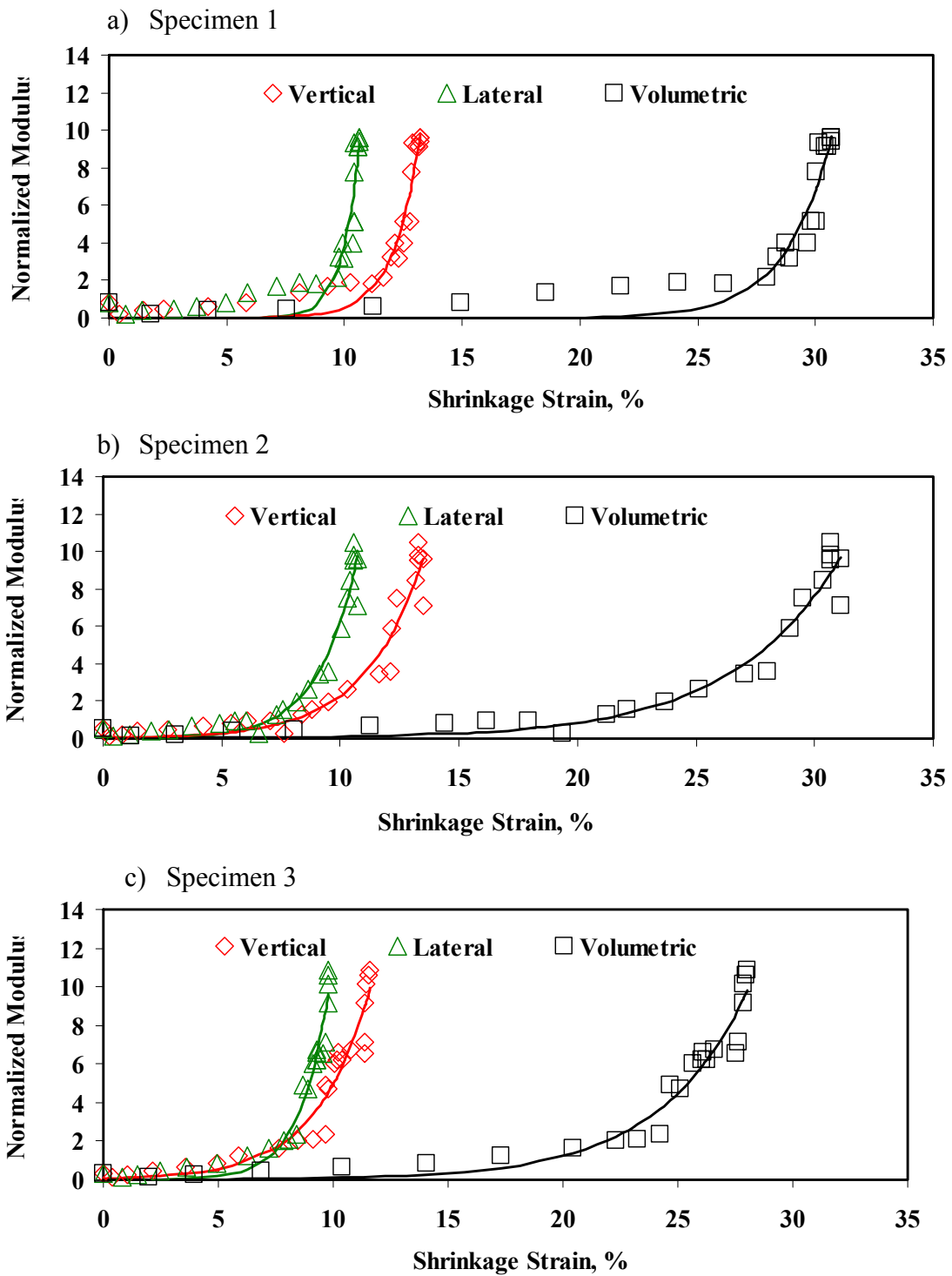


Figure J.6 Typical Variations in Shrinkage Strain and NMC for Clay from Paris District

APPENDIX K - Expansion Strain VS Time – SFO Results

Table K.1 –Correlation Analysis between E Parameter from Equation 5.7 and Index Properties of Clays

Expansion Mode	Plasticity Index	Liquid Limit	Plastic Limit	Optimum Moisture Content	Dry Unit Weight	Seismic Modulus at OMC
Vertical	0.79	0.68	0.34	0.61	-0.54	0.92
Lateral	0.73	0.43	0.02	0.48	-0.20	0.77
Volumetric	0.81	0.61	0.23	0.58	-0.44	0.93

Table K.2 –Relationships between Parameter and Index Properties of Soils

Index Property	Mode of Shrinkage	Parameter - E				
		Slope	Intercept	R ²	F	G
Plasticity Index	Vertical	0.28	-0.66	0.61	2	1.22
	Lateral	0.08	1.62	0.55	1	0.55
	Volumetric	0.28	1.18	0.68	2	1.36
Liquid Limit	Vertical	0.16	-1.40	0.70	2	1.40
	Lateral	0.04	1.49	0.54	1	0.54
	Volumetric	0.16	0.55	0.76	2	1.52
Optimum Moisture Content	Vertical	0.57	-4.95	0.50	1	0.50
	Lateral	0.16	0.28	0.49	1	0.49
	Volumetric	0.58	-3.31	0.58	1	0.58
Dry Unit Weight	Vertical	-0.25	30.94	0.75	2	1.50
	Lateral	-0.06	9.58	0.53	1	0.53
	Volumetric	-0.24	32.44	0.80	4	3.20
Seismic Modulus OMC	Vertical	0.48	-0.62	0.87	4	3.48
	Lateral	0.09	2.15	0.44	1	0.44
	Volumetric	0.45	1.62	0.88	4	3.52

**Table K.3 – Weighting Functions for Each Index Parameter of Houston Clay
(See Equation 5.13)**

Index Property	Vertical Shrinkage	Lateral Shrinkage	Volumetric Shrinkage
	Strain	Strain	Strain
W_{PI}	0.15	0.22	0.13
W_{LL}	0.17	0.21	0.15
W_{OMC}	0.06	0.19	0.06
W_{DUW}	0.18	0.21	0.31
W_{SM OMC}	0.43	0.17	0.34

Table K.4 – Estimated E* Parameter for Different Shrinkage Types for Houston Clay (See Equation 5.14)

Parameter	Vertical	Lateral	Volumetric
E*	7.87	3.79	9.50

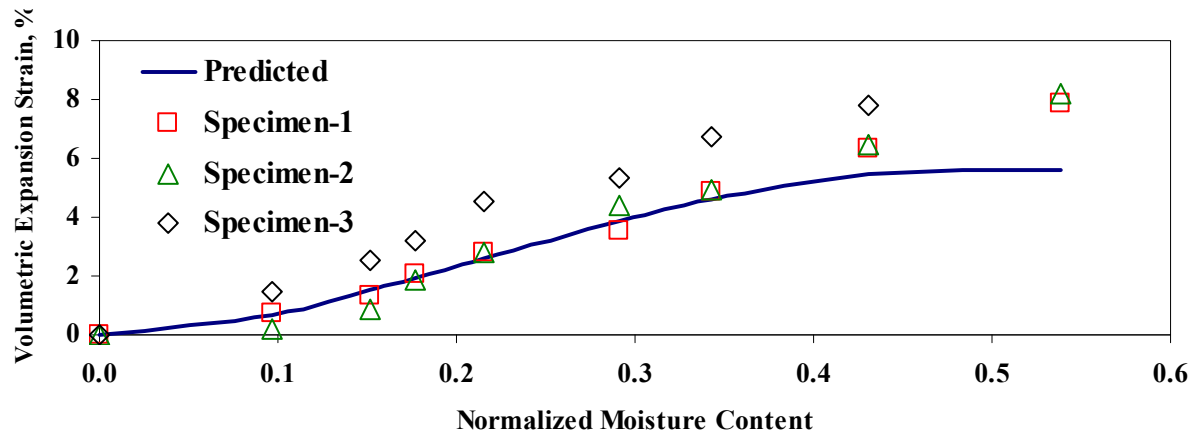
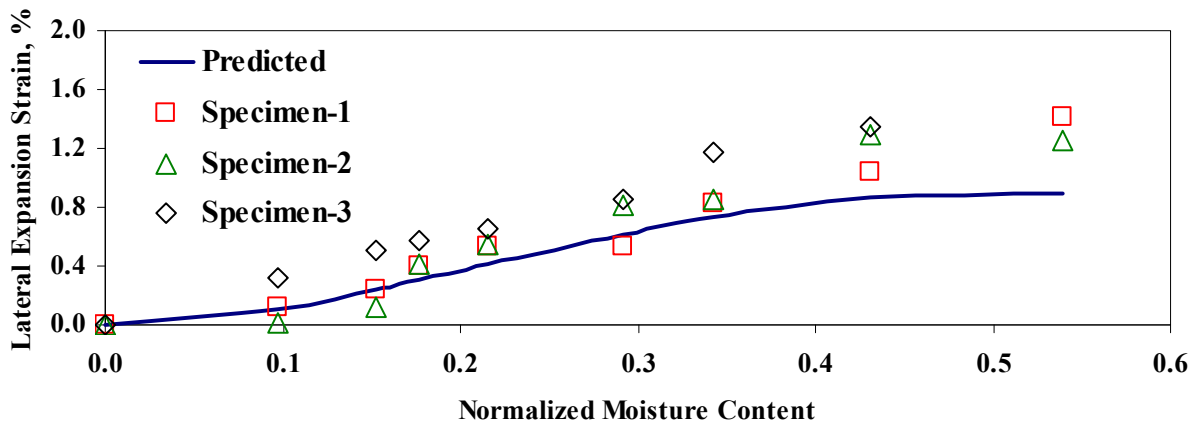
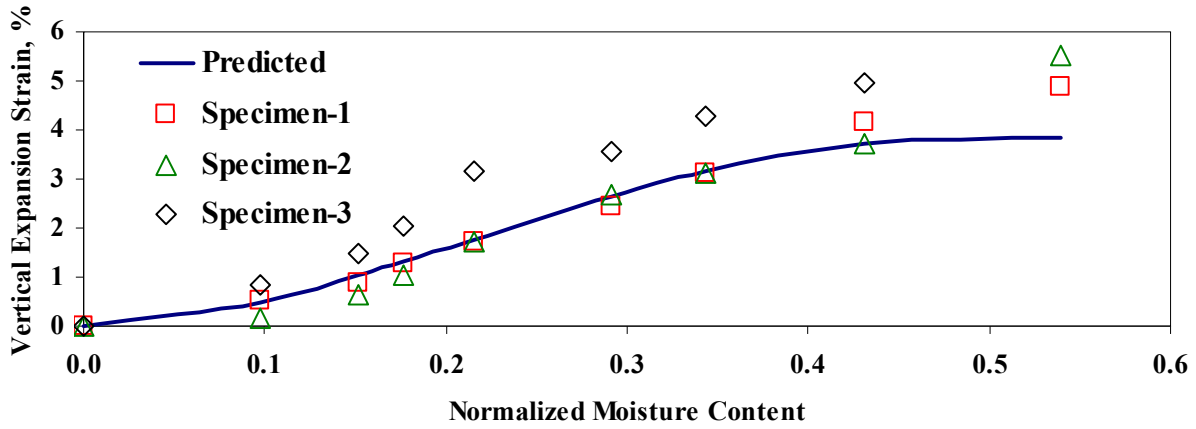


Figure K.1 - Comparison of Measured and Predicted Expansion Strain Data and Moisture Content for Three Specimen of the Houston Clay Material

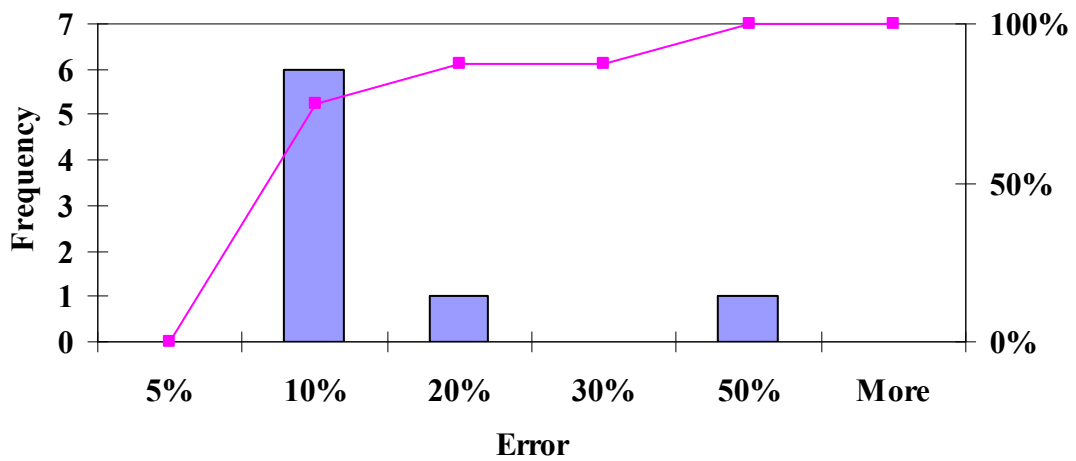
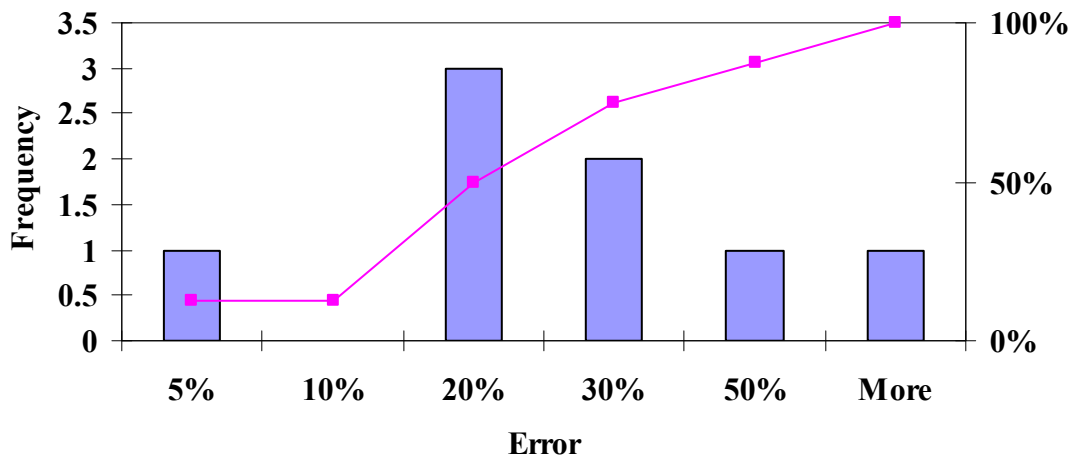
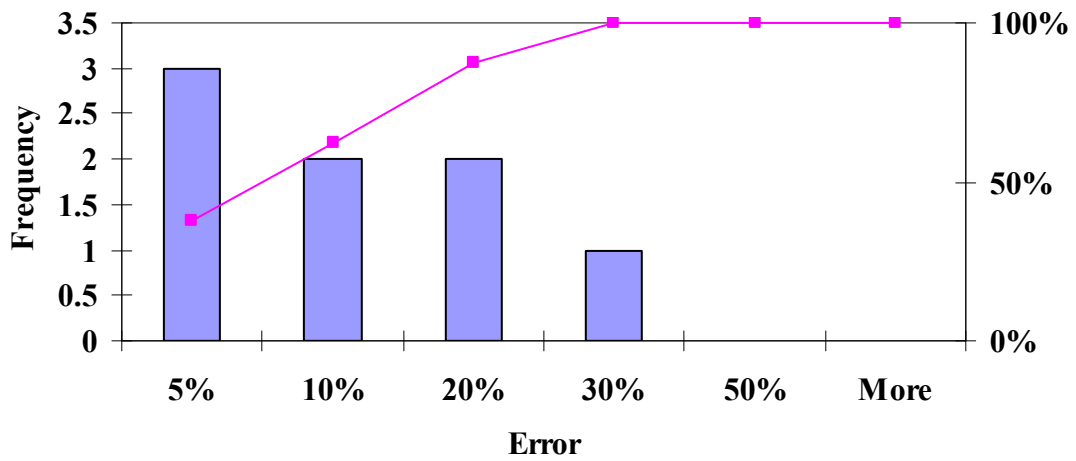


Figure K.2 –Histograms of Differences between Measured and Estimated Strains

Table K.5 –Correlation Analysis between J Parameter from Equation 5.10 and Index Properties of Clays

Shrinkage Mode	Plasticity Index	Liquid Limit	Plastic Limit	Optimum Moisture Content	Dry Unit Weight	Seismic Modulus at OMC
Vertical	0.91	0.88	0.54	0.87	-0.74	0.85
Lateral	0.85	0.86	0.57	0.86	-0.74	0.76
Volumetric	0.89	0.89	0.56	0.88	-0.74	0.82

Table K.6 –Relationships between Parameter and Index Properties of Soils

Index Property	Mode of Shrinkage	Parameter - J				
		Slope	Intercept	R ²	F	G
Plasticity Index	Vertical	0.10	-0.85	0.79	2	1.58
	Lateral	0.05	0.49	0.73	2	1.46
	Volumetric	0.08	0.86	0.80	4	3.20
Liquid Limit	Vertical	0.05	-0.69	0.73	2	1.46
	Lateral	0.03	0.52	0.76	2	1.52
	Volumetric	0.04	0.95	0.78	2	1.56
Optimum Moisture Content	Vertical	0.22	-2.56	0.71	2	1.42
	Lateral	0.13	-0.57	0.74	2	1.48
	Volumetric	0.17	-0.57	0.77	2	1.54
Dry Unit Weight	Vertical	-0.05	7.33	0.48	1	0.48
	Lateral	-0.03	5.50	0.56	1	0.56
	Volumetric	-0.05	7.53	0.55	1	0.55
Seismic Modulus OMC	Vertical	0.12	-0.12	0.67	2	1.34
	Lateral	0.07	0.93	0.58	1	0.58
	Volumetric	0.09	1.41	0.68	2	1.36

**Table K.7 – Weighting Functions for Each Index Parameter of Houston Clay
(See Equation 5.13)**

Index Property	Vertical Shrinkage	Lateral Shrinkage	Volumetric Shrinkage
	Strain	Strain	Strain
W_{PI}	0.39	0.26	0.24
W_{LL}	0.19	0.27	0.24
W_{OMC}	0.18	0.26	0.23
W_{DUW}	0.07	0.10	0.08
W_{SM OMC}	0.17	0.10	0.21

**Table K.8 – Estimated J* Parameter for Different Shrinkage Types for San Antonio Clay
(See Equation 5.14)**

Parameter	Vertical	Lateral	Volumetric
J*	2.28	2.15	3.18

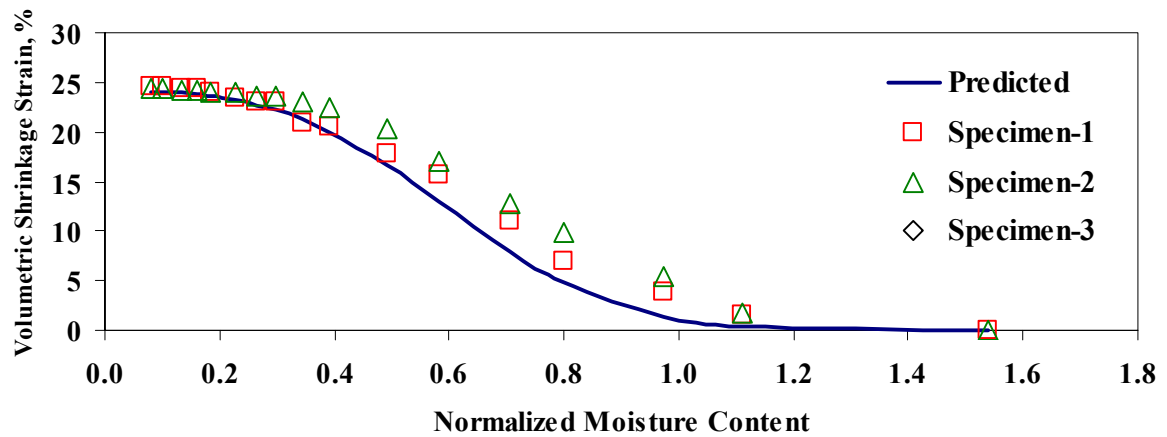
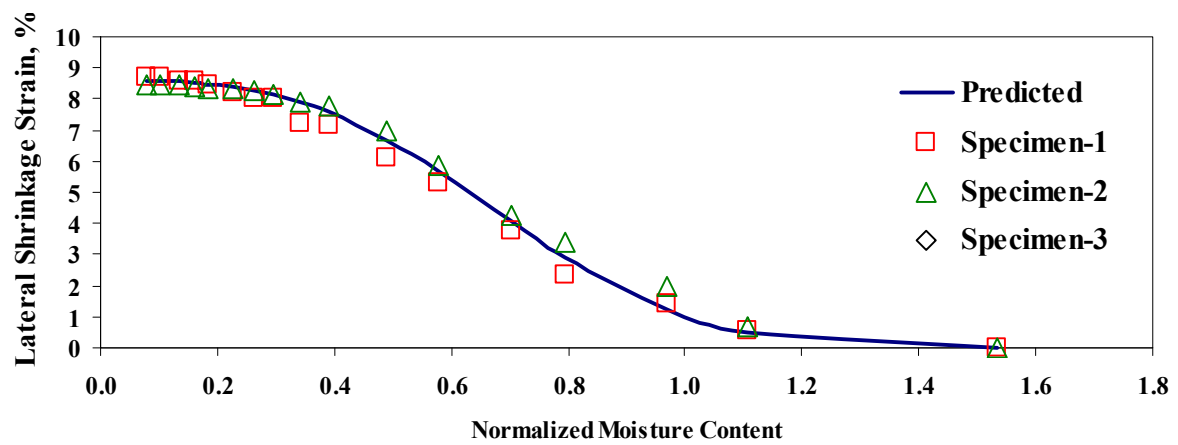
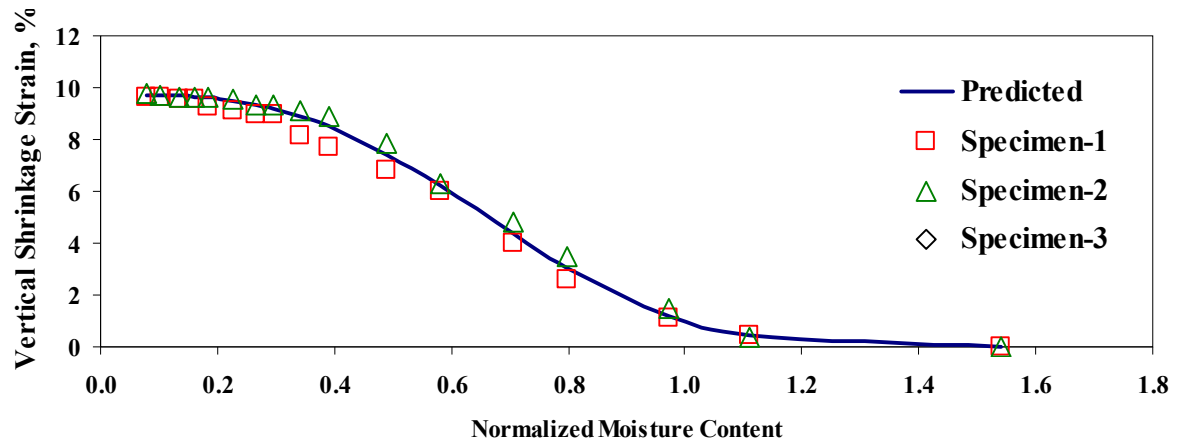


Figure K.3 - Comparison of Measured and Predicted Shrinkage Strain Data and Moisture Content for Three Specimen of the Houston Clay Material

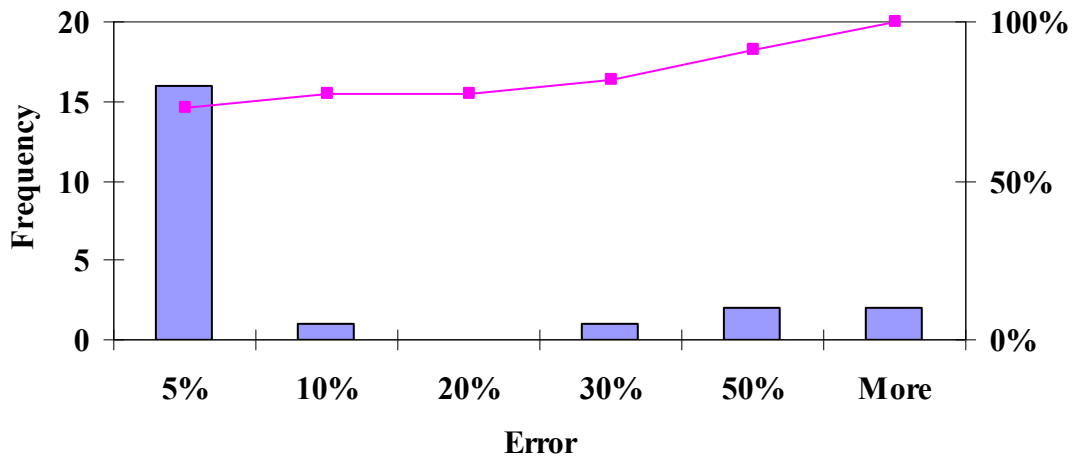
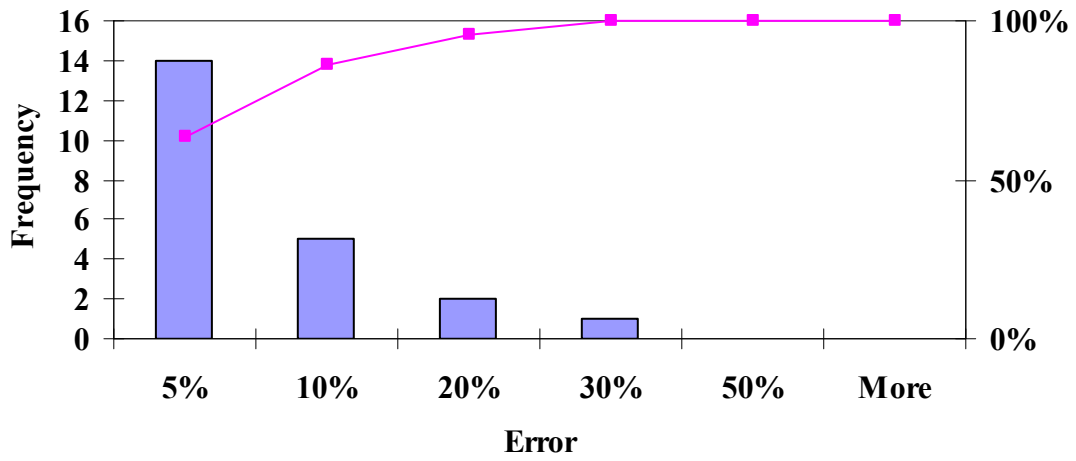
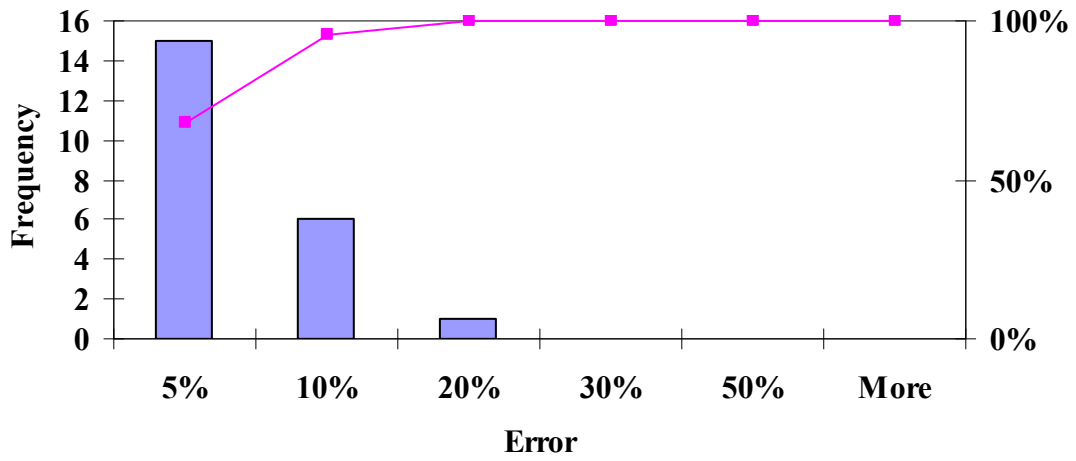


Figure K.4 –Histograms of Differences between Measured and Estimated Strains

Table K.9 –Correlation Analysis between B and C Parameter from Equation 5.5 and Index Properties of Clays

Parameter	Plasticity Index	Liquid Limit	Plastic Limit	Optimum Moisture Content	Dry Unit Weight	Seismic Modulus at OMC
B	-0.51	-0.65	-0.50	-0.46	0.58	-0.87
C	-0.70	-0.86	-0.65	-0.75	0.78	-0.83

Table K.10 –Relationships between Parameter and Index Properties of Soils

Index Property	Parameter	Relationship				
		Slope	Intercept	R ²	F	G
Plasticity Index	B	-0.05	3.85	0.26	1	0.26
	C	-0.17	7.96	0.49	1	0.49
Liquid Limit	B	-0.03	4.22	0.42	1	0.42
	C	-0.11	9.1	0.75	2	1.50
Optimum Moisture Content	B	-0.1	4.58	0.22	1	0.22
	C	-0.41	11.8	0.56	1	0.56
Dry Unit Weight	B	0.04	-1.27	0.33	1	0.33
	C	0.13	-9.73	0.60	2	1.20
Seismic Modulus	B	-0.11	4.36	0.75	2	1.50
OMC	C	-0.26	7.77	0.68	2	1.36

Table K.11 – Weighting Functions for Each Index Parameter of Houston Clay (See Equation 5.13)

Index Property	B	C
W _{PI}	0.058	0.143
W _{LL}	0.001	0.238
W _{OMC}	0.208	0.163
W _{DUW}	0.013	0.218
W _{SM OMC}	0.721	0.238

Table K.12 – Estimated B* and C* Parameter for Different Shrinkage Types for San Antonio Clay

Parameter	B*	C*
	2.26	2.85

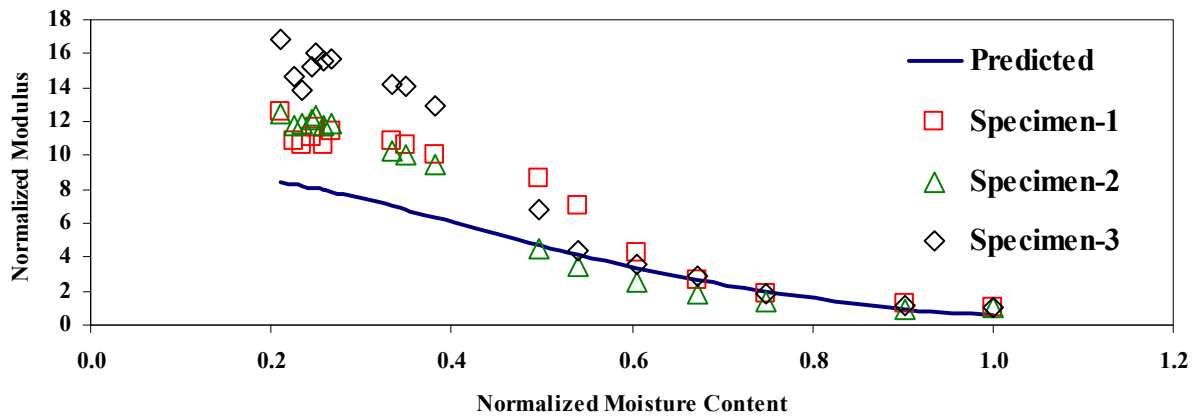


Figure K.5 - Comparison of Measured and Predicted Normalized Modulus Data and Moisture Content for Three Specimen of the Houston Clay Material

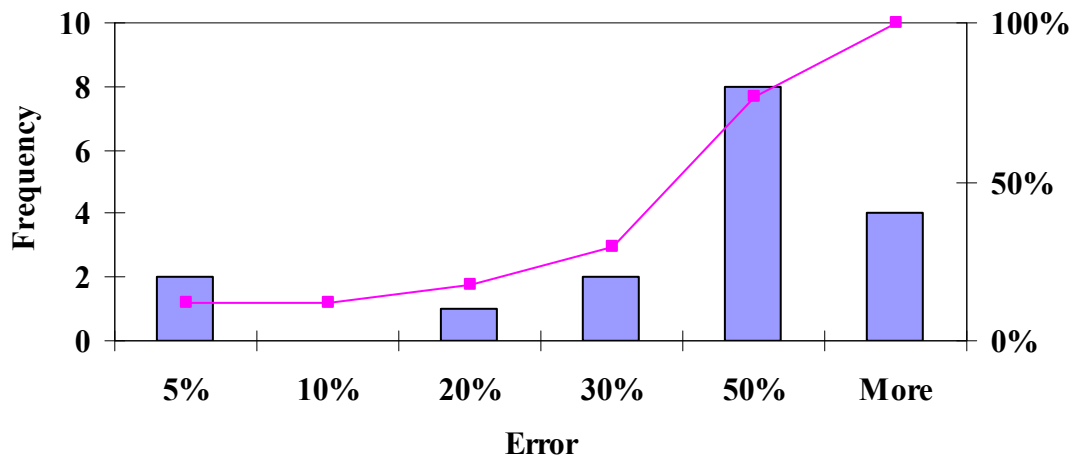


Figure K.6 –Histograms of Differences between Measured and Estimated Strains

Table K.13 –Correlation Analysis between F and G Parameters from Equation 5.8 and Index Properties of Clays

Parameter	Plasticity Index	Liquid Limit	Plastic Limit	Optimum Moisture Content	Dry Unit Weight	Seismic Modulus at OMC
F	-0.68	-0.92	-0.78	-0.84	0.88	-0.06
G	0.08	-0.84	-0.77	-0.54	0.88	0.21

Table K.14 –Relationships between Parameter and Index Properties of Soils

Index Property	Mode of Shrinkage	Relationship				
		Slope	Intercept	R ²	F	G
Plasticity Index	F	-0.77	37.25	0.35	1	0.35
	G	-3.55	151.88	0.31	1	0.31
Liquid Limit	F	-0.59	45.17	0.78	2	1.56
	G	-2.82	192.58	0.73	2	1.46
Optimum Moisture Content	F	-2.37	65.30	0.73	2	1.46
	G	-11.14	285.56	0.67	2	1.34
Dry Unit Weight	F	0.74	-59.28	0.81	4	3.24
	G	3.62	-313.41	0.80	4	3.20

Table K.15 – Weighting Functions for Each Index Parameter of Houston Clay (See Equation 5.13)

Index Property	F	G
W _{PI}	0.068	0.017
W _{LL}	0.495	0.274
W _{OMC}	0.207	0.086
W _{DUW}	0.230	0.623

Table K.16 – Estimated F* and G* Parameter for Different Shrinkage Types for Houston Clay

Parameter	F*	G*
		14.30

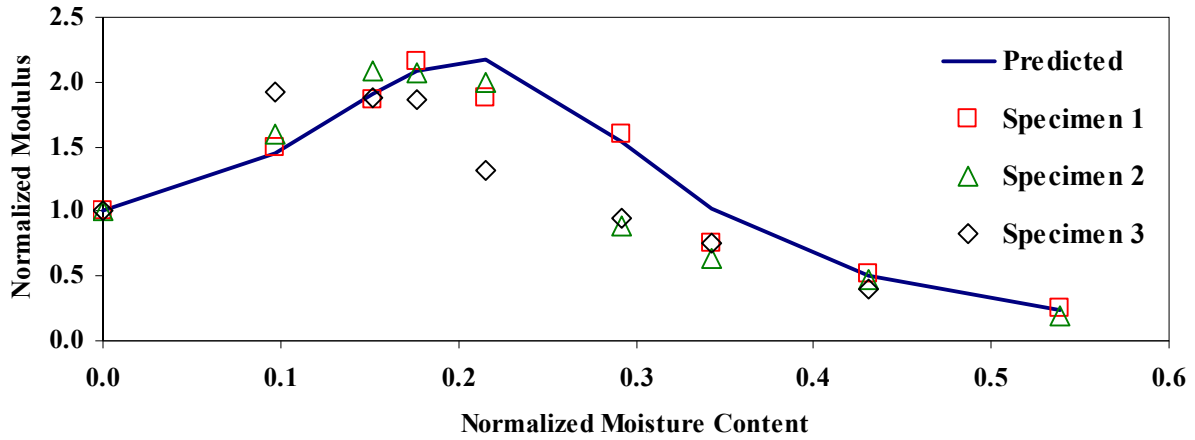


Figure K.7 - Comparison of Measured and Predicted Normalized Modulus Data and Moisture Content for Three Specimen of the Houston Clay Material

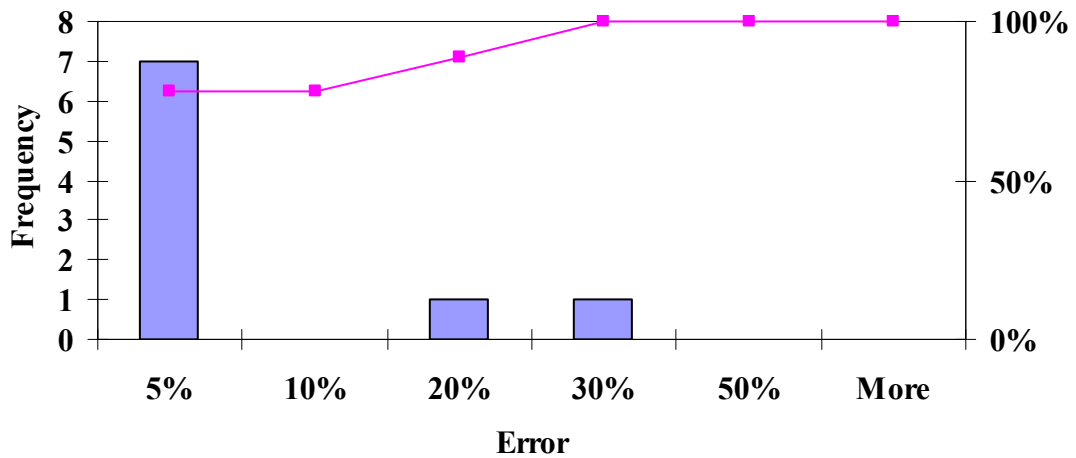


Figure K.8 –Histograms of Differences between Measured and Estimated Strains

Table K.17 –Correlation Analysis between K and L Parameters from Equation 5.11 and Index Properties of Clays

Parameter	Plasticity Index	Liquid Limit	Plastic Limit	Optimum Moisture Content	Dry Unit Weight	Seismic Modulus at OMC
K	-0.68	-0.93	-0.73	-0.86	0.81	-0.64
L	-0.57	-0.46	-0.20	-0.69	0.27	-0.13

Table K.18 –Relationships between Parameter and Index Properties of Soils

Index Property	Parameter	Relationship				
		Slope	Intercept	R ²	F	G
Plasticity Index	K	-0.13	6.38	0.49	1	0.49
	L	-0.38	16.84	0.37	1	0.37
Liquid Limit	K	-0.09	7.39	0.87	2	1.74
	L	-0.18	15.7	0.33	2	0.66
Optimum Moisture Content	K	-0.35	10.12	0.75	2	1.50
	L	-0.99	27.13	0.55	2	1.10
Dry Unit Weight	K	0.11	-7.92	0.70	4	2.80
	L	0.16	-9.36	0.14	4	0.56

Table K.19 – Weighting Functions for Each Index Parameter of Houston Clay (See Equation 5.13)

Index Property	K	L
W_{PI}	0.07	0.35
W_{LL}	0.51	0.17
W_{OMC}	0.22	0.44
W_{DUW}	0.20	0.04

Table K.20 – Estimated K* and L* Parameter for Different Shrinkage Types for Houston Clay

Parameter	K*	L*
		2.60

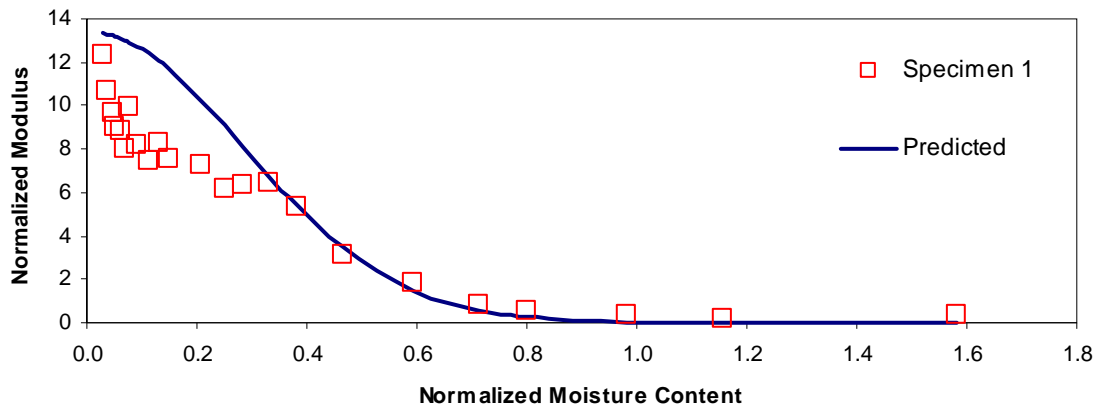


Figure K.9 - Comparison of Measured and Predicted Normalized Modulus Data and Moisture Content for Three Specimen of the Houston Clay Material

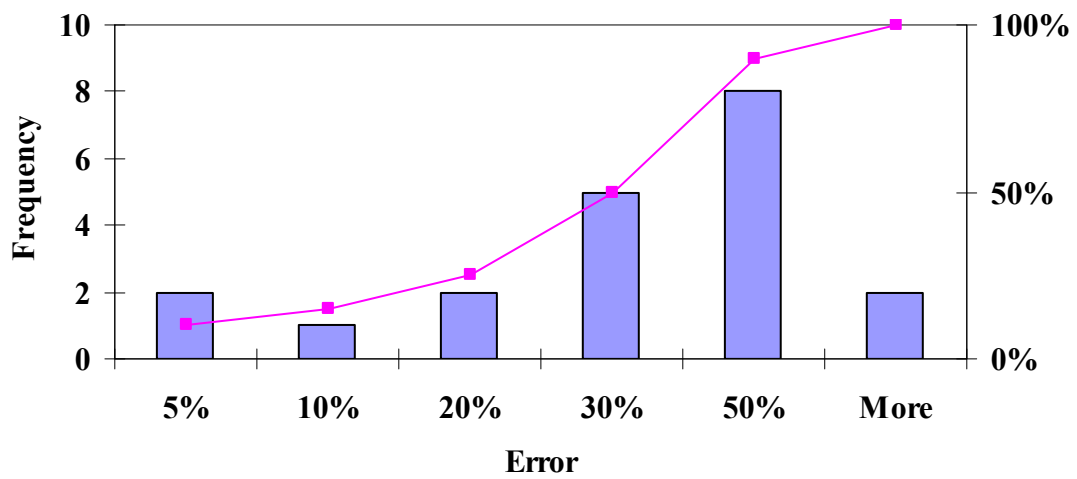


Figure K.10 –Histograms of Differences between Measured and Estimated Strains